

**Biomechanics of Skull Fracture and Intracranial Injury in Young  
Children as a Consequence of a Low Height Fall**

By

Jonathon Hughes

A thesis is submitted to Cardiff University for the degree of Doctor of Philosophy

School of Engineering and School of Medicine  
Cardiff University  
2014

## Declaration

This work has not previously been accepted in substance for any degree and is not concurrently submitted in candidature for any degree.

Signed.....(candidate)                      Date .....

This thesis is being submitted in partial fulfilment of the requirements for the degree of PhD

Signed.....(candidate)                      Date .....

This thesis is the result of my own independent work/investigation, except where otherwise stated. Other sources are acknowledged by explicit references.

Signed.....(candidate)                      Date .....

I hereby give consent for my thesis, if accepted, to be available for the photocopying and for the inter-library loan, and for the title and summary to be made available to outside organisations.

Signed.....(candidate)                      Date .....

I hereby give consent for my thesis, if accepted, to be available for the photocopying and for the inter-library loans after expiry of a bar on access previously approved by the Graduate Development Committee

Signed.....(candidate)                      Date .....

## **Acknowledgments**

First off I would like to state that this research and thesis has by no means been a sole effort, where numerous people have made contributions from small to large.

Initially I would like to thank the staff in the emergency department and in the medical records department at the University Hospital of Wales Cardiff. The staff always happy to help researchers even though they are incredibly busy with their work.

To the research team working with Professor Kemp and Dr Maguire, many thanks for the support in helping throughout the project. A special thank you to statisticians Lazlo Trefan and Daniel Farewell who aided with numerous technical discussions.

To my supervisors, both medical and engineering. working between two research teams can be challenging. However in this research area it is paramount that a multidiscipline approach is adopted in order to find a unified solution. I am grateful to both Dr Jones and Dr Theobald for giving me this opportunity and for their continued support throughout the project. I am also thankful to both Professor Kemp and Dr Maguire, who have been instrumental in helping me through many aspects of this project, particularly for their support whilst presenting in the United States.

Finally to my family and friends who have to endured numerous stressful moments. I extremely thankful for all the support throughout this project and I know I would not have made it to the finish line without it.

## **Abstract**

### **Background**

A challenge for clinicians when presented with a significant head injury in a young child and a postulated fall height is to determine the plausibility of such an injury. Previous authors have aimed to determine the head injuries that can result from a low height fall, however due to a lack of clarity it is difficult to determine a fall height at which certain head injuries including skull fracture and intra cranial injury (ICI) becomes more likely. Biomechanical thresholds aimed at young children exist for skull fracture and adult thresholds for subdural haemorrhage, however they have not been assessed against the injuries seen in a clinical setting. Consequently this study investigated low height falls in a paediatric clinical setting to determine differentiating variables and characteristics in the mechanism of head injury between children with a minor head injury and those with a skull fracture and / or ICI. The primary aim of which was to determine a fall height threshold for skull fracture and / ICI in young children. Following this, biomechanical methods were used to include, the development of an accurate anthropomorphic testing device (ATD) and a finite element model of an infant head, to investigate the differentiating variables and ultimately the clinical fall height threshold.

### **Method**

A case control study of children  $\leq 48$  months of age who had a minor head injury and those with a skull fracture and / or ICI, to identify variables and characteristics of falls that influenced injury severity. Children were ascertained from those who attended the University Hospital of Wales Cardiff from a low height fall. The clinical characteristics and biomechanical variables evaluated included the mechanism of injury, surface of impact, site of impact and fall height (taking into consideration height of object and centre of gravity of the child's body and head mass). Categorical variables were assessed using a Chi Square test and continuous variables using Student t-test or the non parametric equivalent. A modified logistic regression was used to evaluate the likelihood of sustaining a skull fracture and /or ICI based on fall height.

Initially to investigate the differentiating variables a biofidelic infant headform was designed via image processing and segmentation of computed tomography (CT) datasets and manufactured using materials with similar properties to the bone and soft tissues of the head. The headform impact response was initially validated against infant cadaver data and then it was subject to tests classed as sub-injurious based on the clinical data collected from the hospital. The headform was dropped at impact angles of 90°, 75° and 60° at three velocities (2.4m/s, 3m/s, 3.4m/s) corresponding to three heights (0.3m, 0.45m, 0.6m), onto four domestic surfaces (carpet, carpet & underlay, laminate and wood) using two skin friction surrogates (latex, polyamide). A Student t-test was used to measure the affect of the coefficient of static friction and a three factorial ANOVA to measure the affect of impact velocity, surface type and angle of impact had on kinematic variables (peak g, HIC, rotational acceleration, change in rotational velocity and duration of impact).

Finally to investigate the differentiating variables a finite element (FE) model of an infant head was developed, again through image processing of infant head CT datasets. The FE model consisted of the scalp, sutures, cranial bones, dura membranes, cerebral spinal fluid, bridging veins and the brain and the impact response was also initially validated against infant cadaver data. Post validation a parametric test across four different scenarios (0.3m impact onto the occipital, frontal, vertex and parietal areas of the head) was conducted to assess the affect material properties have on impacted response of the model. Finally the FE was used to assess the affect height (0.3m, 0.6m, 1.2m) and anatomical site of impact have on the impact response of the head, including kinematic variables and material response variables.

## **Results**

Identified cases included 416 children with a minor head injury and 47 with a skull fracture and / or ICI. The mean fall height for minor head injuries was significantly lower than for a fall causing skull fracture and / or ICI ( $P < 0.001$ ). Utilising the height of centre of gravity of the head, no skull fracture and / or ICI was sustained in children who fell  $< 0.6\text{m}$  (2ft). Skull fractures and / or ICI were more likely in children  $\leq 12$

months ( $P<0.001$ ), following impacts to the temporal/parietal or occipital region of the head ( $P<0.01$ ), and impacts onto wood ( $P<0.05$ ).

All tests using the biofidelic headform were conducted with impact velocities corresponding to fall heights  $\leq 0.6\text{m}$ , where an increase in impact velocity, increase in surface stiffness and a decrease in impact angle significantly affected both rotational and translation kinematic variables ( $P<0.05$ ). Peak rotational accelerations at 90 degrees were  $11,363\text{ rad/s}^2$  on wood at an impact velocity corresponding to a height of  $0.6\text{m}$  and significantly increased to  $16,980\text{ rad/s}^2$  with a 30 degree decrease in impact angle ( $P<0.001$ ). However head injury criterion (HIC) decreased for wood at impact velocity corresponding to  $0.6\text{m}$  from 245 to 121 for a 30degree decrease in impact angle ( $P<0.001$ ).

The parametric test using the finite element model indicated that the skull stiffness has the greatest affect on the dynamic response of the head, an increase in the skull stiffness of 7% increased HIC by 26%. Height and anatomical site of impact affected kinematic and material response variables. The mean value of peak G and HIC at the clinical defined threshold of  $0.6\text{m}$  fall height was 85g and 284g, respectively. An increase in fall height to The stiffest parts of the head were the frontal areas and the least stiff were impacts focal to the sutures. Impacts focal to sutures indicated high stress zones on adjacent bones, for example an impact to the vertex indicated high stress zones on the left and right parietal bones.

The greatest strain on the connectors used to model the bridging veins was at the most focal impact point, the vertex. For a  $1.2\text{m}$  fall the greatest peak stretch ratio for a vertex impact was 1.31.

### **Conclusion**

A threshold above which skull fracture and / or ICI of  $0.6\text{m}$  was proposed. The corresponding mean values for peak g and HIC using the finite element models at a  $0.6\text{m}$  fall corresponded well with current biomechanical thresholds for skull fracture, particularly the current National Highway Transport Safety Administration standard. This study highlights the importance of developing threshold specific to young children that are both clinically and biomechanically relevant. A clinical finding was that head injury severity was influence by

anatomical site of impact. This was supported by the biomechanical analysis where skull fracture risk and strain on the bridging veins were both influenced by site of impact. The high stress on adjacent bones from a single impact focal to the sutures, suggest the potential for fracture on multiple cranial bones from a single point of impact. Whilst further research is required to validate fracture patterns, it highlights the potential for a bi-parietal fracture from a vertex impact.

## Glossary

**Abusive Head Trauma (AHT)**- An injury to the head where the mechanism is non accidental.

**Acceleration** -Rate of change of velocity over time.<sup>1</sup>

**Bilateral Skull Fracture** – Fracture of multiple cranial bones on the right and left aspects of head<sup>2</sup>.

**Bridging vein** –Veins that bleed from the cerebral hemispheres into the superior sagittal sinus<sup>3</sup>.

**Bulk Modulus** – Material property, ratio of pressure to volumetric strain.<sup>1</sup>

**Cerebral Oedema** –Accumulation of fluid on the brain<sup>3</sup>.

**Comminuted Skull Fracture** – Fracture in which bone is broken or crushed in a number of places<sup>2</sup>.

**Contracoup** – Injury opposite the site of impact beneath the skull<sup>4</sup>.

**Coup injury** – Injury direct beneath the skull at the site of impact.<sup>4</sup>

**Diffuse Axonal Injury (DAI)** – An injury that results in widespread lesions to the white matter as the result of shearing of axons due to rotation<sup>5</sup>.

**Depressed Skull Fracture** - A break in a cranial bone with an inward depression<sup>2</sup>.

**Diastatic fracture** – A fracture that involves widening of sutures<sup>2</sup>.

**Epidural Haematoma (EDH)** - A bleed in the space between the meningeal layer and the skull<sup>3</sup>.

**Extra axial haemorrhage** –A bleed outside the brain<sup>3</sup>.

**Falx cerebri** – Dura layer separates the left and right cerebral hemispheres<sup>3</sup>.

**Glasgow Coma Scale (GCS)** – Scale to measure the level of neurological dysfunction in three separate components; motor, verbal and eye opening responses.<sup>6</sup>

**Intracranial Injury (ICI)** An injury inside the cranial bones<sup>3</sup>.

**Linear Skull Fracture** – Single fracture of a single cranial bone<sup>2</sup>.

**Shear Modulus** – Material property, ratio of shear stress to shear strain<sup>1</sup>.

**Strain**- Elongation relative to its original length<sup>1</sup>.

**Stress** – Force per unit area<sup>1</sup>.

**Subarachnoid Haematoma (SAH)**- A bleed beneath the arachnoid meningeal layer<sup>3</sup>.



**Subdural Haematoma (SDH)** - A bleed in the space between the dura and arachnoid meningeal layer<sup>3</sup>.

**Tentorium Cerebellum** - Dura matter that separates the cerebellum from the occipital lobe<sup>3</sup>.

**Traumatic Brain Injury** - A nondegenerative, noncongenital insult to the brain from an external mechanical force, possibly leading to permanent or temporary impairment of cognitive, physical, and psychosocial functions, with an associated diminished or altered state of consciousness<sup>7</sup>.

**Velocity** - Rate of change of distance with time<sup>1</sup>.

**Viscoelastic** -Property of material that has both elastic and viscous characteristics<sup>1</sup>.

**Young Modulus** - Material property, ratio of stress to strain<sup>1</sup>.

## **References**

1. Rees DW. *Basic solid mechanics*: Macmillan; 1997.
2. Bilo RA, Robben SG, van Rijn RR. *Forensic aspects of paediatric fractures*: Springer; 2010.
3. Standring S. Gray's anatomy. *The anatomical basis of clinical practice*. 2008;3.
4. Drew LB, Drew WE. The contrecoup-coup phenomenon. *Neurocritical care*. 2004;1(3):385-390.
5. Smith DH, Meaney DF, Shull WH. Diffuse axonal injury in head trauma. *The Journal of head trauma rehabilitation*. 2003;18(4):307-316.
6. Teasdale G, Jennett B. Assessment of coma and impaired consciousness: a practical scale. *The Lancet*. 1974;304(7872):81-84.
7. Dawodu A. Traumatic Brain Injury (TBI)-Definition, Epidemiology, Pathophysiology. Medscape. 2013.

## Contents Page

<b>1</b>	<b>Chapter 1 – Introduction.....</b>	<b>21</b>
1.1	Introduction.....	22
1.1.1	Aims and objectives .....	24
1.1.2	Thesis overview.....	26
1.2	References.....	29
<b>2</b>	<b>Chapter 2 – Literature Review.....</b>	<b>32</b>
2.1	Epidemiology of Head Injuries Children .....	33
2.2	Head Injury Severity.....	33
2.3	Biomechanics of Head Injury .....	34
2.3.1	Mechanisms of Injury .....	35
2.3.2	Head Injury Thresholds.....	37
2.3.2.1	Translational Accelerations .....	37
2.3.2.2	Rotation Accelerations .....	40
2.3.3	Material Properties .....	41
2.3.3.1	Skull .....	42
2.3.3.2	Suture.....	44
2.3.3.3	Scalp .....	45
2.3.3.4	Cerebrospinal Fluid (CSF).....	46
2.3.3.5	Brain.....	46
2.3.3.6	Dura Matter .....	48
2.3.3.7	Bridging Veins .....	49
2.4	Key Area to Address From the Literature.....	51
2.5	References.....	54
<b>3</b>	<b>Chapter 3 - Clinical Assessment of Head Injuries in Young Children .....</b>	<b>59</b>
3.1	Introduction.....	60
3.1.1	Background .....	60
3.1.1.1	Low height fall.....	61
3.1.1.2	Definition of a low height fall.....	61
3.1.1.3	Biomechanical variables.....	62
3.1.1.4	Evaluations/Quality of history provided .....	63
3.1.1.5	Injury severity .....	63
3.1.2	Aims and Objectives.....	70
3.2	Method.....	71

3.2.1	Initial Study Design .....	71
3.2.2	Injury Severity Classification .....	71
3.2.3	Age classification.....	73
3.2.4	Inclusion / Exclusion Criteria .....	73
3.2.5	Ethical & Design Issues and Approvals .....	73
3.2.6	Head Injury Assessment Form Development .....	74
3.2.7	Biomechanical Variables.....	76
3.2.7.1	Documented Fall Height (H <sub>f</sub> ).....	76
3.2.7.2	Height of head centre of gravity (H <sub>HCoG</sub> ).....	77
3.2.7.3	Height of body centre of gravity (H <sub>BCoG</sub> ) .....	78
3.2.7.4	Estimated Fall Height (EFH) .....	78
3.2.7.5	Impact Velocity of the Body (V <sub>Body</sub> ).....	79
3.2.7.6	Impact Velocity of the Head (V <sub>Head</sub> ).....	79
3.2.7.7	Body impact momentum (M <sub>Body</sub> ) .....	80
3.2.7.8	Body kinetic energy (KE <sub>Body</sub> ) .....	80
3.2.7.9	Head impact momentum (M <sub>Head</sub> ) .....	81
3.2.7.10	Head kinetic energy (KE <sub>Head</sub> ) .....	81
3.2.8	Statistical Analysis.....	82
3.2.8.1	Sample Size Calculation .....	82
3.2.8.2	Comparison between categorical and continuous data .....	82
3.2.8.3	Injury Risk Curves.....	83
3.2.9	Nomenclature.....	85
3.3	Results.....	86
3.3.1.1	Clinical Data.....	87
3.3.1.2	Biomechanics of Injury .....	89
3.3.1.3	Injury risk probability .....	92
3.3.1.4	Skull fracture and / or ICI .....	95
3.3.1.5	Infant versus toddler .....	98
3.4	Discussion.....	103
3.4.1	Fall Height.....	103
3.4.2	Fall from carer's arms .....	104
3.4.3	Anatomical Site of Impact.....	104
3.4.4	Impact Surface .....	105
3.4.5	Biomechanical Variables.....	105

3.4.6	Child's Age .....	106
3.4.7	Implementation.....	107
3.4.8	Limitations .....	107
3.5	Conclusion.....	109
3.6	References.....	110
<b>4</b>	<b><i>Chapter 4 –Physical Modelling of Infant Head Impacts .....</i></b>	<b><i>114</i></b>
4.1	Introduction.....	115
4.1.1	Background .....	115
4.1.2	Aims and objectives .....	118
4.2	Materials and Method.....	120
4.2.1	Headform Design Methodology.....	120
4.2.1.1	Radiological Datasets.....	120
4.2.1.2	Headform Design and Development.....	121
4.2.2	Material Selection and Manufacture .....	126
4.2.2.1	Skin Friction .....	128
4.2.3	Experimental Procedure- Headform Validation .....	130
4.2.4	Experimental Protocol.....	130
4.2.5	Data Acquisition and Analysis .....	132
4.2.6	Statistical Analysis.....	133
4.2.7	Nomenclature.....	135
4.3	Results.....	136
4.3.1	Validation.....	136
4.3.2	Experimental Protocol.....	137
4.3.2.1	Friction .....	140
4.3.2.2	Peak Rotational Acceleration ( $\alpha_p$ ) .....	142
4.3.2.3	Peak change in rotational velocity ( $\Delta\omega$ ).....	147
4.3.2.4	Peak resultant linear accelerations (Peak $G_R$ ) .....	153
4.3.2.5	Resultant head injury criterion ( $HIC_R$ ) .....	157
4.3.2.6	Impact Duration ( $\Delta t$ ).....	161
4.4	Discussion.....	165
4.4.1	Impact Angle.....	165
4.4.2	Impact Velocity.....	166
4.4.3	Impact Surface .....	167
4.4.4	Skin Friction.....	168

4.4.5	Biomechanics of injury .....	169
4.4.6	Thresholds.....	170
4.4.6.1	Thresholds - Overview .....	170
4.4.6.2	Thresholds - Application .....	171
4.4.6.3	Thresholds – SDH/Bridging vein rupture.....	171
4.4.6.4	Thresholds – Skull fracture .....	174
4.4.7	Limitations .....	175
4.4.8	Implications .....	175
4.5	Conclusion.....	177
4.6	References.....	178

**181**

**5 Chapter 5 – Finite Element Analysis of Infant Head Impacts..... 181**

5.1	Introduction.....	182
5.1.1	Aims and objectives .....	188
5.2	Materials and Methods.....	191
5.2.1	Finite element model development and validation.....	191
5.2.1.1	Overview finite element modelling and image based meshing... 191	
5.2.1.2	FE Model Design and Development .....	193
5.2.1.3	Materials- Model Validation.....	198
5.2.1.4	Analysis Procedure.....	206
5.2.2	Parametric study.....	209
5.2.3	Overview .....	209
5.2.3.1	Skull .....	209
5.2.3.2	Scalp .....	213
5.2.3.3	Dura .....	213
5.2.3.4	Brain.....	213
5.2.3.5	Interactions .....	215
5.2.3.6	Bridging vein.....	215
5.2.3.7	Impact scenarios, output variables and statistical comparisons 217	
5.2.4	Assessment of key clinical features (Height and anatomical site of impact).....	220
5.2.4.1	Impact Scenarios .....	220
5.2.4.2	Statistical Comparisons .....	221
5.2.5	Nomenclature.....	222

5.3	Results.....	223
5.3.1	Validation.....	223
5.3.2	Parametric Analysis.....	226
5.3.2.1	Skull Stiffness.....	226
5.3.2.2	Scalp Stiffness.....	228
5.3.2.3	Membrane Stiffness.....	228
5.3.2.4	Bulk Modulus.....	229
5.3.2.5	Brain Stiffness.....	229
5.3.2.6	Interactions.....	229
5.3.2.7	Bridging Veins.....	229
5.3.3	Assessment of key clinical features using validated FE model.....	230
5.3.3.1	Peak G.....	230
5.3.3.2	HIC.....	232
5.3.3.3	Duration of impact.....	234
5.3.3.4	Rotational acceleration.....	234
5.3.3.5	Peak change in rotational velocity ( $\Delta\omega$ ).....	238
5.3.3.6	Head deformation.....	238
5.3.3.7	Maximum principle stress of the bone.....	243
5.3.3.8	Bridging Veins.....	250
5.4	Discussion.....	256
5.4.1	Validation.....	256
5.4.2	Parametric Analysis.....	257
5.4.2.1	Skull Stiffness.....	258
5.4.2.2	Scalp Stiffness.....	259
5.4.2.3	Membrane Stiffness.....	260
5.4.2.4	Bulk Modulus of the Brain.....	260
5.4.2.5	Brain Stiffness.....	260
5.4.2.6	Bridging Veins.....	261
5.4.3	Assessment of key clinical features.....	263
5.4.3.1	Height.....	263
5.4.3.2	Site of impact.....	263
5.4.4	Deformation.....	266
5.4.5	Threshold.....	267
5.4.5.1	Skull fracture.....	267

5.4.5.2	Bridging vein rupture .....	270
5.4.6	Limitations .....	274
5.4.7	Implications .....	274
5.5	Conclusion .....	276
5.6	References .....	278
<b>6</b>	<b><i>Chapter 6 – Final Conclusions.....</i></b>	<b>282</b>
6.1	Final Conclusions.....	283
6.1.1	Key findings.....	283
6.1.1.1	Clinical .....	283
6.1.1.2	Biomechanical .....	284
6.1.2	Future Research .....	285
6.1.3	Implications .....	286
6.2	References .....	288
<b>7</b>	<b><i>Chapter 7 – Appendices .....</i></b>	<b>289</b>
7.1	Appendix 1 .....	290
7.2	Appendix 2 .....	292
7.3	Appendix 3 .....	297
7.4	Appendix 4 .....	299
7.5	Appendix 5 .....	308
7.6	Appendix 6 .....	310
7.7	References .....	321

## List of Figures

Figure 1. Skull deformation on impact with a surface. ....	35
Figure 2. Translation acceleration on impact with a surface (A), pressure gradient formed on intracranial soft tissues due to a translational impact (B), rotational acceleration induced on the head (C). ....	36
Figure 3. Workflow for development of the Head Injury Assessment form from its initial design through to the final design. Emergency Department (ED).....	75
Figure 4. Heights assessed to differentiate head injury severity. ....	77
Figure 5. Exponential curve fit to calculate head mass based on the characteristic length. Graph recreated from Loyd et al <sup>52</sup> in order to develop an equation that related head mass to the characteristic length. ....	81
Figure 6. Child head injury cases from the prospective and retrospective data collection. ....	86
Figure 7. Injury risk curves developed and assessed for the height of the head centre of gravity ( $H_{HCoG}$ ). ....	93
Figure 8. Height of centre of gravity of the head $H_{HCoG}$ for minor head injury, skull fracture or ICI (Intracranial Injury) resulting from falls in children $\leq 48$ months of age.....	94
Figure 9. Logistic regression curve illustrating the probability (with 5 <sup>th</sup> and 95 <sup>th</sup> percentile values) of sustaining a skull fracture or ICI (Intracranial Injury), based on the height of head centre of gravity $H_{HCoG}$ for the range of heights reported. ....	95
Figure 10. Threshold filter applied to the CT dataset and image then aligned with Frankfurt plane. ....	124
Figure 11. Development of the antropomorphic test device through image processing of a 5 week old male CT dataset. ....	124
Figure 12. Final design of the headform. Frontal view of the headform (A). coronal view, illustrating occipital plate fixed and positioned to basal section (B), Side view, illustrating the positioning of the occipital plate(C), (D) Image of inside of the headform. ....	126
Figure 13. Comparison between the Infant headform design (A) and the manufactured headform (B) .....	128
Figure 14. Manufacturing stages of the headform from the output of the selective laser-sintering machine to the headform used for impact testing .....	128
Figure 15. Apparatus set up for 60cm fall onto wood for a 90deg impact.....	131



Figure 16. Spectral analysis, used to determine cut off frequency for filter.....	133
Figure 17. Acceleration vs time graphs for 30cm impacts on the forehead (A), vertex (B), occiput (C), right parietal (D) comparing the experimental results with those of Prange et al <sup>8</sup> . Blue line with error bars refer to response corridors from Prange et al <sup>8</sup> and red line is the infant headform response.....	137
Figure 18. Headform deformation on impact from 60cm drop onto laminate, (A) prior to Impact, (B) 4ms post impact, (C) 8ms post impact and (D) 12 ms post impact.....	138
Figure 19. Acceleration output from the rotational accelerometer and the x, y and z axis of the translational accelerometer. Output from the rotational accelerometer, illustrating the acceleration and deceleration phase (A). Output from the Z axis of the translational accelerometer, illustrating how the headform decelerates on impact (B). Output from the y axis of the translational accelerometer (C). Output from the x axis of the translational accelerometer (D).....	139
Figure 20. The effect that changing impact velocity and impact surface has on peak rotational acceleration at a 90 degree impact angle. Error bars equal standard of error.....	145
Figure 21. The effect that changing impact velocity and impact surface has on peak rotational acceleration at a 75 degree impact angle. Error bars equal standard of error.....	146
Figure 22. The effect that changing impact velocity and impact surface has on peak rotational acceleration at a 60 degree impact angle. Error bars equal standard of error.....	146
Figure 23. Rotational acceleration versus rotation velocity with varying impact surface and impact velocity at a 90 degree impact angle. Dotted lines indicate bridging vein rupture thresholds.....	150
Figure 24. Rotational acceleration versus rotation velocity with varying impact surface and impact velocity at a 75 degree impact angle. Dotted lines indicate bridging vein rupture thresholds.....	151
Figure 25. Rotational acceleration versus rotation velocity with varying impact surface and impact velocity at a 60 degree impact angle. Dotted lines indicate bridging vein rupture thresholds.....	152

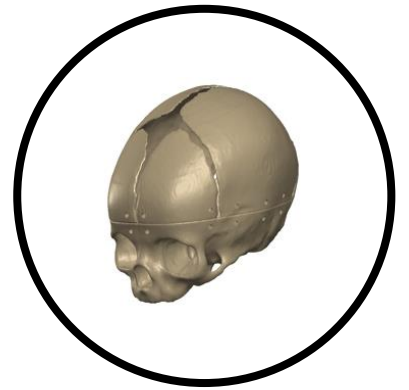
Figure 26. Peak translational acceleration variation with changing impact velocity and impact surface at a 90 degree angle of impact. Dotted lines refer to head injury thresholds in children $\leq 12$ months. ....	155
Figure 27. Peak translational acceleration variation with changing impact velocity and impact surface at a 75 degree angle of impact. Dotted lines refer to head injury thresholds in children $\leq 12$ months. ....	156
Figure 28. Peak translational acceleration variation with changing impact velocity and impact surface at a 90 degree angle of impact. Dotted lines refer to head injury thresholds in children $\leq 12$ months. Error bars equal standard of error. ....	156
Figure 29. Head Injury Criterion (HIC) variation with changing impact velocity and impact surface for a 90 degree angle of impact. Dotted lines refer to skull fracture thresholds in children $\leq 12$ months. ....	160
Figure 30. Resultant Head Injury Criterion (HIC) variation with changing impact velocity and impact surface for a 75 degree angle of impact. Dotted lines refer to skull fracture thresholds in children $\leq 12$ months. ....	160
Figure 31. Resultant Head Injury Criterion (HIC) variation with changing impact velocity and impact surface for a 75 degree angle of impact. Dotted lines refer to skull fracture thresholds in children $\leq 12$ months. ....	161
Figure 32. Element types. Hexahedral element with mid sides nodes (A), Tetrahedral element with mid sided nodes (B).....	193
Figure 33. Masks generated of the skull, suture, meningeal layers, and brain for the meshing procedure. ....	195
Figure 34. Flow diagram for the meshing procedure for the finite element model. ....	196
Figure 35. The error in the peak force compared to densest mesh. ....	198
Figure 36. Connectors used to model bridging veins inserted into model. Connector 1 is most posterior and 10 is most anterior. ....	205
Figure 37. Connectors inserted into in a posterior facing direction. ....	216
Figure 38. Impact locations used in finite element analysis. A vertex impact with an arrow illustrating superior-inferior (SI) measurements (A), a frontal impact with an arrow illustrating anterior-posterior (AP) measurement (B), a parietal impact with an arrow illustrating the left-right (LR) measurement (C), an occipital impact (D), a fronto-parietal impact with an arrow illustrating a distal-floor (DF)	

measurement (E), a parieto-occipital measurement (F), A-Anterior of head, P – Posterior of head.....	219
Figure 39. Comparison of compression at rate of 50mm/s in anterior-posterior (AP) and left-right (LR) direction between model B4 and the cadaver head used by Prange et al <sup>16</sup> .....	226
Figure 40. Variation of peak G with changing height and location of impact. ....	232
Figure 41. Variation of HIC with changing height and site of impact.....	233
Figure 42. Variation in duration of impact between fall height and site of impact. ....	234
Figure 43. Peak rotational acceleration in the sagittal, coronal and axial planes for an occipital impact, .....	235
Figure 44. Peak rotational accelerations versus peak change in rotational velocities for all fall heights and sites of impact investigated. ....	237
Figure 45. Estimation of headform deformation using the high-speed video from 0.6m fall onto wood. Prior to impact to impact no head deformation (A), 10.5mm deformation at 4ms post impact (B), 15.5mm deformation at 7ms post impact (C), 14.4mm deformation 10ms post impact (D). ....	239
Figure 46. Vertex impact for a 0.6m fall height with the FE model. Prior to impact to impact no head deformation (A), 11.6mm deformation at 4ms post impact (B), 12.9mm deformation at 7ms post impact (C), 8.5mm deformation 10ms post impact (D).....	240
Figure 47. Comparison of deformation between the finite element model (FE) and the anthropomorphic testing device (ATD). ....	241
Figure 48. Example of impact response from an 0.6m occipital impact. Anterior-posterior (AP), left-right (LR), superior-inferior (SI).....	241
Figure 49. Strain in anterior-posterior (AP), superior-inferior (SI) and left-right (LR) directions for all occipital impacts.....	242
Figure 50. Peak head strain for all sites of impact across all fall heights investigated.....	243
Figure 51. Correlation between maximum principle stress values and peak G (A), correlation between maximum principle stress and HIC (B). ....	246
Figure 52. Stress zones (blue) in excess ultimate stress for 0.82cm parieto-occipital impact. View from left parieto-occipital area, looking from posterior left to anterior right.....	249

Figure 53. A 1.2m fall onto vertex illustrating stress zones in excess of bone ultimate stress values. Intracranial view of skull in an inferior superior direction .....	250
Figure 54. A 1.2m fall onto parietal area illustrating stress zones in excess of bone ultimate stress values. Intracranial view from right to left.....	250
Figure 55. Stretch ratio versus time for the left sides connectors for a 0.6m vertex impact.....	251
Figure 56. Peak stretch ratio for each fall height and site of impact.....	253
Figure 57. Correlation between peak rotational acceleration and peak stretch ratio (A), correlation between peak rotational change in rotational velocity and peak stretch ratio (B).....	255

---

# Chapter 1 – Introduction



## 1.1 Introduction

Head injuries in young children as the result of a low height fall represent a challenging issue for clinicians, biomechanical engineers and medico-legal experts. The developmental nature of infants and young children, increasing mobility combined with underdeveloped muscles and reflexes, means that head injuries as the result of a fall are a common occurrence in most households<sup>1</sup>. However the majority of such incidents are thought to be benign, with only 4.8 % leading to hospital attendance and <1% of falls resulting in either a concussion or skull fracture in infants<sup>1</sup>. Despite this, Parslow *et al*<sup>2</sup> concluded that the most common cause of traumatic brain injury (TBI) in the 0-4 age group was a fall (38%). However, investigating only infants (age <1 years old), falls only accounted for 19% of the TBI cases with the most common cause of TBI being suspected assault (52%)<sup>2</sup>. The percentage of children hospitalised with abusive head trauma (AHT) varies with age, however studies have estimated the frequency as being between 25-30%<sup>3</sup>. Due to this, clinicians are faced with the dilemma of trying to differentiate head injuries that have resulted from abuse and those that have not, particularly for this age group, when the child is unable to give a history themselves. A fall is an incident that further confounds the problem, as whilst it is a common cause of head injuries presenting to hospital, it is also a common false account given by parents/carers later suspected of abuse<sup>4-7</sup>. As a result researchers from differing professional backgrounds, clinical, legal and engineering, have attempted to establish what injuries could result from a low height fall. This thesis utilises both a clinical and biomechanical approach to investigate head injuries resulting from a low height fall in infants and young children.

There is no strict definition of a low height fall. Original research conducted by Helfer *et al*<sup>8</sup> investigated children < 5years old who had fallen from a bed or sofa and used a cut off of <0.91m. Since then it has variably been defined, with authors using cut off heights of 0.91m<sup>9,10</sup>, 1m<sup>11</sup>, 1.22m<sup>4,7,12,13</sup> and 1.52m<sup>14</sup>. Previous authors have also document mean heights for moderate/serious head injury when

comparing head injury severity groupings<sup>15-17</sup>. Mean heights have been reported between 0.91m<sup>10, 15</sup> and 1.32m<sup>17</sup>. A low height fall is an incident that is further confounded by there being no clear classification criteria. Consequently there has been variation in the calculated height ranging from the height of the surface fallen from<sup>10, 18</sup> to the height of the head relative to the impacted surface<sup>5, 19</sup>, the classification of incidents where for example a fall from a carers arms has been defined from >0.91m<sup>10</sup> to >1.22m<sup>5</sup>, and also whether a consideration should be made for the accuracy of the height estimated by the carer<sup>19</sup>. Due to all these factors it is difficult to establish a clear cut off for a low height fall and thereby making it problematic to define head injuries that can result from such incidents.

The controversy surrounding low height fall is mainly attributed to it being a common false history provided by parents suspected of child abuse<sup>4-7</sup>. Chadwick *et al*<sup>4</sup> documented 7 fatal head injury cases with an initial history of a low height fall which the authors later attributed to abuse. Of which, 2 were the result of standing fall, 2 were a fall from a bed or table and 2 were the result of fall from an adults arms. Tarantino *et al*<sup>7</sup> documented 2 cases of children admitted after rolling off a couch, however both cases were later deemed to have been abused. Duhaime *et al*<sup>5</sup> investigated the mechanisms of head injury in children <2 years old, and there were 24 cases classed as an inflicted injury. Of these cases, 8 had history of fall <1.22m, which the authors defined as fall from a standing height, or fall from a bed, sofa or table. Feldman *et al*<sup>6</sup> investigated the mechanisms of a subdural haemorrhage (SDH) and in the abuse group, 41% (n=16/39) presented with a history of a fall <1.22m. This therefore illustrates a low height fall is a common false history given by parents suspected of abuse, and in particular a fall from household furniture or a standing height. A history low height fall is further confounded by previous biomechanical studies using an anthropomorphic testing device (ATD) reporting similar or greater accelerations as the result of fall to that seen in shaking<sup>20, 21</sup>, a common mechanism with or without impact associated with abuse<sup>5, 21, 22</sup>. However the biofidelity of the ATDs<sup>22, 23</sup> and the head injury thresholds used have been question by other authors<sup>22-26</sup>.

Differentiating between an accident and child abuse remains challenging regardless of the hypothesised mechanism of abuse. The plausibility of head injuries typically associated with abuse, including multiple SDH over the convexity, interhemispheric haemorrhages, posterior fossa SDH, hypoxic-ischaemic injury and cerebral oedema<sup>3</sup> resulting from a low height fall remains debatable. Likewise, the possibility of certain injuries such as a complex skull fracture resulting from a single impact remain in question. Different approaches have been taken, with the aim of defining the injuries that can result from a low height fall, despite its lack of an explicit definition. A clinical perspective has been to define injuries associated with a low height fall, with some authors only documenting a simple skull fracture<sup>8, 27</sup>, others highlighting the possibility of an intracranial injury (ICI)<sup>5, 9-11, 13, 15, 17, 19, 28, 29</sup> or death<sup>4, 30-32</sup>. Despite this research, there remains no clear threshold in terms of height for the different forms of head injury. Biomechanical investigations have included developing testing devices, both physical<sup>21, 23, 33, 34</sup> and computational<sup>33, 35-39</sup>, in order to develop and assess thresholds for head injury in terms of translation and rotational accelerations. Whilst previous models have been developed, few have been validated with human cadavers<sup>34, 37, 38</sup> and then used to assess biomechanical thresholds against injuries commonly seen in a clinical setting.

### 1.1.1 Aims and objectives

This thesis therefore aims to further the understanding of the biomechanics of head injuries in young children, in particular infants, as the result of a low height fall. A unique approach was adopted in order to complete this assessment. Head injuries as the result of a fall in young children ( $\leq 48$  months) were assessed from a clinical setting such that differentiating features could be developed (both clinical and biomechanical) between minor head trauma and those resulting in skull fracture and/or intracranial injury (ICI). The aim of this phase was to develop a clinical threshold, which could be analysed using biomechanical tools, including both physical and computational modelling, in order to evaluate current biomechanical thresholds for skull and intracranial injuries. Therefore this thesis



is split into four areas, literature review, clinical assessment of head injuries as the result of a low height fall, physical modelling of head impacts and finite element analysis of head impacts. An overview of the aim of each chapter is outlined below:

- Literature review (Chapter 2)

Assess the previous literature on the epidemiology of head injuries in young children. Review current debated mechanisms on the biomechanics of head injuries with an aim of evaluating current thresholds aimed at young children. Evaluate material properties of infant cranial bone and soft tissues of the head to inform the development of the physical and computational model of the head.

- Clinical assessment of head injuries as the results of a low height fall (Chapter 3)

Review the clinical literature on low height falls in order to determine the head injuries that have been reported from this particular incident.

Conduct a case control study between children aged  $\leq 48$  months with a minor head injury and those with a skull fracture and/or ICI as the result of a low height fall. The primary aim of which was to establish a threshold in terms of fall height for skull and/or ICI. The secondary aims of were to develop differentiating clinical and biomechanical features between the two injury groupings.

- Physical modelling of head impact (Chapter 4)

Review the literature on previous young child testing dummies developed and used to investigate kinematic response of the head on impact from a low height fall. Develop an anthropomorphic testing device (ATD) of an infant head that was validated against human infant cadaver data. Then use the ATD to investigate key differentiating features from Chapter 3, with an aim of assessing current biomechanical thresholds against the clinical threshold.

- Finite element modelling of head impacts (Chapter 5)

Review literature on finite element models developed of an infant head and used to investigate the impact response from a low height fall. Develop a finite element model of an infant head that was validated against human cadaver

data. Again use the FE model of an infant head to investigate key differentiating features from Chapter 3 and further evaluate biomechanical thresholds against the clinical threshold. Also investigate how the dynamic response of an infant head may potentially make it more or less susceptible to different forms of traumatic head injury.

### 1.1.2 Thesis overview

An overview of the results and conclusions from each section is outlined below.

- Literature review (Chapter 2)

Biomechanical threshold for skull fracture relevant to children exist but they have not been assessed against injuries seen in a clinical setting. Thresholds for bridging vein rupture exist for adults, although a correct method for scaling to infants and young children has yet to be established. Material properties exist for the human infant cranial bone, sutures and bridging veins, but not for other soft tissues of the head, including the meningeal layers, brain and the scalp.

- Clinical assessment of head injuries as the results of a low height fall (Chapter 3)

A review of head injuries in young children as the result of a fall deduced that whilst uncommon, injuries including a SDH, subarachnoid haemorrhage (SAH), epidural haemorrhage (EDH), complex fracture and simple fracture have been reported from heights classed within a low fall height range. Although there does not exist a clear cut off in terms of height for each injury. A prospective study of minor head injury yielded 416 cases and a retrospective review of injuries including skull fracture and/or ICI produced 47 cases. Skull fracture and/or ICI was significantly associated with an increase fall height, age (infants  $\leq 12$  months), anatomical site of impact (parietal/temporal, occipital area) and surface impacted (wood). No cases of skull fracture and/or ICI occurred below a fall height of 0.6m, based on the height of centre of gravity of the head.

- Physical modelling of head impact (Chapter 4)

Previous authors have developed ATDs aimed at young children and infants, yet few have been validated against cadaver data. An infant headform was

designed from image processing of CT images and manufactured using additive layer technologies with biofidelic materials. The impact response of the headform was validated against infant human cadaver data and subsequently used to measure the affect of impact velocity (corresponding to fall height), impact angle, skin friction and impact surface have on the dynamic response of the head on impact. A decrease in impact angle increased rotational output variables and an increase in impact velocity increased both rotational and translation output variables. An increase in surface stiffness also increased rotational and translation output variables but the affect varied with impact velocity and angle. Only sub injurious fall heights were investigated ( $\leq 0.6\text{m}$ ), thereby allowing current biomechanical thresholds to be assessed. Few thresholds were substantiated by the clinical data, with exception of the current National Highway Transport Safety Administration (NHTSA) standard<sup>40</sup>.

- Finite element modelling of head impacts (Chapter 5)

Finite element models of infant head have been developed and some have been validated against cadaver data<sup>37, 38</sup>. However few have investigated a range of fall scenarios with the aim of establishing a threshold for head injury.

A finite element model of an infant head was designed using image based meshing from CT images of a 19-day-old infant. Initially four different FE models were developed and assessed against validation output variables. The model utilising optimised material properties<sup>36</sup> had the most similar dynamic response to human infant cadaver heads and was classed as validated. A parametric test of material properties was conducted across a range of impact scenarios. Skull stiffness was shown to have the greatest affect in the dynamic response of the FE model. Post completing the parametric test, the model was used to assess two of the key clinical differentiating features, height and anatomical site of impact. Height increased kinematic output variables. The mean value of peak G and HIC at the clinically defined threshold of 0.6m fall height was 85g and 284 respectively. Both these values correlated well with infant biomechanical skull fracture thresholds<sup>34, 40</sup>, although there were still

differences in the level of risk. Anatomical site of impact affected kinematic output variables and material failure properties. An occipital impact had the greatest risk of fracture and an impact focal to a suture indicated possibility of fracture in adjacent bones. The greatest strains on the bridging veins in the model were at impacts focal to the veins and at the least stiff aspects of the head, although they did not exceed previously reported failure values for the heights investigated ( $\leq 1.2\text{m}$ ).

**1.2 References**

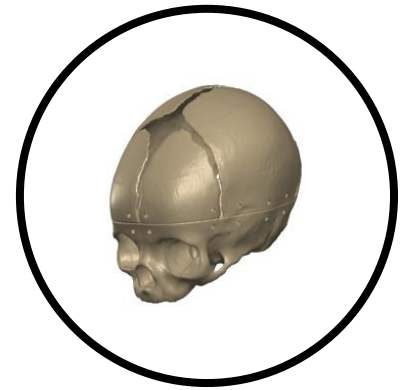
1. Warrington SA, Wright CM, Team AS. Accidents and resulting injuries in premobile infants: data from the ALSPAC study. *Archives of Disease in Childhood*. 2001;85(2):104-107.
2. Parslow RC, Morris KP, Tasker RC, Forsyth RJ, Hawley CA. Epidemiology of traumatic brain injury in children receiving intensive care in the UK. *Archives of Disease in Childhood*. 2005;90(11):1182-1187.
3. Kemp A, Jaspan T, Griffiths J, Stoodley N, Mann M, Tempest V, et al. Neuroimaging: what neuroradiological features distinguish abusive from non-abusive head trauma? A systematic review. *Archives of disease in childhood*. 2011;96(12):1103-1112.
4. Chadwick DL, Chin S, Salerno C, Landsverk J, Kitchen L. Deaths from Falls in Children: How Far is Fatal? *The Journal of Trauma*. 1991;31(10):1353-1355.
5. Duhaime AC, Alario AJ, Lewander WJ, Schut L, Sutton LN, Seidl TS, et al. Head injury in very young children: mechanisms, injury types, and ophthalmologic findings in 100 hospitalized patients younger than 2 years of age. *Pediatrics*. 1992;90(2):179.
6. Feldman KW, Bethel R, Shugerman RP, Grossman DC, Grady MS, Ellenbogen RG. The cause of infant and toddler subdural hemorrhage: a prospective study. *Pediatrics*. 2001;108(3):636.
7. Tarantino CA, Dowd MD, Murdock TC. Short vertical falls in infants. *Pediatric emergency care*. 1999;15(1):5.
8. Helfer RE, Slovis TL, Black M. Injuries Resulting When Small Children Fall Out of Bed. *Pediatrics*. 1977;60(4):533-535.
9. Hettler J, Greenes DS. Can the initial history predict whether a child with a head injury has been abused? *Pediatrics*. 2003;111(3):602-607.
10. Ibrahim NG, Wood J, Margulies SS, Christian CW. Influence of age and fall type on head injuries in infants and toddlers. *International Journal of Developmental Neuroscience*. 2011.
11. Park SH, Cho BM, Oh SM. Head injuries from falls in preschool children. *Yonsei Medical Journal*. 2004;45:229-232.
12. Duhaime A, Margulies S, Durham S, O'Rourke M, Golden J, Marwaha S, et al. Maturation-dependent response of the piglet brain to scaled cortical impact. *Journal of Neurosurgery: Pediatrics*. 2000;93(3).
13. Reece RM, Sege R. Childhood Head Injuries: Accidental or Inflicted? *Arch Pediatr Adolesc Med*. 2000;154(1):11-15.
14. Williams RA. Injuries in Infants and Small Children Resulting from Witnessed and Corroborated Free Falls. *The Journal of Trauma*. 1991;31(10):1350-1352.
15. Claudet I, Gurrera E, Honorat R, Rekhroukh H, Casasoprana A, Grouteau E. [Home falls in infants before walking acquisition]. *Archives de pediatrie: organe officiel de la Societe francaise de pediatrie*. 2013;20(5):484-491.
16. Thompson AK, Bertocci GE. Paediatric bed fall computer simulation model development and validation. *Computer methods in biomechanics and biomedical engineering*. 2011(ahead-of-print):1-10.

17. Thomas AG, Hegde SV, Dineen RA, Jaspán T. Patterns of accidental craniocerebral injury occurring in early childhood. *Archives of disease in childhood*. 2013;98(10):787-792.
18. IDB. The Injury Database (IDB) version 1.1: Consumer Safety Institute. Amsterdam and AIHW National Injury Surveillance Unit, Adelaide; 2005.
19. Thompson AK, Bertocci G, Rice W, Pierce MC. Pediatric short-distance household falls: Biomechanics and associated injury severity. *Accident Analysis and Prevention*. 2011;43(1):143-150.
20. Duhaime A-C, Gennarelli TA, Thibault LE, Bruce DA, Margulies SS, Wiser R. The shaken baby syndrome: a clinical, pathological, and biomechanical study. *Journal of neurosurgery*. 1987;66(3):409-415.
21. Prange M, Coats B, Duhaime A, Margulies S. Anthropomorphic simulations of falls, shakes, and inflicted impacts in infants. *Journal of Neurosurgery: Pediatrics*. 2003;99(1).
22. Cory C, Jones M. Can shaking alone cause fatal brain injury? A biomechanical assessment of the Duhaime shaken baby syndrome model. *Medicine, science and the law*. 2003;43(4):317-333.
23. Coats B, Margulies S. Potential for head injuries in infants from low-height falls. *Journal of Neurosurgery: Pediatrics*. 2008;2(5):321-330.
24. Morrison N. The Dynamics of Shaken Baby Syndrome: The University of Birmingham; 2002.
25. Thibault KL, Margulies SS. Age-dependent material properties of the porcine cerebrum: effect on pediatric inertial head injury criteria. *Journal of Biomechanics*. 1998;31(12):1119-1126.
26. Prange MT, Kiralyfalvi G, Margulies SS. Pediatric rotational inertial brain injury: the relative influence of brain size and mechanical properties. Stapp Car Crash Conference Proceedings; 1999.
27. Lyons TJ, Oates RK. Falling out of Bed: A Relatively Benign Occurrence. *Pediatrics*. 1993;92(1):125-127.
28. Schutzman SA, Barnes PD, Mantello M, Scott RM. Epidural hematomas in children. *Annals of emergency medicine*. 1993;22(3):535-541.
29. Chiesa A, Duhaime AC. Abusive head trauma. *Pediatric clinics of North America*. 2009;56(2):317-331.
30. Chadwick DL, Bertocci G, Castillo E, Frasier L, Guenther E, Hansen K, et al. Annual Risk of Death Resulting From Short Falls Among Young Children: Less Than 1 in 1 Million. *Pediatrics*. 2008;121(6):1213-1224.
31. Hall JR, Reyes HM, Horvat M, Meller JL, Stein R. The mortality of childhood falls. *The Journal of Trauma*. 1989;29(9):1273.
32. Plunkett J. Fatal pediatric head injuries caused by short-distance falls. *The American Journal of Forensic Medicine and Pathology*. 2001;22(1):1.
33. Klinich K, Hulbert G, Schneider L. Estimating infant head injury criteria and impact response using crash reconstruction and finite element modeling. *Stapp car crash journal*. 2002;46:165.
34. Van Ee C, Moroski-Browne B, Raymond D, Thibault K, Hardy W, Plunkett J. Evaluation and refinement of the CRABI-6 anthropomorphic test device injury criteria for skull fracture. 2009: ASME.

35. Coats B, Ji S, Margulies S. Parametric study of head impact in the infant. *Stapp Car Crash J.* 2007;51:1-15.
36. Li Z, Hu J, Reed MP, Rupp JD, Hoff CN, Zhang J, et al. Development, Validation, and Application of a Parametric Pediatric Head Finite Element Model for Impact Simulations. *Annals of Biomedical Engineering.* 2011:1-14.
37. Li Z, Luo X, Zhang J. Development/global validation of a 6-month-old pediatric head finite element model and application in investigation of drop-induced infant head injury. *Computer methods and programs in biomedicine.* 2013;112(3):309-319.
38. Roth S, Raul JS, Willinger R. Finite element modelling of paediatric head impact: Global validation against experimental data. *Computer methods and programs in biomedicine.* 2010;99(1):25-33.
39. Roth S, Vappou J, Raul J, Willinger R. Child head injury criteria investigation through numerical simulation of real world trauma. *Computer methods and programs in biomedicine.* 2009;93(1):32-45.
40. Eppinger R, Sun E, Bandak F, Haffner M, Khaewpong N, Maltese M, et al. Development of improved injury criteria for the assessment of advanced automotive restraint systems–II. *National Highway Traffic Safety Administration.* 1999.

---

Chapter 2 – Literature  
Review





## **2.1 Epidemiology of Head Injuries Children**

Traumatic brain injury (TBI) is significant problem worldwide, the World Health Organisation estimates incidence rates of mild TBI between 100-300 per 100,000<sup>1</sup>. However the rates have been shown to vary between countries, age, gender and definition of TBI<sup>2,3</sup>. Hawley *et al*<sup>4</sup> investigated minor head injury (GCS 13-15) in the paediatric population, and concluded annual rates of 5,099 per 100,000 in the 0-4 year age group. In the USA, the 0-4 year age group has the highest emergency department (ED) incident rate of TBI, estimated at 1,256.2 per 100,000<sup>5</sup>. Hawley *et al*<sup>6</sup> concluded that 280 per 100,000 children (<16 years old) were admitted with TBI each year. A small, but significant, minority of these warrant admission to Intensive Care with TBI, 5.1/100,000. Previous authors have documented a rate of 5.1 per 100,00 of children (0-4 years) admitted to an intensive care unit with TBI<sup>7</sup>.

The severity of the head injury also varies depending on the mechanism of the injury. Among minor head injuries, a fall is the most commonly recorded mechanism in those aged < 1 year (69.4%) and those aged 2-4 years (62.7%)<sup>4</sup>. Investigating children admitted to a paediatric intensive care unit, a fall was the commonest cause of TBI in the 0-4 age group (38%)<sup>7</sup>.

## **2.2 Head Injury Severity**

There is no international classification of head injury severity, therefore it varies between countries, clinicians and journal article authors, which makes it difficult when comparing studies. Severity can be measured according to the presenting neurological status, neurological outcome, mechanism or the extent of primary structural damage as evidenced on neuroimaging<sup>8</sup>. Different authors utilise a different category when evaluating head injury severity.

A classification system for neurological status is based on the Glasgow Coma Score<sup>9</sup>(GCS). The GCS was devised by Teasdale and Jennett<sup>10</sup> and modified in 1976<sup>11</sup> to assess the extent of coma after trauma. It identifies the level of

neurological dysfunction in three separate components; motor, verbal and eye opening responses. Scores from each component are considered separately and combined to form an overall GCS score ranging from a total score of 3-15. In the UK, GCS has been subcategorised into minor/mild (GCS of 13-15), moderate (GCS of 9-12) and severe (GCS <9)<sup>9</sup>.

However despite this, authors have used different methods when evaluating head injury severity particularly from a low height fall, with some documenting specific structural damage as identified on neuroimaging such as skull fracture<sup>12</sup> or a SDH<sup>13</sup> and others using a defined scale such as minor versus serious<sup>14, 15</sup>. This will be discussed further in the clinical literature review section of this thesis (Section 3.1.1.5). When authors categorise severity groups such as minor versus serious, the definitions are as per the authors definition and are outlined in Appendix 4. In this thesis, as will be discussed in Section 3.2.2, minor head injury was differentiated from injuries that have resulted in structural damage that could be seen on computed tomography (CT) imaging, including skull fracture and the different forms of structural ICI (SDH, EDH, SAH etc). This was because an aim of this thesis was to evaluate head injuries seen clinically with current biomechanical thresholds for skull fracture and bridging vein rupture, however this will be discussed further in Chapter 3.

### **2.3 Biomechanics of Head Injury**

The application of engineering methods to the understanding of injuries in the human body was first pioneered in the automotive industry. The work by John Stapp in the 1950s progressed the understanding of tolerance levels of the human body and thus furthered the knowledge of crash protection<sup>16</sup>. Since this original work, the field of biomechanics has focussed on understanding the mechanical response of the body when exposed to an applied load to appreciate the factors that causes head injury and to improve safety.

### 2.3.1 Mechanisms of Injury

A comprehensive overview of the mechanisms of head injury has been outlined by previous authors<sup>17-19</sup>, but a general description is outlined below. The biomechanics of head injury has historically been split into two main areas, translation accelerations as the result of direct impact and rotational accelerations as a consequence of an indirect load such as an impact to the thorax producing whiplash on the head. Yet as it has been described by others, rarely would translation and rotational accelerations be seen in isolation, from either a direct or indirect impact to the head<sup>17</sup>. Upon impact with an object, the head would deform and decelerate, thereby resulting in translational acceleration. Severe translation accelerations have been found to correlate with focal injuries including skull fracture and local brain contusion<sup>20</sup>, although they have also been linked with contracoup injuries<sup>21</sup>.

On impact with a flat surface, the skull deforms, bending inwards and produces a wave like pattern (Figure 1). This results in tension on the inner surface and also on the outer surface of skull, as depicted in Figure 1. The fracture can initiate at the inner surface that is under tension and thus propagates towards the outer surface (Figure 1)<sup>22</sup>. Fracture can also initial on the outer surface in areas of tension<sup>22</sup>.

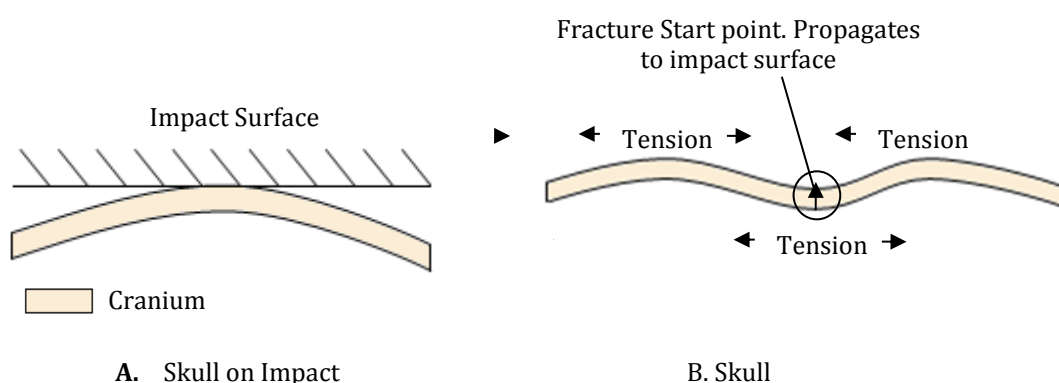
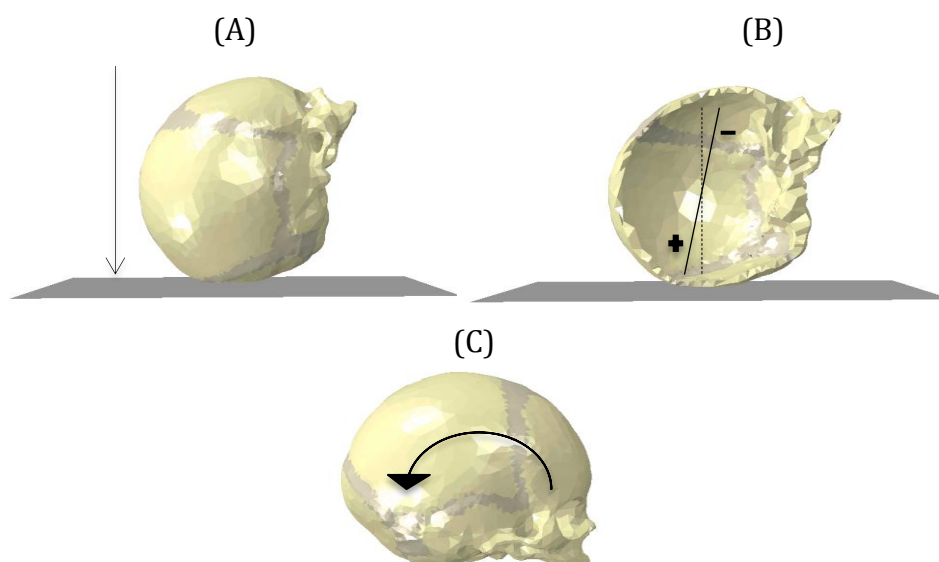


Figure 1. Skull deformation on impact with a surface.

Intracranial damage was generally thought to occur as a consequence of skull deformation from a translational impact, which can lead to brain motion and thus

potentially causing a focal haematoma<sup>23</sup>. Other authors have proposed that such injury may also be caused as a consequence of a pressure gradient established during translational impact<sup>24-26</sup>. At the site of impact, the focal intracranial tissues would be exposed to a positive pressure and, due to motion of brain, locations distal to the impact site would be exposed to negative pressure<sup>18</sup> (Figure 2). It has been suggested that this pressure gradient subjects the brain to shear stresses<sup>27</sup> and thus causes cavitation<sup>28,29</sup>, whilst the positive pressure has been linked with the focal injuries. The negative pressure and cavitation theory in relation to contracoup injury has, however, been heavily debated by authors<sup>23,30,31</sup> and thus its application is still in question.



*Figure 2. Translation acceleration on impact with a surface (A), pressure gradient formed on intracranial soft tissues due to a translational impact (B), rotational acceleration induced on the head (C).*

Holburn<sup>32</sup> was the first author to state that it was rotation, as opposed to translation, accelerations that causes brain injury, producing injurious shear stress and strains. The theory was subsequently supported by authors using primates and physical models<sup>20,33-37</sup>, where it was concluded that shear strains on the brain bridging veins were as the result of rotation and also caused diffuse patterns of injury, such as diffuse axonal injury and SDH. Longer impact durations with

reduced magnitudes of acceleration were associated with DAI, yet shorter durations with increased acceleration were related to SDH <sup>36</sup>. Rotational accelerations have also been attributed to bridging vein rupture in human cadavers <sup>38, 39</sup>, Whilst mechanisms of injury have generally been split between translational and rotational accelerations, authors have stated that injury to head and, more specifically the brain, is likely through a combination of both <sup>23</sup>.

### **2.3.2 Head Injury Thresholds**

Head injury thresholds have generally been developed through subjecting human cadavers or primates to accelerations (translation or rotational) and evaluating any consequential injuries. Recently, investigators are further exploring these thresholds through the use of numerical modelling and accident reconstruction, using an anthropomorphic testing device (ATD) or a computational model. Thresholds in terms of kinematic variables provide a marker with which incidents can be assessed. Post experimentation, the input accelerations are correlated with injury patterns, usually using logistic regression, to develop a threshold in terms of a kinematic variables such as the peak linear acceleration (peak G). The thresholds for head injury, and in particular those relating to infants and young children, will be discussed in terms of translational and rotational accelerations.

#### **2.3.2.1 Translational Accelerations**

The original kinematic variable developed as a head injury threshold was the Wayne State Tolerance curve, based on human cadaver, animal and volunteer work<sup>40, 41</sup>, and it related peak G to the duration of impact. Whilst providing injury assessment values, limitations of the curve were highlighted including difficulty in plotting single values for acceleration and time when both would vary on impact <sup>42</sup>. A logarithmic plot of the Wayne State Tolerance curve resulted in linear line with a slope of -2.5 and this was used by Gadd <sup>43</sup> to develop the Gadd Severity Index (GSI), Equation (1). A value in excess of 1000 was regarded as injurious.

$$GSI = \int_0^T a^{2.5} dt \quad (1)$$

where  $a$  is acceleration and  $T$  is time duration.

This was then updated by Versace <sup>44</sup> to only investigate the injurious aspect of the acceleration time curve, which led to the development of the Head Injury Criterion (HIC), Equation (2).

$$HIC = |(t_2 - t_1) \left\{ \frac{\int_{t_1}^{t_2} a dt}{(t_2 - t_1)} \right\}^{2.5}|_{max} \quad (2)$$

where again  $a$  is acceleration and  $t_2-t_1$  is a portion of the acceleration time waveform.

A number of experimental studies were conducted on adult cadavers, with Prasad and Mertz <sup>45</sup> presenting the collated data to establish a level of risk with HIC. Here, a 16% risk of severe or fatal head injury was associated with a HIC value of 1000 <sup>45</sup>, considered initially at a time duration  $(t_2 - t_1)$  at 36ms, although this was later updated to 15ms <sup>16</sup> and the threshold reduced to 700. The original research by Prasad and Mertz <sup>45</sup> identified brain injury and skull fracture to have the same level of risk in terms of HIC <sup>16</sup>. Consequently, the HIC value of 700 was associated with skull fracture and a level of risk of 31%. Given the original data related to adults, NHTSA proposed methods to scale for children, to extend their research through the use of their child family of ATDs. Original scaling methods were based on head measurement and skull stiffness properties <sup>46</sup>, although this was later updated to be based on brain material properties. The skull fracture risk for adult developed by the NHTSA is outlined in Equation (3).

$$p(\text{fracture}) = N \left( \frac{\ln(HIC) - \mu}{\sigma} \right) \quad (3)$$

where  $N()$  is a normal distribution,  $\mu$  is equal to 6.96 and  $\sigma$  is equal to 0.85. The corresponding scaling factor for a 12 month old was 0.555 <sup>16</sup>. Whilst providing a useful scaling value, due to a lack of infant material properties, assumptions had to be made in the scaling calculations. Therefore it is difficult to assess the accuracy of this scaling value. In spite of this, there are no cases in the published literature where infant or young child cadavers have been subject to an injurious impact scenario and the kinematic variables on impact have been measured. Prange *et al*

<sup>47</sup> performed compression and impact tests with the head from three infant cadavers at sub-injurious levels. The cadavers were aged 1, 3 and 11 days old. The compression tests were conducted at rates of 0.05mm/s, 1mm/s, 5mm/s and 50mm/s in order measure the stiffness of the head in anterior-posterior direction and also the left-right direction. Finally the three heads were subject to impacts onto five anatomical locations (vertex, forehead, occiput, left parietal and right parietal) at two different fall heights (0.15m, 0.3m). This research provided stiffness values for an infant head, thus enabling the biofidelity of testing devices (physical and computational models) to be assessed. As no skull fractures were documented across all the testing completed by Prange *et al* <sup>47</sup>, therefore providing a lower threshold for skull fracture. However the authors did not investigate greater heights, consequent it is difficult to determine a height as which fracture might occur.

Klinich *et al* <sup>48</sup> used a 6 month Child Restraint Airbag Interaction (CRABI) ATD to reconstruct road traffic accidents from the National Highway Traffic Safety Administration (NHTSA) database. The 6 month CRABI ATD was subsequently shown to have a similar impact response to cadavers heads used by Prange *et al* <sup>47</sup>, for all impact locations except the parietal. Consequently Klinich *et al* <sup>48</sup> developed 50% skull fracture threshold based on peak G and HIC, the corresponding values were 85g and 220 respectively. Weber <sup>49,50</sup> completed injurious impact tests with infant cadavers, however the kinematic response on impact was not measured. The authors aimed to investigate a single legal case, to determine if skull fracture was possible from a specific scenario. The scenario was a 0.82m fall from a changing table onto the parietoccipital area of the head. Weber <sup>49</sup> initially tested three surfaces (stone, carpet and foam supported linoleum) using 5 infant cadavers (aged between 1 and 9 months old) per surface. All 15 impacts resulted in skull fracture. Weber <sup>50</sup> completed a further 35 impacts using 35 cadavers. Ten impacts were onto foam and 25 impacts were double folder camel hair blanket. Of the foam impacts 2 resulted in fracture and of the camel hair blanked impacts 4 resulted in fracture. Van Ee *et al* <sup>51</sup> used a 6 month CRABI ATD to create the

cadaver impact tests conducted by Weber<sup>49, 50</sup> to develop skull fracture thresholds. The authors developed a 50% skull fracture threshold at a peak G value of 82g and HIC value 290<sup>51</sup>. However in the original cadaver cases series the stiffness properties of surfaces or cadaver heads used was not reported. Thus it is unclear if the surfaces used by Van Ee *et al*<sup>51</sup> were similar to those used in the cadaver tests. In conjunction the CRABI 6 month ATD was validated against young infant cadavers aged 1,3 and 11 days old, but the cadavers used by Weber<sup>49,50</sup> were aged between 1 and 9 months. Therefore it is unknown if the CRABI 6 months ATD is representative of this older age group. Thus again whilst providing an age appropriate threshold, it is difficult to assess how accurate they are. However the purpose of this thesis is to evaluate these thresholds against the head injuries seen in a clinical setting.

### 2.3.2.2 Rotation Accelerations

Whilst Holburn<sup>32</sup> was the first to suggest that rotational accelerations cause head injuries, the initial thresholds for SDH were developed by Löwenhielm<sup>39</sup>. Utilising adult cadaver impact tests, an initial bridging vein threshold was developed of 4,500 rad/s<sup>2</sup> in conjunction with a change in rotational velocity of 50 rad/s<sup>39</sup>. Later work by the same authors utilising a mathematic model, edited the change in rotational velocity to 70 rad/s<sup>52</sup> and then further edited it to 30 rad/s<sup>53</sup> for bridging vein rupture. Depreitere *et al*<sup>38</sup> completed impacts tests on adult cadavers using a swinging pendulum. The authors concluded a bridging vein threshold of 10,000 rad/s<sup>2</sup> for pulse durations less than 10ms, and that the 4,500 rad/s<sup>2</sup> threshold is adequate for longer impact durations. A limitation of both these thresholds is that the percentage level of risk is not document. In the tests conducted by Depreitere *et al*<sup>38</sup>, certain cadavers had no bridging vein rupture from accelerations in excess of 10,000 rad/s<sup>2</sup>, thus it is not a 100% risk.

The research conducted by Duhaime *et al*<sup>54</sup> compared accelerations from shaking to that of an impact using an ATD. In their research, they developed thresholds in relation to infants that were scaled relative to adult primates. The thresholds,



defining SDH, identified rotational acceleration of 35,000 rad/s<sup>2</sup> in combination with a change in rotational velocity of 110 rad/s. Whilst unclear<sup>55</sup>, it is believed the thresholds for adult primates documented by Gennarelli and Thibault<sup>35</sup> were scaled using the method documented by Bur<sup>32</sup>. In conjunction, this method only related adult primates to adult humans, thus the assumption for the scaling relationship including similar geometry and identical material properties would be incorrect<sup>55</sup>. Consequently, Thibault and Margulies<sup>56</sup> proposed altered scaling relationship, Equation (4).

$$\theta_{Infant} = \theta_{Adult} \left( \frac{M_{Adult}}{M_{Infant}} \right)^{\frac{2}{3}} \left( \frac{G'_{Infant}}{G'_{Adult}} \right) \quad (4)$$

Where  $\theta$  is rotational acceleration,  $M$  is brain mass and  $G'$  is storage modulus.

Using this relationship, the updated threshold for SDH was estimated at a rotational accelerations value of 23,700 rad/s<sup>2</sup> and change in rotational velocity of 67 rad/s. In spite of this updated equation, there is no agreed method for scaling rotational accelerations from an adult to an infant. Scaling based on geometry indicates greater tolerance levels in children, yet material properties also have to be considered, as documented by previous authors<sup>57</sup>. Consequently, the possibility of a SDH has been inferred from thresholds proposed by Löwenhielm<sup>39</sup> and Depreitere *et al*<sup>38</sup>.

### 2.3.3 Material Properties

The impact response of either a physical or computational head models will be dependent on the material properties used to develop them. Therefore for either the physical or computational models to act as appropriate biofidelic surrogates then the material properties used in their development need to resemble those of a human infant. Thus the literature has been reviewed to gain an understanding of the mechanical testing that has taken place on the bone and soft tissue structures of the head in infants and adults, to gain an understand of their material properties so that an appropriate surrogate can be chosen. A comprehensive overview of the

material properties relevant to infants and young children has been published by previous authors<sup>58</sup> and overview of the relevant literature is outlined below.

### **2.3.3.1 Skull**

Very few studies have completed testing on infant cranial bone compared to that completed on adult cranial bone<sup>59-63</sup>. McPherson and Kriewall<sup>64</sup> investigated the mechanical properties of fetal cranial bone to assess the deformation of a fetal head during labour using finite element analysis (FEA)<sup>65</sup>. They completed three point bending tests on 86 specimens from 6 different fetal heads aged between 24-40 weeks gestation and also a specimen from a 6 year old head. Specimens were taken from frontal and parietal bones in both fibre orientations, parallel and perpendicular to the long axis. As the material properties were going to inform an FEA of head deformation through the birth canal, the rate of testing was quasistatic at a rate of only 0.5mm/min with a maximum deflection of 1.5mm. The data was then subdivided into two groups, 24-30 weeks gestation (Pre terms) and 36-40 weeks gestation (Term). The authors found that age (pre term vs term) and fibre orientation (parallel vs perpendicular) had significant influence on the elastic modulus ( $P < 0.001$ ), where the older infant and fibre orientation parallel increased  $E$  (Table 1). This highlights that bone stiffness should be considered orthotropic and that age should be taken into consideration when selecting material properties. The reported elastic moduli are documented in Table 1.

The study provided the first basic material properties for fetal bone, however other material properties such as yield stress or yield strain were not described thus making it difficult to fully understand failure properties of fetal bone. Also no specimens of infants (1-12 months) were investigated.

*Table 1. Effect of age and orientation on bone elasticity. Reproduced from McPherson and Kriewall <sup>64</sup>. Mean±Standard Deviation.*

Age	Fibre Orientation	
	Elasticity Parallel / MPa	Elasticity Perpendicular / MPa
Pre term	1650±1170	145±62
Term	3880±780	951±572

Margulies and Thibault <sup>66</sup> completed three point bending tests from 4 infant cadavers aged 25 weeks to 6 months, to define age-dependent material properties of the skull. All specimens were tested with the fibre direction perpendicular to the long axis, at two different strain rates, 2.54mm/min and 2554mm/min. For the human samples the elastic modulus, rupture modulus and energy to absorption all increased with age (birth to 6 months) and ultimate strain decreased, but due to small sample size statistical comparison could not be drawn. Their results were comparable with the McPherson and Kriewall <sup>64</sup>. The authors completed testing, both three point bending and tensile on cranial bone and suture samples from neonate pigs. The authors state that the properties were comparable between the human and porcine, yet no statistical comparisons were possible due to the small sample size; thus, it is unknown if this comparison is valid. The infant porcine cranial bone, however, showed strain rate dependency, with the elastic modulus, rupture modulus and energy to absorption increasing with strain rate, which is similar to adult material properties <sup>61</sup>. However it is unclear if this would be true for human infant bone.

To assess the effect of rate dependency of infant cranial bone, at rates comparable to a low height fall, Coats and Margulies <sup>67</sup> completed three point bending tests on 46 specimens from 21 infant craniums aged < 1 year old. Whilst measuring the rate dependent effects, the authors also measured the effect of age and homogeneity of infant cranial bone. Samples were dissected from the parietal and occipital bone to assess homogeneity. The authors aimed to conduct their testing

at rates equivalent to a 0.3m and a 0.9m fall (equivalent speeds of 2.41m/s and 4.23m/s respectively), yet due to frictional losses the average impact rates were 1.58 m/s and 2.81m/s respectively. Their results showed the location of the specimen (i.e parietal versus occiput) and age significantly influenced the elastic modulus and ultimate tensile strength, with both properties increasing with age and for the parietal specimens relative to occipital specimens. The significant effect of age again further illustrates the essential need for age specific material properties<sup>64, 66</sup>. Utilising their data with previously reported value for infant human cranium<sup>64, 66</sup>, strain rate was shown not to significantly affect the elastic modulus or the ultimate tensile strength. This differs from adult cranial bone<sup>61</sup> and neonate porcine samples<sup>66</sup>, thus illustrating that caution should be adopted before assuming that porcine or adults samples are an adequate surrogate for human infants. Similarly to Margulies and Thibault <sup>66</sup> the bone stiffness was not significantly different from the original values reported by McPherson and Kriewall <sup>64</sup> for fibres perpendicular to the long axis, showing repeatability in bone stiffness across the 3 independent studies . Whilst providing essential data on the material properties of infant cranial bone where the fibre orientation was perpendicular to the long axis, due to a limited number of samples the authors were unable to measure the material properties where the fibres are parallel to the long axis. Consequently, the effect of factors including strain rate, age and homogeneity may differ with a parallel fibre orientation. This study was essential as it provided age specific material properties for infants, which will be used by this study.

### **2.3.3.2 Suture**

Whilst measuring the material properties of infant cranial bone, Coats and Margulies <sup>67</sup> also measured tensile properties of infant human suture. Fourteen specimens from 11 calvaria were subject to tensile tests. The suture was shown to be significantly less stiff compared to bone ( $P=0.011$ ), whilst it had a significantly higher ultimate strain ( $P<0.001$ ). The material properties of the sutures were not age dependent, which differed from the bone whilst, similarly to bone, the

properties of the suture were not strain rate dependent. This study was first to measure the material properties of infant suture, thus provided essential material properties for the development of both physical and finite element infant head models. However prior to this Margulies and Thibault <sup>66</sup> measured the properties of porcine suture due to similarities between infant cranial bone and neonate porcine cranial bone. The infant suture showed rate dependency, with the rupture modulus and elastic modulus increasing with strain rate. This, combined with the elastic modulus of the porcine data being 22-80 stiffer than those of human, again further illustrates that caution should be adopted prior to using porcine material properties as a surrogate for human<sup>67</sup>.

### 2.3.3.3 Scalp

The scalp is a layer of soft tissue that covers the cranium and consists of five layers: skin (1), connective tissue (2), galea (3), connective tissue (4), periocranium (5)<sup>68</sup>. The thickness of the scalp varies with age, particularly in infants<sup>58</sup>. No studies have completed mechanical testing of paediatric scalp tissue, and few have completed tests on adult scalp tissue<sup>69,70</sup>. Gadd *et al* <sup>69</sup> completed compression tests and showed that the scalp stiffens with compression. An estimate of the elastic modulus from their results indicates a value from 0.9MPa to 29.5MPa when compression was increased up to 50%. Raposio and Nordström <sup>70</sup> completed tensile tests on 20 scalp tissue samples from 10 humans. The samples only consisted of the top 3 layers of the scalp. The authors documented load displacement values, utilising the reported dimensions along with average thickness properties from the literature<sup>58</sup> to estimate an elastic modulus of 0.13MPa<sup>70</sup>. The variations might be attributed to differences in the direction of testing (compression versus tensile) which potentially highlights the anisotropic nature of the scalp tissue; furthermore, Raposio and Nordström <sup>70</sup> did not include all 5 layers of the scalp in their testing. Finally Galford and McElhaney <sup>71</sup> completed compression and tensile tests on adult rhesus monkey scalp tissue and documented time dependent behaviour, with a dynamic modulus of 1.58MPa. Whilst based on adult and monkey properties, the scalp is potentially anisotropic

and potentially rate dependent, it is unclear if these properties exist in paediatric scalp tissue.

#### 2.3.3.4 Cerebrospinal Fluid (CSF)

The cerebrospinal fluid (CSF) provides nutrients to the brain, whilst also reducing brain motion from translation accelerations<sup>72</sup>. It flows from the ventricular system in the brain to subarachnoid layer and then into the body venous systems via the arachnoid granulations<sup>68</sup>. The viscosity of infant CSF is similar to distilled water, 0.727mPas<sup>58</sup>, although this was based on a single sample.

#### 2.3.3.5 Brain

Experiments conducted aiming to define the material properties of the brain have shown there is a large variation in the mechanical response of the brain under an applied load. The brain consists mainly of water (78%)<sup>73</sup>, thus it's bulk modulus is assumed to be equivalent of water<sup>74</sup>. Most mechanical experiments conducted on the brain samples have measured it under a shear load since it is believed to be weaker in shear as opposed to compression<sup>32, 56</sup>, but compressive and oscillatory tests have been conducted. A frequent approach has been to measure the strain on the brain material under a dynamic shear load. Differing material models have been applied, though commonly a linear viscoelastic model is used. The complex dynamic shear modulus ( $G^*$ ) is measured in terms of the storage modulus ( $G'$ ) and the loss modulus ( $G''$ ), Equation (5),

$$G^* = G' + iG'' \quad (5)$$

An inverse fast fourier transform is commonly used to turn these measurements from the frequency to the time domain, resulting in Equation (6),

$$G(t) = G_\infty + (G_0 - G_\infty)e^{-\beta t} \quad (6)$$

where  $G(t)$  is the shear modulus at time  $t$ ,  $G_0$  is the short term shear modulus,  $G_\infty$  is the long term shear modulus and  $\beta$  is the decay constant.

A range of material tests have been conducted on adult human brain with a large variation in the constants in the viscoelastic model. This variation is partly

explained by different testing procedures<sup>72</sup>, anatomical location<sup>75</sup>, species tested<sup>75</sup>, time post mortem<sup>75</sup>, age<sup>75</sup>, and rate of testing<sup>58, 71, 75</sup>.

Despite this no studies have conducted mechanical testing on human infant brain samples, with few studies conducting tests on infant porcine samples. Thibault and Margulies<sup>56</sup> aimed to quantify the age dependant properties of adult brain tissue. The authors used porcine samples to investigate this, due to similarities in the growth between the central nervous system of a pig and a human<sup>56</sup>. They used harmonic shear testing across a range of frequencies of porcine samples aged 2-3 day old and 1 year old, which corresponded to human ages of approximately 1 month and four years respectively. Their testing was conducted at strain amplitudes of 2.5% and 5%. At 2.5% strain both the storage and loss modulus significantly increased with age, but at 5% strain only the loss modulus significantly increased with age. Therefore again highlighting the age dependency of material properties. The study only examined porcine brains and authors state the results showed similar properties to human samples reported in the literature, particularly the differing frequency behaviour of storage and the loss shear modulus. The scale of the results were an order of magnitude different from some reported human values, which the authors attributed to times post death. Thus it was unclear whether porcine samples are adequate surrogate in terms of brain material properties.

A viscoelastic model is commonly used to model the brain, though the brain has been reported to exhibit a non viscoelastic behaviour at high strains (20-40%) by Galford and McElhaney<sup>71</sup>. Prange and Margulies<sup>75</sup> conducted testing at high strains of up to 50% on porcine adult and infant samples and also human adult samples. Thus the study was also able to investigate differences between human and porcine samples. In conjunction to these two material parameters, Prange and Margulies<sup>75</sup> also assessed the anisotropic and inhomogeneity of brain tissue, where they showed that the brain is inhomogeneous and that certain structures, namely white matter and corpus callosum are anisotropic. The authors concluded

that a non-linear modified 1<sup>st</sup> order Ogden hyperelastic model was the best fit to their results for shear and compressive loading, and that the brain should be modelled as non linear at large strains. The authors comparisons between porcine and fresh human material indicated that the human samples were 29% stiffer compared to porcine. The authors state that the reason for this might be because of differences in the human samples (location of sample and that patients had epilepsy) and that fresh human samples had a far greater comparison compared to the human autopsy data in the literature<sup>75</sup>. Therefore it is inconclusive from the results and the lack of further comparisons in the literature whether porcine sample are an adequate surrogate in terms of brain material properties. Despite this the comparison between adult human and porcine samples allowed for scaling of infant porcine samples to human infant.

Comparison between the infant porcine samples by authors, indicated similar results to Thibault and Margulies <sup>56</sup>, when tested across similar conditions (i.e. 2.5% strain). Whilst adult brain stiffness is greater than infants at small strain, Prange and Margulies <sup>75</sup> results showed that at larger strain the paediatric tissue is stiffer compared to adults.

### **2.3.3.6 Dura Matter**

The dura is one of the meningeal layers that surrounds the skull. A fold in the dura matter that separates the right and left cerebral hemispheres is called the falx cerebri and a fold that separate the occipital lobe from the cerebellum is called the tentorium cerebellum<sup>68</sup>. Only two studies in the literature measured the material properties of human dura. Galford and McElhaney <sup>71</sup> measured the elastic modulus of adult human dura under a free vibration test and reported an elastic modulus of 31.5MPa. Bylski *et al* <sup>76</sup> measured the stiffness of fetal dura matter in bi axial tension from 7 foetuses . Whilst the research on fetal dura is more age appropriate to this study, the elastic modulus was not reported.



### 2.3.3.7 Bridging Veins

The bridging veins drain blood from the cerebral portion of the brain into the superior sagittal sinus. They pass from the cerebral cortex across the pia matter, across the subarachnoid space, through the arachnoid layer, the potential subdural space, the dural layer and into the superior sagittal sinus<sup>68</sup>. Rupture of the bridging veins is a commonly suggested mechanism for a subdural haemorrhage<sup>38, 39</sup>. In spite of this, relatively few studies have conducted mechanical tests on human bridging veins. Despite the bridging veins passing through the different meningeal layers, with the majority occupying the subarachnoid space, a SDH is more common compared to a SAH as the result of head trauma. Yamashima and Friede<sup>77</sup> attributed this to variable wall thickness, a lack of arachnoid trabecular cells and the arrangement of the collagen fibres of the bridging vein in the subdural area.

Despite rupture of the bridging veins forming an intrinsic part of the mechanisms of traumatic SDH, relatively few studies have measured their mechanical properties<sup>72, 78-80</sup>. Original work by Löwenhielm<sup>79</sup>, subjected 22 veins to strain rates between  $2s^{-1}$  and  $1000s^{-1}$ . The veins were taken from 11 humans aged between 13 and 87 years. Their research suggested that the bridging veins were strain rate dependent, with the ultimate stretch ratio of the bridging veins being a function of the strain rate, with reported ultimate stretch ratios between 1.14 and 1.83<sup>72, 79</sup>.

Research later conducted on the mechanical properties of bridging veins by Lee and Haut<sup>78</sup>, however, concluded that the failure properties were not strain rate dependent. The authors completed testing on 139 veins dissected from 8 humans aged between 62 and 85 years, where the veins were tested at a low strain rate of  $0.1-2.5s^{-1}$  and a high strain rate of  $100-250s^{-1}$ . Whilst the rates used were not as large as those reported by Löwenhielm<sup>79</sup>, the rate dependency of Löwenhielm<sup>79</sup> was within the strain rates used by Lee and Haut<sup>78</sup>. The ultimate stretch ratios varied between 1.15 and 2 across the different strain rates with a mean of

1.51±0.24 at rates 0.1-2.5s<sup>-1</sup>, and 1.55±0.15 at 100-250s<sup>-1</sup>. Disparities between the results was attributed to slippage at the clamps by Löwenhielm <sup>79</sup>.

Meaney <sup>80</sup> also conducted mechanical testing of human bridging veins to assess the effect of strain rate on the failure properties, whilst also measuring the effect of perfusion and age. A total of 59 veins were taken from cadavers 3 to 62 years, and tested at rates up to 250s<sup>-1</sup>. In agreement with Lee and Haut <sup>78</sup>, strain rate did not significant effect the ultimate failure properties. Age and perfusion also did not significantly affect the failure properties of the bridging veins.

Whilst failure properties of the bridging veins were not shown to be age dependent by Meaney <sup>80</sup>, the minimum age measured was 3 years and it has been shown that material properties can vary at younger closer to infant ages <sup>67,75</sup>, as has been discussed by previous authors<sup>81</sup>. Morrison <sup>72</sup> aimed to address the differences in the mechanical properties of bridging veins in the previous literature, whilst ultimately assessing the strain rate dependency of infant human bridging veins. However due to ethical reasons the authors had difficulty in obtaining infant human samples, thus limiting their conclusions. In spite of this they obtained 6 bridging veins from 3 infants aged between 0-12 weeks, whilst also conducted tests on 32 veins from 2 pigs age 16-17 weeks ( n.b. The age of the pigs would not equate to an infant human age). As a consequence of their small sample they only investigated low strain rates, between 5.8 and 32.7s<sup>-1</sup>. The ultimate stretch ratio for the infant humans were reported between 1.1 and 1.72, therefore coinciding with the range of previous reported values. The variation between the results was attributed a number of factors by Morrison <sup>72</sup>, namely the potential slippage at the clamps, procurement and storage of the bridging veins and the method of actuation. The authors also discussed that the variation within the individual donors was small compared to the variation between the donors, thus it is also potentially attributed to the natural variation between humans. Yet due to the difficulty in getting access to samples, there will also be variation in the

circumstances leading to the death, with two of samples from Morrison <sup>72</sup> being the result of head trauma.

Whilst experiments conducted on bridging veins by Morrison <sup>72</sup> were limited to a small sample, they provide the only properties that are specific to infants and values fall within previous reported values for adults. Consequently, the stiffness properties reported will be used by this study.

*Table 2. Properties on bridging veins reported in the literature*

<b>Author</b>	<b>Age</b>	<b>Strain Rate / s<sup>-1</sup></b>	<b>Ultimate Stretch Ratio</b>
Löwenhielm <sup>79</sup>	Adult	2 - 1000	1.556±0.154
Lee and Haut <sup>78</sup>	Adult	0.1-2.5 & 100 - 250	1.575±0.425
Meaney <sup>80</sup>	3-62 years	250	1.5±0.2
Morrison <sup>72</sup>	Infant	5.8 - 32.7	1.433±0.308

## **2.4 Key Area to Address From the Literature**

Thresholds for skull fracture in terms of kinematic variables exist for infants and young children<sup>16, 48, 51</sup>. In addition adult thresholds exist for bridging vein rupture and have been used to infer potential injury in young children<sup>38, 39</sup>. The biomechanical thresholds however have not been evaluated against what has been seen clinically. Given the limited data on which the thresholds are based, an evaluation of clinical relevance is essential prior to application.

There is considerable paucity of data on the properties of bone and in particular the intra/extra cranial soft tissue structures for young children and in particular infants. Consequently selection of correct material properties needs to take this into consideration and thus evaluate the effect of differing properties prior to selecting appropriate values.

Due to the limitations of the previously published scientific literature, this research has been split into three sections, which are outlined below.

It was hypothesised that developing a fall height threshold from clinical information about the mechanisms leading to head injury would allow current biomechanical thresholds to be evaluated and potentially enable a threshold to be proposed by this study. Consequently an initial aim of this research was to conduct a clinical study to determine a fall height threshold for skull fracture and / or ICI.

As will be discussed in section 3.1.1, there is no clear cut off in terms of fall height for skull fracture and/or ICI from previous clinical based studies. It was hypothesised that collecting and only using accurate fall heights would allow for the identification of a clear cut off in terms of height below which a skull fracture and/or ICI is unlikely. It was hypothesised that a potential threshold exists between 0.3m and 0.82m<sup>47, 49, 50</sup>, based on cadaver data. In conjunction, through using a case control study it was hypothesised that there would be a significant difference in other biomechanical variables including the mechanism of injury and surface of impact.

Post conducting a clinical study, in order to evaluate current biomechanical threshold, accurate biomechanical devices needed to be developed. It was believed that utilising modern image processing and manufacturing techniques would aid in the development of geometrically accurate physical and computational models. It was hypothesised that if CT scans were selected with similar head anthropomology to the infant cadaver heads used in previous biomechanical experiment, it would aid in the validation process.

Post validation it was hypothesised that if the devices were only used to investigate the clinically significant features, fall heights and biomechanical variables it would provide biomechanical evidence to support the clinical findings.

Finally due to limited material properties of the bone and soft tissue structures of an infant head, it was hypothesised that conducting a parametric analysis within limits of reported material properties would demonstrate a range of kinematic responses that a single infant head might produce.

## 2.5 References

1. Cassidy JD, Carroll L, Peloso P, Borg J, von Holst H, Holm L, et al. Incidence, risk factors and prevention of mild traumatic brain injury: results of the WHO Collaborating Centre Task Force on Mild Traumatic Brain Injury. *Journal of Rehabilitation Medicine*. 2004;36(0):28-60.
2. Yates PJ, Williams WH, Harris A, Round A, Jenkins R. An epidemiological study of head injuries in a UK population attending an emergency department. *Journal of Neurology, Neurosurgery & Psychiatry*. 2006;77(5):699.
3. Tagliaferri F, Compagnone C, Korsic M, Servadei F, Kraus J. A systematic review of brain injury epidemiology in Europe. *Acta neurochirurgica*. 2006;148(3):255-268.
4. Hawley C, Wilson J, Hickson C, Mills S, Ekeocha S, Sakr M. Epidemiology of paediatric minor head injury: Comparison of injury characteristics with Indices of Multiple Deprivation. *Injury*. 2013;44(12):1855-1861.
5. Laker SR. Epidemiology of concussion and mild traumatic brain injury. *PM&R*. 2011;3(10):S354-S358.
6. Hawley CA, Ward AB, Long J, Owen DW, Magnay AR. Prevalence of traumatic brain injury amongst children admitted to hospital in one health district: a population-based study. *Injury*. 2003;34(4):256-260.
7. Parslow RC, Morris KP, Tasker RC, Forsyth RJ, Hawley CA. Epidemiology of traumatic brain injury in children receiving intensive care in the UK. *Archives of Disease in Childhood*. 2005;90(11):1182-1187.
8. Maconochie I, Ross M. Head injury (moderate to severe). *Clinical evidence*. 2010;2010.
9. NICE. Head Injury Triage, assessment, investigation and early management of head injury in infants, children and adults. <http://www.nice.org.uk/nicemedia/live/11836/36260/36260.pdf>. Published 2007. Accessed 01/04/2011, 2011.
10. Teasdale G, Jennett B. Assessment of coma and impaired consciousness: a practical scale. *The Lancet*. 1974;304(7872):81-84.
11. Teasdale G, Jennett B. Assessment and prognosis of coma after head injury. *Acta neurochirurgica*. 1976;34(1-4):45-55.
12. Leventhal JM, Thomas SA, Rosenfield NS, Markowitz RI. Fractures in young children: distinguishing child abuse from unintentional injuries. *Archives of Pediatrics and Adolescent Medicine*. 1993;147(1):87.
13. Feldman KW, Bethel R, Shugerman RP, Grossman DC, Grady MS, Ellenbogen RG. The cause of infant and toddler subdural hemorrhage: a prospective study. *Pediatrics*. 2001;108(3):636.
14. Claudet I, Gurrera E, Honorat R, Rekhroukh H, Casasoprana A, Grouteau E. [Home falls in infants before walking acquisition]. *Archives de pediatrie: organe officiel de la Societe francaise de pediatrie*. 2013;20(5):484-491.
15. Thompson AK, Bertocci G, Rice W, Pierce MC. Pediatric short-distance household falls: Biomechanics and associated injury severity. *Accident Analysis and Prevention*. 2011;43(1):143-150.

16. Eppinger R, Sun E, Bandak F, Haffner M, Khaewpong N, Maltese M, et al. Development of improved injury criteria for the assessment of advanced automotive restraint systems–II. *National Highway Traffic Safety Administration*. 1999.
17. King AI, Yang KH, Zhang L, Hardy W, Viano DC. Is head injury caused by linear or angular acceleration. IRCOBI conference; 2003. p. 1-12.
18. Post A, Hoshizaki TB. Mechanisms of brain impact injuries and their prediction: a review. *Trauma*. 2012;14(4):327-349.
19. Zhang L, Yang KH, King AI. Biomechanics of neurotrauma. *Neurological Research*. 2001;23(2-3):144-156.
20. Gennarelli T, Thibault L, Ommaya A. Pathophysiologic responses to rotational and translational accelerations of the head. *SAE Technical Paper*. 1972;720970.
21. Ommaya AK, Grubb Jr RL, Naumann RA. Coup and contre-coup injury: observations on the mechanics of visible brain injuries in the rhesus monkey. *Journal of neurosurgery*. 1971;35(5):503-516.
22. Bilo RA, Robben SG, van Rijn RR. *Forensic aspects of paediatric fractures*: Springer; 2010.
23. Gurdjian E. Re-evaluation of the biomechanics of blunt impact injury of the head. *Surgery, gynecology & obstetrics*. 1975;140(6):845-850.
24. Gurdjian E, Lissner H. Mechanism of Head Injury as Studied by the Cathode Ray Oscilloscope\* Preliminary Report. *Journal of neurosurgery*. 1944;1(6):393-399.
25. Gurdjian E, Lissner H, Evans F, Patrick L, Hardy W. Intracranial pressure and acceleration accompanying head impacts in human cadavers. *Surgery, gynecology & obstetrics*. 1961;113:185-190.
26. Goldsmith W. Biomechanics of head injury. Prentice-Hall, Inc., NJ; 1972.
27. Thomas L, Roberts V, Gurdjian E. Impact-Induced Pressure Gradients Along Three Orthogonal Axes in the Human Skull\*. *Journal of neurosurgery*. 1967;26(3):316-321.
28. Gross AG. Impact thresholds of brain concussion. *The Journal of aviation medicine*. 1958;29(10):725-732.
29. Lubock P, Goldsmith W. Experimental cavitation studies in a model head-neck system. *Journal of Biomechanics*. 1980;13(12):1041-1052.
30. Gurdjian ES. Acute head injury: a review. *Surgery annual*. 1980;12:223-241.
31. Nutsholtz G, Lux P, Kaiker P, Janicki MA. Head impact response-Skull deformation and angular accelerations 1984. Report No.: 0898837111.
32. Holburn AH. Mechanics of head injuries. *Lancet* 2. 1943:438-441.
33. Gennarelli T, Ommaya A, Thibault L. Comparison of translational and rotational head motions in experimental cerebral concussion. Proc 15th Stapp Car Crash Conference; 1971. p. 797-803.
34. Gennarelli TA, Spielman GM, Langfitt TW, Gildenberg PL, Harrington T, Jane JA, et al. Influence of the type of intracranial lesion on outcome from severe head injury. *Journal of neurosurgery*. 1982;56(1):26-32.
35. Gennarelli TA, Thibault LE. Biomechanics of acute subdural hematoma. *The Journal of Trauma and Acute Care Surgery*. 1982;22(8):680-686.

36. Gennarelli TA, Thibault LE, Adams JH, Graham DI, Thompson CJ, Marcincin RP. Diffuse axonal injury and traumatic coma in the primate. *Annals of neurology*. 1982;12(6):564-574.
37. Ommaya AK, Gennarelli T. Cerebral concussion and traumatic unconsciousness correlation of experimental and clinical observations on blunt head injuries. *Brain*. 1974;97(1):633-654.
38. Depreitere B, Van Lierde C, Sloten JV, Van Audekercke R, Van Der Perre G, Plets C, et al. Mechanics of acute subdural hematomas resulting from bridging vein rupture. *Journal of neurosurgery*. 2006;104(6):950-956.
39. Löwenhielm P. Strain tolerance of the vv. cerebri sup.(bridging veins) calculated from head-on collision tests with cadavers. *Zeitschrift für Rechtsmedizin*. 1974;75(2):131-144.
40. Lissner H, Lebow M, Evans F. Experimental studies on the relation between acceleration and intracranial pressure changes in man. *Surgery, gynecology & obstetrics*. 1960;111:329-338.
41. Patrick L, Lissner H, Gurdjian ES. Survival by design : head protection. In Proceedings of the 7th Stapp Car Crash Conference; 1965. p. 483-499.
42. Cory C, Jones M, James D, Leadbeatter S, Nokes L. The potential and limitations of utilising head impact injury models to assess the likelihood of significant head injury in infants after a fall. *Forensic Science International*. 2001;123(2-3):89-106.
43. Gadd CW. Criteria for injury potential. *Impact Acceleration Stress*. 1962;977:141.
44. Versace J. A review of the severity index. In *Proceedings of the Stapp Car Crash Conference* 1970. p. 771-796.
45. Prasad P, Mertz HJ. The position of the United States delegation to the ISO working group on the use of HIC in the automotive environment. *SAE transactions*. 1985;94:106-116.
46. Melvin J. Injury assessment reference values for the CRABI 6-month infant dummy in a rear-facing infant restraint with airbag deployment. *SAE Paper No 950872*. 1995.
47. Prange M, Luck J, Dibb A, Van Ee C, Nightingale R, Myers B. Mechanical properties and anthropometry of the human infant head. *Stapp car crash journal*. 2004;48:279.
48. Klinich K, Hulbert G, Schneider L. Estimating infant head injury criteria and impact response using crash reconstruction and finite element modeling. *Stapp car crash journal*. 2002;46:165.
49. Weber W. Experimental studies of skull fractures in infants]. *Zeitschrift für Rechtsmedizin Journal of legal medicine*. 1984;92(2):87.
50. Weber W. [Biomechanical fragility of the infant skull]. *Zeitschrift für Rechtsmedizin Journal of legal medicine*. 1985;94(2):93.
51. Van Ee C, Moroski-Browne B, Raymond D, Thibault K, Hardy W, Plunkett J. Evaluation and refinement of the CRABI-6 anthropomorphic test device injury criteria for skull fracture. 2009: ASME.
52. Löwenhielm P. Mathematical simulation of gliding contusions. *Journal of Biomechanics*. 1975;8(6):351-356.

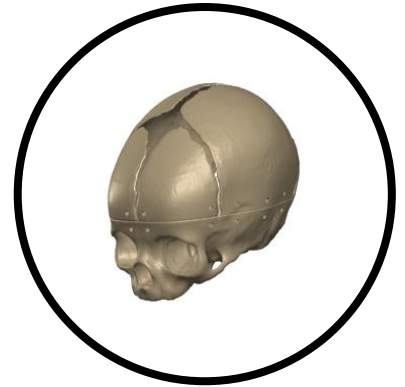


53. Löwenhielm P. Tolerance level for bridging vein disruption calculated with a mathematical model. *Journal of bioengineering*. 1978;2(6):501.
54. Duhaime A-C, Gennarelli TA, Thibault LE, Bruce DA, Margulies SS, Wiser R. The shaken baby syndrome: a clinical, pathological, and biomechanical study. *Journal of neurosurgery*. 1987;66(3):409-415.
55. Cory C, Jones M. Can shaking alone cause fatal brain injury? A biomechanical assessment of the Duhaime shaken baby syndrome model. *Medicine, science and the law*. 2003;43(4):317-333.
56. Thibault KL, Margulies SS. Age-dependent material properties of the porcine cerebrum: effect on pediatric inertial head injury criteria. *Journal of Biomechanics*. 1998;31(12):1119-1126.
57. Coats B, Margulies S. Potential for head injuries in infants from low-height falls. *Journal of Neurosurgery: Pediatrics*. 2008;2(5):321-330.
58. Margulies S, Coats B. Experimental Injury Biomechanics of the Pediatric Head and Brain. *Pediatric Injury Biomechanics*: Springer; 2013. p. 157-189.
59. McElhaney JH, Fogle JL, Melvin JW, Haynes RR, Roberts VL, Alem NM. Mechanical properties of cranial bone. *Journal of Biomechanics*. 1970;3(5):495-511.
60. Melvin JW, McElhaney J, Roberts V. Development of a mechanical model of the human Head–Determination of tissue properties and synthetic substitute materials. *Analysis*. 1970;2013:03-18.
61. Wood JL. Dynamic response of human cranial bone. *Journal of Biomechanics*. 1971;4(1):1-12.
62. Hubbard RP, Melvin JW, Barodawala IT. Flexure of cranial sutures. *Journal of Biomechanics*. 1971;4(6):491-496.
63. Evans FG, Lissner HR. Tensile and compressive strength of human parietal bone. *Journal of applied physiology*. 1957;10(3):493-497.
64. McPherson GK, Kriewall TJ. The elastic modulus of fetal cranial bone: a first step towards an understanding of the biomechanics of fetal head molding. *Journal of Biomechanics*. 1980;13(1):9-16.
65. McPherson GK, Kriewall TJ. Fetal head molding: An investigation utilizing a finite element model of the fetal parietal bone. *Journal of Biomechanics*. 1980;13(1):17-26.
66. Margulies S, Thibault K. Infant skull and suture properties: measurements and implications for mechanisms of pediatric brain injury. *Journal of Biomechanical Engineering*. 2000;122:364.
67. Coats B, Margulies S. Material properties of human infant skull and suture at high rates. *Journal of neurotrauma*. 2006;23(8):1222-1232.
68. Standring S. Gray's anatomy. *The anatomical basis of clinical practice*. 2008;3.
69. Gadd CW, Nahum AM, Schneider DC, Madeira RG. Tolerance and properties of superficial soft tissues in situ. *SAE Technical Paper 700910*. 1970.
70. Raposio E, Nordström RE. Biomechanical properties of scalp flaps and their correlations to reconstructive and aesthetic surgery procedures. *Skin Research and Technology*. 1998;4(2):94-98.

71. Galford JE, McElhaney JH. A viscoelastic study of scalp, brain, and dura. *Journal of Biomechanics*. 1970;3(2):211-221.
72. Morrison N. The Dynamics of Shaken Baby Syndrome: The University of Birmingham; 2002.
73. Ommaya AK. Mechanical properties of tissues of the nervous system. *Journal of Biomechanics*. 1968;1(2):127-138.
74. McElhaney JH, Melvin J, Roberts VL, Portnoy HD. Dynamic characteristics of the tissues of the head. *Perspectives in Biomedical Engineering*. 1973:215-222.
75. Prange M, Margulies S. Regional, directional, and age-dependent properties of the brain undergoing large deformation. *Journal of Biomechanical Engineering*. 2002;124:244.
76. Bylski DI, Kriewall TJ, Akkas N, Melvin JW. Mechanical behavior of fetal dura mater under large deformation biaxial tension. *Journal of Biomechanics*. 1986;19(1):19-26.
77. Yamashima T, Friede R. Why do bridging veins rupture into the virtual subdural space? *Journal of Neurology, Neurosurgery & Psychiatry*. 1984;47(2):121-127.
78. Lee MC, Haut RC. Insensitivity of tensile failure properties of human bridging veins to strain rate: Implications in biomechanics of subdural hematoma. *Journal of Biomechanics*. 1989;22(6-7):537-542.
79. Löwenhielm P. Dynamic properties of the parasagittal bridging veins. *International Journal of Legal Medicine*. 1974;74(1):55-62.
80. Meaney DF. Biomechanics of acute subdural hematoma in the subhuman primate and man. 1991.
81. Coats B, Eucker SA, Sullivan S, Margulies SS. Finite element model predictions of intracranial hemorrhage from non-impact, rapid head rotations in the piglet. *International Journal of Developmental Neuroscience*. 2012.

---

Chapter 3 - Clinical  
Assessment of Head  
Injuries in Young Children



### 3.1 Introduction

Biomechanical thresholds for head injury in young children exist for skull fractures<sup>1, 2</sup> and adult thresholds exist for intracranial injuries including a SDH<sup>3-5</sup>. Skull fractures and intra cranial, including a SAH, SDH, EDH<sup>6</sup>, are the result of trauma<sup>7</sup> that results in material failure, whether it be fracture of a cranial bone or rupture of a bridging vein between the brain and sagittal venous sinus within the subdura. However the biomechanical thresholds for these injuries have not been assessed against the clinical features present in a young child who presents to a hospital having suffered from a head injury. Consequently a clinical study was developed to identify factors that influence the likelihood of skull fracture and/or ICI. This section of the research aimed to establish differentiating factors between low height falls that have not resulted in material failure (skull fracture and/or intracranial injury) and those that have. It was hypothesised that comparing the biomechanical features of falls that resulted in skull fracture or intracranial injury (ICI) with those that did not, would inform current paediatric head injury thresholds. These features included the fall height, surface of impact and age of the child. Establishing these markers could inform the clinical and forensic assessment of head injury in young children when physical child abuse may be suspected, inform head injury prevention strategies and also inform biomechanical studies, both physical and computational.

#### 3.1.1 Background

Whilst falls are a common mechanism of TBI (Section 2.1), it is the injuries that may result from a *low height fall* that raises controversy. Therefore the literature was reviewed to determine the injuries that have been documented as a consequence of this.

One of the first authors to investigate the possible head injuries young children sustain from low height falls was Helfer *et al*<sup>8</sup>. The authors investigated children less than or equal to 5 years old who had fallen from a bed or sofa, which the authors described as less than 0.91m. The study collected 246 cases through a 6

year review of hospital incident reports at a children's hospital, combined with parents completing a questionnaire whilst visiting their private paediatrician, if their child had fallen out of bed. Of the 246 cases only three had a fractured skull, thus leading the authors to conclude that serious head injuries were not possible from low height falls.

### 3.1.1.1 Low height fall

The first challenge in reviewing the literature relating to low height falls is defining what is meant by this term. Further issues include, whether the incident was witnessed, whether abuse was considered as a possible mechanism and whether other biomechanical variables were considered. The relevant articles with regards to these issues are outlined in Appendix 4 and are further discussed below.

### 3.1.1.2 Definition of a low height fall

The height used to categorise a low height fall has variably been defined as 0.91m to 1.52m<sup>8-15</sup>. A common approach when estimating the fall height has been to infer the height based on the description. For example Helfer *et al*<sup>8</sup> classed falls from beds and sofas as <0.91m. However this is a potentially erroneous method for establishing fall height, although it has frequently used by other authors<sup>10, 12, 13</sup>, in particular, when classifying falls from a bed or sofa, or a fall from a persons arms. Without a detailed description of the incident, including details such as the type of furniture fallen from (adult bed compared to a child's bed), position of the child prior to falling (standing versus sitting) and the height of the person, and their position prior to dropping the child, it is difficult to estimate the true fall height. This is highlighted by the difference in estimates of fall height, for example falls from a bed were classed as <0.91m by Helfer *et al*<sup>8</sup> and as <1.22m by Duhaime *et al*<sup>10</sup>. A fall from a person's arms has also had varying height estimations<sup>10, 12</sup>. Ibrahim *et al*<sup>12</sup>, estimated height of fall from carers arms as greater than 0.91m, when a specific height was not available. However, within their results, there were 10 cases where the fall height was less than 0.91m,

although the mechanism was reported as a fall from a person's arms. A similar finding was reported by other authors<sup>16</sup>. This illustrated the difficulty in estimating height without a very detailed description of the incident. Another problem with categorisation of low height falls has been defining what height is being used (Head height or surface height). Few authors have considered using the height of the head in their estimations <sup>17, 18</sup> (Appendix 4), thereby classing a fall from a standing position and a lying position as being the same, which would not be true. The final issue with the height estimation used when aiming to determine injuries that can result from a low height fall, is the accuracy of the estimated height. Thompson *et al* <sup>18</sup>, completed at home investigations of the incidents described at the Emergency Department (ED) and found that the *estimated* fall heights at the ED overestimated the *true* fall height when measured at the homes. This indicates how cautious one needs to be when interpreting the history provided by a carer or parent in the emergency situation.

### 3.1.1.3 Biomechanical variables

In the epidemiology research, fall height has often been the only biomechanical variable considered to have an effect on head injury severity. However, it has been clearly shown that other variables including surface impacted, body mass and point of impact have the potential to influence head injury severity <sup>18-20</sup>. A limited number of authors have investigated variables other than height (Appendix 4), Lyons and Oates <sup>21</sup> investigated the momentum on impact and found no significant difference between the injured and the non injured groups. Although it was unclear if the authors considered the *position* of the child prior to falling, however they did take general measurements of the height fallen. Only Thompson *et al* <sup>18</sup>, considered other biomechanical factors when conducting epidemiology research relating to injuries from low height falls. The variables investigated included impact velocity, potential energy, change in momentum, impacted surface (Measured via the coefficient of restitution), fall characteristics (pre & post fall position, fall dynamics), and patient characteristic (Mass, Body Mass Index (BMI)) which were compared between minor and moderate/serious injuries. They

observed that furniture height, fall height (Vertical distance to the centre of mass of body), impact velocity and BMI were significantly different between the minor and moderate/serious injury groupings ( $P < 0.05$ ). Whilst the authors analysed considerable detail on the falls, they only investigated children who attended the Emergency Department (ED), thus limiting the number of serious injuries captured and as a result the final sample size. A larger sample size may have resulted in further variables, e.g. potential energy and momentum, being significantly different between the minor and moderate/serious injuries.

#### **3.1.1.4 Evaluations/Quality of history provided**

An uncertainty when evaluating mechanisms of head injury in young children is the potential for AHT. Consequently when reviewing the literature, articles were evaluated to determine if the authors considered abuse as an aetiology and whether cases were excluded or separated out in the analysis. In conjunction articles were further evaluated to determine whether only witnessed incidents were included in order to determine if an accurate history was provided. This criteria for relevant articles can be seen in Appendix 4.

#### **3.1.1.5 Injury severity**

Whilst there a number of the discrepancies involved in the definition of a low height fall, the potential injuries explored from such incidents have also varied. The documented injuries from a low height fall vary between studies. As previously noted, Helfer *et al*<sup>8</sup> only documented skull fractures from falls less than 0.91m, whereas others for example have documented SDH as a consequence of a low height fall<sup>11, 14, 22</sup>.

##### **3.1.1.5.1 Simple fracture**

Simple skull fractures are thought to be possible from low height falls, with a number of authors documenting this<sup>10, 13-16, 21-26</sup>. Simple fractures have been defined as linear fracture of a single bone. Very few authors have documented no

skull fractures from a low height falls<sup>27</sup>, details of which are shown in Appendix 4. Whilst numerous studies report isolated skull fractures from low height falls<sup>12, 22, 24</sup>, few stratified out the different types of fracture whilst also reporting height<sup>10, 16, 28</sup>. Duhaime *et al*<sup>10</sup> investigated the mechanisms of head injury and reported that simple skull fractures were as likely to occur from falls <1.22m as they were from falls >1.22m, but the number of cases were not reported. Greenes and Schutzman<sup>25</sup> investigated the mechanisms of isolated skull fracture and 78 had a simple fracture. Of the total 101 cases, 55 fell < 1.52m and 18 fell from <0.91m. Of the 18 cases, 17 were infants. The number of simple fractures from a low height fall was not reported. Leventhal *et al*<sup>16</sup> studied fracture and reported 8 cases of simple skull fractures from falls <0.6m (n=24) and 17 were reported from heights between 0.6m and 1.19m (n=33)<sup>16</sup>. The lowest reported height of a skull fracture was not documented by the authors. Reece and Sege<sup>14</sup> investigated head injuries in children aged <6.5 years old and reported 62 accidental cases from fall <1.22m of which 38 (61%) had simple fractures. Thus it is clear that simple fractures have been reported from heights within a low height fall range. The lowest height reported in the literature reviewed for a simple fracture was by Thomas *et al*<sup>22</sup>, who reported this type of fracture at a height 0.5m, although it was unclear how the heights were calculated. The commonest site of skull fractures resulting from trauma is the parietal bone<sup>16, 22, 25</sup>, with second most common being either the occipital or temporal bone<sup>16, 22, 25</sup>, although it was unclear if this was specific to a low height fall.

#### 3.1.1.5.2 Complex fractures

In the literature it has been shown that simple skull fractures are possible from low height falls, yet the plausibility of complex fractures from such incidents has been debated. While previous authors have debated whether complex skull fractures including multiple<sup>29-31</sup>, depressed<sup>29</sup>, diastatic<sup>31</sup>, crossing suture<sup>30</sup> and bilateral<sup>30</sup> are associated with AHT, the unintentional injuries assessed were not specific to low height falls.

Duhaime *et al*<sup>10</sup> stated that complex fractures required greater heights which involved greater impact forces in comparison to simple fractures, with all



unintentional depressed skull fractures resulting from heights >1.2m. Leventhal *et al*<sup>16</sup> documented six complex skull fractures from heights between 0.6 - 1.19m (n=33), six between 1.2-2.1m (n=26) and 2 from heights greater than 2.1m (n=7). The 0.6-1.19m range lies within the parameters of a low height fall as described by previous authors<sup>8, 10, 12, 13</sup>. Thus disagreeing with Duhaime *et al*<sup>10</sup> and illustrating the possibility of a complex fracture from a low height fall. Although the height measurement and classification used was unclear (Appendix 4). In contrast to Duhaime *et al*<sup>10</sup>, Greenes and Schutzman<sup>25</sup> investigated historical features associated with isolated skull fracture, and found that 6 of the 22 cases of depressed fracture had a reported history of a fall less than 0.91m and 3 of 9 cases of multiple fractures occurred from 'minor trauma', one of which was a fall from 0.6m. Reece and Sege<sup>14</sup> noted there were 62 cases where the fall height was classed as less than 1.2m, 8% (n=5/62) of which were complex fracture. Hiss and Kahana<sup>32</sup> documented four cases of bilateral skull fractures as consequence of a low height fall, however three cases were deemed to be the result of a crushing mechanism, thus potentially only leaving a single case. Arnholz *et al*<sup>33</sup> reported a single case of a bilateral fracture from a single impact onto the midline posterior aspect of head where the fall height was between 0.6m and 0.9m.

Thus it is clear that complex fractures, whilst infrequent in comparison to simple fractures, may be possible from a low height fall. Biomechanical studies using infant cadavers also support this argument. Weber<sup>34, 35</sup> impacted 50 infant cadavers aged between 1-9 months from 0.82m onto 5 different surfaces. Of the total impacts 20 resulted in a fracture, of which 5 involved fractures of multiple cranial bones<sup>34, 35</sup>.

It is often the presence of an intracranial injury (ICI) from a low height fall that raises the suspicion of AHT, particularly a Subdural Haemorrhage (SDH)<sup>10, 29, 36, 37</sup>. Only a limited numbers of authors have documented intracranial injuries from a low height fall, and few have separated out the different types of ICI (Appendix 4). The prevalence of ICI from a low height fall varies between studies<sup>12, 13</sup>. Park *et al*

<sup>13</sup> investigated children < 6 years who had fallen, and 18.4% of the ‘low level falls’ (classed as <1m) had an intracranial haemorrhage. Whilst abuse cases were excluded from the analysis, it was unclear how abuse was defined, and whether the cases were witnessed or not. In the large study by Ibrahim *et al* <sup>12</sup>, 55% of the 67 infant falls <0.91m and 42% of the 31 toddler falls <0.91m had a primary intracranial injury (Appendix 4). Also, 5% of the 67 infants falling <0.91m had secondary intracranial injury (Appendix 4). The plausibility of different types of ICI from a ‘low height fall’ and their association with abuse varies <sup>10,36</sup>, thus they have been reviewed separately to determine their likelihood from a low height fall.

#### 3.1.1.5.3 Epidural/ extradural haematoma (EDH)

Schutzman *et al* <sup>38</sup> completed a 10 year retrospective review of children <19 years old who were diagnosed with a traumatic EDH and found that 45.3% (n=24/53) of the epidural haemorrhages were the result of a fall <1.52m.

The authors documented the location of the EDH, 47.5% (n=19/40) of which were in the temporal region and 25% (n=10/40) in the temporo-parietal region. However the study was not specific to young children, with only 13 of the 53 occurring in children < 2years old, and the authors did not document the aetiology or location of the EDH for those aged <2 years. The authors did not state explicitly whether abuse was actively excluded or not, nor the details of the fall height calculations.

Other studies focussing on young children have noted a similar number of cases of low height falls as an aetiology for EDH. Shugerman *et al* <sup>37</sup> identified 34 cases of EDH, 91% of which (n=31) were classed as unintentional. Sixteen of the 34 cases (47%) with EDH had a reported history of a fall less than 1.83m. Whilst this height is higher than that previously reported for a low height fall, it again shows the potential for an EDH in young children from what was classed by the authors as a ‘minor trauma’ incident. Of the 26 cases reported to have fallen <1.22m by Duhaime *et al* <sup>10</sup>, 3 cases (11.5%) had an EDH. This percentage is lower than that reported by Schutzman *et al* <sup>38</sup> and Shugerman *et al* <sup>37</sup>, which may be due to the

authors using different classifications of height and also investigating different age ranges; where Duhaime *et al*<sup>10</sup> only examined children less than 2 years of age. Hettler and Greenes<sup>11</sup> reported thirty nine cases as low-impact trauma, which the authors defined as <0.91m or other low-impact non fall mechanism. Thirty three percent (n=13/39) of these had an EDH. Thomas *et al*<sup>22</sup> reported a single case of an EDH beneath a fracture from a 1m fall. The prevalence of an EDH resulting from a ‘low height’ fall illustrates that this type of injury should be regarded as possible from a low height fall, particularly from an impact to the temporal/parietal region<sup>38</sup>.

#### 3.1.1.5.4 Subdural Haematoma (SDH)

Duhaime *et al*<sup>10</sup> only found SDH in motor vehicles collisions however patients with a SDH from a low height fall were part of their algorithm for determining AHT. Of the 39 ‘low impact trauma’ cases reported by Hettler and Greenes<sup>11</sup>, 54% (n=21) had a SDH, following exclusion of abuse. In the retrospective review of children aged < 6.5 years of age by Reece and Sege<sup>14</sup> 8% (n=5) had a SDH from ≤1.22m. . Two of the 19 (10.5%) moderate to severe unintentional injuries had SDH from a low height fall in the research conducted by Thompson *et al*<sup>18</sup>. One case was a 42 month girl who fell from 1m, and the other was a one month old girl who fell from 0.86m. The infant had a skull fracture with SDH whereas the older child did not. Feldman *et al*<sup>39</sup> aimed to determine the most common mechanisms of SDH in 66 children < 3years old. Sixty-six cases were captured and each case was assessed for abuse, and assigned to one of three categories, unintentional (n=15, 23%), indeterminate (n=12, 18%) and abuse (n=39, 59%). No child who fell <1.22m (n=15) in the unintentional group had a SDH. Thomas *et al*<sup>22</sup> investigated children < 2 years old undergoing a head Computerised Tomography (CT). They reported 17 cases of a thin subdural haemorrhage beneath a fracture, with mean fall height of 1.57m and 2 cases of isolated SDH with a mean fall height of 0.7m.

In summary, the literature reviewed supports the argument that low height falls rarely result in a SDH, yet they have been documented from such incidents, with

the largest group being reported by Hettler and Greenes <sup>11</sup> (54%, n=21/39). In spite of this, it was unclear in the literature if the type of SDHs seen from the low height falls were different to those commonly associated with abuse. Feldman *et al* <sup>39</sup> stated that, 'However, it is unlikely that normal, short childhood falls (<4 feet) cause SDH that is associated with significant concurrent brain injury. Conversely, short falls may cause simple contact SDH.' (Feldman *et al* <sup>39</sup>, p.634). Thus it may be possible that the SDH seen in the literature from low height falls differ from the interhemispheric subdural hemorrhages and hemorrhages in multiple locations that are associated with abuse <sup>36</sup>. If a SDH is the result of a contact injury then it might be accompanied by an overlying fracture or extra cranial soft tissue swelling as reported by Hymel *et al* <sup>40</sup>. Three of the four cases by Hymel *et al* <sup>40</sup> and one of the two cases by Thompson *et al* <sup>18</sup> with SDH from a low height fall had a skull fracture reported, yet extra cranial soft tissue injuries were not documented. Thomas *et al* <sup>22</sup> reported the greatest number of cases with an accompanying skull fracture, where 17 thin SDH were underneath the fracture. Conversely, other evidence of contact might not always be evident; Amongst the infant and toddler falls from <0.91m with primary intracranial injury reported by Ibrahim *et al* <sup>12</sup>, approximately 30% (n=15/50) had no fracture and 18% had neither fractures nor soft tissue injuries. Of all the falls, one third had no fracture and 8% had no fracture or soft tissue injury with primary intracranial injury <sup>12</sup>. Thus the presence of a intracranial from an impact injury may not necessarily result in a fracture.

#### 3.1.1.5.5 Subarachnoid Haematoma (SAH)

Vinchon *et al* <sup>41</sup> documented 3 cases of mild SAH from a 'trivial fall', which the authors defined as falls from hospital beds or a person's arms (n=5). Reece and Sege <sup>14</sup> only reported a single SAH (2%, n=1/62) from falls <1.22m. The highest incidence of SAH from a low height fall was documented by Hettler and Greenes <sup>11</sup> (23%, n=9/39). Thomas *et al* <sup>22</sup> documented three cases of patchy SAH in combination with SDH, where the average fall height was 1.57m.

#### 3.1.1.5.6 Parenchymal Injury

Relatively few authors have documented injuries specific to the brain from a low height fall. Reece and Sege<sup>14</sup> reported 2 cases of brain contusion from falls <1.22m, Hettler and Greenes<sup>11</sup> reported 5 cases of haemorrhagic contusion from a low impact trauma and recently Thomas *et al*<sup>22</sup> reported a single cases of parenchymal brain injury from a 1.5m fall. Ibrahim *et al*<sup>12</sup> reported 5 cases of secondary brain injury, classed as cerebral oedema, ischemia, infarct, or loss of gray-white matter differentiation, in infants from fall <0.91m (n=98). Consequent an injury to the brain appears extremely rare from a low height fall.

#### 3.1.1.5.7 Moderate/Serious Head Injuries

In order to determine head injuries that can result from a low height fall, a methodology applied by some authors has been to differentiate between two injury groupings, for example minor versus moderate/serious. Therefore the they have not distinguished between ICI and skull fractures. Thompson *et al*<sup>18</sup> compared minor versus moderate/serious head injuries, where the moderate/serious was defined as an abbreviated injury score of 2-3. Whilst not specific to head injury, the average fall height of the moderate/serious group was 0.91m. Claudet *et al*<sup>42</sup> aimed to analyse pre mobile infants (<9months) who had been admitted as the result of a fall at home. A total 55 cases of traumatic brain injury were identified and had a mean fall height of 0.91m. The definition of traumatic brain injury was not clear and neither was the estimation of fall height. Thomas *et al*<sup>22</sup> recorded a mean fall height of 1.16m for those with a normal CT, 1.4m for those with an isolated skull fracture and 1.5m for those with an ICI. The lowest reported fall height for a skull fracture was 0.5m. Though the authors did not state how they estimated their heights. Thus the greater mean fall heights, might be attributed to the authors methodology, where all mechanisms of head injuries were investigated, yet the other authors only investigated domestic falls<sup>12, 42</sup>.

### 3.1.1.5.8 Overview

It is clear from the literature that simple fractures have resulted from a low height, although less frequent, complex fractures have also been recorded. Whilst Thomas *et al*<sup>22</sup> documented the lowest reported fall height resulting in a skull fracture of 0.5m, the height calculations were unclear. Epidural haemorrhages have also been reported from a low height fall, particularly for a temporal or temporo-parietal impact<sup>38</sup>. Subdural haemorrhages have been reported for low height falls and there appears broad agreement that they are contact SDHs with an overlying fracture<sup>22,39</sup> or soft tissue injury as opposed to the multiple and inter hemispheric haemorrhages associated with abuse. Both SAH and parenchymal injuries have been reported infrequently from a low height fall. However there remains no clear cut off in terms of height for different forms of head injury, particularly for complex fracture or intracranial injuries. Studies refer to heights as less than a value, but do not reference a height below which injuries were not seen.

### 3.1.2 Aims and Objectives

Few of the previous epidemiological studies have attempted a methodology that would allow for identification of a fall height threshold above which an anatomical material failure (skull fracture and/or intracranial injury) becomes more likely. In addition the prior research has focussed on children who have been admitted to hospital with a head injury, and thus fails to compare the mechanisms resulting in head injuries across a range of severities. Thus the primary objective of this section of the research was to study all head injuries in young children ( $\leq 48$  months) attending a single regional hospital as a result of a low height fall, to quantify the essential biomechanical characteristics of the scenarios leading to head injuries and to determine differentiating features that influence head injury severity. Secondary objectives were to determine the probability of a head injury resulting in material failure based on multiple variables, including height, age and surface.

## **3.2 Method**

### **3.2.1 Initial Study Design**

A case control study was developed to compare the characteristics that differentiated children who suffered a minor head injury (controls) from those who sustained a skull fracture and/or ICI (cases) as a consequence of a low height fall.

Data were collected about children younger than or equal to 48 months old who presented to the Emergency Department (ED) at the University Hospital of Wales (UHW) Cardiff, with a witnessed accidental head injury as a consequence of a low height fall between June 2011 to October 2011.

A prospective study design was chosen to ensure the capture of accurate and relevant information. A Head Injury Assessment Form was introduced into the ED at the UHW in order to capture the relevant information (Appendix 1).

The prevalence of skull fracture and/or ICI head injuries in children, is relatively low<sup>43</sup>. In order to achieve statistically significant results (based on the sample size calculation) retrospective data collection from case note review of children who had sustained skull fracture and/or ICI from head injury was initiated. These children within the same age range, were ascertained retrospectively from the radiology data base at the UHW and supplemented with the Paediatric Intensive Care Unit (PICU) database of children admitted with a head injury at the same hospital between January 2002 and October 2012.

### **3.2.2 Injury Severity Classification**

To ensure relevant case ascertainment, a head injury classification system was developed in order to differentiate between minor head injuries with no skull fracture and / or ICI and more serious head injuries that had resulted in material failure, namely skull fracture and/or intracranial injury visible on neuro imaging.

The cases consisted of children who had a CT scan that identified a skull fracture, with or without ICI, or ICI alone and were considered to be children with structural cranial or intracranial damage, as per the Public Health Observatory England, definition<sup>44</sup>. The National Institute for Health and Clinical Excellence (NICE) implement guidelines for when to do a head CT<sup>45</sup>, based on a clinical decision rule Dunning *et al* <sup>46</sup>, which had a sensitivity of 98% and specificity 87% for the prediction of a clinically significant head injury. Consequently the control group contained minor head injuries and consisted of those children who were asymptomatic based on NICE head injury guidelines where no head CT was undertaken, and those who were symptomatic but had a normal head CT. Children who were symptomatic but did not undergo a head CT were excluded from the study. The cases group consisted of those with an abnormal CT and included children with simple and complex skull fractures with or without ICI and children who had ICI alone *Table 3*.

*Table 3. Head injury severity classification.*

<b>Case: Skull Fracture and/or Intracranial Injury</b>	<b>Control: Minor Head Injury</b>
Simple skull fracture (linear fracture involving a single bone)	No visible injuries
Complex skull fracture (fracture involving multiple cranial bones, diastatic, depressed)	Soft tissue injury (bruise/haematoma, swelling, laceration, abrasion)
Intracranial Injury (ICI): Extra axial haemorrhage (epidural, subdural, subarachnoid), cerebral contusion, cerebral oedema, diffuse axonal injury, hypoxic ischaemic injury	



### **3.2.3 Age classification**

Infants were defined as children aged less or equal to 12 months and toddlers as children aged between 13 and 48 months.

### **3.2.4 Inclusion / Exclusion Criteria**

#### **Fall height**

It has been previously stated that a low height fall have been variably defined from <0.91m to < 1.52m with others using a 1.83m cut off<sup>11</sup>. In addition authors have classed falls >3.05m as high level<sup>12, 23, 24</sup>. Falls <3.05m were investigated, enabling a margin to calculate a fall height threshold for injury from domestic falls. Thus domestic or playground incidents were included such as falling from a standing or sitting height, from a toy or playground ride, from a raised surface such as a bed or chair, from a person's arms and a stair fall.

All motor vehicle crashes, birth related trauma, and unwitnessed cases of accidental injury were excluded from the study. All cases of AHT were excluded, if a patients' head injuries were initially suspected to be as a result of abuse, yet later deemed accidental following a full multidisciplinary review by the Cardiff and Vale Child Protection and Safeguarding team, then the child was included; If they were deemed intentional or inconclusive they were excluded.

### **3.2.5 Ethical & Design Issues and Approvals**

Data collection with waived patient informed consent was chosen in order to capture a large enough sample, which was informed by a power calculation (Section 3.2.8.1). Finally as the plan was to analyse, report and disseminate only non identifiable data then it was believed that waived consent was the optimal approach. An application to National Information Governance Board to undertake the study was submitted on the 24/02/2011 and was accepted on the 10 /06/2011 (Reference:ECC 3-04(h)/2011). An application was made to the South Wales Research Ethics Panel B Committee meeting on the 15/06/2011 and was

approved (Reference: 11/WA/0167). Research and Development approval at the UHW Cardiff involved application to the Cardiff and Vale Research Review Service (CaRRS) The researcher was granted a research passport and an honorary research contract 27/05/2011 (Reference : 11/RPM/5090 ). CaRRS application was submitted for review on the 24/04/2011 and approved on the 26/05/2011.

**3.2.6 Head Injury Assessment Form Development**

A data collection proforma was developed to ensure consistent data collection for the children who presented to the emergency department and those who were admitted to the children’s hospital. The Head Injury Assessment Form was initially designed to capture precise biomechanical information surrounding the causal incident. This included projectile speed and position of impact relative to the item fallen from (Appendix 1). However post discussions within the research team and with clinicians, it became clear that such data collection was not practical in the clinical setting. The Head Injury assessment form was expanded into a standardised form that incorporated mechanism of injury with all the necessary clinical information that would allow it to be used as part of routine care. The development of the Head Injury Assessment Form from its initial design, is described in Figure 3. The form was then piloted with emergency staff clinicians at the UHW including David Farrell (Paediatric team leader ED, UHW) and paediatrician Dr Alison Mott (named Dr Child Protection). The final version of the Head Injury Form can be seen in Appendix 1

The items deemed important to include on the Head Injury Assessment Form included the position of the child before and after the incident such that vertical distance through the child’s head fell from could be estimated. Details including how the child fell and part of the body that landed on were incorporated so that only head injury cases were included. Parents were asked to give an estimate of the height of the object fallen to aid with the height calculations. In section 3.1.1.2, it is outlined how previous authors have discussed that parents overestimate fall height when presenting their child to an emergency department. Whilst height

charts were added to the emergency rooms, a study was undertaken to evaluate if people over estimate or under estimate, so that comparisons could be made with previous authors. This study is shown in Appendix 5.

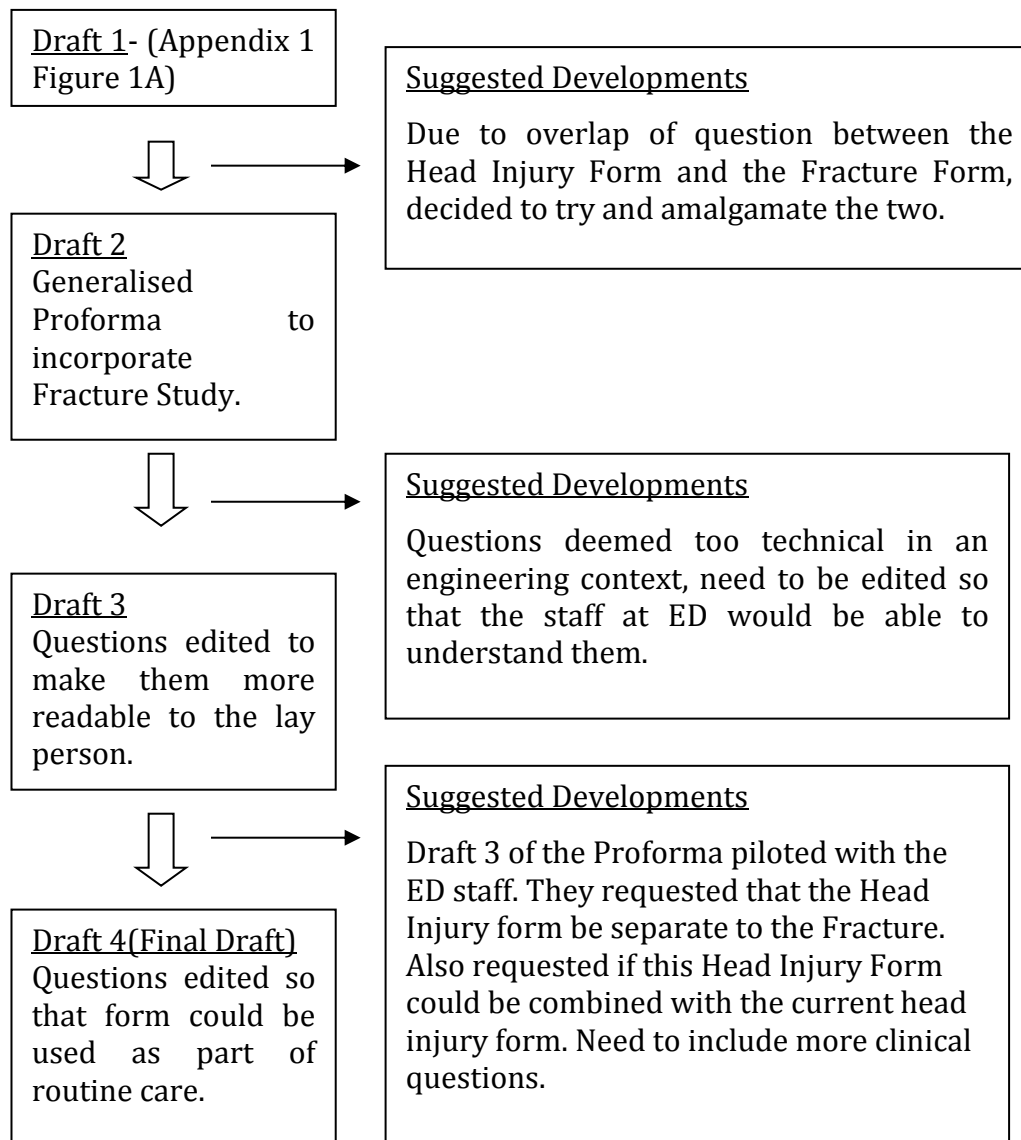


Figure 3. Workflow for development of the Head Injury Assessment form from its initial design through to the final design. Emergency Department (ED).

#### Data Collection

A Head Injury Assessment Form was completed by the admitting clinician in the ED or in the paediatric wards (see appendix 1) from June 2011 – October 2011 for

every child who presented with witnessed accidental head injury as part of their baseline clinical assessment. Data recorded included details of the activity undertaken by the child, the position of the child before and after the incident. Information on the dynamics of the fall, included the estimated height of fall, surface material impacted and object fallen from. The anatomical location of the acute soft tissue injuries were recorded and used to inform the likely site of impact.

Further data recorded included child demographics, and details of the nature and extent of the soft tissue injuries to other parts of the body, neurological symptoms including Glasgow Coma Score (GCS), and details of radiological investigations (X-ray, CT, MRI). The same data set was retrieved from the retrospective review of the case notes by the researcher when available.

### **3.2.7 Biomechanical Variables**

Initial categorisation of head injury causation was defined as per the Injury Database manual (as adopted by the European Union<sup>47</sup>). Consequently, the data recorded in the proforma were grouped into the following categories, falling from: standing or sitting; a moving object; a raised surface, such as a bed or sofa; down stairs; whilst being carried by a carer (adult, child or in a child product, such as a car seat), on the flat or whilst on the stairs.

#### **3.2.7.1 Documented Fall Height (Hf)**

The documented fall height referred to that recorded on Head Injury Assessment Form or that documented in the medical records. In cases where the child had fallen from an object, it referred to the height of the object (Figure 4). This height was used because it is often the only height available to clinicians and has been the height used by previous authors investigating head injuries in children<sup>8, 12, 15, 21, 25, 48</sup>.

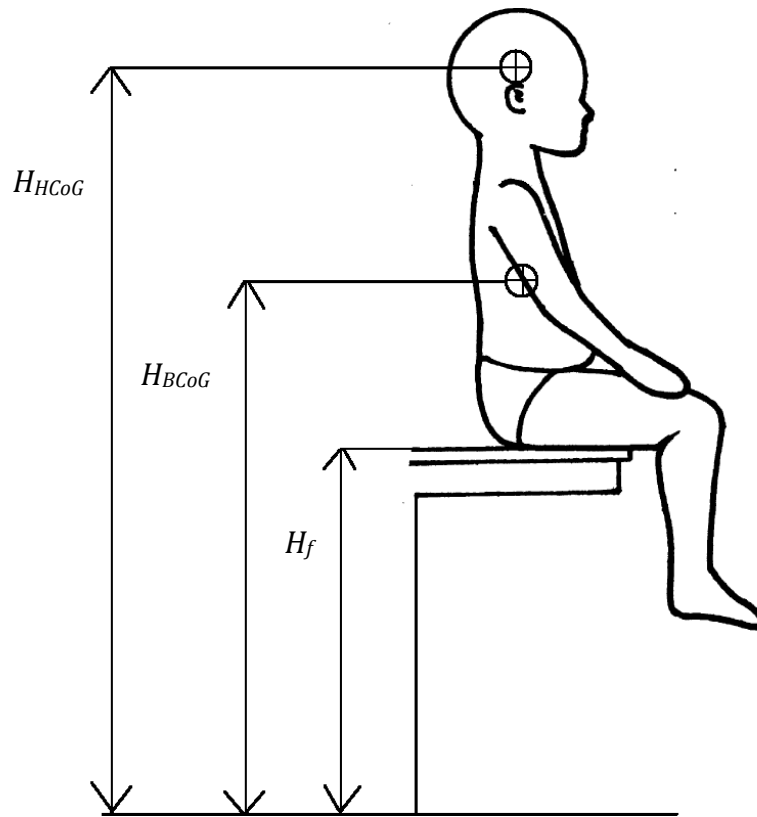


Figure 4. Heights assessed to differentiate head injury severity.

### 3.2.7.2 Height of head centre of gravity ( $H_{HCoG}$ )

If the object fallen from was clearly documented, for example height of sofa or table, then an extra height to account for the position of the child prior to falling was calculated. For cases where the position of the child was documented (standing, sitting, crawling) the height of the head relative to impact surface was then calculated via Equation (7). The estimations of standing, sitting and crawling positions were made from the 50th percentile anthropomorphic measurements for the age and gender (Appendix 2). For cases where the position of the child was unknown, an imputation strategy was used. To evaluate the lowest possible height, the child's head height was assumed to be equivalent of the documented fall height. This imputation was incorporated into Equation (7),

$$H_{HCoG} = H_f + HCoGx \quad (7)$$

Where  $H_{HCoG}$  and  $H_f$  have been previously defined and  $H_{CoGx}$  is the position of the centre of gravity of the head with respect to the weight bearing surface. The calculation of  $H_{CoGx}$  is shown in Appendix 2.

An addition imputation was used to assess the highest height the head could be for the cases where the position of the child was not documented. In these cases the child was assumed to be in a standing position. This measurement was defined as  $H_{HCoGM}$ .

This head CoG measurement was used to account for the position of the child prior to falling and therefore give an estimation of the vertical distance travelled by the head prior to impact.

**3.2.7.3 Height of body centre of gravity ( $H_{HCoG}$ )**

The position of the centre of gravity of the body was based on the 50th percentile data published by Snyder *et al* <sup>49</sup> for both the standing and sitting position. The calculation of  $H_{BCoG}$  is shown in Equation (8).

$$H_{BCoG} = H_f + BCoGx \tag{8}$$

Where  $H_{BCoG}$  and  $H_f$  have been previously defined and  $B_{CoGx}$  is the position of the body centre of gravity with respect to the weight bearing surface. The calculation of  $B_{CoGx}$  is shown in Appendix 2.

This measurement was used to allow comparisons to be made with previous authors<sup>12</sup>.

**3.2.7.4 Estimated Fall Height (EFH)**

Documented fall heights were reliant on those stated by the parent. Whilst height charts were placed in the ED to facilitate height estimation there is a potential for error in the height given. Thompson *et al* <sup>18</sup> completed at home investigation of the incidents described at the ED and found that the height given by the parent overestimated the true fall height. Appendix 4, outlines a further study that

supports this, where a groups of adults were shown to overestimate the height of household furniture. Therefore an extra variable, Estimate Fall Height (EFH) was calculated, based on the work by Thompson *et al* <sup>18</sup>, to account for parents/carers inaccurate estimations of the fall height (9).

$$EFH = 0.718H_f + 0.11736 \quad (9)$$

Where  $H_f$  has been previously defined (Nomenclature *Table 4*).

As this was based upon documented fall height, an extra height was added to account for the position of the head centre gravity. Equation (10) was used respectively, when the child’s position prior to falling was clearly documented. This led to an extra variable, the position of the head centre of gravity incorporating the estimated fall height ( $EFH_{HCoG}$ ), Equation (10).

$$EFH_{HCoG} = EFH + HCoGx \quad (10)$$

Where EFH and HCoGx have been previously defined (Nomenclature *Table 4*).

**3.2.7.5 Impact Velocity of the Body ( $V_{Body}$ )**

The impact velocity of the body was calculated based on Equation (11)

$$V_{Body} = \sqrt{2g H_{BCoG}} \quad (11)$$

Where  $g$  is gravity ( $9.81m/s^2$ ) and  $H_{BCoG}$  has been previously defined.

**3.2.7.6 Impact Velocity of the Head ( $V_{Head}$ )**

The impact velocity of the head was calculated based on Equation (12)

$$V_{Head} = \sqrt{2g H_{HCoG}} \quad (12)$$

Where  $g$  and  $H_{HCoG}$  have been previously defined.

**Body Mass ( $m_B$ )**

Body mass was estimated in order to inform momentum and kinetic energy calculations, Equations (13) and (14) respectively. The body mass used in Equations (13) and (14) was based on the value documented on the Head Injury Assessment form or in the clinical case notes. If the mass was not recorded then

the 50th percentile for the age and gender was derived from the World Health Organisation (WHO) growth charts <sup>50</sup>.

**3.2.7.7 Body impact momentum ( $M_{Body}$ )**

The body Impact momentum was calculated using Equation (13)

$$M_{Body} = m_B V_{Body} \tag{13}$$

Where  $m_B$  and  $V_{Body}$  have been previously defined.

**3.2.7.8 Body kinetic energy ( $KE_{Body}$ )**

The kinetic energy on impact was calculated using Equation (14)

$$KE_{Body} = \frac{1}{2} m_B V_{Body}^2 \tag{14}$$

Where  $m_B$  and  $V_{Body}$  have been previously defined.

**Head Mass ( $m_H$ )**

Head mass was estimated in order to inform momentum and kinetic energy calculations, Equations (16) and (17) respectively. Lloyd *et al* <sup>51</sup> documented the head masses of the 14 paediatric cadaver heads (aged from 31 weeks gestation to 16 years old with 10 cadavers < 12 months old ) used in their study and also illustrated an exponential curve fit based on the characteristic length for the cadaver heads. This information was used to develop an equation for head mass based on the characteristic length, Equation (15).

$$m_H = 0.0889e^{0.0044CL} \tag{15}$$

Where  $m_H$  is the head mass and CL is the characteristic length. The calculation of characteristic length is shown in Equation (57), Appendix 2. The head length, width and circumference used in the characteristic length calculation were calculated using the equations developed by Loyd *et al* <sup>52</sup>. The head mass equation based on characteristic length is illustrated in Figure 5.



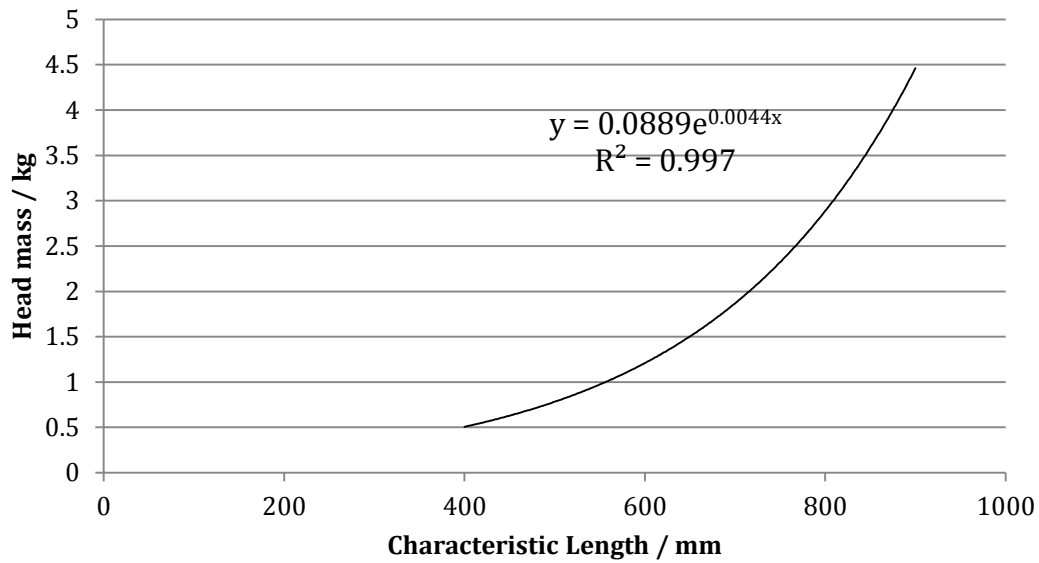


Figure 5. Exponential curve fit to calculate head mass based on the characteristic length. Graph recreated from Loyd et al <sup>52</sup> in order to develop an equation that related head mass to the characteristic length.

### 3.2.7.9 Head impact momentum ( $M_{Head}$ )

The head impact momentum was calculated using equation (16).

$$M_{Head} = m_H V_{Head} \quad (16)$$

Where  $m_H$  and  $V_{Head}$  have been previously defined. The head mass used in Equations (16) was based on equation (15).

### 3.2.7.10 Head kinetic energy ( $KE_{Head}$ )

The kinetic energy on impact was calculated using equation (17).

$$KE_{Head} = \frac{1}{2} m_H V_{Head}^2 \quad (17)$$

Where  $m_H$  and  $V_{Head}$  have been previously defined.

The head mass used in Equation (17) was based on equation (15).

### **3.2.8 Statistical Analysis**

#### **3.2.8.1 Sample Size Calculation**

The sample size calculation was based on a comparison of the mechanism of head injury between those with a minor head and those with a skull fracture and / or ICI, where the mechanism was a fall and the height was documented. This field of research is relatively new, and there was little published data to an accurate power size calculation. Thompson *et al* <sup>18</sup> published information on short-distance household falls comparing biomechanical variables between children with minor head injuries to those with moderate or serious head injuries for children under 4 years old. This paper had only 2 cases classed as skull fracture and /or ICI, where a specific height was documented compared to 60 minor head injuries where an mean height was reported. Plunkett <sup>53</sup> also looked at injury severity from short-distance falls, where there were 8 cases equating to skull fracture and / or ICI in children less than 4 years of age. Therefore the sample size was based on a comparison of the biomechanical variable fall height between those 10 cases (8 from Plunkett <sup>53</sup> and 2 from Thompson *et al* <sup>18</sup>) and minor injury data from Thompson *et al* <sup>18</sup>. A minimum sample size of 50 significant head injuries was indicated with alpha set at 0.05 and using a power of > 80%. This value of 50 was taken as a guide to follow. Due to the small amount of data on which to base this sample size calculation, a level of uncertainty was placed on the value of 50. As a result a power calculation to determine a statistically significant result was continually reassessed throughout the data collection.

#### **3.2.8.2 Comparison between categorical and continuous data**

Statistical differences between cases and controls for the categorical variables were assessed using Chi square test, where expected numbers were small, Fishers Exact was used. Logistic regression was used to further evaluate the sub groups of the categorical variables (mechanism of injury, impact surface and site of impact).The reference category for mechanism of injury was a fall from a standing

height, for impact surface it was carpet and for site of impact it was a forehead impact.

The continuous variables, including fall height, kinetic energy etc, were initially assessed for normality using the Kolomogorov-Smirnov test. If the data was normally distributed then statistical significance was evaluated using a student t-test, otherwise the non the parametric equivalent (Mann Whitney Test) was used. The same statistical tests were completed when comparing continuous and categorical variables between infants and toddlers.

SPSS (Version 20, IBM) was used for all the statistical comparisons, where statistical significance was set at  $p = 0.05$ .

### 3.2.8.3 Injury Risk Curves

Injury risk curves were developed to relate the probability in terms of a binary outcome, minor head injury versus skull fracture and / or ICI, to the biomechanical variables. Various statistical methods have been adopted in injury biomechanics to estimate injury risk in terms of biomechanical variables. Historically the maximum likelihood method has been used, most notably the logistic method<sup>54, 55</sup>. The logistic regression model is shown in equation (5). The a and b variable are optimised in terms of the goodness of fit based on the maximum likelihood method.

$$P(x) = \frac{1}{1 + e^{-(a+bx)}} \quad (18)$$

Another technique commonly used in biomechanics is the Mertz/Weber method<sup>56</sup>. This technique involves ordering both binary outcomes from the smallest to largest in order to identify the overlap between the two outcomes. The overlap region is then assumed to have a normal distribution and median ranking values are assigned to the largest value of the non-injured group and lowest value of the injured group. Normal distribution probability paper is then used to plot these two points and a line is drawn through both, such that the estimates of percent of

injury can be determined. After this a cumulative distribution function can be created based on a normal distribution. The final injury risk curve assessed is the modified maximum likelihood developed by Nakahira *et al* <sup>54</sup>.

Two assumptions were used in order to evaluate the injury risk curves against the collected data. The first was that when the biomechanical variable approaches zero the injury risk approaches zero. Equation (19) was used to assess this assumption, as has been used by previous authors <sup>54</sup>.

$$A1 = 1 - \{1 - P(0)\}^n \tag{19}$$

Where P(0) is the probability and point 0 and n is the sample size.

The second assumption was that the injury should have the maximum goodness of fit. The log likelihood function was used to assess this assumption, Equation (20), was used, as has been used by previous authors<sup>54</sup>, the larger the value for this assumption the better the goodness of fit.

$$EB = \frac{1}{n} \log\{(\Pi_i y_i)(\Pi_j (1 - y_j))\} \tag{20}$$

Where n is the sample size,  $y_i$  is the predictor of injured cases and  $y_j$  is the the predictors of uninjured cases.

The three different forms of logistic regression were assessed against the two assumptions. The different forms of logistic regression were assessed based on  $H_{CoG}$ . The best suited method was then used for the logistic regression on the other biomechanical variables.

### 3.2.9 Nomenclature

Table 4. Nomenclature of biomechanical variables measured

Symbol	Definition
$H_f$	Documented fall height
$H_{B\text{CoG}}$	Height of the body centre of gravity
$H_{H\text{CoG}}$	Height of the head centre of gravity. Imputation based on lowest possible height, thus cases where position of child unknown assumed to be lying.
$H_{H\text{CoGM}}$	Height of the head centre of gravity. Imputation based on highest possible height, thus cases where position of child unknown assumed to be standing.
EFH	Estimated fall height
$EFH_{H\text{CoG}}$	Height of the head centre of gravity with estimated fall height incorporated
$EFH_{H\text{CoGM}}$	Height of the head centre of gravity with estimated fall height incorporated. Imputation based on highest possible height, thus cases where position of child unknown assumed to be standing.
$m_B$	Body mass
$m_H$	Head mass
$V_{\text{Body}}$	Impact velocity body
$V_{\text{Head}}$	Impact velocity head
$M_{\text{Body}}$	Momentum of body on impact
$M_{\text{Head}}$	Momentum of head on impact
$KE_{\text{Body}}$	Kinetic energy of the body on impact
$KE_{\text{Head}}$	Kinetic energy of the head on impact

### 3.3 Results

The prospective data collection yielded 494 minor head injury cases, of which 416 met the inclusion criteria and the retrospective case note review captured 63 cases of skull fracture and / or ICI, of which 47 met the inclusion criteria ( Figure 6), two of which were ascertained in the same period as the prospective data collection. A fall height was documented in 108 cases of minor head injury and 25 of the skull and / or ICI group. Whilst this is lower compared to the sample size calculation, it still produced a significant result (Table 6).

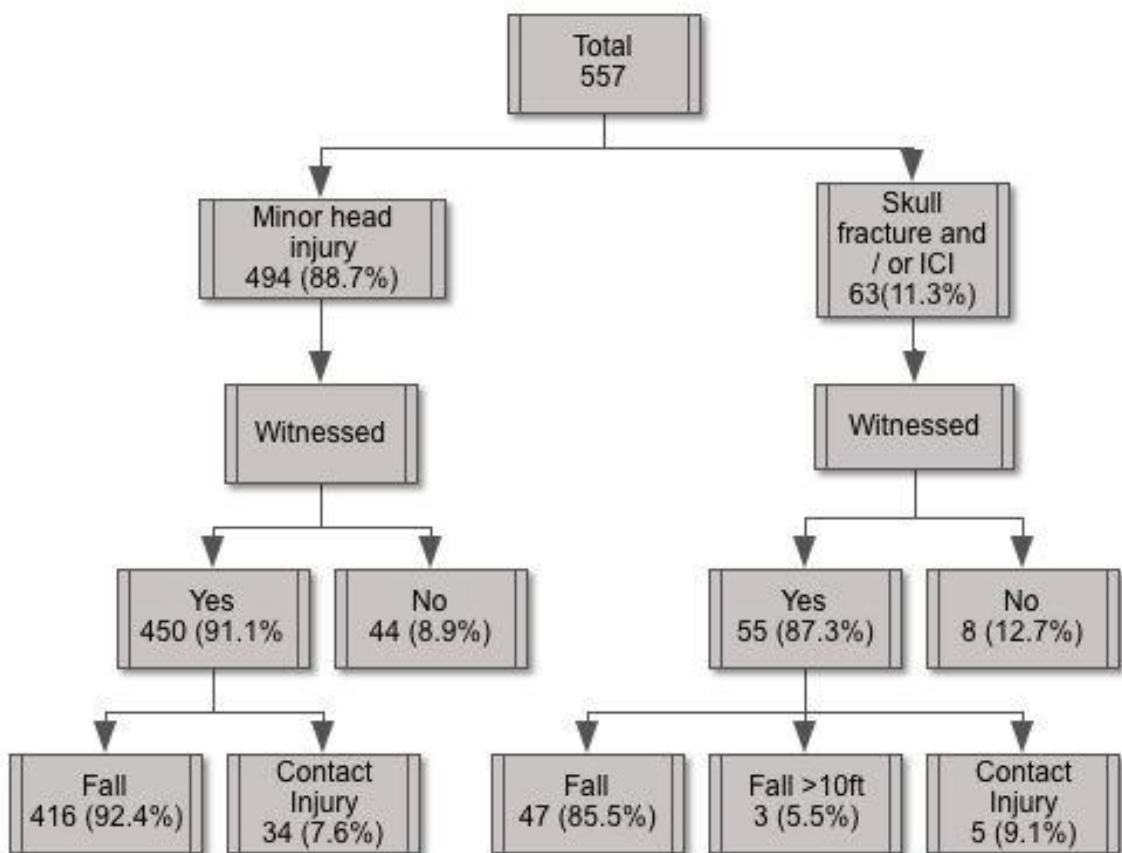


Figure 6. Child head injury cases from the prospective and retrospective data collection.

Gender did not differ significantly between the case and control groups ( $p = 0.642$ , Table 5), with 60.3% of minor head injury and 63.8% of children with a skull and / or ICI being male. Age influenced the risk of injury severity. The mean age of children with a skull fracture and / or ICI was  $11 \pm 2$  months, which was significantly lower than those with a minor and head injury ( $23 \pm 1$  months,

$P < 0.001$ ). A significantly greater proportion of children with a skull fracture and/or ICI were aged  $\leq 12$  months ( $P < 0.001$ , Table 5) compared to those aged between 13-48 months.

### 3.3.1.1 Clinical Data

Twenty-four children had a simple skull fracture (51.1%), of which seven cases had co existing ICI. Complex fractures were documented in nineteen cases and comprised of seven depressed fractures, six multiple fractures, four bilateral fractures and three complex fractures (i.e. crossing the suture line) (note: some children had multiple fracture types). Intracranial injury was seen in 44.7% (21/47) of children with a skull fracture and / or ICI, of which 76.2% (16/21) had an isolated extra axial haemorrhage. The remaining children (5/21) had more than one extra axial haemorrhage or intracerebral injury.

There was a significant difference in the likely site of impact between children with minor head injury and those with a skull fracture and / or ICI ( $P < 0.001$ ). In children with skull fracture and/or ICI, significantly greater proportions were the result of impacts to the parietal/temporal (63.5% vs 5%) and occipital regions (23.1% vs 9.2%), whilst minor head injuries were the result of impacts to the forehead (47.1% vs  $< 10\%$ ) or facial region (24.8% vs 0%, Table 5). Logistic regression indicated parietal/temporal ( $P < 0.001$ ) and occipital impacts ( $P < 0.001$ ) significantly increased the likelihood of a skull fracture and / or ICI compared to forehead impact.

*Table 5. Comparison of clinical and demographic variables and their association with head injury severity from low height falls in children ≤4 years old.*

	<b>Cases: Skull fracture or ICI (n=47) / n (%)</b>	<b>Controls: Minor head injury (n=416) / n(%)</b>	<b>P Value</b>
<b>Gender</b>			
Male	30 (63.8)	251 (60.3)	P=0.642
Female	17 (36.1)	165 (39.7)	
<b>Age (months)</b>	<b>Mean±SE</b>	<b>Mean±SE</b>	
	11 (2)	23 (1)	P<0.001
<b>Age group (months)</b>			P<0.001
Infants (≤12 months)	36 (76.6)	100 (24.0)	
Toddlers (13-48 months)	11 (23.4)	316 (76.0)	
<b>Soft Tissue Injury</b>			P<0.001
Bruise	6 (12.8)	91 (21.9)	
Swelling	27 (57.4)	21 (5.0)	
Bruise and swelling	<10%*	6 (1.4)	
Laceration	0 (0)	61 (14.7)	
<b>GCS<sup>§</sup></b>	<b>(n=27)</b>	<b>(n=392)</b>	
GCS =15	23 (85.2)	391 (99.7)	
GCS<15	4 (14.8)	<1%	
<b>Site of soft tissue injury/ impact</b>	<b>n=(52)<sup>∞</sup></b>	<b>n=(444)<sup>∞</sup></b>	P<0.001
Parietal or temporal	33 (63.5)	22 (5.0)	
Occipital	12 (23.1)	41 (9.2)	
Forehead	<10%*	209 (47.1)	
Vertex	0 (0)	7 (1.6)	
Face	0 (0)	110 (24.8)	
No visible injuries recorded	<10%*	55 (12.4)	
<b>Skull fracture and/or ICI</b>	<b>n</b>		
Simple fracture w/o ICI	17 (36.2)	N/A	
Complex fracture or ICI with or without fracture	30 (63.8)	N/A	

\* Due to small study numbers specific values cannot be stated as it could lead to patients being identified, as directed by ethics committee. <sup>∞</sup> Total number of cases differs due to some cases having more than one soft tissue injury. <sup>§</sup> GCS (Glasgow Coma Score), SE ( Standard Error), ICI ( Intracranial Injury), n (Number of cases).



### 3.3.1.2 Biomechanics of Injury

The mechanism most commonly associated with a minor head injury was a fall from a standing or sitting height (47.8%, 199/416). The logistic regression revealed that that likelihood of a skull fracture and / or ICI increased as the result of fall whilst being carried ( $P < 0.001$ ), and a fall whilst carried on stairs ( $P < 0.001$ ) relative to a fall from a standing or sitting height.

#### Fall Height

Fall height was documented for 133 falls (108 minor head injury and 25 skull fracture and / or ICI). Of these cases, 70.7% ( $n=94/133$ ) were falls from a raised surface (mean  $H_f = 0.66 \pm 0.03m$ ) and 17.3% ( $n=23/133$ ), from carer's arms (mean documented fall height ( $H_f$ ) =  $0.92 \pm 0.10m$ ).

Children with a minor head injury fell from a mean height ( $H_f$ ) =  $0.62 \pm 0.03m$ , a statistically lower height ( $p < 0.001$ ) than those with a skull fracture and / or ICI ( $1.09 \pm 0.07m$ ). The mean height of centre of gravity of the body ( $H_{BCoG}$ ) and  $H_{HCoG}$  for those children with a skull fracture and / or ICI were  $1.12 \pm 0.07m$  and  $1.14 \pm 0.07m$  respectively, both of which were significantly greater ( $p < 0.01$ ) than children with a minor head (mean  $H_{BCoG} = 0.78 \pm 0.03m$ , mean  $H_{HCoG} = 0.89 \pm 0.04m$ ; Table 6). Utilising  $H_{HCoG}$ , no skull fracture/ICI cases were sustained from a height  $< 0.6m$  (Figure 8). Investigating the imputation strategy where the highest possible height was assumed, the mean value for  $H_{HCoGM}$  for those with a skull fracture and / or ICI was  $1.47 \pm 0.09m$ , again significantly greater compared to those with minor head injury (mean  $H_{HCoGM} = 1.15 \pm 0.04m$ ,  $P = 0.001$ ).

Accounting for the carer/parent's potential to overestimate the fall height and utilising the EFH, the mean height for skull fracture and / or ICI fell to  $0.90 \pm 0.05m$  (Table 6), which was significantly greater than those with a minor head injury (mean  $EFH = 0.56 \pm 0.02m$ ,  $P < 0.001$ , Table 6). However incorporating the height of the head,  $EFH_{HCoG}$  for children with a skull fracture and / or ICI was greater compared to those with a minor head injury ( $0.96 \pm 0.06m$  versus  $0.83 \pm 0.04m$ ), but

the difference did not reach statistical significance ( $P=0.071$ ). Again using this height ( $EFH_{HCoG}$ ), no children sustained a skull fracture and / or ICI from a fall height  $<0.55m$ .

### Impact Velocity

The impact velocity of both the body and head were significantly different between the two injury severity groups ( $P<0.05$ ). The mean  $V_{Head}$  was  $4.68m/s$  for the those with a skull fracture and / or ICI and it fell to  $4.05m/s$  for the children with a minor head injury ( $P<0.05$ ).

### Impact Momentum

Neither the momentum of the body nor the momentum of the head was significantly different between the two head injury severity groups ( $P\geq 0.319$ , Table 6).

### Kinetic Energy

The kinetic energy of the body was significantly different between those with a minor head injury and those with a skull fracture and / or ICI ( $83.45J$  vs  $121.58J$ ,  $P=0.034$ , Table 6), however the kinetic energy of the head on impact was not ( $P=0.099$ , Table 6).

### Impact Surface

Impact surface was significantly different between those with a minor head injury and those with a skull fracture and / or ICI ( $P<0.001$ ). The logistic regression showed that only an impact onto wood ( $P=0.004$ ) significantly increased the likelihood of skull fracture/ICIs compared to a carpet impact. A greater proportion of minor head injuries were the result of impacts onto concrete ( $37.9\%$  vs  $17.1\%$ ). However a greater proportion of minor head injuries as the result of an impact onto concrete were to the forehead ( $n=46/80$ ,  $57.5\%$ ), as a consequence of a fall from a standing height ( $n=33/80$ ,  $41.2\%$ ) and in children  $>12$  months ( $n=65/80$ ,  $81.3\%$ ), whereas the skull/ICI cases were to the parietal/temporal area

(n=4/7,57.1%), as a result of a fall from a carer’s arms (n=3/7,42.9%) and in children ≤12 months (n=5/7, 71.4%).

*Table 6. Biomechanical variables influencing the severity of head injury in children ≤ 4years experiencing a low height fall.*

	<b>Cases: Skull fracture or ICI (n=47)</b>	<b>Controls: Minor head injury (n=416)</b>	P Value	Statistical Power / %
<b>Mechanism of Injury †</b>	(n=47) n (%)	(n=416) n (%)	P<0.001	
Fall from standing height	<10%*	199 (47.8)		
Fall from moving object	<10%*	<5%*		
Fall from raised surface	15 (31.9)	136 (32.7)		
Fall whilst being carried	14 (29.8)	19 (4.6)		
Fall involving stairs or steps	<10%	42 (10.1)		
Fall whilst being carried on stairs	13 (27.2)	<5%*		
<b>Surface Impacted †</b>	(n=41) n (%)	(n=211) n (%)	P<0.001	
Concrete	7 (17.1)	80 (37.9)		
Carpet	14 (34.1)	72 (37.1)		
Laminate	6 (14.6)	43 (20.4)		
Wooden	7 (17.1)	6 (2.8)		
Tile	5 (12.2)	9 (4.3)		
<b>Biomechanical Variable §</b>	(n=25) Mean (SE)	(n=108) Mean (SE)		
H <sub>f</sub> / m	1.09 (0.07)	0.62 (0.03)	P <0.001	100.0
H <sub>BCoG</sub> / m	1.12 (0.07)	0.78 (0.03)	P=0.003	99.4
H <sub>HCoG</sub> / m	1.14 (0.07)	0.89 (0.04)	P <0.001	85.1
H <sub>HCoGM</sub> / m	1.47 (0.09)	1.15 (0.04)	P=0.001	

EFH / m	0.90 (0.05)	0.56 (0.02)	P<0.001	100.0
EFH <sub>HCoG</sub> / m	0.96 (0.06)	0.83 (0.04)	P=0.071	99.5
V <sub>Body</sub> / m/s	4.64 (0.15)	3.81 (0.08)	P<0.001	99.9
V <sub>Head</sub> / m/s	4.68 (0.16)	4.05 (0.1)	P<0.05	96.1
M <sub>Body</sub> / kgm/s	49.5 (6.24)	40.99 (1.67)	P=0.319	37.2
M <sub>Head</sub> / kgm/s	7.14 (0.43)	6.74 (0.22)	P=0.405	21.0
KE <sub>Body</sub> / J	121.58	83.45 (4.94)	P=0.034	60.6
KE <sub>Head</sub> / J	17.3 (1.47)	14.71 (0.79)	P=0.099	46.2

† Chi square test used for the statistical comparisons, for cases where expected numbers were small Fishers exact test was used. § Mann and Whitney used to test significance. \* Due to small study numbers specific values cannot be stated as it could lead to patients being identified. H<sub>f</sub> (Documented fall height), H<sub>BCoG</sub> (Height of the body centre of gravity), H<sub>HCoG</sub> (Height of the head centre of gravity Imputation based on lowest possible height, thus cases where position of child unknown assumed to be lying.), H<sub>HCoGM</sub> (Height of the head centre of gravity. Imputation based on highest possible height, thus cases where position of child unknown assumed to be standing.), EFH (Estimated fall height), EFH<sub>HCoG</sub> (Height of the head centre of gravity with estimated fall height incorporated), EFH<sub>HCoGM</sub> (Height of the head centre of gravity with estimated fall height incorporated. Imputation based on highest possible height, thus cases where position of child unknown assumed to be standing.), V<sub>Body</sub> (Impact velocity of body), V<sub>Head</sub> (Impact velocity of head), M<sub>Body</sub> (Momentum of body on impact), M<sub>Head</sub> (Momentum of head on impact), KE<sub>Body</sub> (Kinetic energy of the body on impact), KE<sub>Head</sub> (Kinetic energy of the head on impact). m (Metre). n (Number of cases), SE (Standard error of the mean).

### 3.3.1.3 Injury risk probability

The three different types of injury risk curves for H<sub>HCoG</sub> are shown in Figure 7. The output for the two assumptions used to assess the three different injury risk curves is shown in Table 7. As can be seen the maximum likelihood method has the greatest value for assumption B, and thus the best goodness of fit, however it fails assumption A. Therefore based on the criteria used to assess the injury risk curves, the modified maximum likelihood method was shown to be best, and was used for development of injury risk curves for the other biomechanical variables.

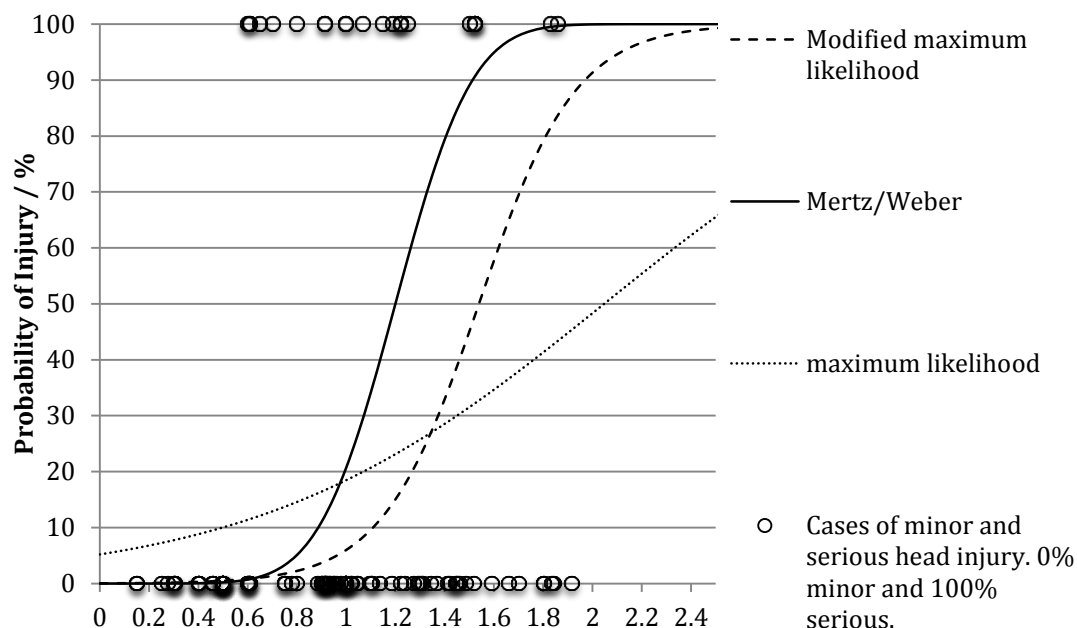


Figure 7. Injury risk curves developed and assessed for the height of the head centre of gravity ( $H_{HCoG}$ )

Table 7. Assessment of the injury risk curves against assumption A and B

Injury risk curve	Assumption A	Assumption B
Maximum likelihood	0.999	-0.456
Modified maximum likelihood	0.05	-0.596
Mertz/Weber	0	-0.831

The logistic regression curve shows the probability of sustaining a skull fracture and / or ICI based on  $H_{HCoG}$  for the range of heights reported (Figure 9), with the  $H_{HCoG}$  for both minor and skull fracture and / or ICI cases shown in Figure 8. The probability of sustaining a skull fracture and / or ICI is estimated as 50% when  $H_{HCoG} = 1.54m$  (CI 1.41m to 1.69m) (Figure 9). Accounting for parents over-estimating fall heights, resulted in the 50% probability of sustaining a skull fracture and /or ICI reducing to 1.4m (CI 1.29m to 1.54m). Finally allowing for the imputation where the highest height of the head was assumed ( $H_{HCoGM}$ ), the 50%

probability increased to  $H_{HCoGM} = 1.77m$  (CI 1.64m to 1.93m). The logistic curves for the biomechanical variables,  $H_f$ ,  $H_{HCoGM}$ , EFH and  $EFH_{HCoG}$  can be seen in Appendix 3.

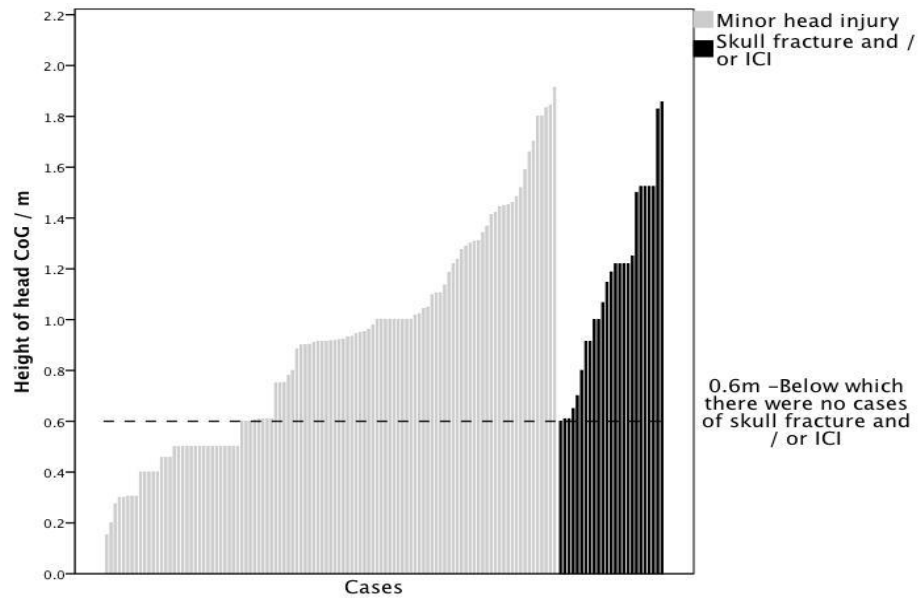


Figure 8. Height of centre of gravity of the head  $H_{HCoG}$  for minor head injury, skull fracture or ICI (Intracranial Injury) resulting from falls in children  $\leq 48$  months of age.

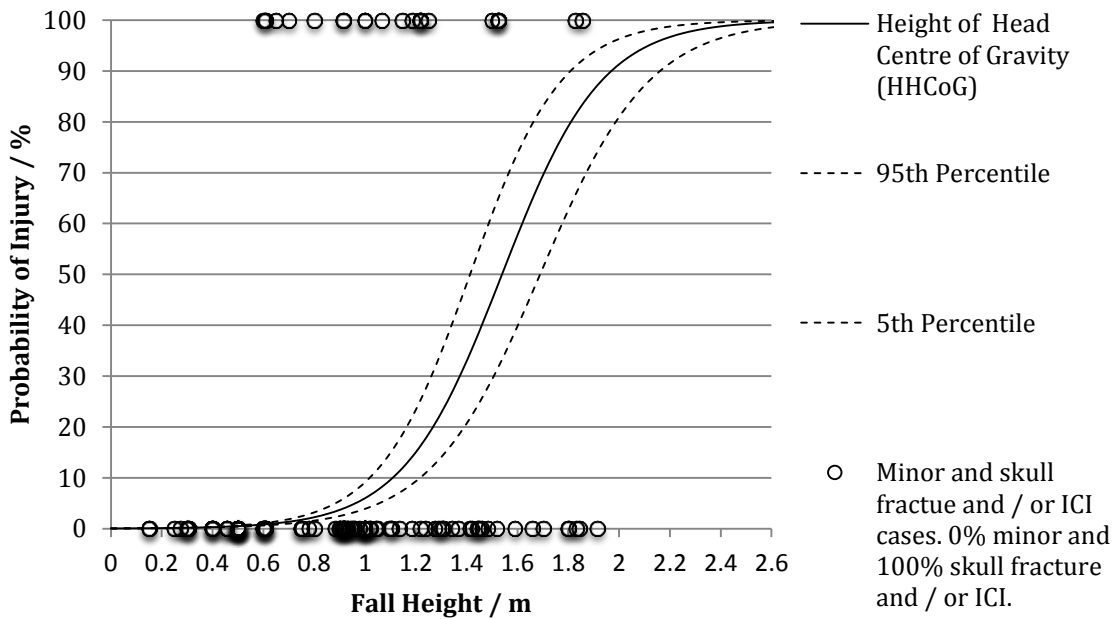


Figure 9. Logistic regression curve illustrating the probability (with 5<sup>th</sup> and 95<sup>th</sup> percentile values) of sustaining a skull fracture or ICI (Intracranial Injury), based on the height of head centre of gravity  $H_{HCoG}$  for the range of heights reported.

### 3.3.1.4 Skull fracture and / or ICI

The cases group consisted of skull fractures and/or intracranial injuries. Consequently simple fractures were compared with complex fracture and / or ICI, to determine if there were significant differences between the two groups in terms of the clinical and biomechanical variables (Table 8). It can be seen in Table 8 that there was no significant difference in terms of age, site of impact, mechanism of injury, surface of impact, or any of the biomechanical variables between the two groups ( $p > 0.067$ ).

*Table 8. Comparison biomechanical variables between children with simple skull fracture and those with complex fracture or intracranial injury with or without fracture in children  $\leq 4$  years experiencing a low height fall.*

	Simple Fracture	Complex fracture or ICI with or without fracture	P Value	Statistical Power / %
Age (months)	Mean $\pm$ SE	Mean $\pm$ SE		
	13.7 (3.6)	9.1 (2.3)	0.326	
Site of Soft Tissue Injury/ Impact †	N= 17	N= 30	0.686	
Parietal or Temporal	10 (58.8)	23 (65.7)		
Occipital	5 (29.4)	7 (20.0)		
Forehead	<10%	4 (11.4)		
No visible injuries recorded	<10%	<10%		
Mechanism of Injury			0.642	
Fall from standing height	0 (0)	<10%		
Fall from raised surface	8 (47.1)	7 (23.3)		
Fall whilst being carried	5 (29.4)	9 (30.0)		
Fall involving stairs or steps	2 (11.8)	<10%		
Fall whilst being carried on stairs	2 (11.8)	11 (36.7)		
Surface Impacted			0.585	
Concrete	4 (23.5)	3 (10.3)		
Carpet	7 (41.2)	7 (24.1)		
Laminate	<10%	5 (17.2)		
Wooden	2 (11.8)	5 (17.2)		
Tile	<10%	4 (13.8)		
Biomechanical Variable	(n=10)	(n=15)		
	Mean (SEM)	Mean (SEM)		



### Chapter 3 – Clinical Assessment of Head Injuries in Young Children

$H_f / m$	1.12 (0.10)	1.07 (0.10)	0.735	6.5
$H_{BCoG} / m$	1.12 (0.10)	1.13 (0.10)	0.939	5.1
$H_{HCoG} / m$	1.12 (0.10)	1.16 (0.11)	0.77	6.1
$EFH / m$	0.92 (0.07)	0.88 (0.07)	0.735	6.8
$EFH_{HCoG} / m$	0.92 (0.07)	0.98 (0.08)	0.619	8.3
$V_{Body} / m/s$	4.63 (0.22)	4.71 (0.22)	0.826	5.3
$V_{Head} / m/s$	1.12 (0.1)	1.16 (0.11)	0.77	7.9
$M_{Body} / kgm/s$	52.18 (6.18)	47.72 (9.72)	0.285	10.4
$M_{Head} / kgm/s$	7.77 (0.73)	6.73 (0.52)	0.244	31.5
$KE_{Body} / J$	124.71 (18.72)	119.49 (30.21)	0.397	6.7
$KE_{Head} / J$	18.56 (2.39)	16.46 (1.9)	0.496	16.9

§ T-test used to test significance.  $H_f$  (Documented fall height),  $H_{BCoG}$  (Height of the body centre of gravity),  $H_{HCoG}$  (Height of the head centre of gravity Imputation based on lowest possible height, thus cases where position of child unknown assumed to be lying.),  $H_{HCoGM}$  (Height of the head centre of gravity. Imputation based on highest possible height, thus cases where position of child unknown assumed to be standing.),  $EFH$  (Estimated fall height),  $EFH_{HCoG}$  (Height of the head centre of gravity with estimated fall height incorporated),  $EFH_{HCoGM}$  (Height of the head centre of gravity with estimated fall height incorporated. Imputation based on highest possible height, thus cases where position of child unknown assumed to be standing.),  $V_{Body}$  (Impact velocity of body),  $V_{Head}$  (Impact velocity of head),  $M_{Body}$  (Momentum of body on impact),  $M_{Head}$  (Momentum of head on impact),  $KE_{Body}$  (Kinetic energy of the body on impact),  $KE_{Head}$  (Kinetic energy of the head on impact).  
ICI ( Intracranial injury), m (metre), n (Number of cases), SE ( Standard error of mean).

### **3.3.1.5 Infant versus toddler**

There were 136 infant (100 minor and 36 skull fracture and / or ICI) and 327 toddler (316 minor and 11 skull fracture and / or ICI) cases. A significantly greater proportion of cases with a skull fracture and / or ICI were infants compared to toddlers ( $P < 0.001$ ). The differences in head injury severity between infants and toddlers in terms of clinical and biomechanical variables are described in Table 9 and Table 10.

#### **3.3.1.5.1 Clinical Data (Infant versus toddler)**

Simple fractures without ICI accounted for 30.6% (11/36) of infant cases and 55% (6/11) of the toddler cases. Complex fractures were documented in 44.4% (16/36) of infant cases and comprised of four depressed fractures, four bilateral and three multiple fractures (note: some children had multiple fracture types). Intracranial injury was seen in 47.2% (17/36) of the infants, of which 58.8% (10/17) had an isolated extra axial haemorrhage.

The site of the soft tissue injury was significantly different between infants and toddler for both those with a minor head injury and those with a skull fracture and / or ICI ( $P \leq 0.001$ ). A greater proportion of parietal/temporal impacts leading to a skull fracture and/or ICI were in infants (75% vs 18.2%, Table 9) and a greater proportion of occipital impacts were in toddlers (54.5% vs 16.7%, Table 9). A greater proportion of children with a minor head injury as the result of a forehead impact were toddlers (53.2% vs 38.0%, Table 9)

*Table 9. Comparison of clinical variables between infants and toddlers and their association with head injury severity (Minor head injury and skull fracture and / or ICI) from a low height fall.*

	Skull fracture and / or ICI			Minor head injury		
	Infant / n(%)	Toddler / n (%)	P value	Infant / n(%)	Toddler / n (%)	P value
Site of Soft Tissue Injury/ Impact †	n=36	n=11	0.001			<0.001
No visible injuries	0 (0.0)	2 (18.2)		33 (33.0)	22 (7.0)	
Forehead	3 (8.3)	<10%		38 (38.0)	168 (53.2)	
Parietal or Temporal	27 (75)	2 (18.2)		4 (4.0)	17 (5.4)	
Occiput	6 (16.7)	6 (54.5)		10 (10.0)	30 (9.5)	
Face	0 (0.0)	<10%		15 (15.0)	72 (22.8)	
Vertex	0 (0.0)	<10%		0 (0)	7 (2.2)	
Skull fracture and / or ICI			0.171			
Simple fracture w/o ICI	11 (30.6)	6 (54.5)		N/A	N/A	N/A
Complex fracture or ICI with or without ICI	25 (69.4)	5 (45.5)		N/A	N/A	N/A

### 3.3.1.5.2 Biomechanical variables (Infant versus toddler)

The mechanism of head injury was significantly different between infants and toddlers for both those with a minor head injury ( $P < 0.001$ ) and those with a skull fracture and / or ICI ( $P = 0.016$ ), Table 10. The most common mechanism leading to minor head injury in infants was a fall from a raised surface (46%, 46/100, Table 10) and for a toddlers it was fall from a standing height (52%, 168/316). A greater proportion of children with a skull fracture and / or ICI as a result of fall whilst being carried on the stairs were infants compared to toddlers (36.1% versus 0%,

Table 10) and a significantly greater proportion of toddlers with a skull fracture and / or ICI had a fall from raised surface (63.6% versus 22.2%, Table 10).

#### 3.3.1.5.2.1 Surface (Infant versus toddler)

Surface impacted was significantly different between infants and toddlers for the minor head injuries ( $P=0.002$ ) but not for the children with a skull fracture and / or ICI (0.541). A greater proportion of minor head injuries as the result of impact onto carpet were infants compared to toddlers (48.5% versus 28.1%, Table 10), whereas a greater proportion of toddler minor head injuries were the results of impacts onto concrete (46.8% versus 20.8%, Table 10). Investigating only head injuries in infants, there was no significant difference in impact surface between those with minor head injury and those with a skull fracture and / or ICI (0.095) but investigating only toddlers impact surface was significantly different between the cases and control groups ( $P=0.005$ ).

#### 3.3.1.5.2.2 Fall Height (Infant versus toddler)

A fall height was recorded for 61 falls involving infants (45 Minor and 16 Skull fracture and / or ICI) and 72 cases involving toddlers (63 Minor and 9 Skull fracture and / or ICI). The mean height of the centre of gravity of the head of the infants with a skull fracture and / or ICI was  $1.06 \pm 0.09\text{m}$  and this was lower compared to toddlers but this difference was not significant ( $P=0.112$ ), Table 10. However  $H_{\text{HCoG}}$  was significant lower for infants with a minor head injury compared to toddlers ( $P<0.001$ ), Table 10. Utilising  $EFH_{\text{HCoG}}$  the mean height of the infants with a skull fracture and / or ICI was  $0.89 \pm 0.06\text{m}$ . Based on  $H_{\text{HCoG}}$  no infants with a skull fracture and / or ICI occurred from  $<0.61\text{m}$  and using  $EFH_{\text{HCoG}}$  none were  $<0.56\text{m}$ .

#### 3.3.1.5.2.3 Impact Velocity (Infant versus toddler)

Impact velocity for both the body ( $V_{\text{Body}}$ ) and head ( $V_{\text{Head}}$ ) were significantly different between infants and toddlers for the cases with minor head injury

( $P \leq 0.003$ ), however not for the cases with skull fracture and / or ICI ( $P \geq 0.074$ ), Table 10.

*Table 10. Differences in biomechanical variables between infants and toddlers influencing the severity of head injury experiencing a low height fall.*

	Skull fracture and / or ICI			Minor head injury		
	Infant / n(%)	Toddler / n(%)	P value	Infant / n(%)	Toddler / n(%)	P value
<b>Mechanism of Injury</b>			0.016			<0.001
Fall standing height	<10%	<10%		31 (31)	168 (53.2)	
Fall from moving object	0 (0)	0 (0)		<10%	16 (5.1)	
Fall from raised surface	8 (22.2)	7 (63.6)		46 (46)	90 (28.5)	
Fall from person arms	12 (33.3)	2 (18.2)		15 (15)	4 (1.3)	
Fall involving stairs	<10%	<10%		5 (5)	37 (11.7)	
Fall from person arms on stairs	13 (36.1)	0 (0)		<10%	<10%	
<b>Surface Impacted</b>			0.541			0.004
Concrete Floor	5 (15.2)	2 (25)		15 (20.8)	65 (46.8)	
Carpet Floor	12 (36.4)	2 (25)		33 (45.8)	39 (28.1)	
Laminate	6 (18.2)	<20%		18 (25)	25 (18.0)	
Wooden	5 (15.2)	2 (25)		3 (4.2)	3 (2.2)	
Tile	4 (12.1)	<20%		3 (4.2)	6 (4.3)	
<b>Biomechanical Variable</b>	n=16	n=9		n=16	n=9	
H <sub>f</sub> / m	1.02 (0.09)	1.21 (0.1)	0.215	0.61 (0.04)	0.63 (0.04)	0.907
H <sub>BCoG</sub> / m	1.04 (0.09)	1.27 (0.1)	0.074	0.67 (0.05)	0.85 (0.04)	0.003
H <sub>HCoG</sub> / m	1.06 (0.09)	1.3 (0.12)	0.112	0.72 (0.06)	1.01 (0.05)	<0.001
EFH / m	0.84 (0.07)	0.98 (0.07)	0.215	0.55 (0.03)	0.57 (0.03)	0.907

### Chapter 3 – Clinical Assessment of Head Injuries in Young Children

EFH <sub>HCoG</sub> / m	0.89 (0.06)	1.08 (0.1)	0.108	0.66 (0.05)	0.95 (0.05)	<0.001
V <sub>Body</sub> / m/s	4.47 (0.19)	4.94 (0.23)	0.074	3.52 (0.13)	4.01 (0.1)	<0.001
V <sub>Head</sub> / m/s	4.49 (0.19)	5 (0.25)	0.117	3.62 (0.15)	4.36 (0.12)	0.003

H<sub>f</sub> (Documented fall height), H<sub>BCoG</sub> (Height of the body centre of gravity), H<sub>HCoG</sub> (Height of the head centre of gravity Imputation based on lowest possible height, thus cases where position of child unknown assumed to be lying.), H<sub>HCoGM</sub> (Height of the head centre of gravity. Imputation based on highest possible height, thus cases where position of child unknown assumed to be standing.), EFH (Estimated fall height), EFH<sub>HCoG</sub> (Height of the head centre of gravity with estimated fall height incorporated), EFH<sub>HCoGM</sub> (Height of the head centre of gravity with estimated fall height incorporated. Imputation based on highest possible height, thus cases where position of child unknown assumed to be standing.), V<sub>Body</sub> (Impact velocity of body), V<sub>Head</sub> (Impact velocity of head), M<sub>Body</sub> (Momentum of body on impact), M<sub>Head</sub> (Momentum of head on impact), KE<sub>Body</sub> (Kinetic energy of the body on impact), KE<sub>Head</sub> (Kinetic energy of the head on impact). ICI ( Intracranial injury), m (metre), n (Number of cases), SE ( Standard error of mean).

### 3.4 Discussion

Current literature suggests that low height falls rarely result in skull fracture and/or intracranial injury<sup>9, 10, 15, 21, 23, 27, 48</sup>. This comprehensive analysis of young children with head injury from low height falls has identified variables that are associated with skull fracture and/or ICI and provides additional evidence that they do not occur below 0.6m (based on CoG of the head) but can occur above this height<sup>12-14, 18, 53</sup>. This study has, compared key biomechanical variables, in head injuries that have and have not resulted in material failure thereby permitting the definition of injury thresholds<sup>57</sup>.

#### 3.4.1 Fall Height

Previous studies have attempted to define fall height thresholds for skull fracture in children<sup>9, 10, 12, 15, 23, 53, 58</sup>. In this study, no skull fracture and / or ICI occurred from a  $H_{HCoG} < 0.6m$ . Taking into account parents' over estimation of height fallen resulted in a minimum fall height  $EFH_{HCoG} < 0.55m$ . Thus, a height of between 0.55-0.6m is proposed as a potential threshold for when risk of sustaining a skull fracture and/or ICI increases. This threshold coincides with existing infant skull fracture data, where experimental infant cadaver drop tests have inferred that a skull fracture threshold exists between 0.3m<sup>59</sup> and 0.82m<sup>34, 35</sup>. Considering our data against the lowest bounds (i.e. 0.3m), no skull fracture and/or ICIs were reported from falls at this height. Considering the upper bounds presented in the literature where 42% of infant cadaver heads impacted from 0.82m exhibited skull fracture<sup>34, 35</sup>, indicating that 0.82m exceeds a skull fracture threshold. Hence, our proposed 0.55-0.6m threshold corresponds to comparable published data, which is broadly supported by our theoretical regression analysis. Whilst differing biomechanical thresholds exist for skull fracture and ICI, a comparison between isolated skull fracture and complex fracture and or ICI resulting in no significant difference between the two, indicating the threshold is applicable across different forms of head injury severity.

Published studies have also identified thresholds to define low height falls, typically based upon the head height<sup>10, 12, 18</sup> or surface height<sup>47, 60</sup>. Various thresholds have been proposed that broadly attempt to define a boundary between those that resulted in an anatomical material failure and those that have not (0.91m<sup>8, 11, 12</sup>, 1m<sup>13</sup>, 1.22m<sup>9, 10, 14, 15</sup>, or 1.52m<sup>23</sup>). This is perhaps due to inconsistent estimations in the biomechanical variables (e.g. a fall from a sofa or bed has been variably classified as <0.91m to <1.22m<sup>8, 10-13, 15, 24</sup>). Whilst this variation in thresholds limits a direct comparison of data, children in these studies sustained simple skull fractures below the defined thresholds, providing further justification for the proposed 0.6m head injury threshold. It should be noted that Leventhal *et al*<sup>16</sup> did document skull fractures from falls <0.61m, although the fall height definition lacked clarity. Similarly the lowest reported fall height for a skull fracture by Thomas *et al*<sup>22</sup> was 0.5m, but again the fall height definition was unclear.

### **3.4.2 Fall from carer's arms**

Almost one-third (29.8%) of those children sustaining a skull fracture and/or ICI in this data set fell from a carer's arms, from a mean height of 0.92 ± 0.10m. Previous authors documented an association between this mechanism and skull fracture or ICI<sup>15, 42</sup>. Whilst this ratio is consistent with previous literature<sup>12</sup>, there is (unsurprisingly) a range of fall heights associated with such fall scenarios (>0.9m to >1.2m<sup>10, 12</sup>). In some instances, falls from arms were <0.9m, although outcomes were not reported in these studies<sup>12, 16</sup>. The increased risk from this particular mechanism may be attributed to a number of factors including an increased height and potential hitting more vulnerable aspects of the head such as the parietal/temporal area.

### **3.4.3 Anatomical Site of Impact**

The site of impact contributes to a range of potential injury severity. The temporal or parietal and occipital areas in this dataset were associated with skull fracture



and/or ICI. While parietal fractures are common in children with an accidental injury, the site of impact has not previously been systematically recorded<sup>16</sup>. Localised bone thickness and stiffness characteristics may potentially be why parietal and occipital regions are greater risk to fracture compared to frontal areas<sup>61-63</sup>, however this will be investigated further using biomechanical models. Temporal and temporoparietal impacts also have shown to be commonest location of EDH<sup>38</sup>. This could potentially be attributed to the location of the middle meningeal artery.

#### **3.4.4 Impact Surface**

This study indicates that impacts onto wooden surfaces were significantly associated with children sustaining a skull fracture and/or ICI, data that is consistent with anthropomorphic test device studies<sup>2, 19, 62, 64, 65</sup>. However there is nothing to suggest why a wooden impact would be more injurious than a concrete or a tile impact. Also a greater proportion of minor head injuries were the result of impacts onto concrete. This counterintuitive result may be due to a complex interplay of factors, such as age, height fallen, surface and anatomical site of impact. The relationship between minor head injury from falls onto concrete and falls from standing, frontal impacts in toddlers would go some way to support this theory. It could also potentially be due to parental anxiety and an increased likelihood to seek clinical reassurance when a child has a head injury from a fall onto concrete.

#### **3.4.5 Biomechanical Variables**

Relatively few other epidemiological studies investigating falls have considered variables other than height that influence head injury severity<sup>18, 21</sup>. Consistent with previous authors, momentum of the body did not significantly differ between the two head injury severity groups<sup>21</sup>. Velocity of the body on impact however did, which is an agreement with previous authors<sup>18</sup>. Thompson *et al*<sup>18</sup> concluded that the potential energy did not significantly change between minor and

moderate/serious head injuries, which differ from this research where kinetic energy (equivalent to potential energy) of the body did. This study uniquely assessed the head in isolation on impact, however neither impact momentum or kinetic energy of the head significantly changed between the head injury groups. Even though a head does not impact in isolation in a real scenario, cadavers experimental are often conducted with just a head, thus it allows for cross comparison. Whilst implementation of these variables (kinetic energy and momentum) could potentially be difficult, they could be used to investigate other non-fall impact trauma scenarios from a forensic perspective.

#### **3.4.6 Child's Age**

The data shows that a skull fracture and/or ICI were more prevalent in  $\leq 12$  month old infants as a result of an accidental fall. Other studies note an age-related susceptibility of children sustaining serious head injury from 'short falls'<sup>12, 16, 66</sup>, whilst Ibrahim *et al*<sup>12</sup> noted that infants were more likely than a toddler to be hospitalized, have a soft tissue injury and a skull fracture from falls  $< 0.91\text{m}$ . In the comparison between infants and toddlers with skull fracture and / or ICI in this study, the height of the centre of gravity was lower but not significantly. Whilst potentially indicating a decrease in the threshold for younger infants, the minimum height for the cases with skull fracture and/or ICI for this age was between 0.56-0.61m, thus similar to the overall age. Differences in the mechanism of injury and surface impacted between infants and toddlers were seen in this study, further highlighting age related differences. Investigating only infant head injuries, surface impacted did not significantly affect head injury severity, highlighting that the effect of surface varies with age. Anatomical site of impact also significantly varied between infants and toddlers with skull fracture and / or ICI, potentially showing infants are maybe more susceptible to skull fracture and/or ICI from a parietal/temporal impact.

The published literature on the potential injuries from a low height fall indicates that while infrequent, injuries including EDH, SDH and SAH can occur<sup>9, 10, 15, 21, 23, 27,</sup>

<sup>48</sup>. While extra axial haemorrhages were identified in the majority of the cases that had an ICI, there were no interhemispheric or multiple subdural haemorrhages as are classically seen in abusive and other head trauma <sup>36</sup>.

### **3.4.7 Implementation**

This study highlights some key variables that influence the likelihood of a skull fracture and / or ICI in young children, providing greater clinical guidance. Hence, variables that could be recorded when evaluating a young child with head injury include the age of the child, the surface impacted, anatomical site of impact and fall height based on the head CoG. The height of the head CoG relative to the weight bearing surface could be calculated based upon the reported position of the child to estimate the height of the head and through the use of standard sitting or standing height charts as is appropriate. The logistic regression curve could be used to estimate the likelihood of skull fracture and / or ICI when the height of the CoG of the head has been estimated.

### **3.4.8 Limitations**

A limitation of this study was the small number of cases with a skull fracture and/or ICI, as a result of a fall, highlighting their rarity, with only 47 presenting to a regional pediatric unit, serving a population of approximately 465,000 over a ten-year period. This resulted in a low statistical power when comparing the extent of the head injury (simple fracture versus complex or ICI with or without fracture) and limited a more detailed analysis of the biomechanics of low height falls with respect to explicit neuropathological patterns of intra cranial injury. The small sample size also restricted the development of a multi variable logistic model, consequently only height was included in the logistic model. However a separate analysis was completed purely on children aged  $\leq 12$  month, thereby highlighting the changing affect of the covariates. As with any retrospective data collection, the skull fracture and/or ICI cases were limited by the quality of the data recorded in the patient case notes<sup>16</sup>. As such, the accuracy and level of detail of the

information meant that certain comparisons, such as the initial position of the child, prior to the fall, could not be assessed in all cases. Consistent with previous literature, the heights used in this study were those reported by carer's, however the effect of parents incorrectly estimating height was incorporated into the analysis. The prospective aspect of the data collecting in this study were those seen at the ED and therefore, represent those children whose parents were sufficiently concerned to attend hospital, which may skew the data, since it may not reflect all minor head trauma that this population sustains.

### 3.5 Conclusion

This study provides a unique insight into the distinguishing biomechanical variables between children aged  $\leq$  four years old who have and have not had a skull fracture or ICI from an accidental fall. Skull fracture and/or ICI were significantly associated with:

- Fall height, where the head centre of gravity was  $>0.55-0.6\text{m}$ .
- Age  $\leq 12$  months.
- Site of impact on the head, namely impacts to the parietal/temporal, or occipital area.
- Surface impacted.

This study highlights the need to record full details of falls when children present with a head injury, including the height/object from which they fell, their position prior to the fall and the surface and body part on which they impacted. These features have the potential to inform both clinical decisions, when assessing young children with a head injury. The clinical and biomechanical differentiating variables provided variables to assess for the physical and computational models. The clinical fall height threshold of between  $0.55-0.6\text{m}$  provides a marker with which current biomechanical thresholds can be assessed.

### 3.6 References

1. Klinich K, Hulbert G, Schneider L. Estimating infant head injury criteria and impact response using crash reconstruction and finite element modeling. *Stapp car crash journal*. 2002;46:165.
2. Van Ee C, Moroski-Browne B, Raymond D, Thibault K, Hardy W, Plunkett J. Evaluation and refinement of the CRABI-6 anthropomorphic test device injury criteria for skull fracture. 2009: ASME.
3. Depreitere B, Van Lierde C, Sloten JV, Van Audekercke R, Van Der Perre G, Plets C, et al. Mechanics of acute subdural hematomas resulting from bridging vein rupture. *Journal of neurosurgery*. 2006;104(6):950-956.
4. Löwenhielm P. Dynamic properties of the parasagittal bridging veins. *International Journal of Legal Medicine*. 1974;74(1):55-62.
5. Löwenhielm P. Strain tolerance of the vv. cerebri sup.(bridging veins) calculated from head-on collision tests with cadavers. *Zeitschrift für Rechtsmedizin*. 1974;75(2):131-144.
6. King AI, Yang KH, Zhang L, Hardy W, Viano DC. Is head injury caused by linear or angular acceleration. IRCOBI conference; 2003. p. 1-12.
7. Bilo RA, Robben SG, van Rijn RR. *Forensic aspects of paediatric fractures*: Springer; 2010.
8. Helfer RE, Slovis TL, Black M. Injuries Resulting When Small Children Fall Out of Bed. *Pediatrics*. 1977;60(4):533-535.
9. Chadwick DL, Chin S, Salerno C, Landsverk J, Kitchen L. Deaths from Falls in Children: How Far is Fatal? *The Journal of Trauma*. 1991;31(10):1353-1355.
10. Duhaime AC, Alario AJ, Lewander WJ, Schut L, Sutton LN, Seidl TS, et al. Head injury in very young children: mechanisms, injury types, and ophthalmologic findings in 100 hospitalized patients younger than 2 years of age. *Pediatrics*. 1992;90(2):179.
11. Hettler J, Greenes DS. Can the initial history predict whether a child with a head injury has been abused? *Pediatrics*. 2003;111(3):602-607.
12. Ibrahim NG, Wood J, Margulies SS, Christian CW. Influence of age and fall type on head injuries in infants and toddlers. *International Journal of Developmental Neuroscience*. 2011.
13. Park SH, Cho BM, Oh SM. Head injuries from falls in preschool children. *Yonsei Medical Journal*. 2004;45:229-232.
14. Reece RM, Sege R. Childhood Head Injuries: Accidental or Inflicted? *Arch Pediatr Adolesc Med*. 2000;154(1):11-15.
15. Tarantino CA, Dowd MD, Murdock TC. Short vertical falls in infants. *Pediatric emergency care*. 1999;15(1):5.
16. Leventhal JM, Thomas SA, Rosenfield NS, Markowitz RI. Fractures in young children: distinguishing child abuse from unintentional injuries. *Archives of Pediatrics and Adolescent Medicine*. 1993;147(1):87.
17. Duhaime A, Margulies S, Durham S, O'Rourke M, Golden J, Marwaha S, et al. Maturation-dependent response of the piglet brain to scaled cortical impact. *Journal of Neurosurgery: Pediatrics*. 2000;93(3).

18. Thompson AK, Bertocci G, Rice W, Pierce MC. Pediatric short-distance household falls: Biomechanics and associated injury severity. *Accident Analysis and Prevention*. 2011;43(1):143-150.
19. Cory C, Jones M. Development of a simulation system for performing in situ surface tests to assess the potential severity of head impacts from alleged childhood short falls. *Forensic Science International*. 2006;163(1-2):102-114.
20. Lee MC, Haut RC. Insensitivity of tensile failure properties of human bridging veins to strain rate: Implications in biomechanics of subdural hematoma. *Journal of Biomechanics*. 1989;22(6-7):537-542.
21. Lyons TJ, Oates RK. Falling out of Bed: A Relatively Benign Occurrence. *Pediatrics*. 1993;92(1):125-127.
22. Thomas AG, Hegde SV, Dineen RA, Jaspán T. Patterns of accidental craniocerebral injury occurring in early childhood. *Archives of disease in childhood*. 2013;98(10):787-792.
23. Williams RA. Injuries in Infants and Small Children Resulting from Witnessed and Corroborated Free Falls. *The Journal of Trauma*. 1991;31(10):1350-1352.
24. Gruskin KD, Schutzman SA. Head trauma in children younger than 2 years: are there predictors for complications? *Archives of pediatrics & adolescent medicine*. 1999;153(1):15.
25. Greenes DS, Schutzman SA. Infants with isolated skull fracture: what are their clinical characteristics, and do they require hospitalization? *Annals of emergency medicine*. 1997;30(3):253-259.
26. ROS SP, CETTA F. Are skull radiographs useful in the evaluation of asymptomatic infants following minor head injury? *Pediatric emergency care*. 1992;8(6):328.
27. Macgregor DM. Injuries associated with falls from beds. *Injury Prevention*. 2000;6(4):291-292.
28. Wood JN, Christian CW, Adams CM, Rubin DM. Skeletal surveys in infants with isolated skull fractures. *Pediatrics*. 2009;123(2):e247-e252.
29. Hobbs CJ. Skull fracture and the diagnosis of abuse. *Archives of Disease in Childhood*. 1984;59(3):246.
30. Meservy CJ, Towbin R, McLaurin RL, Myers PA, Ball W. Radiographic characteristics of skull fractures resulting from child abuse. *American Journal of Roentgenology*. 1987;149(1):173.
31. Stewart G, Meert K, Rosenburg N. Trauma in infants less than three months of age. *Pediatric emergency care*. 1993;9(4):199.
32. Hiss J, Kahana T. The medicolegal implications of bilateral cranial fractures in infants. *The Journal of Trauma*. 1995;38(1):32.
33. Arnholz D, Hymel KP, Hay TC, Jenny C. Bilateral pediatric skull fractures: Accident or abuse? *The Journal of Trauma*. 1998;45(1):172.
34. Weber W. [Experimental studies of skull fractures in infants]. *Zeitschrift für Rechtsmedizin Journal of legal medicine*. 1984;92(2):87.
35. Weber W. [Biomechanical fragility of the infant skull]. *Zeitschrift für Rechtsmedizin Journal of legal medicine*. 1985;94(2):93.

36. Kemp A, Jaspan T, Griffiths J, Stoodley N, Mann M, Tempest V, et al. Neuroimaging: what neuroradiological features distinguish abusive from non-abusive head trauma? A systematic review. *Archives of disease in childhood*. 2011;96(12):1103-1112.
37. Shugerman RP, Paez A, Grossman DC, Feldman KW, Grady MS. Epidural hemorrhage: is it abuse? *Pediatrics*. 1996;97(5):664-668.
38. Schutzman SA, Barnes PD, Mantello M, Scott RM. Epidural hematomas in children. *Annals of emergency medicine*. 1993;22(3):535-541.
39. Feldman KW, Bethel R, Shugerman RP, Grossman DC, Grady MS, Ellenbogen RG. The cause of infant and toddler subdural hemorrhage: a prospective study. *Pediatrics*. 2001;108(3):636.
40. Hymel KP, Rumack CM, Hay TC, Strain JD, Jenny C. Comparison of intracranial computed tomographic (CT) findings in pediatric abusive and accidental head trauma. *Pediatric radiology*. 1997;27(9):743-747.
41. Vinchon M, de Foort-Dhellemmes S, Desurmont M, Delestret I. Confessed abuse versus witnessed accidents in infants: comparison of clinical, radiological, and ophthalmological data in corroborated cases. *Child's nervous system*. 2010;26(5):637-645.
42. Claudet I, Gurrera E, Honorat R, Rekhroukh H, Casasoprana A, Grouteau E. [Home falls in infants before walking acquisition]. *Archives de pediatrie: organe officiel de la Societe francaise de pediatrie*. 2013;20(5):484-491.
43. Warrington SA, Wright CM, Team AS. Accidents and resulting injuries in premobile infants: data from the ALSPAC study. *Archives of Disease in Childhood*. 2001;85(2):104-107.
44. England PHOi. [http://www.apho.org.uk/default.aspx?QN=INJURY\\_PAGE02](http://www.apho.org.uk/default.aspx?QN=INJURY_PAGE02). Accessed 11/03/2013, 2013.
45. NICE. Head Injury Triage, assessment, investigation and early management of head injury in infants, children and adults. <http://www.nice.org.uk/nicemedia/live/11836/36260/36260.pdf>. Published 2007. Accessed 01/04/2011, 2011.
46. Dunning J, Daly JP, Lomas J, Lecky F, Batchelor J, Mackway-Jones K. Derivation of the children's head injury algorithm for the prediction of important clinical events decision rule for head injury in children. *Archives of disease in childhood*. 2006;91(11):885-891.
47. IDB. The Injury Database (IDB) version 1.1: Consumer Safety Institute. Amsterdam and AIHW National Injury Surveillance Unit, Adelaide; 2005.
48. Nimityongskul P, Anderson LD. The likelihood of injuries when children fall out of bed. *Journal of Pediatric Orthopaedics*. 1987;7(2):184.
49. Snyder RG, Spencer ML, Owings CL, Schneider LW. Physical Characteristics of Children. *US Consumer Product Safety Commission, Bethesda, MD*. 1975.
50. WHO. The WHO Child Growth Standards. <http://www.who.int/childgrowth/standards/en/>. Published 2011. Accessed 18/8/2011, 2011.
51. Lloyd J, Willey EN, Galaznik JG, Lee III WE, Luttner SE. Biomechanical Evaluation of Head Kinematics During Infant Shaking Versus Pediatric Activities of Daily Living. *Journal of Forensic Biomechanics*. 2011.



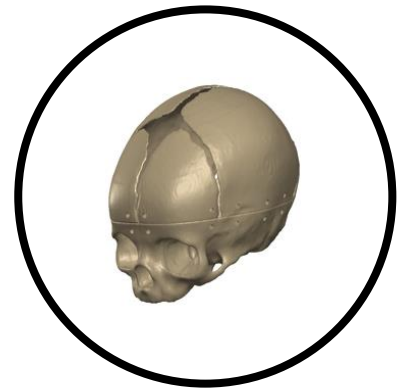
52. Loyd AM, Nightingale R, Bass CR, Mertz HJ, Frush D, Daniel C, et al. Pediatric head contours and inertial properties for ATD design. *Stapp car crash journal*. 2010;54:167.
53. Plunkett J. Fatal pediatric head injuries caused by short-distance falls. *The American Journal of Forensic Medicine and Pathology*. 2001;22(1):1.
54. Nakahira Y, Furukawa K, Niimi H, Ishihara T, Miki K, Matsuoka F. A combined evaluation method and a modified maximum likelihood method for injury risk curves. 2000.
55. Banglmaier R, Wang L, Prasad P. Various statistical methods for the analysis of experimental chest compression data. *Proceedings of the American Statistical Association, Section on Physical & Engineering Sciences*. 2002.
56. Mertz H, Weber D. Interpretations of the impact responses of a three-year-old child dummy relative to child injury potential. *Automatic Occupant Protection Systems*. 1988.
57. Alem NM, Nusholtz GS, Melvin JW. Head and neck response to axial impacts 1984. Report No.: 0898837111.
58. Hall JR, Reyes HM, Horvat M, Meller JL, Stein R. The mortality of childhood falls. *The Journal of Trauma*. 1989;29(9):1273.
59. Prange M, Luck J, Dibb A, Van Ee C, Nightingale R, Myers B. Mechanical properties and anthropometry of the human infant head. *Stapp car crash journal*. 2004;48:279.
60. ICECI. International Classification of External Causes of Injuries (ICECI) version 1.2: Consumer Safety Institute. Amsterdam and AIHW National Injury Surveillance Unit, Adelaide; 2004.
61. Margulies S, Coats B. Experimental Injury Biomechanics of the Pediatric Head and Brain. *Pediatric Injury Biomechanics*: Springer; 2013. p. 157-189.
62. Coats B, Margulies S. Potential for head injuries in infants from low-height falls. *Journal of Neurosurgery: Pediatrics*. 2008;2(5):321-330.
63. Coats B, Margulies S. Material properties of human infant skull and suture at high rates. *Journal of neurotrauma*. 2006;23(8):1222-1232.
64. Prange M, Coats B, Duhaime A, Margulies S. Anthropomorphic simulations of falls, shakes, and inflicted impacts in infants. *Journal of Neurosurgery: Pediatrics*. 2003;99(1).
65. Ibrahim N, Margulies S. Biomechanics of the toddler head during low-height falls: an anthropomorphic dummy analysis. *Journal of Neurosurgery: Pediatrics*. 2010;6(1):57-68.
66. Crowe LM, Catroppa C, Anderson V, Babl FE. Head injuries in children under 3 years. *Injury*. 2012.

---

Chapter 4 –Physical

Modelling of Infant

Head Impacts



## 4.1 Introduction

It has been demonstrated that a skull fracture and / or ICI in a young child, as the result of a postulated low height fall is a contentious issue. Previous researchers have aimed to determine a threshold for skull fracture and / or ICI, based on the height of the fall, as described in section 3.1.1. However, due to inconsistencies in the reporting of fall heights (0.91-1.52m) and the seriousness of the resulting head injuries from a low height fall, there is no clear ‘cut off’ for a skull fracture and / or ICI apparent in the literature. Chapter 3 addressed this issue, detailing the establishment of 0.6m as a potential threshold for skull fracture and / or ICI. Other significant variables were age, site of impact and surface impacted.

### 4.1.1 Background

An anthropomorphic testing device (ATD) is often used by biomechanical engineers when trying to assess the likelihood of an injury from a given incident. The impact response of the ATDs is often quantified in terms of kinematic variables associated with head injury severity, generalised into translational and rotational accelerations, as previously discussed. The use of an ATD has been used in the automotive industry to act as a surrogate to cadaver testing. The development of ATDs ultimately led to the development of the Hybrid III dummy, aimed at 50<sup>th</sup> percentile adult. Post the development of this dummy, a family of dummies were developed and the Child Response Airbag Interaction (CRABI) ATDs were aimed at young children<sup>1,2</sup> (6, 12, 18 month dummies). In conjunction with these commercially available ATDs initially designed for the automotive industry, research institutes have developed their own specific ATDs<sup>3-5</sup>. The literature was reviewed to evaluate where ATDs aimed at young children had been used to investigate low height falls.

Duhaime *et al*<sup>4</sup> was the first to develop an ATD aimed at child protection research, where they investigated differences in kinematic variables between shaking with or without impact. However Prange *et al*<sup>5</sup> was the first to use this approach to investigate low height falls in young children, where the authors developed a 1.5

month old dummy. The authors measured the rotational velocity, rotational acceleration and duration of impact of the head when the ATD was impacted onto the occiput from the supine position from three different heights (0.3m, 0.9m and 1.5m) onto 3 different domestic surfaces (crib mattress, carpet and concrete). The study concluded that the peak rotational velocity increased with falls onto harder surfaces and the duration of the impact decreased from the greater heights, though the acceleration and velocity were not significantly different for any surface when comparing the 0.9m to the 1.5m falls. Interestingly the response of the carpet and concrete were indistinguishable except for the peak rotational acceleration at 1.5m. A limitation of the study was that the head of the dummy was simplified to a 2.25mm thick solid homogenous plastic, therefore no account was given for the sutures and the fact that skull is made up of plates, this would likely cause a more stiffened response and probably output higher values in comparison to an actual infant head. Consequently the study addressed this by stating that the results were likely to be a worst-case scenario.

Coats and Margulies <sup>3</sup> developed an infant ATD with increased biofidelity, where the head was constructed from copolymer plates and connected by silicon rubber to resemble the bone and suture characteristics of an infant head. The experimental procedure in the study followed a similar pattern to that of Prange et al <sup>5</sup>, yet the heights dropped from were 0.3m, 0.6m and 0.9m. Accelerations were measured in the six degrees freedom and forces were measured in three planes axial, coronal and sagittal. It was concluded that an increase in height significantly increased the peak rotational accelerations, drops onto stiffer surfaces (carpet and concrete vs mattress) also produced larger rotational accelerations. Similarly to Prange et al <sup>5</sup> no significant differences were seen for the peak rotational accelerations between the carpet and the concrete in the axial, coronal and sagittal planes except for 0.3m falls, where there were significantly higher peak rotational accelerations for the drops onto carpet in the coronal and axial planes. The lack of significant difference in rotational accelerations at higher heights led the authors to believe that carpet had fully compressed by 0.6m, however upon looking at the

impact force data no significant differences were seen between the carpet drops at 0.3m and 0.6m yet there were differences between 0.6m and 0.9m, thus full compression of the carpet was likely between 0.6m and 0.9m. The results from the ATD used by Coats and Margulies <sup>3</sup> found a decrease in the peak rotational accelerations and velocities in comparison to Prange *et al* <sup>5</sup>, underlying the importance of increased dummy biofidelity when measuring impact response.

A limitation of the of the work by Prange *et al* <sup>5</sup> and Coats and Margulies <sup>3</sup>, was that only three simplified surfaces were used in the impact tests, and no considerations were made for the full surface make up. Corry and Jones <sup>6</sup> was the first to complete a thorough analysis of the domestic surfaces which infants are prone to impact. Variations between the underlying surface, different types of the same surface (i.e woollen carpet against polypropylene carpet) and point of impact relative to the underlying joists and supports were investigated. Linear accelerations in terms of a critical fall height to cause a HIC value of 1000 were measured (value linked to a 16% likelihood of life threatening brain injury in adults). Point of impact in relation to the distances relative to the joists, type of floorboard (chipboard vs wooden), presence of underlay, and the rigidity of the top surface layer were all shown to have an effect on the critical fall height. The study clearly indicated that the full mixture from the supports to the top surface layer need to be considered prior to trying to determining the injurious effect of a surface, however the aluminium hemisphere headform used in the study was calibrated to adult data and as result had a impact response of an adult head, plus the HIC value of 1000 relates to adult injury threshold, as a result it was unclear if the varying surface mixtures would have the same effect on the response of an infant head on impact.

The research by Van Ee *et al* <sup>7</sup> measured the effect of varying domestic surfaces using the 6 month Child Restrain Airbag Interaction (CRABI-6) ATD, which has been shown to have a similar response to infant cadavers <sup>8</sup>. Again it was shown that a decrease in surface stiffness (Concrete, carpet, carpet & pad, foam, camel hair blanket) decreased the response measurements (Peak g, HIC, Peak rotational

accelerations) illustrating, with particular reference to the carpet vs carpet & pad, that the full surface make up needs to be considered. However the aim of the study was to replicate the cadaver impact tests completed by Weber <sup>9,10</sup>, to develop infant skull fracture thresholds, as result the ATD was only dropped from a single height (single height used by Weber <sup>9,10</sup>), therefore the interaction between height and surface stiffness was not documented.

### 4.1.2 Aims and objectives

The aim of this section of the research was to develop a biofidelic infant headform, using materials with similar properties to those reported for the scalp, cranial suture, cranium and brain <sup>11,12</sup> and then to subject the headform to a validation procedure, based on the infant cadaver response data, published by Prange *et al* <sup>8</sup>. Post validation, it was intended that the study combine and progress the work of Cory and Jones <sup>6</sup> and Coats and Margulies <sup>3</sup>. Utilising an in depth analysis of common domestic surfaces, accounting for the potential effects of the presence of underlay and supporting joists, whilst also measuring the rotational accelerations on impact.

The aim, post validation, was to address a key limitation with all previous studies using infant ATDs, that they only measure the head injury outcome from a 90° translational impact; yet in reality, very few circumstances would result in such a situation. With particular reference to the pre-mobile infant, often, low height falls result from either a child falling from a raised surface, such as a table or sofa, or being dropped from a carer's arms (Chapter 3), both of which, would likely involve an oblique angle of impact. This was not assessed in Chapter 3, since during the development of the proforma, it was felt that the question would be misinterpreted and thus, not filled in correctly by the ED staff. Also, due to this issue not currently being addressed in the literature, it was not routinely assessed by clinicians and thus, was not documented in the retrospective analysis of methods in Chapter 3.

Certain types of TBI are caused by rotational accelerations, as opposed to translational accelerations<sup>13,14</sup>, thus, the potentially injurious effect of domestic surfaces, with increasing height from an oblique impact, have yet to be determined. Coats and Margulies<sup>3</sup> concluded that the rotational accelerations, in the axial plane, were larger in comparison to the sagittal or horizontal plane, yet the change in peak-to-peak rotational velocities, were lower. The reason given was that ‘. . . frictional force between the surrogate scalp and the impact surface prevents the head from sliding laterally, but rather grips the head at the occiput causing rapid axial acceleration about this pivot point.’ (Coats and Margulies<sup>3</sup>, p.328). It was hypothesised, that an impact at an oblique angle could amplify this effect and cause greater rotational accelerations in comparison to a perpendicular impact.

Finally, section 2.3.2 addressed the current proposed young child head injury thresholds, for skull fracture and traumatic brain injury, in terms of the kinematic variables. Since these thresholds were not assessed against the paediatric clinical setting, the final aim was to assess these thresholds against the 0.6m proposed from Chapter 3, to determine if there was a disconnect between the biomechanical and clinical thresholds.

## 4.2 Materials and Method

### 4.2.1 Headform Design Methodology

Prange *et al*<sup>8</sup> conducted infant cadaver head drop tests from 2 heights (0.15m and 0.3m) with three heads (1,3 and 11 days old), onto a smooth anvil, where the impact was measured with a load cell. As this is the only current published data on cadaver head response, it provides the only information to which, validation of a head model can be achieved. Therefore, the design and manufacture of the experimental headform was tailored to resemble the anthropometry of the cadaver heads used by Prange *et al*<sup>8</sup>.

#### 4.2.1.1 Radiological Datasets

To develop a geometrically accurate headform, computed tomographic (CT) datasets from infants less than 3 months of age were used. CT data sets, with a small axial thickness, were used as it enabled the geometry of the skull to be closely replicated, whilst also allowing for a smooth surface configuration. This particular age was chosen, as the epidemiological review in Chapter 3 highlighted a significantly greater proportion of children  $\leq 12$  months sustaining a serious head and also the infant cadavers in the Prange *et al*<sup>8</sup> data series were less  $\leq 11$  days old.

At the University Hospital of Wales (UHW), Cardiff, all radiographic datasets that are completed as part of routine care, can be accessed through the Radiology Management System. This study created an anonymised copy of CT and MRI datasets of children  $< 10$  years old on a separate system. Images for children  $< 10$  years old were collected, to cover the age ranges researched by Trauma Biomechanics research team at Cardiff School of Engineering (n.b. all ages were covered under the same ethical approval process). An application to collect the CT images from UHW Cardiff was submitted to the South Wales Research Ethics Committee, Panel C on the 28/09/2011 and approval was received on the 28/10/2011 (11/WA/0304). In conjunction, application for Cardiff and Vale University Health Board R&D approval was submitted on the 29/09/2011 and



received on the 28/10/2011 (Cardiff and Vale UHB Project Ref:11-DTD-5178, National Institute for Social Care and Health Research Ref:76154). Dr Andrea Liu (Paediatric Consultant Radiologist, UHW) and Dr Jonathan Bainbridge (Radiologist, UHW) were the local collaborators at the UHW Cardiff.

All paediatric radiological datasets were anonymised; imaging the skull, intracranial structures, craniocervical junction and the cervical vertebrae. The inclusion criteria were, that all radiological images were classed as normal, that is, that no congenital and traumatic pathology affected the skeletal or soft tissue structures, or, that any other visible abnormalities of the cranium or intracranial tissues were present. If a child had functional neurological problems, such as autism or epilepsy, yet the structure of the skull and brain were normal, then they were eligible for use. The identification and anonymisation of the datasets, conforming to this inclusion and exclusion criteria, was performed by Dr Jonathan Bainbridge and Dr Andrea Liu .

A total of 195 CT scans were collected (15 per age group), to cover the following developmental ages - 3, 6, 9, 12, 15, 18, 24, 30, 36, 48, 72, 96 and 120 months.

### **4.2.1.2 Headform Design and Development**

Only four CT datasets were available for the anthropomorphic analysis, prior to the design and manufacture of the headform. This was due to funds being available, to manufacture the headform for a short period of time, March 2012 – April 2012, it was therefore, decided to proceed with the design of the headform prior to capturing the full 15 datasets.

All CT image datasets were of an axial slice thickness of 0.625mm and a resolution of 512 x 512. Processing the images involved importing the CT datasets as DICOM images into ScanIP (Version 4.2, Simpleware Ltd <sup>15</sup>) and then aligning each dataset with the Frankfurt Plane, using ScanIP (Version 4.2, Simpleware Ltd <sup>15</sup>) , which involved aligning a vector from the left to the right external acoustic meatus to be

parallel with x axis. Then a vector from left external acoustic meatus to the inferior aspect of the left orbit was aligned to be parallel with the y axis. Markers were then placed at the most distal aspects of the head anteriorly (A), posteriorly (P), lateral (left), lateral (right), vertex and finally at the external acoustic meatus, using ScanIP (Version 4.2, Simpleware Ltd <sup>15</sup>) . The local coordinates, for these markers, were then exported from ScanIP (Version 4.2, Simpleware Ltd <sup>15</sup>) into Excel format. The head length, width and height for each of the data sets were calculated using Equations(21), (22) and (23).

$$Patient\ Head\ Length\ (PHL) = A_x - P_x \quad (21)$$

$$Patient\ Head\ Width\ (PHW) = LL_y - LR_y \quad (22)$$

$$Patient\ Head\ Height\ (PHH) = V_z - LEAM_z \quad (23)$$

Where  $A_x$  is the X coordinate of anterior marker,  $P_x$  is the x coordinate of posterior marker,  $LL_y$  is the y coordinate of left lateral marker,  $LR_y$  is the y coordinate of right lateral marker,  $LR_z$  is the z coordinate of vertex marker and  $LEAM_z$  z coordinate of left external acoustic meatus.

The Root Mean Square (RMS) error for the three dimensions was then calculated, between each dataset and each of the three cadaver heads used by Prange et al <sup>8</sup>. The calculation of the RMS is shown in (24).

$$RMS = \sqrt{\frac{(PrHL - PHL)^2 + (PrHW - PHW)^2 + (PrHH - PHH)^2}{3}} \quad (24)$$

Where PHL is the head length , PrHL is the head length from Prange *et al* <sup>8</sup> data series, PHW is the head width, PrWL is the head width from Prange *et al* <sup>8</sup> data series, PHH is the head height and PrHH is the head height from Prange *et al* <sup>8</sup> data series.

The CT image with the lowest Root Mean Square (RMS) error was used for the model development.

*Table 11. Head measurement of the Computed Tomography datasets collected from the UHW Cardiff compared to the Prange et al<sup>8</sup> data series.*

Patient age / days	Head length / mm	Head width / mm	Head height / mm	RMS (1 day old)	RMS (3 day old)	RMS (11 day old)
Measurements of infant heads in Prange <i>et al</i> <sup>8</sup> dataset						
1	103.0	108.0	112.0			
3	85.0	88.0	104.0			
11	75.0	88.0	92.0			
Measurements of the infant heads in this study						
56	138.9	106.2	92.0	26.0	20.8	15.6
35	136.8	103.6	91.0	24.1	19.0	*14.3
84	136.6	98.4	97.8	24.7	18.5	14.9
90	139.8	128.1	100.0	35.8	30.4	21.8
* CT dataset with the lowest RMS. RMS – Root mean square error.						

The chosen CT dataset was of a 5-week-old male infant. Image segmentation, using the threshold filter, was completed to differentiate the cranium from the soft tissue structures<sup>15</sup>. A greyscale threshold was applied to the CT datasets, a threshold between greyscale values of 105-255 was implemented to differentiate the bones from the soft tissues, as shown in *Figure 10*. A histogram of a profile line, moving across the bone, was used to determine the greyscale values.

A cavity fill filter was applied to the mask of cranial bones to remove small holes in basal bones. The cervical vertebrae and the mandible were removed to replicate the cadaver heads used by Prange *et al*<sup>8</sup> (*Figure 11*).

The basal section of the headform was then edited, to allow for a probe to be attached to the base section and also, to enable the occipital plate to be attached to the basal section, as shown in *Figure 11*.

Chapter 4 – Physical Modelling of Infant Head Impacts

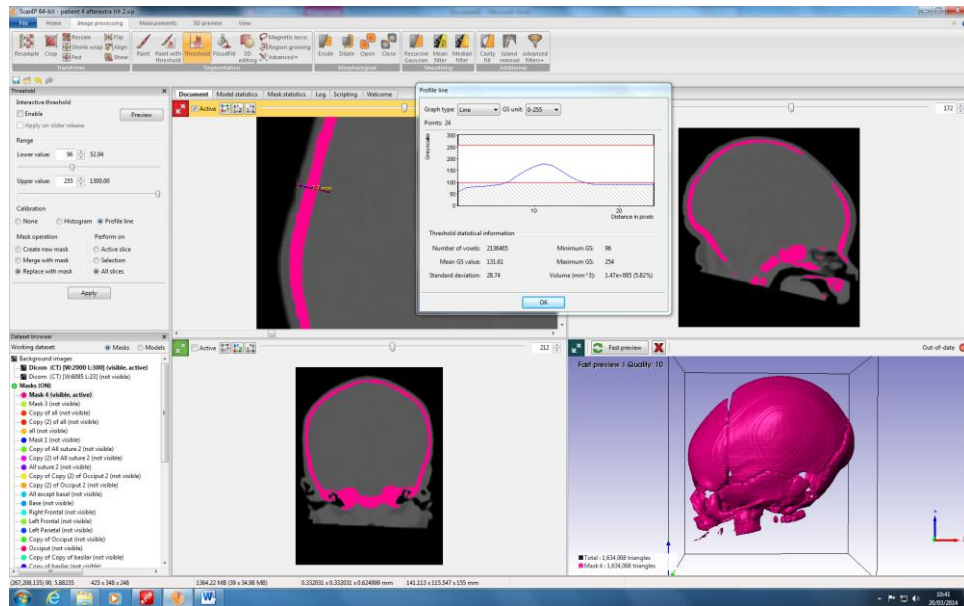


Figure 10. Threshold filter applied to the CT dataset and image then aligned with Frankfort plane.

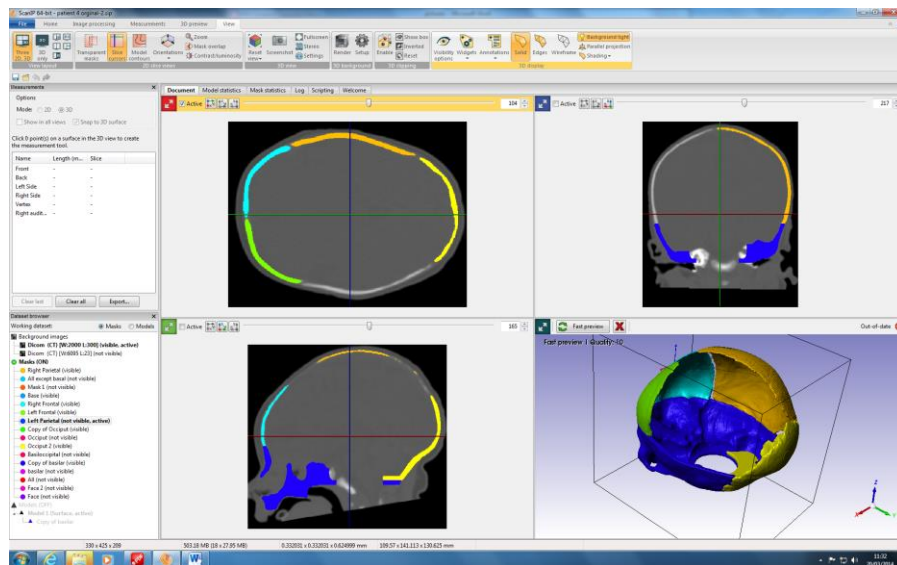
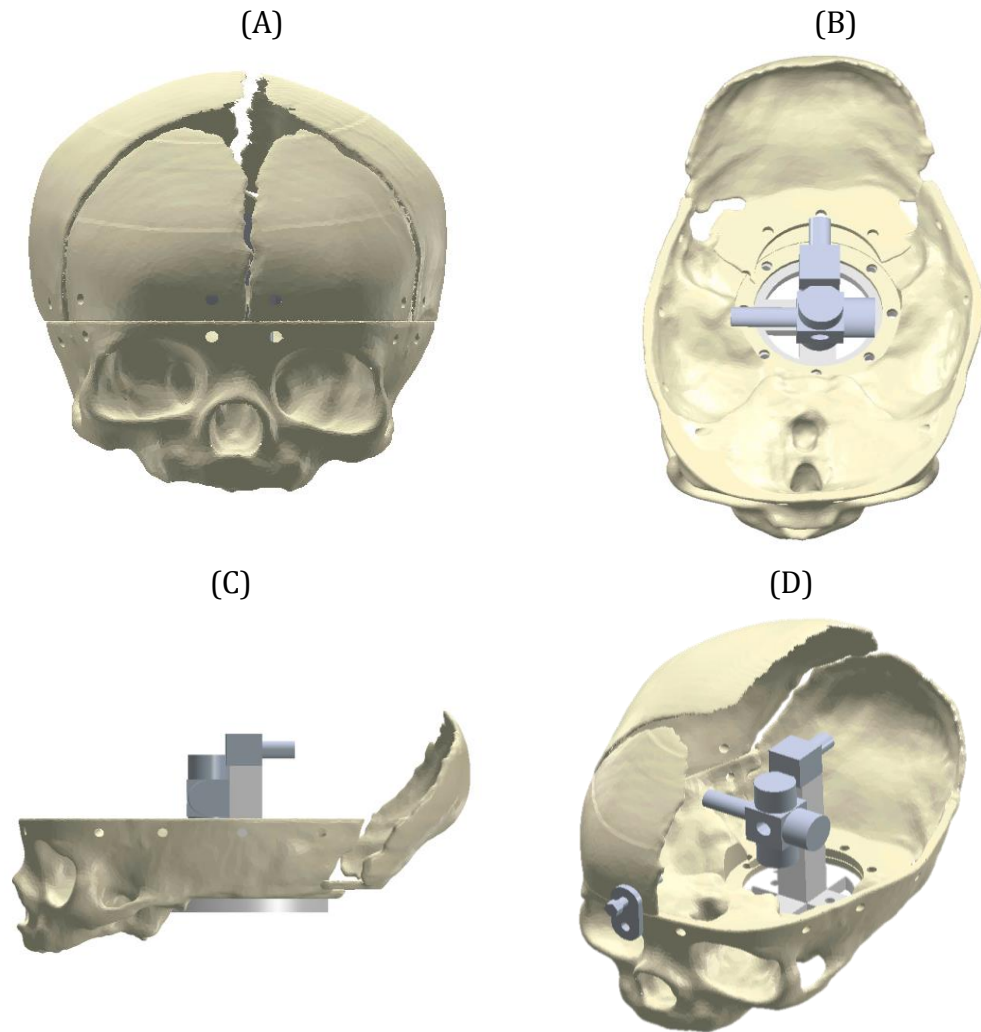


Figure 11. Development of the antropomorphic test device through image processing of a 5 week old male CT dataset.

The headform model was then exported as a Stereolithography (STL) file into Solidworks (Version 2011, DSS 16). The STL drawing was then edited, such that the model consisted of 6 different parts: two frontal plates, two parietal plates, an

occipital plate and a basal section. Holes were produced on each plate of 3mm diameter (2 per frontal plate, 4 per parietal plate, 3 in the occipital plate and 18 in the basilar plate). The frontal and parietal plates were connected via lugs/washers and 2.5mm steel screws. The occipital plate was attached to the basal section via 2.5mm steel screws. The probe was designed to allow for attachment of the translation tri-axial accelerometer (Type 8763B, Kistler Instrumentation Corp, Amherst, NY) and a rotational accelerometer (Type 8838, Kistler Instrumentation Corp, Amherst, NY). The probe length was designed, such that sensors would be close to the position of the centre of mass, as reported by Prange et al <sup>8</sup>, approximately 29mm from the external acoustic meatus in the z axis direction. The final headform design can be seen in *Figure 13*.



*Figure 12. Final design of the headform. Frontal view of the headform (A). coronal view, illustrating occipital plate fixed and positioned to basal section (B), Side view, illustrating the positioning of the occipital plate(C), (D) Image of inside of the headform.*

#### **4.2.2 Material Selection and Manufacture**

The head was then manufactured out of Duraform Polyamide (PA), using a Selective Laser Sintering machine (EOSINT P700, EOS, Munich). This manufacturing technique was chosen, as it allowed for a cost effective method of obtaining accurate geometry. The properties of the duraform polyamide were similar to the upper limit of the elastic modulus, reported for bone fibres oriented

perpendicular to the long axis, by Coats and Margulies <sup>11</sup> and lower than the mean values reported by McPherson and Kriewall <sup>12</sup>, for foetal cranial bone, with fibres parallel to the long axis, as shown in *Table 13*. The gaps, representing the cranial sutures, between each plate, as shown in *Figure 13*, were filled with silicone rubber and then the head subsequently covered with latex rubber, since they possess similar stiffness properties to infant sutures and human scalp, respectively <sup>3,11,17</sup>. The latex was applied over the headform in the final assembly stage and thus, set into the shape of the headform,

*Figure 14*. To resemble the brain, a polyethylene bag was placed inside the headform and filled with gelatine (10% gelatine & 90% water), in accordance with a previous study modelling the brain <sup>18</sup>. The gelatine mould was left to solidify, prior to the sensors being attached. The brain surrogate weighed 460g. A visual comparison between the designed and manufactured headform is presented in *Figure 13*.

A triaxial accelerometer was positioned in the sagittal, coronal and axial planes to measure translational accelerations and the rotational sensor was connected to measure rotational accelerations ( $\alpha$ ) about the sagittal plane (

*Figure 14*). A small ferrous plate, size 29mm x 9mm x 2mm and mass 0.0005kg, was attached the base of the headform using two 2.5mm screws, allowing for attachment to an electromagnet. All total head dimensions can be seen in *Table 12*.

*Table 12. Headform Dimensions*

Variable	Headform	Prange <i>et al</i> <sup>8</sup>		
age / days	35	1	3	11
Head Length / cm	13.7	10.8	10.3	11.2
Head Width / cm	10.4	8.8	8.5	10.4
Head Height / cm	9.0	8.8	7.5	9.2
Head Mass / g	682 (Without Sensors), 729 (With Sensors)	666.5	491.5	701.9

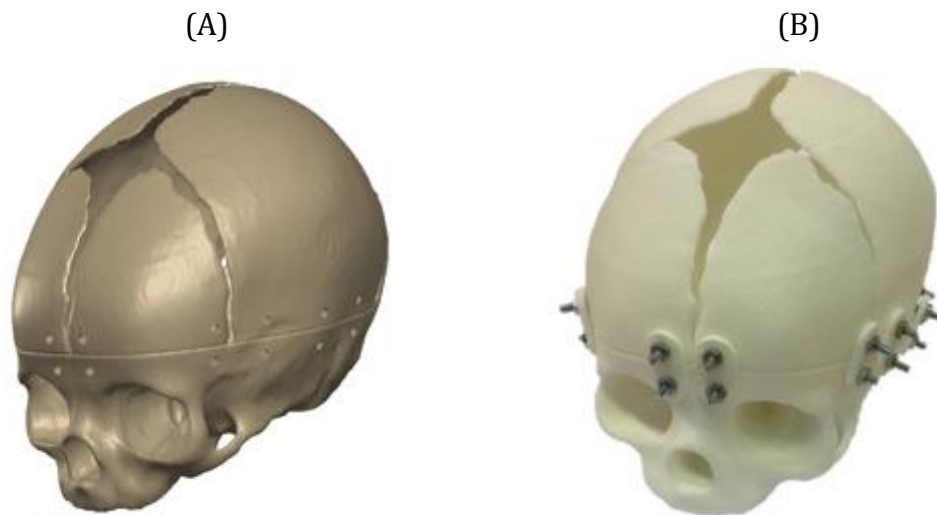


Figure 13. Comparison between the Infant headform design (A) and the manufactured headform (B)

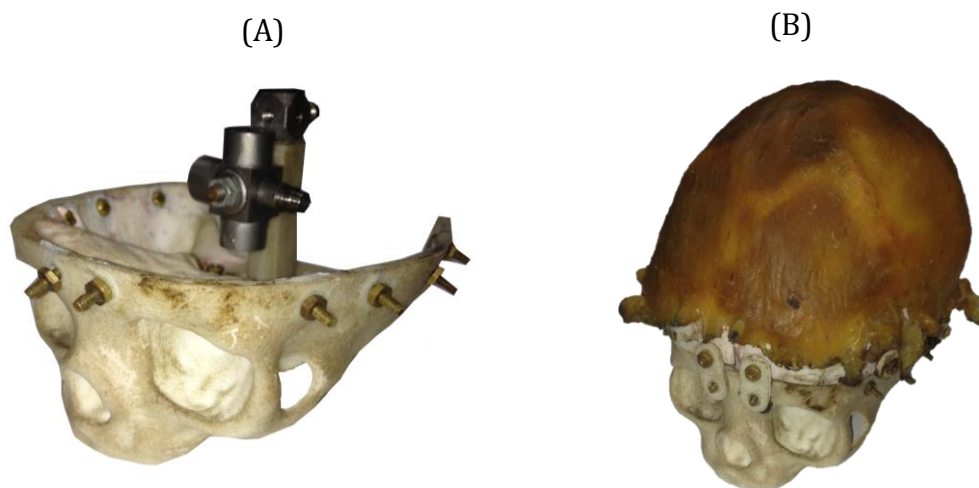


Figure 14. Manufacturing stages of the headform from the output of the selective laser-sintering machine to the headform used for impact testing.

#### 4.2.2.1 Skin Friction

As discussed earlier, Coats and Margulies<sup>3</sup> hypothesised that skin friction may cause the head to rotate during impact. To address this issue, the coefficient of static friction was measured between adult human skin and common domestic surfaces. A study was conducted to assess the static frictional properties of human



skin on a range of domestic surfaces at trauma lab at Cardiff University by undergraduate students (Analysis presented in this thesis was completed by the author).

Fifteen adults were subject to the different surfaces (wood, carpet, and laminate) being pulled tangentially across the forehead via belt pulley and mass system. Masses of 5 different weights (20g, 30g, 40g, 50g, 60g) were pulled, tangentially across the forehead using a newton metre. Hydrated and non-hydrated (volar) skin was tested.

In addition, a series of tests were conducted to investigate a skin simulant, which could be used to cover the ATD head. The materials tested, as possible surrogates in terms of skin friction, were latex, chamois, leatherette, polypropylene, polyamide and saturated polyamide.

Table 6A in Appendix 6 documents mean values  $\pm$  standard error for the coefficient of static friction for the 15 adults and also the skin surrogates onto the different domestic surfaces. The significant difference between the three domestic surfaces and volar, or saturated, skin are documented in Table 6A, Appendix 6. Of the skin surrogates tested, none had a coefficient of static friction that was significantly similar to human skin, across the six different combinations of skin hydration and domestic surfaces. However, the closest match was the polyamide, as can be seen in Table 6B, Appendix 6, which was statistically similar in 50% (3/6) of the combinations of skin hydration and surface type. The coefficient of friction for latex was significantly greater than human skin across 83% (5/6) of the different combinations, however, it was significantly similar to saturated skin on laminate. Thus, two separate skin surrogates, polyamide and latex were used in the headform design, to determine if friction has a significant affect on the kinematic variables during impact. The polyamide was chosen, due to its similarities to human skin and latex as it was been used by previous authors, whilst also accounting for the higher coefficient of static friction documented

(Table 6B, Appendix 6) for laminate. The polyamide was attached on top of the latex using adhesive.

#### 4.2.3 Experimental Procedure- Headform Validation

In accordance with the experimental methodology of Prange *et al* <sup>8</sup>, the biofidelic infant headform was placed inside a net and raised to two different heights 15cm and 30cm. It was raised via a length of cord and dropped, by transection of the cord, onto four impact points (approximating the physiological forehead, vertex, right parietal and occiput) onto a metal force plate. The force plate (Type 4060H, Bertec Corporation, Worthington, OH), output voltage, on impact, was measured at a sampling frequency of 10 KHz. The voltage was converted into a corresponding force via a sensitivity value, and the acceleration on impact was extrapolated, using Newton’s 2<sup>nd</sup> law (Equation (25)). The corresponding Head Injury Criterion (HIC) values for a 15ms impact were calculated from the acceleration/time data using Equation (2).

$$F = Ma \tag{25}$$

$$V = \sqrt{2 \times 9.81 \times H} \tag{26}$$

$$\omega = \int_{t_1}^{t_2} \alpha \, dt \tag{27}$$

Where F is force, M is mass, a is translational acceleration, V is velocity, H is height, t is time,  $\omega$  is rotational velocity and  $\alpha$  is rotational acceleration.

#### 4.2.4 Experimental Protocol

To measure the response of the head to angular impacts, the headform was dropped from three different heights, corresponding to three different impact velocities (2.4 m/s, 3.0 m/s, 3.4 m/s) based on Equation (26) (0.30m, 0.45m and 0.60m), onto four different surfaces (carpet (3mm), carpet with underlay (5mm), laminate flooring (8mm) and wood (20mm)), where the angle of impact was set at 90°, 75° and 60°. Each surface was placed over a floorboard system, consisting of

two joists 600mm apart, with chipboard laid on top ( n.b. the wooden surface was not placed over the chipboard). The design of the floorboard system was in accordance with the British standards corresponding to the distance between the joist (BSI <sup>19</sup>).

#### Delivery mechanism

For the 75° and 60° impacts, wooden wedges were placed underneath the floorboard rig at angles of 15° and 30°, respectively. The headform was attached to an electromagnet, via the ferrous plate and raised to the required height and clamped to a rigid aluminium pole. The height was measured from the vertex of the head to the impact surface with a ruler. Each impact was videoed to assess whether the correct impact location was achieved. An example of the experimental rig set up can be seen *Figure 15*. Each test was repeated four times with latex layer and then four times with the polyamide layer added.

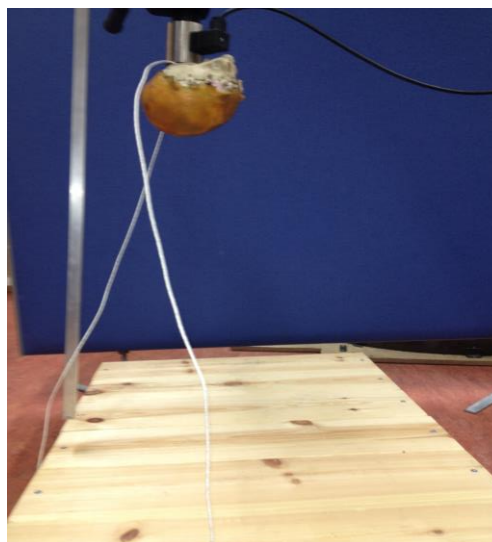


*Figure 15. Apparatus set up for 60cm fall onto wood for a 90deg impact*

#### 4.2.5 Data Acquisition and Analysis

A translational triaxial accelerometer was connected, via a charge amplifier to a National Instruments Data Acquisition Card (NI DAQ) (NI USB 6211), the rotational sensor was connected directly to the NI DAQ card. The voltage output, from both sensors, were passed from the NI DAQ card to a computer, where the output was filtered, using a low pass Butterworth 4<sup>th</sup> order filter set at 1000Hz and captured using National Instruments Data Acquisition Software (NI DAQ, National Instruments) at a rate of 10 KHz. The Society for Automotive Engineering standard for automotive crashes, states that data should filtered between 1000Hz and 1650Hz (SAE <sup>20</sup>). A spectral analysis of the voltage data, which involved completing a fast Fourier analysis on the data and converting from the time domain to the frequency domain, indicated a cut off at 1000Hz (Figure 16). This was completed in Excel (Version 2007, Microsoft Cooperation). This cut off frequency has been used by research institutes investigating ‘low height falls’ using ATDs <sup>21</sup>.

The NI DAQ software was programmed to capture 10ms of data, prior to the impact and 50ms of data, post the impact. The low pass filter was applied to the ‘raw’ voltage values, for each axis of the translation accelerometer and the rotational accelerometer. The voltage output for the x, y and z axes of the translational and the rotational accelerometer were converted to g and  $\alpha$ , respectively, via a sensitivity value in the NI DAQ software. All data, including the raw voltages, filtered voltages and g and  $\alpha$  values were programmed to be recorded in a .txt format in the NI DAQ software. All .txt data files were exported to Matlab (Version R2011a, Mathworks<sup>22</sup>). Matlab code was written to calculate the peak translational acceleration, HIC (Equation (2)) and duration of impact for the x, y and z axes of the translational accelerometer. The resultant peak acceleration (Peak  $G_R$ ) and resultant HIC ( $HIC_R$ ) were calculated.

$$Peak G_R = \sqrt{a_{px}^2 + a_{py}^2 + a_{pz}^2} \quad (28)$$

$$HIC_R = \sqrt{HIC_x^2 + HIC_y^2 + HIC_z^2} \quad (29)$$

Where Peak  $G_R$  is the resultant translational acceleration,  $a_{px}$  peak translation acceleration x axis,  $a_{py}$  peak translational acceleration y axis,  $a_{pz}$  is peak translational acceleration z axis,  $HIC_R$  is the resultant HIC,  $HIC_x$  is HIC in the x axis,  $HIC_y$  is HIC in the y axis and  $HIC_z$  is HIC in the z axis.

In conjunction with the maximum and minimum rotational accelerations and velocities (Equation (27)) were calculated. The high speed video was set to record 5 seconds of data post the trigger point at a rate of 1000Hz.

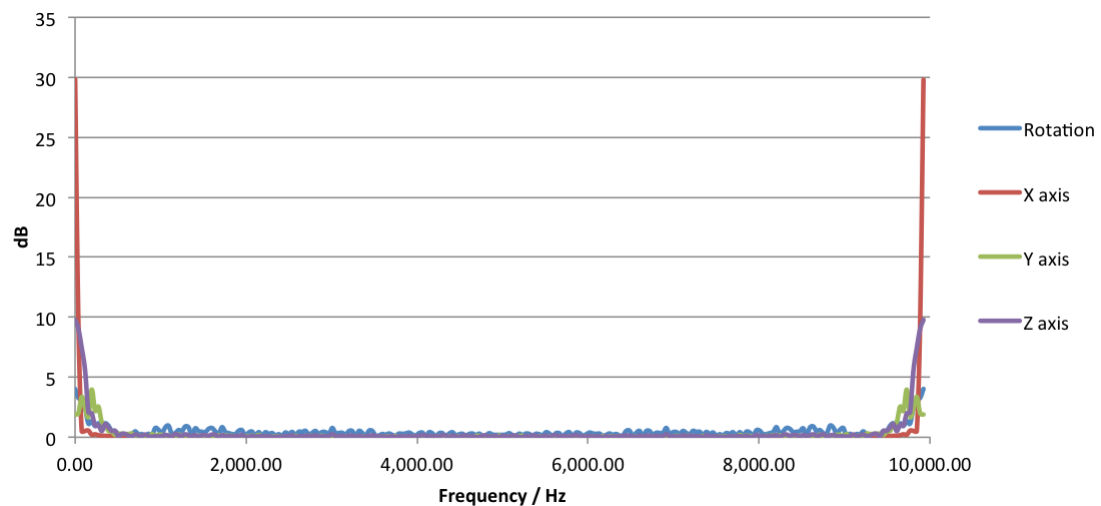


Figure 16. Spectral analysis, used to determine cut off frequency for filter

#### 4.2.6 Statistical Analysis

A one sample student t-test was used to compare peak G, HIC and duration of impact between the ATD response and Prange *et al*<sup>8</sup> data series for the validation process.

A Student’s t-test was used to investigate the effect that the coefficient of static friction has on the kinematic variables. The effect was assessed across each of the 36 different combinations of impact velocity, angle of impact and impact surface.

Parametric and the non parametric equivalence of the three factorial ANOVA were used to determine, if significant differences existed in the peak  $\alpha$ , peak  $\omega$ ,  $a_R$ ,  $HIC_R$  and duration of impact between the varying fall velocity, surface type and angle of impact. The non parametric equivalent was based on the global ranking of the data. SPSS (Version 20, IBM<sup>23</sup>) was used for all the statistical comparisons, where statistical significance was set at  $p = 0.05$ . Post hoc analyses involved using a SNK test.

Table 13. Infant Headform Material Properties

Headform section	Material	Properties	Anatomical equivalent	Source
Skull	Duraform (Polyamide)	Elastic Modulus = 1600MPa	Mean = 315±104.9MPa Max = 1317.6MPa  Mean = 1650 MPa	Coats and Margulies <sup>11</sup>  McPherson and Kriewall <sup>12</sup>
Scalp	Latex rubber	Elastic modulus = 1.4MPa	1.5MPa ( n.b. Rhesus monkey)	Galford and McElhaney <sup>17</sup>
Suture	Silicon rubber	Elastic modulus = 2.1MPa	3.8MPa (2 day old human infant)	Coats and Margulies <sup>11</sup>

#### 4.2.7 Nomenclature

Table 14. Nomenclature of material properties and variables assessed during finite element analysis.

<b>Symbol</b>	<b>Definition</b>
$\sigma$	Stress
$\epsilon$	Strain
E	Elastic Modulus
Peak $G_R$	Resultant peak linear acceleration
$HIC_R$	Resultant Head Injury Criterion
$\Delta t$	Duration of impact
$\alpha_p$	Peak rotational acceleration
$\Delta\omega$	Peak change in rotational velocity

### 4.3 Results

#### 4.3.1 Validation

The experimental infant headform was validated in accordance with the method of Prange *et al*<sup>8</sup>, a total of 18 drop tests were conducted. *Figure 17* illustrates the headform experimental response corridors, which are compared with the results and standard deviation published by Prange *et al*<sup>8</sup>. It can be seen that the headform response shows a close correlation, with 100% of the results falling within the corridors for the vertex and forehead, but only 65% for the occiput and 50% for the right parietal. A one way student t-test was used to compare the Peak g, duration of impact and HIC values against those reported by Prange *et al*<sup>8</sup>, for the 15cm and 30cm drops, onto each impact location. No significant difference was found between any of the variables at both drop heights and impact location (P>0.05).

*Table 15. Peak acceleration, HIC and duration of impact from the validation procedure*

Impact Location	Peak Acceleration / g	Head Injury Criterion	Duration of impact / ms
15cm Drop height			
Vertex	28.7	30.1	18.2
Occiput	26.2	24.2	19.5
Right parietal	25.8	20.6	17.5
Forehead	29.5	26.9	19.1
30cm Drop height			
Vertex	42.3	71.3	17.6
Occiput	39.4	61.0	18.4
Right parietal	49.6	47.1	17.6
Forehead	46.8	55.5	15.3
g-acceleration due to gravity (9.81m/s <sup>2</sup> ), ms-millisecond, cm-centimetre.			



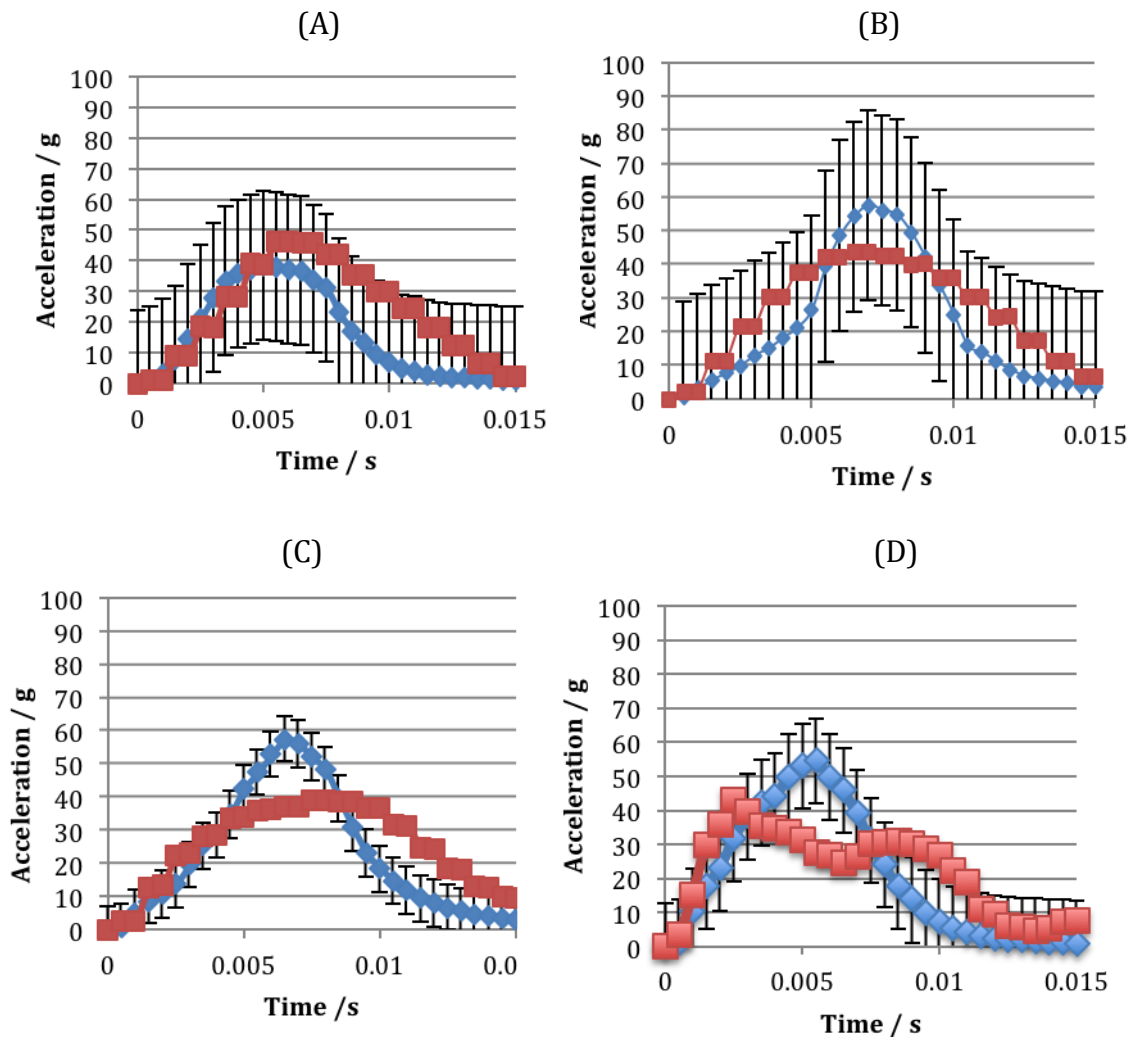
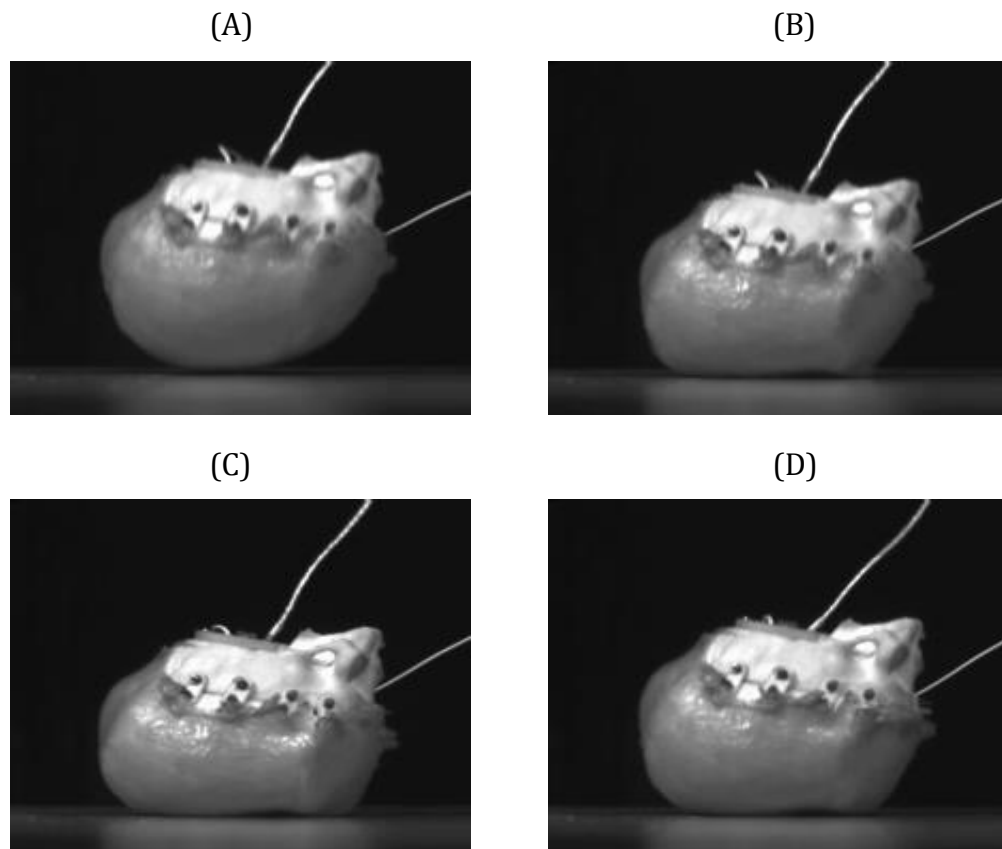


Figure 17. Acceleration vs time graphs for 30cm impacts on the forehead (A), vertex (B), occiput (C), right parietal (D) comparing the experimental results with those of Prange et al<sup>8</sup>. Blue line with error bars refer to response corridors from Prange et al<sup>8</sup> and red line is the infant headform response.

### 4.3.2 Experimental Protocol

Four drops were completed for each combination of friction (polyamide) fall velocity (2.4 m/s, 3 m/s, 3.4 m/s), surface type (carpet & underlay, carpet, laminate, wood) and angle of impact (90°, 75°, 60°), thereby resulting in 288 impacts. A drop test was deemed acceptable based on a vertex area of the headform contacting the impact surface, initially using the high speed and

subsequently the 60Hz video output. A total of 271 drop tests were deemed as ‘acceptable’, 133 with latex and 138 with the polyamide as a skin surrogate. During impact, the head was observed to deform, thereby decelerating, followed by a rapid acceleration as the elastic energy from the head deformation was converted to kinetic energy. An example of the headform deformation is provided in *Figure 18* and an example of the output from the rotational and translational accelerometers shown in *Figure 19*.



*Figure 18. Headform deformation on impact from 60cm drop onto laminate, (A) prior to Impact, (B) 4ms post impact, (C) 8ms post impact and (D) 12 ms post impact.*

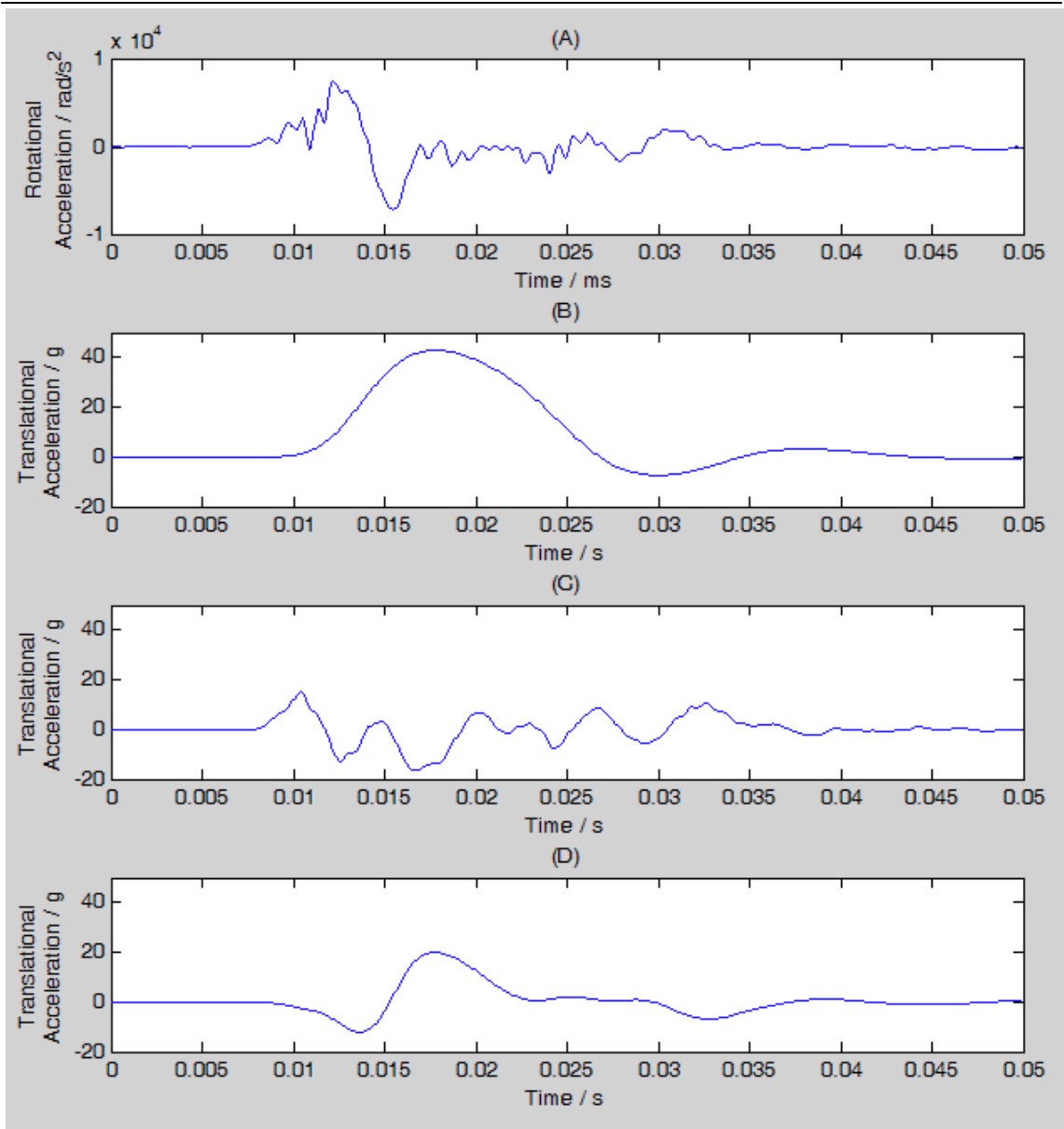


Figure 19. Acceleration output from the rotational accelerometer and the x, y and z axis of the translational accelerometer. Output from the rotational accelerometer, illustrating the acceleration and deceleration phase (A). Output from the Z axis of the translational accelerometer, illustrating how the headform decelerates on impact (B). Output from the y axis of the translational accelerometer (C). Output from the x axis of the translational accelerometer (D).

**4.3.2.1 Friction**

The coefficient of static friction for latex was significantly greater than the polyamide for the carpet, wood and laminate surface contacts ( $P < 0.001$ ), Table 16. The greatest difference was that between the laminate surface and the polyamide, where the coefficient of friction was over 3 times greater for latex, Table 16.

*Table 16. Comparison of the coefficient of static friction between the two skin simulants, latex and polyamide.*

	<b>Polyamide / mean (SE)</b>	<b>Latex / mean (SE)</b>	<b>P value</b>
Wood	0.99(0.02)	1.79(0.05)	$P < 0.001^*$
Laminate	0.36(0.02)	1.19(0.05)	$P < 0.001^*$
Carpet	0.78(0.08)	1.52(0.03)	$P < 0.001^*$
*A student t test used for statistical comparisons, as groups were normality distributed. SE – Standard Error.			

A Student’s t-test was used to determine if friction had a significant effect on kinematic variables (peak  $\alpha$ , peak  $\omega$ ,  $a_R$ ,  $HIC_R$  and duration of impact) with differing impact velocity, angle of impact and impact surface. Across the 36 different combinations of impact velocity, angle of impact and impact surface, the latex skin surrogate significantly increased peak  $\alpha$  for 5 of the 36 (13.9%) combinations and significantly decreased peak  $\alpha$  for 1 (2.8%) combination, Table 17. The greatest increase in the peak  $\alpha$ , as a result of the latex was 36% ( $P = 0.005$ , Table 17) on wood, at an angle of 60 degrees and impact velocity of 2.4m/s, yet, the largest decrease was 23.8% on laminate at an angle 90degrees and impact velocity of 2.4m/s. ( $P = 0.001$ , Table 17). Four of the five cases, where the latex significantly increased the peak  $\alpha_p$ , were at the lowest impact velocity of 2.4m/s.

Table 17. A comparison between latex and polyamide to determine the effect of friction on headform rotation during impact, with varying impact velocity, impact surface and angle of impact.

Impact Velocity (m/s)	Impact Surface	Latex / rad/s <sup>2</sup> Mean±SE	Polyamide / rad/s <sup>2</sup> Mean±SE	P value
90 degree (perpendicular to surface)				
2.4	Carpet-underlay	3686.9(329.2)	2384.6(327.3)	0.020
	Carpet	6593.5(302.4)	6096.9(68.2)	0.160
	Laminate	5181.1(26.7)	6801.8(266.8)	0.001
	Wood	7776.7(161.6)	7122.9(406.9)	0.400*
3.0	Carpet-underlay	5766.4(281)	5082(245.6)	0.116
	Carpet	7615.1(151.3)	7446.6(329.4)	0.658
	Laminate	7992.2(860.2)	8079.3(802.5)	0.945
	Wood	9368.8(575.1)	7966.6(598.1)	0.162
3.4	Carpet-underlay	5848.5(487.8)	6566.9(570.7)	0.404
	Carpet	9140.8(743.1)	8769.1(700.5)	0.728
	Laminate	10464.5(1816.3)	10103.6(819.3)	0.849
	Wood	11004.4(695.4)	11363.3(858)	0.762
75 degree				
2.4	Carpet-underlay	4620.4(397.7)	5059.3(202.5)	0.200*
	Carpet	6995.1(422.6)	6550.5(146.8)	0.359
	Laminate	9647.1(307.5)	7725.2(218.7)	0.005
	Wood	10033.6(234.4)	7959.5(270)	0.001
3.0	Carpet-underlay	8953.6(550.2)	8256.6(460.9)	0.200*
	Carpet	11174.9(496)	9808.8(373)	0.070
	Laminate	11372.6(796.3)	11515.5(528.1)	0.882
	Wood	13512.1(740.7)	14069.7(879.3)	0.645
3.4	Carpet-underlay	11146.9(116.7)	11276.3(139.4)	0.529
	Carpet	13996(322.8)	12568.1(206)	0.010
	Laminate	14741.2(810.4)	13723.5(830.9)	0.414
	Wood	15991.1(435.2)	16060.7(765.2)	0.940
60 degree to Vertical				
2.4	Carpet-underlay	5576.6(464.1)	6950.9(402.2)	0.067

	Carpet	8536.7(355.9)	8836.3(218.1)	0.886*
	Laminate	10379.7(719.1)	10931.3(938.5)	0.665
	Wood	13924.2(492.2)	10239.7(706.2)	0.005
3.0	Carpet-underlay	6906.4(2295.8)	8981.9(528.2)	0.412
	Carpet	12905(405.9)	13100.6(173.3)	0.643
	Laminate	15290.7(600.5)	13357.2(910.8)	0.127
	Wood	17535.3(322.3)	13080.1(164.3)	1.000*
3.4	Carpet-underlay	11509.2(637.9)	14547.9(1605.5)	0.106
	Carpet	17212.1(291.6)	15853.4(503.7)	0.089
	Laminate	19661.8(1197.1)	16440.4(1637.9)	0.163
	Wood	19846.2(970.2)	16980.7(2287.9)	0.313

A similar pattern was seen when comparing the peak change in rotational velocity where 6 of the 36 (16.7%) were significantly affected by the change in coefficient of static friction, again 4 of which, were at the lowest impact velocity of 2.4m/s. A comparison between latex and the polyamide, in terms peak change in rotational velocity, can be seen in Appendix 6.

From this point forward, for this chapter only, all results will be based on the polyamide but the results for the latex can be found in Appendix 6.

#### **4.3.2.2 Peak Rotational Acceleration ( $\alpha_p$ )**

Peak rotational accelerations significantly increased with increasing impact velocity ( $P < 0.001$ ), increasing surface stiffness ( $P < 0.001$ ) and decreasing impact angle ( $P < 0.001$ ). The interaction between angle of impact and impact velocity had a significant affect on  $\alpha_p$  ( $P < 0.001$ ), as did the interaction between the impact surface and angle of impact ( $P = 0.019$ ). However, the interaction between impact surface and impact velocity ( $P = 0.547$ ) did not. A three factorial ANOVA concluded that the three-way interaction of impact velocity, surface and angle of impact, significantly affected  $\alpha_p$  ( $P = 0.040$ ). The mean  $\alpha_p$  values for the different scenarios tested can be seen in *Figure 20*, *Figure 21* and *Figure 22*.

#### 4.3.2.2.1 Impact Velocity ( $\alpha_p$ )

An increase in impact velocity, from 2.4m/s to 3.4m/s, significantly increased  $\alpha_p$  for all impact angles and impact surface ( $P < 0.05$ ). For a 90-degree impact onto wood,  $\alpha_p$  increased from 7,123 rad/s<sup>2</sup> to 11,363 rad/s<sup>2</sup> ( $P < 0.001$ ). However, for the 90 degree impact,  $\alpha_p$  only significantly increased for the carpet-underlay surface, when the impact velocity increased from 2.4m/s to 3m/s ( $P = 0.005$ ). Similarly, for the 90 degree impact, increase in impact velocity from 3m/s to 3.4m/s, did not significantly increase  $\alpha_p$  for all surfaces. Only for the stiffest surfaces (wood and laminate), did  $\alpha_p$  significantly increase ( $P < 0.05$ ).

For both the 60 and 75 degree impacts, an increase in impact velocity from 2.4m/s to 3m/s and also from 3m/s to 3.4m/s, significantly increased  $\alpha_p$  for all surfaces ( $P < 0.05$ ).

#### 4.3.2.2.2 Impact Surface ( $\alpha_p$ )

The carpet-underlay surface significantly reduced  $\alpha_p$ , compared to all other surfaces, for the 90 degree impacts ( $P < 0.05$ ). The mean  $\alpha_p$ , at a 90 degree impact at 3.4m/s onto wood, was 11,363 rad/s<sup>2</sup>, yet for the same conditions onto carpet-underlay,  $\alpha_p$  reduced to 6566 rad/s<sup>2</sup> ( $P < 0.001$ ), *Figure 20*. Wood and laminate were not significantly different from each other, across all impacts velocities at a 90 degree impact ( $P > 0.222$ ). In conjunction with differences to carpet-underlay, only the carpet surface, alone, significantly reduced  $\alpha_p$  compared to wood at an impact velocity of 3.4m/s and at a 90 degree angle ( $P = 0.013$ ).

For the 75 degree impacts, carpet-underlay did not significantly reduced  $\alpha_p$ , compared to carpet, for all impact velocities ( $P > 0.105$ ). However, when comparing carpet-underlay to both wood and laminate,  $\alpha_p$  significantly reduced across all impact velocities ( $P < 0.02$ ). At this angle and impact velocity of 3.4m/s, carpet-underlay reduced  $\alpha_p$  by 29.8% to 11,276 rad/s<sup>2</sup>, relative to wood ( $P < 0.001$ ), *Figure*

21. The carpet surface significantly reduced  $\alpha_p$ , compared to wood at both the 3m/s to 3.4m/s ( $P < 0.001$ ), at this impact angle, Figure 21.

At a 60 degree impact angle, carpet-underlay significantly reduced  $\alpha_p$ , compared to all other surfaces for both the 2.4m/s and 3m/s impact velocities ( $P < 0.05$ ). At a 3.4m/s impact velocity, only impacts onto wood were significantly different to carpet-underlay ( $P = 0.029$ ), where the mean  $\alpha_p$  was reduced from 16,891 rad/s<sup>2</sup> to 14,548 rad/s<sup>2</sup>. Carpet did not significantly reduce  $\alpha_p$ , compared to wood or laminate at this angle, for the 3m/s or the 3.4m/s impacts. Also, there was no significant difference between wood and laminate across all impact velocities at the 60 degree impact angle ( $P > 0.5$ ).

#### 4.3.2.2.3 Impact Angle ( $\alpha_p$ )

A decrease in impact angle from 90 to 60 degrees, significantly increased  $\alpha_p$  for all surfaces across all impact velocities ( $P < 0.01$ ). An impact onto wood at 3.4m/s increased mean  $\alpha_p$  from 11,363 rad/s<sup>2</sup> to 16,881 rad/s<sup>2</sup>, when the impact angle reduced from 90 to 60 degrees ( $P < 0.001$ ). Further comparisons can be seen by comparing *Figure 20* to *Figure 22*.

A decrease in impact angle from 90 to 75 degrees, significantly increased  $\alpha_p$  for all surfaces, for both the 3m/s and 3.4m/s impacts ( $P < 0.02$ ), but not for the 2.4m/s impact. For an impact onto the laminate surface at 3.4m/s, this angle reduction increased mean  $\alpha_p$  from 10,104 rad/s<sup>2</sup> to 13,723 rad/s<sup>2</sup> ( $P < 0.001$ ). Further comparisons can be made, by comparing *Figure 20* to *Figure 21*. For the 2.4m/s impact,  $\alpha_p$  only significantly reduced for carpet-underlay ( $P = 0.006$ ).

A decrease in impact angle from 75 to 60 degrees, significantly increased  $\alpha_p$  at 2.4m/s for all surfaces ( $P < 0.02$ ). For the 3.4m/s impact this reduction in angle,  $\alpha_p$ , was only significantly increased for carpet-underlay, carpet and laminate ( $P < 0.01$ ). At 3m/s, only carpet significantly increase  $\alpha_p$ , for this angle reduction ( $P = 0.001$ ).



The level on increase in  $\alpha_p$  due to the 75 to 60 degree angle reduction can be seen through comparing *Figure 21* to *Figure 22* .

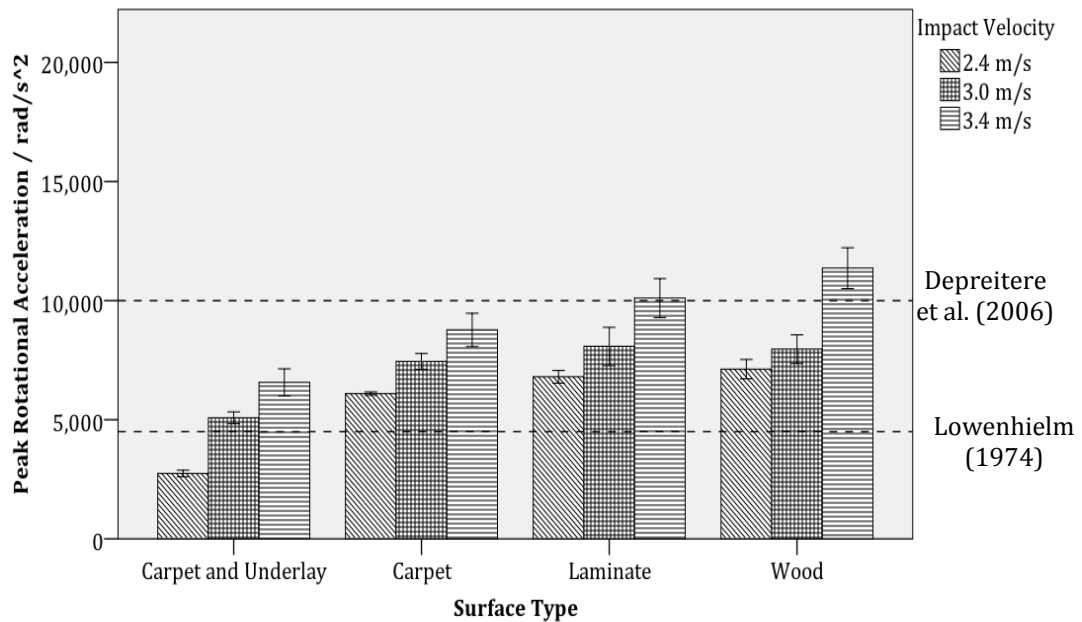


*Figure 20. The effect that changing impact velocity and impact surface has on peak rotational acceleration at a 90 degree impact angle. Error bars equal standard of error.*

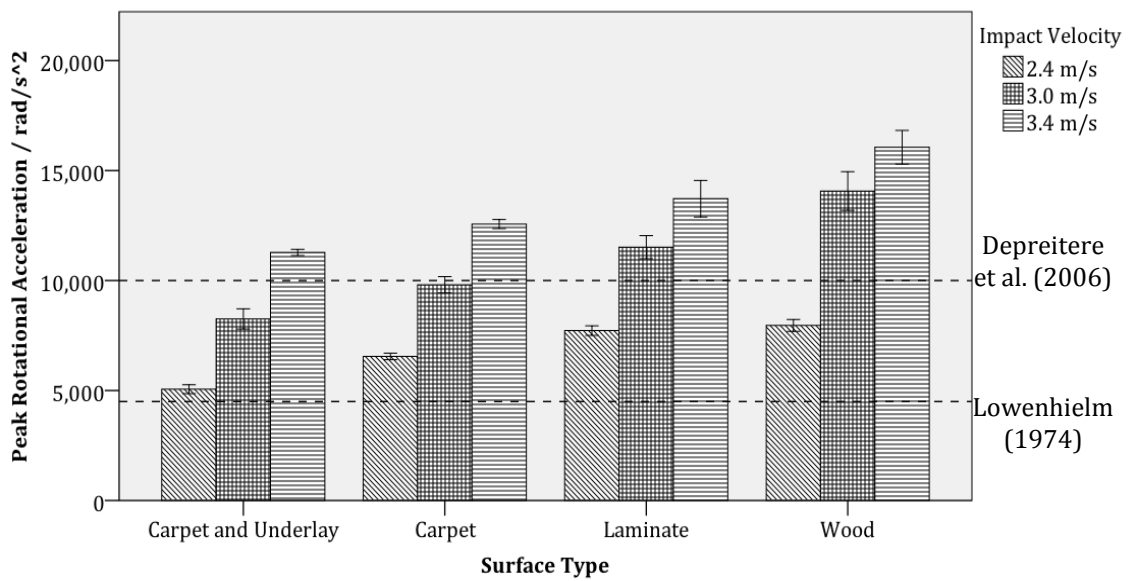


Figure 21. The effect that changing impact velocity and impact surface has on peak rotational acceleration at a 75 degree impact angle. Error bars equal standard of error.

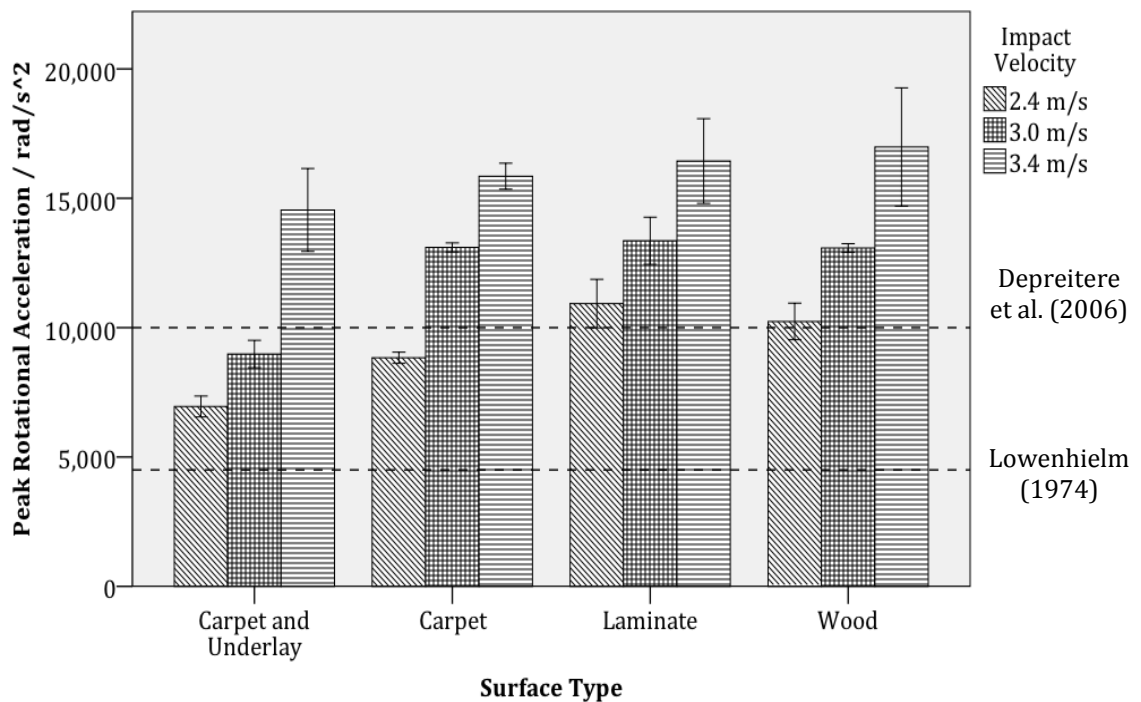


Figure 22. The effect that changing impact velocity and impact surface has on peak rotational acceleration at a 60 degree impact angle. Error bars equal standard of error.

### 4.3.2.3 Peak change in rotational velocity ( $\Delta\omega$ )

Rotational velocities were significantly influenced by impact velocity, impact surface and impact angle ( $P \leq 0.001$ ). The interaction between angle of impact and impact velocity had a significant effect on  $\Delta\omega$  ( $P < 0.001$ ), as did the interaction between the impact surface and angle of impact ( $P = 0.026$ ). However, the interaction between impact surface and impact velocity ( $P = 0.347$ ) did not. A three factorial ANOVA concluded that the three-way interaction of impact velocity, surface and angle of impact, significantly affected the  $\Delta\omega$  ( $P = 0.024$ ). The mean  $\Delta\omega$  values for the different scenarios tested can be seen in *Figure 23*, *Figure 24* and *Figure 25*.

#### 4.3.2.3.1 Impact Velocity ( $\Delta\omega$ )

At a 90 degree impact angle, an increase in impact velocity from 2.4m/s to 3.4m/s significantly increased  $\Delta\omega$  for the carpet-underlay, laminate and wood surfaces ( $P < 0.01$ ). An impact onto wood, at 90 degrees, increased  $\Delta\omega$  from 12.5 rad/s to 21.6 rad/s when impact velocity increased from 2.4m/s to 3.4m/s, *Figure 23*. An increase in impact velocity from 2.4m/s to 3m/s was only significant for carpet-underlay and laminate, at a 90 degree impact angle ( $P < 0.01$ ). The increase in impact velocity from 3m/s to 3.4m/s only significantly affected  $\Delta\omega$  for the wood surface ( $P = 0.001$ ).

At a 75 degree impact angle, all increases in impact velocity (2.4m/s to 3m/s, 3m/s to 3.4m/s and 2.4m/s to 3.4m/s) significantly increased  $\Delta\omega$  across all surfaces ( $P < 0.05$ ). All except, the increase from 3m/s to 3.4m/s onto carpet-underlay ( $P = 0.063$ ). At this impact angle, the peak  $\Delta\omega$  was 40.8 rad/s and occurred for the impact onto wood at 3.4m/s, increasing from 26.3 rad/s at an impact velocity 2.4m/s ( $P < 0.001$ ) (*Figure 24*).

Similar results were seen for the 60 degree impact, where again all increases in impact velocity significantly increased  $\Delta\omega$  across all surfaces tested ( $P < 0.01$ ). The peak  $\Delta\omega$  was 46.5 rad/s and again, it occurred for the impacts onto wood at 3.4m/s, increasing from 31.3 rad/s for the 2.4m/s impact ( $P < 0.001$ ) (*Figure 25*).

#### 4.3.2.3.2 Impact Surface ( $\Delta\omega$ )

Few significant differences were seen in  $\Delta\omega$  as a result of surface for a 90 degree impact angle. However, carpet-underlay significantly reduced  $\Delta\omega$ , compared with all other surfaces, at an impact velocity of 2.4m/s ( $P<0.01$ ). Carpet-underlay also significantly reduced  $\Delta\omega$ , compared with wood and laminate, at an impact velocity of 3.4m/s ( $P<0.03$ ). Peak change in rotational velocity decreased from 21.6rad/s to 15.3 rad/s, when comparing wood to carpet-underlay at an impact velocity of 3.4m/s ( $P=0.01$ ) (*Figure 23*). There were also significant differences in  $\Delta\omega$  between wood and laminate at 3m/s ( $P=0.005$ ).

A decrease in impact angle to 75 degree, saw a similar pattern in the results, where again impact surface had a limited affect on  $\Delta\omega$ . Only carpet-underlay significantly reduced  $\Delta\omega$ , compared to other surfaces and this was at an impact velocity of 3.4m/s ( $P<0.05$ ). Comparing carpet-underlay to wood, at an impact velocity of 3.4m/s and angle of 75 degrees, it can be seen that  $\Delta\omega$  is significantly reduced from 40.7 rad/s to 34 rad/s ( $P=0.003$ ) (*Figure 24*).

A further decrease in impact angle to 60 degrees, resulted in impact surface having less of a significant effect on  $\Delta\omega$ . Across all impact velocities tested, surface did not significantly affect  $\Delta\omega$  ( $P<0.02$ ), at this impact angle (60 degrees).

#### 4.3.2.3.3 Impact Angle ( $\Delta\omega$ )

A decrease in impact angle from 90 to 60 degrees significantly increased  $\Delta\omega$  across all surfaces and impact velocities ( $P<0.001$ ). An impact onto wood at 3.4m/s and at a 90 degree angle resulted in a  $\Delta\omega$  of 21.6 rad/s, for the same impact scenario at 60 degree this increased to 46.5rad/s ( $P<0.001$ ). Further comparisons can be made by investigating *Figure 23* and *Figure 25*.

Similarly, a decrease from 90 to 75 degrees significantly increased  $\Delta\omega$  across all impact velocities and surfaces tested ( $P<0.03$ ). Increases in  $\Delta\omega$ , as a result of this reduction in angle can be seen by comparing *Figure 23* and *Figure 24*.

A decrease from 75 to 60 degrees had a similar affect on  $\Delta\omega$ , where  $\Delta\omega$  significantly increased for all velocities and surfaces tested ( $P<0.05$ ), except for laminate at 3m/s ( $P=0.105$ ). Increases in  $\Delta\omega$ , as a result of this angle reduction can seen by comparing Figure 24 and Figure 25.

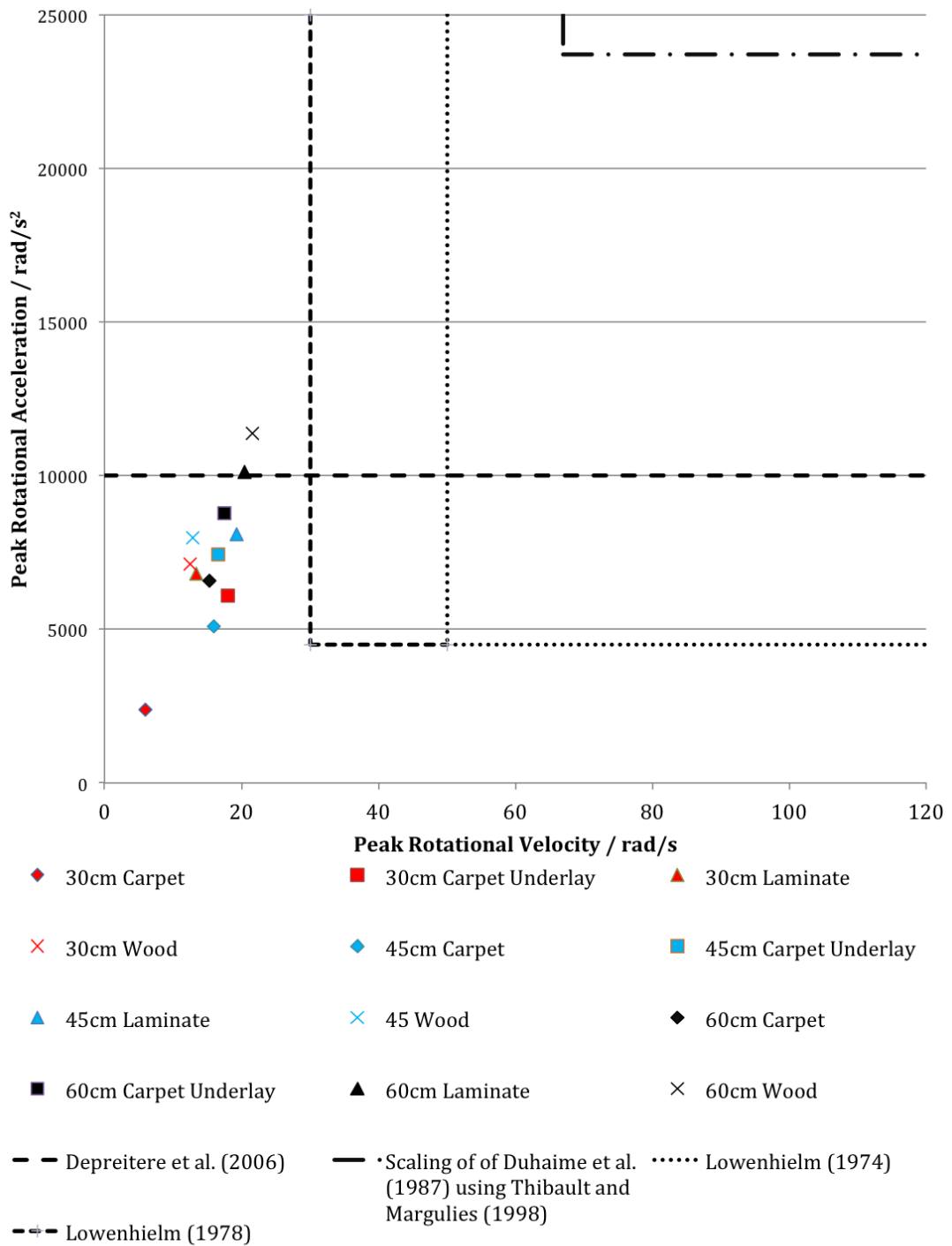


Figure 23. Rotational acceleration versus rotation velocity with varying impact surface and impact velocity at a 90 degree impact angle. Dotted lines indicate bridging vein rupture thresholds.

Chapter 4 – Physical Modelling of Infant Head Impacts

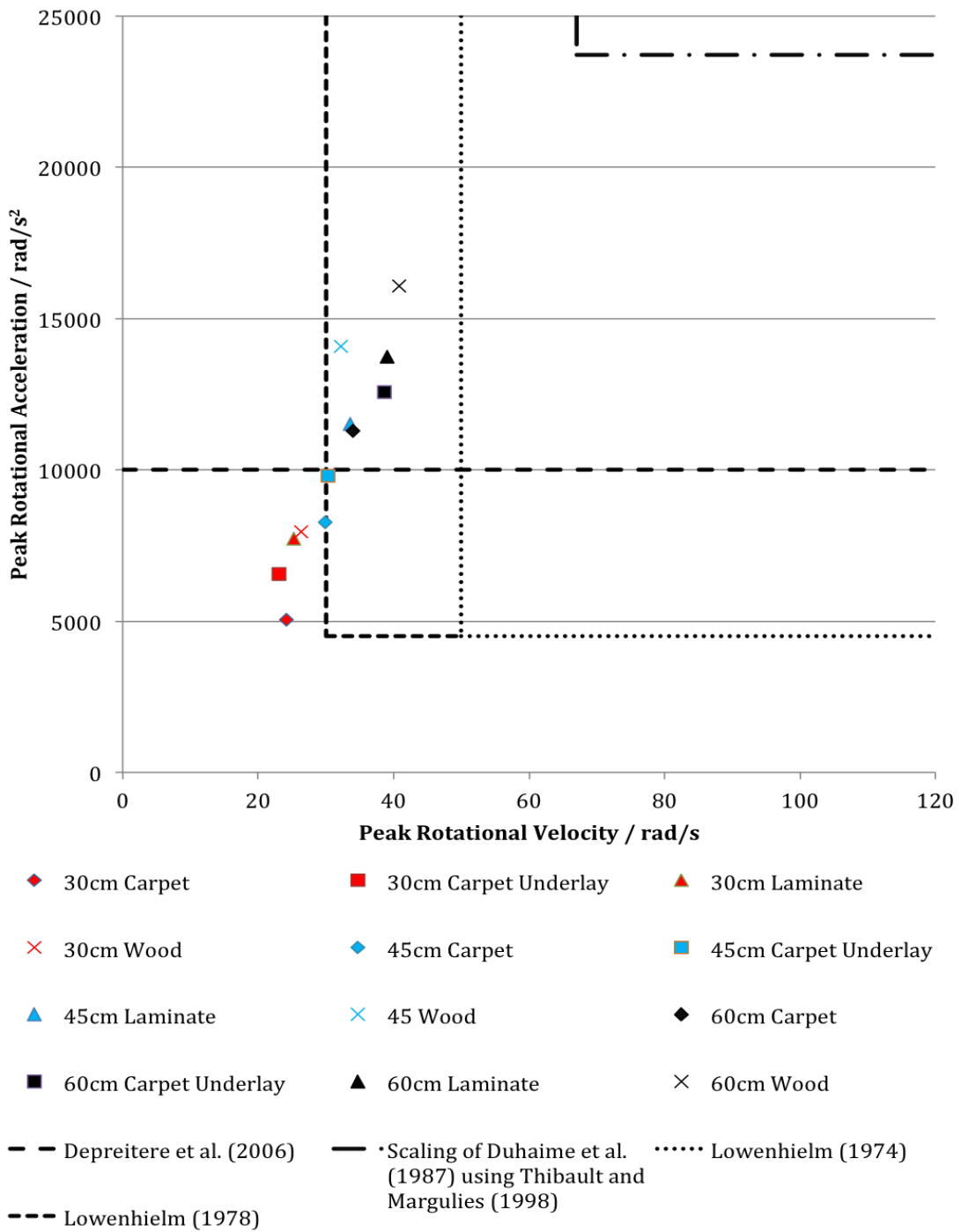


Figure 24. Rotational acceleration versus rotation velocity with varying impact surface and impact velocity at a 75 degree impact angle. Dotted lines indicate bridging vein rupture thresholds.

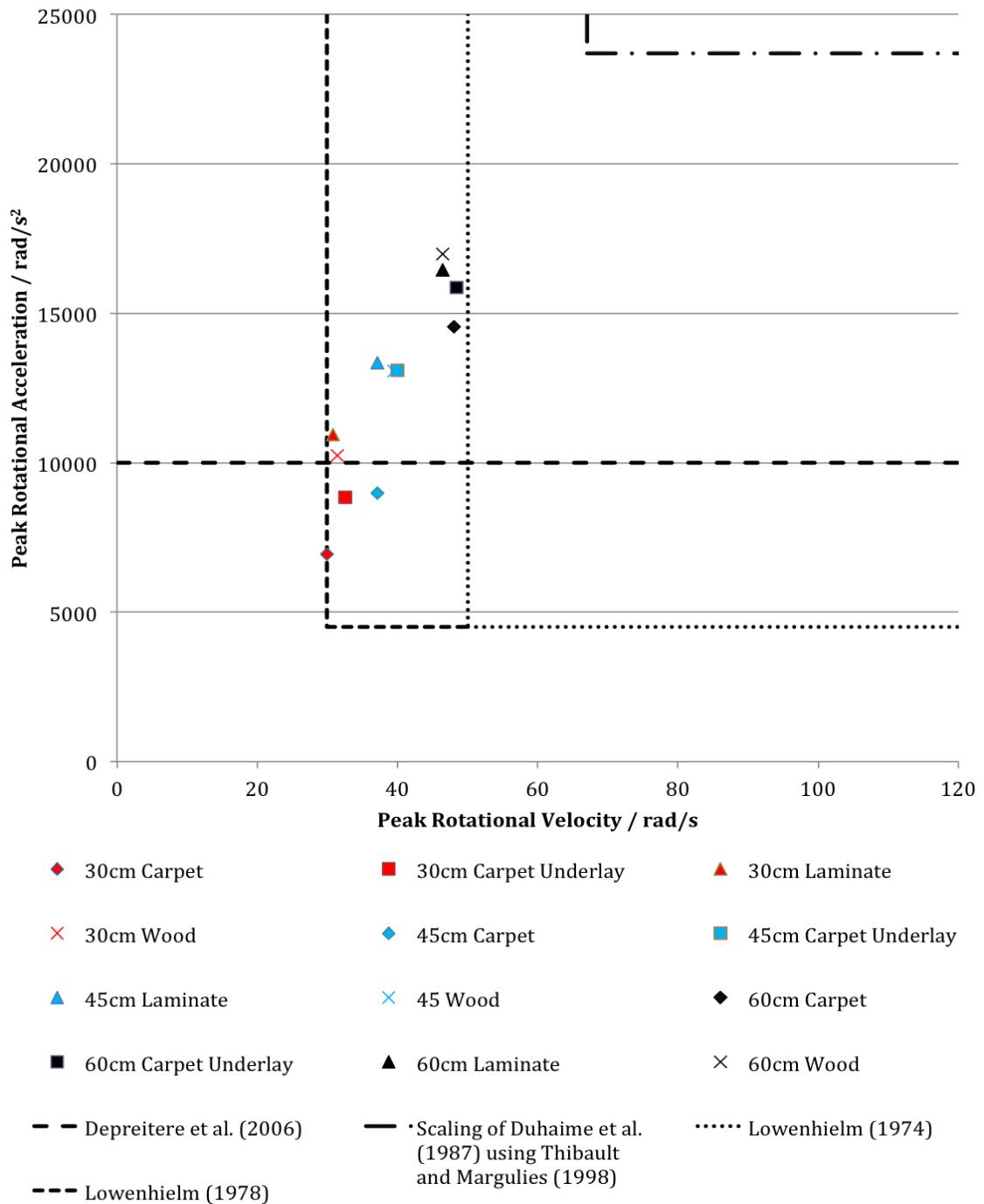


Figure 25. Rotational acceleration versus rotation velocity with varying impact surface and impact velocity at a 60 degree impact angle. Dotted lines indicate bridging vein rupture thresholds.



#### 4.3.2.4 Peak resultant linear accelerations (Peak $G_R$ )

Peak resultant linear accelerations (Peak  $G_R$ ) were calculated by taking the resultant value from the peak translational accelerations in the X, Y and Z components. Peak  $G_R$  significantly increased with increasing impact velocity ( $P < 0.001$ ), increasing surface stiffness ( $P < 0.001$ ) and decreased with decreasing impact angle ( $P < 0.001$ ). The interaction, between angle of impact and impact velocity, did not have a significant effect on peak  $G_R$  ( $P = 0.19$ ). The same was true for the interaction between the impact surface and impact velocity ( $P = 0.511$ ). However, the interaction between impact surface and impact angle did ( $P < 0.001$ ). A three factorial ANOVA concluded that the three-way interaction of impact velocity, surface and angle of impact significantly affected peak  $G_R$  ( $P = 0.028$ ). The mean peak  $G_R$  values, for the different scenarios tested, can be seen in Figure 26, Figure 27 and Figure 28.

##### 4.3.2.4.1 Impact Velocity (Peak $G_R$ )

Increase in impact velocity significantly increased peak  $G_R$  for all surfaces for the 90 degree, 75 degree and 60 degree impacts ( $P < 0.001$ ). For the 90-degree impacts, as impact velocity was increased from 2.4m/s to 3.4m/s, the mean peak  $G_R$  increased from 50.0g to 75.2g on carpet-underlay ( $P < 0.001$ ) and from 61.0g to 100.4g on wood ( $P < 0.001$ ). Further increases in peak  $G_R$ , as consequence of increasing impact velocity, can be seen in Figure 26, Figure 27 and Figure 28.

##### 4.3.2.4.2 Impact Surface (Peak $G_R$ )

At a 90 degree impact, carpet-underlay significantly reduced peak  $G_R$ , compared to carpet for the 2.4m/s and 3m/s impact velocities ( $P < 0.03$ ), however, it did not at 3.4m/s ( $P = 0.101$ ). At the 3m/s impact velocity, carpet increased the mean peak  $G_R$  to 70.6g from a mean value of 61.8g on the carpet-underlay surface ( $P = 0.02$ ). Compared to wood, carpet-underlay significantly reduced peak  $G_R$  across all impact velocities ( $P < 0.01$ ) and again, compared to wood, carpet significantly reduced it for the 3m/s and 3.4m/s impacts ( $P < 0.002$ ). Laminate and wood were

significantly different from each other, for the 2.4m/s and 3m/s impacts ( $P < 0.05$ ), but not at 3.4m/s ( $P = 0.396$ ), at this impact angle.

For the 75 degree impacts, again the carpet-underlay surface significantly reduced peak  $G_R$ , compared to wood, across all impact velocities ( $P < 0.001$ ). Also, compared to laminate, carpet-underlay significantly reduced peak  $G_R$  for the 2.4m/s and 3.4m/s impacts ( $P < 0.02$ ). There was no significant difference between the carpet-underlay and carpet surface, across all impact velocities, at the 75 degree angle ( $P > 0.5$ ). The same was true when comparing wood to laminate to wood ( $P > 0.05$ ).

A reduction in the impact angle, to 60 degrees, resulted in the carpet-underlay surface significantly reducing peak  $G_R$ , relative to carpet for 2.4m/s and 3m/s impacts ( $P < 0.01$ ). A similar pattern was seen when comparing the carpet-underlay surface to wood, where significant differences were seen for the 2.4m/s and the 3m/s impacts ( $P < 0.04$ ). Again, no significant differences were seen when comparing laminate and wood across all impacts velocities at this angle ( $P < 0.15$ ).

#### 4.3.2.4.3 Impact Angle (Peak $G_R$ )

A decrease in impact angle had a limited effect on peak  $G_R$ . For the carpet-underlay surface, only a reduction in impact angle from 90 to 60 degrees, at an impact velocity of 2.4m/s, significantly reduced peak  $G_R$  ( $P = 0.047$ ). For the same reduction in impact angle (90 to 60 degrees), there was no significant effect on peak  $G_R$  across all impact velocities for the carpet and laminate surfaces. However, impacts onto wood, at both 3m/s and 3.4m/s, did significantly reduce as the result of this angle reduction (90 to 60 degrees) ( $P < 0.002$ ). At an impact velocity of 3.4m/s, this angle reduction decreased peak  $G_R$  for wood, from 100.4g to 85.1g ( $P = 0.001$ ).

A 15 degree reduction in impact angle, from 90 to 75 degrees, also significantly reduced peak  $G_R$  for the carpet-underlay surface at 2.4m/s ( $P = 0.025$ ). A similar trend was seen for carpet, where peak  $G_R$  only significantly reduced for the 2.4m/s

impact for this reduction in angle (90 to 75 degrees) ( $P < 0.001$ ). Impacts onto laminate at 3.4m/s also resulted in a significant reduction in peak  $G_R$  ( $P = 0.003$ ), when the impact angle was reduced from 90 to 75 degrees.

A decrease in impact angle from 75 to 60 degrees did not significantly affect peak  $G_R$  for the carpet-underlay or laminate surfaces across all impact velocities ( $P > 0.12$ ). However, for the carpet surface, peak  $G_R$  significantly decreased for the 2.4m/s and 3.4m/s impacts for this angle reduction (75-60 degrees) ( $P < 0.05$ ). For this reduction in impact angle (75 to 60 degrees), peak  $G_R$  significantly reduced for wood at both the 3m/s and 3.4m/s impacts ( $P < 0.02$ ). Comparisons between *Figure 27* and *Figure 28* illustrate the level of decrease in terms of peak  $G_R$ .

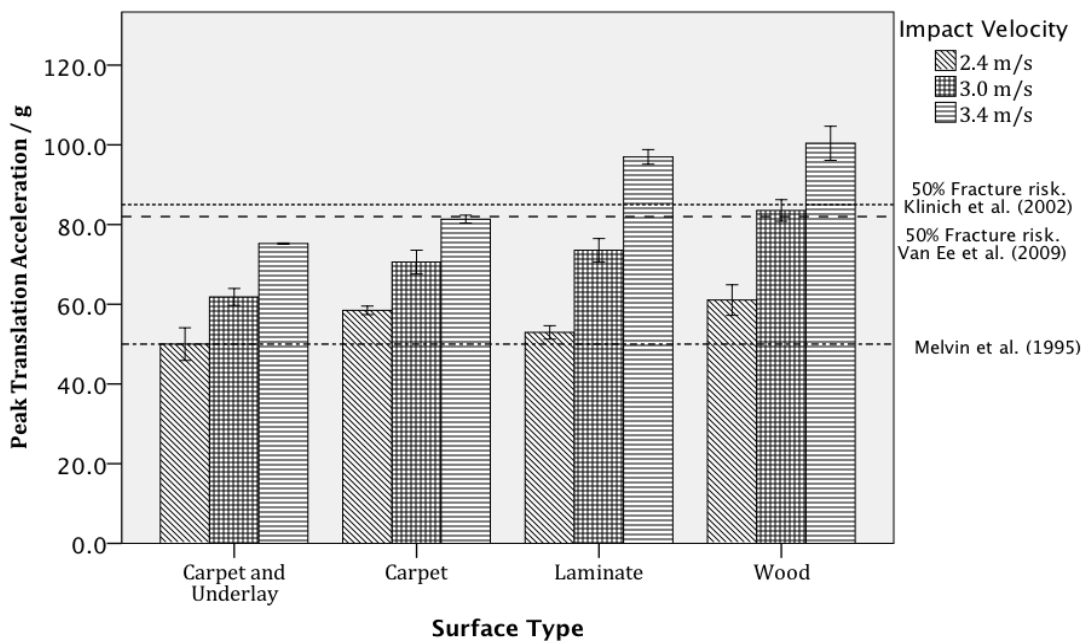


*Figure 26. Peak translational acceleration variation with changing impact velocity and impact surface at a 90 degree angle of impact. Dotted lines refer to head injury thresholds in children  $\leq 12$  months.*

Chapter 4 – Physical Modelling of Infant Head Impacts

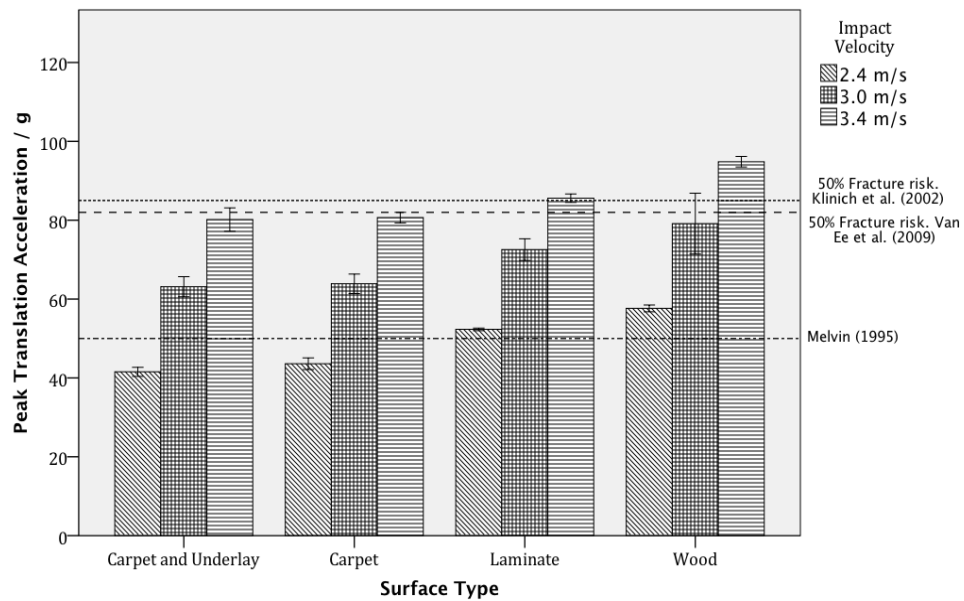


Figure 27. Peak translational acceleration variation with changing impact velocity and impact surface at a 75 degree angle of impact. Dotted lines refer to head injury thresholds in children  $\leq 12$  months.

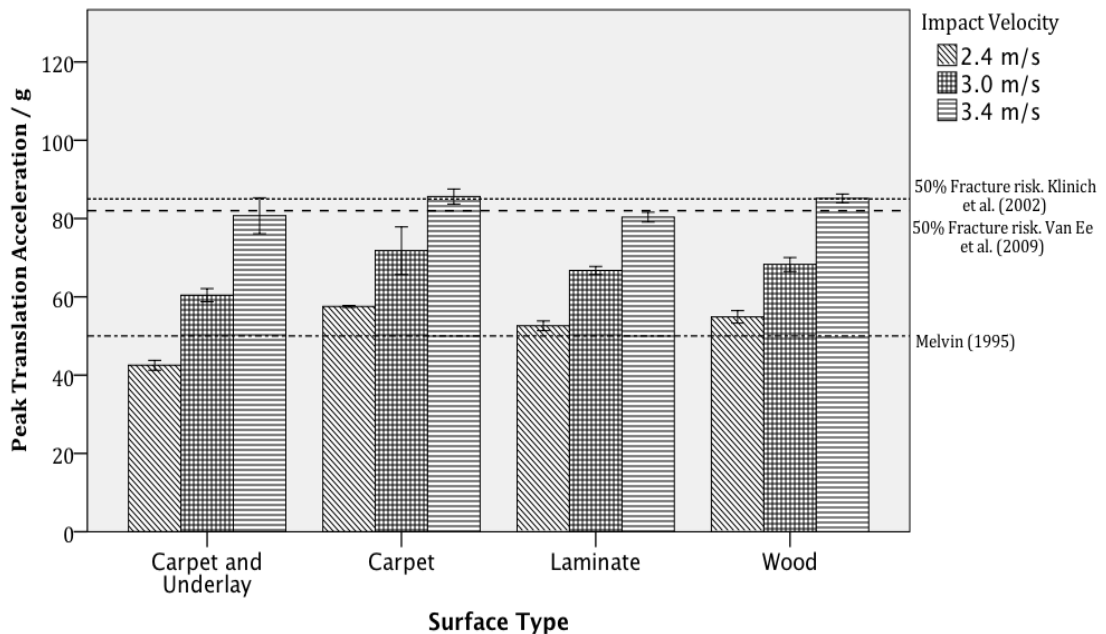


Figure 28. Peak translational acceleration variation with changing impact velocity and impact surface at a 90 degree angle of impact. Dotted lines refer to head injury thresholds in children  $\leq 12$  months. Error bars equal standard of error.

#### 4.3.2.5 Resultant head injury criterion (HIC<sub>R</sub>)

Resultant head injury criterion (HIC<sub>R</sub>) significantly increased, with increasing surface stiffness, increasing impact velocity and decreased with a decrease in the impact angle (P<0.001). The interaction between angle of impact and impact velocity (P<0.001), impact surface and impact velocity (P<0.001) and impact surface and impact angle (P<0.001) all significantly affected HIC<sub>R</sub>. A three factorial ANOVA concluded that the three-way interaction of impact velocity, surface and angle of impact significantly affected HIC<sub>R</sub> (P=0.013). The mean HIC<sub>R</sub> values for the different scenarios tested can be seen in Figure 29, *Figure 30* and *Figure 31*.

#### Impact Velocity (HIC<sub>R</sub>)

Similarly to peak G<sub>R</sub>, all increases in impact velocity significantly increased HIC<sub>R</sub> across all impact surfaces and angles (P<0.004). The lowest mean HIC<sub>R</sub>, for a 90 degree impact, was 63 and occurred on the carpet-underlay surface at an impact velocity of 2.4m/s. Increasing the impact velocity to 3.4m/s, for the same impact conditions, significantly increased HIC<sub>R</sub> to 159. Further increases in HIC<sub>R</sub>, as the result of impact velocity across the three angles of impact, can be seen in Figure 29, *Figure 30* and *Figure 31*.

##### 4.3.2.5.1 Impact Surface (HIC<sub>R</sub>)

At a 90 degree impact angle and 2.4m/s impact velocity, few significant differences were seen between the surfaces tested in terms of HIC<sub>R</sub>. However, carpet significantly reduced HIC<sub>R</sub>, compared to both the wood and laminate surfaces (P<0.02). An increase in the impact velocity to 3m/s, at this impact angle, saw the carpet-underlay surface significantly reduce HIC<sub>R</sub>, compared to all other surfaces (P<0.05). Carpet significantly reduced HIC<sub>R</sub> relative to wood (P<0.001) and laminate was significantly different to wood (P<0.001) for this impact conditions (90 degrees at 3m/s). A further increase in the impact velocity, to 3.4m/s at a 90 degree impact angle, resulted in all surfaces having significantly different HIC<sub>R</sub> values (P<0.02). The carpet-underlay surfaces significantly reduced HIC<sub>R</sub> relative to the other three surfaces (P<0.02) and carpet, also significantly reduced HIC<sub>R</sub>,

compared to wood and laminate ( $P < 0.02$ ). An impact onto wood increased the mean  $HIC_R$  to 245 from 159 on carpet-underlay for a 3.4m/s impact. Laminate also reduced  $HIC_R$ , compared to wood ( $P < 0.001$ ). The affect of impact surface on  $HIC_R$ , at this impact angle can be seen in Figure 29.

A similar pattern was seen when comparing the significance of  $HIC_R$  between surfaces for the reduced impact angle of 75 degrees. At the lowest impact velocity of 2.4m/s, impact surface did not significantly influence  $HIC_R$  ( $P \geq 0.05$ ). An increase in the impact to velocity to 3m/s, resulted in impact surface significant affecting  $HIC_R$  for certain comparisons. The carpet-underlay surfaces significantly reduced  $HIC_R$ , compared to both laminate and wood ( $P < 0.05$ ), but not carpet ( $P = 0.042$ ). At this impact velocity and angle (3m/s at 75 degrees), carpet was only significantly different to wood in terms of  $HIC_R$  ( $P < 0.001$ ). Laminate and wood were also significantly different at this impact velocity and angle (3m/s at 75 degrees) ( $P = 0.003$ ). A further increase in the impact velocity to 3.4m/s resulted in greater differences between impact surfaces. Again the carpet-underlay surface significantly reduced  $HIC_R$ , compared to laminate and wood ( $P < 0.005$ ), but not carpet ( $P = 0.448$ ). Carpet also significantly reduced  $HIC_R$  relative to both wood and laminate at this impact velocity and angle (3.4m/s at 75 degrees) ( $P < 0.04$ ). The affect of impact surface on  $HIC_R$  at this impact angle can be seen in *Figure 30*.

A decrease in impact angle to 60 degrees resulted in fewer significant differences between the surfaces. The carpet-underlay surface was significantly different to both carpet and wood ( $P < 0.021$ ) at an impact velocity of 2.4m/s. However, carpet was not significantly different from either wood or laminate, and wood and laminate were not significantly different from each other, at this impact angle and velocity (2.4m/s at 60 degrees) ( $P > 0.08$ ). An increase in the impact velocity to 3m/s resulted in only the carpet-underlay surface and wood being significantly different from each other, where carpet-underlay reduced  $HIC_R$  from 80.1 to 60.7 at the 60 degree impact angle ( $P = 0.015$ ). A further increase in the impact velocity to 3.4m/s at the 60 degree impact angle, resulted in surface not having a

significant influence on  $HIC_R$  ( $P>0.5$ ). The effect of impact surface on  $HIC_R$ , at this impact angle (60 degrees), can be seen in Figure 31.

#### 4.3.2.5.2 Impact Angle( $HIC_R$ )

A 30 degree reduction in impact angle, from 90 to 60 degrees, significantly reduced  $HIC_R$  for carpet-underlay, laminate and wood, across all impact velocities ( $P<0.003$ ). For an impact onto wood at 3.4m/s,  $HIC_R$  reduced from 245 to 121 ( $P<0.001$ ). For carpet, a 30 degree decrease in impact angle significantly reduced  $HIC_R$  for the 3m/s and 3.4m/s impacts ( $P<0.001$ ). The effect of the 30 degree reduction in impact angle on  $HIC_R$  can be seen by comparing Figure 29 and Figure 31.

A decrease in impact angle, from 90 to 75 degrees, saw a similar pattern of results, as the reduction from 90 to 60 degrees. Whereby  $HIC_R$  was significantly reduced for carpet-underlay, laminate and wood, across all impact velocities ( $P<0.02$ ). Again, for the carpet surface, this decrease in impact angle only significantly decreased  $HIC_R$  for the 3m/s and 3.4m/s impacts ( $P<0.001$ ). The effect of this 15 degree reduction in impact angle, on  $HIC_R$ , can be seen by comparing Figure 29 and Figure 30.

The reduction in impact angle, from 75 to 60 degrees, resulted in fewer significant differences in terms of  $HIC_R$ . For this decrease in angle, no significant effect was seen for impacts on carpet-underlay, laminate or carpet across all impact velocities ( $P>0.05$ ). However,  $HIC_R$  did significantly reduce, due to the reduction in angle for impacts onto wood at 3m/s and 3.4m/s ( $P<0.001$ ). The effect of this 15 degree reduction in impact angle on  $HIC_R$  can be seen by comparing Figure 30 and Figure 31.

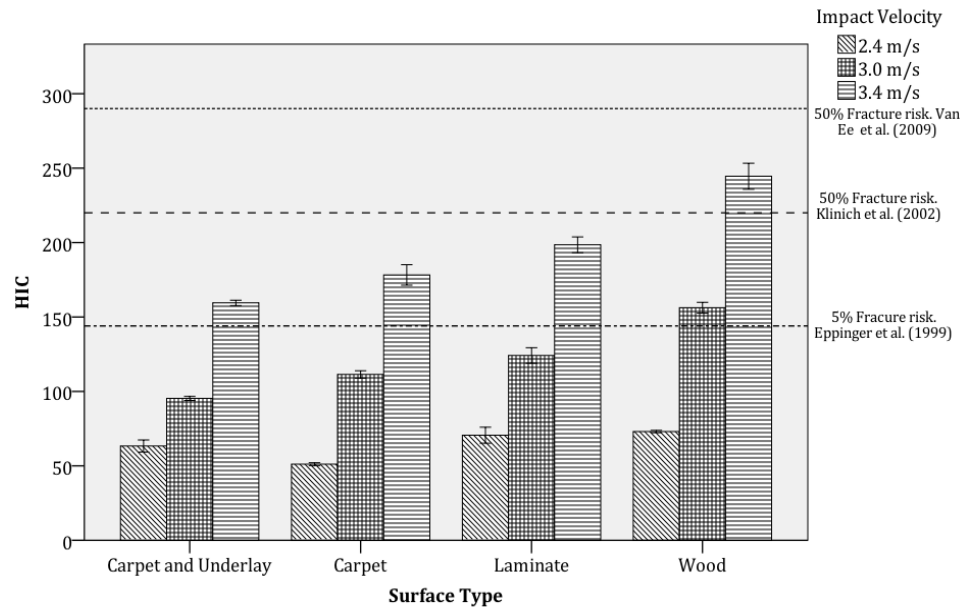


Figure 29. Head Injury Criterion (HIC) variation with changing impact velocity and impact surface for a 90 degree angle of impact. Dotted lines refer to refer skull fracture thresholds in children  $\leq 12$  months.

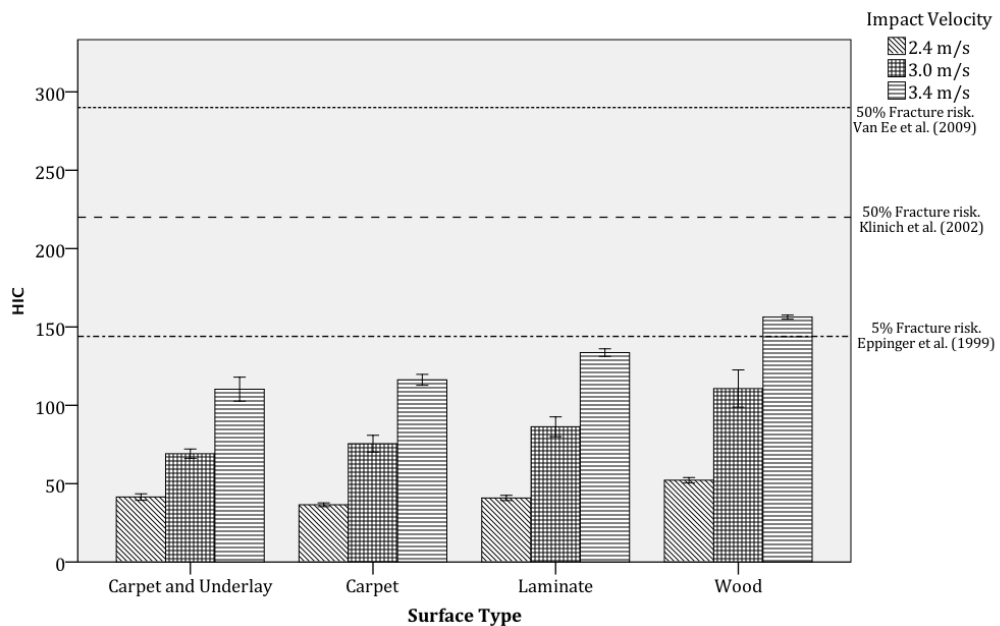


Figure 30. Resultant Head Injury Criterion (HIC) variation with changing impact velocity and impact surface for a 75 degree angle of impact. Dotted lines refer to refer skull fracture thresholds in children  $\leq 12$  months.



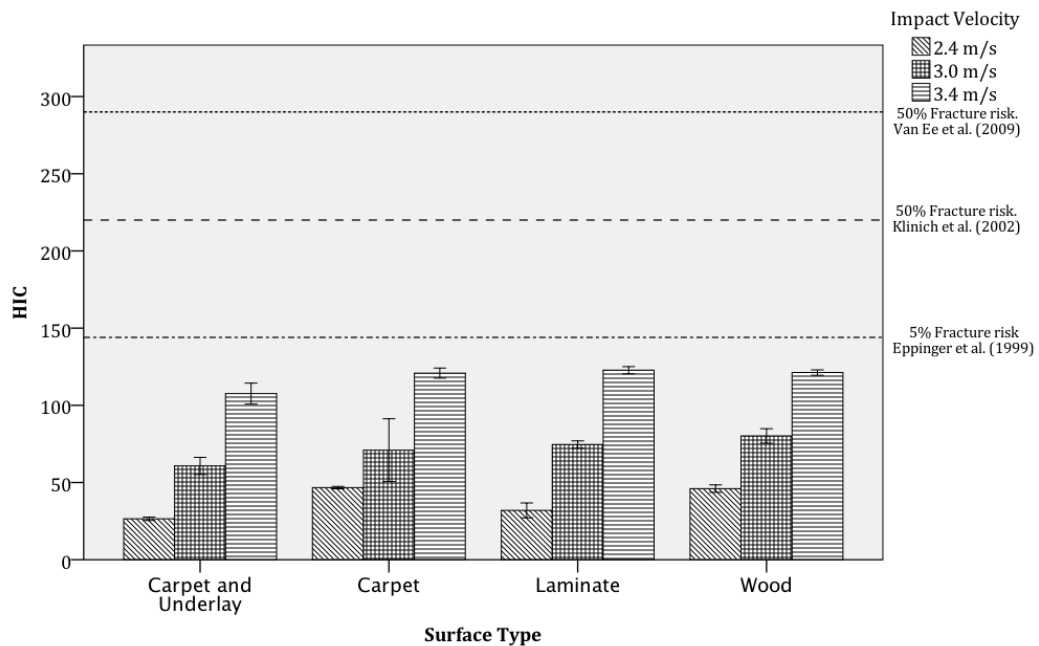


Figure 31. Resultant Head Injury Criterion (HIC) variation with changing impact velocity and impact surface for a 75 degree angle of impact. Dotted lines refer to skull fracture thresholds in children  $\leq 12$  months.

#### 4.3.2.6 Impact Duration ( $\Delta t$ )

Impact duration significantly decreased, with increasing impact velocity ( $P < 0.001$ ), increasing surface stiffness ( $P < 0.001$ ) and was significantly affected by a decreasing impact angle ( $P < 0.001$ ). The interaction between angle of impact and impact velocity did not have a significant effect on  $\Delta t$  ( $P = 0.213$ ). However, the interaction between impact surface and impact angle ( $P < 0.001$ ) and the interaction between impact surface and velocity did ( $P < 0.001$ ). A three factorial ANOVA concluded that the three-way interaction of impact velocity, surface and angle of impact did not significantly affect  $\Delta t$  ( $P = 0.162$ ). The mean  $\Delta t$  values for the different scenarios tested can be seen in Table 18.

##### 4.3.2.6.1 Impact velocity ( $\Delta t$ )

Duration of impact significantly reduced with an increase in impact velocity across all impact surfaces and angles tested ( $P < 0.002$ ). The highest mean  $\Delta t$  was 22ms and occurred on the carpet-underlay surface at an impact velocity of 2.4m/s and at angle of 90 degree, this decreased to 17.8ms when the impact velocity increased to 3.4m/s (Table 18).

### 4.3.2.6.2 Surface ( $\Delta t$ )

At a 90 degree impact angle, the carpet-underlay surface significantly increased  $\Delta t$ , compared to all other surfaces, for both the 2.4m/s and 3.4m/s impacts ( $P < 0.005$ ). However, for the 3m/s impact, at this angle, the carpet-underlay surface only significantly increased  $\Delta t$  compared to carpet and wood ( $P < 0.002$ ). Carpet did not significantly increase  $\Delta t$ , compared to either wood or laminate, across all impact velocities at this angle ( $P > 0.05$ ). At this 90 degree angle, wood and laminate were only significantly different from each other at 3 m/s impact velocity ( $P = 0.007$ ).

For the 75 degree impacts, the carpet-underlay surface significantly increased  $\Delta t$ , compared to all other surfaces across all impact velocities tested ( $P < 0.007$ ). However, at this angle, the carpet surface significantly increased  $\Delta t$ , compared to wood and laminate at a 2.4m/s impact ( $P < 0.002$ ), but not at a 3m/s or 3.4m/s impact ( $P > 0.06$ ). Again wood and laminate were not significantly different in terms of  $\Delta t$  across all impact velocities at this impact angle (75 degrees) ( $P > 0.1$ ).

A decrease in impact angle to 60 degrees resulted in fewer significant differences in  $\Delta t$  as a result of the surface. The carpet-underlay surface only significantly increased  $\Delta t$ , compared to wood and laminate, for the 2.4m/s and 3.4m/s impacts ( $P < 0.04$ ). The carpet-underlay and carpet were not significantly from each other across all impact velocities at this angle ( $P > 0.07$ ). Wood and laminate were only significantly different from each other at an impact velocity of 2.4m/s ( $P = 0.001$ ).

### 4.3.2.6.3 Angle ( $\Delta t$ )

A decrease in impact angle from 90 to 60 degrees had few significant effects on  $\Delta t$ . Only impacts at 2.4m/s onto wood and also carpet-underlay were significantly affected by this angle reduction (90 to 60 degrees) ( $P < 0.02$ ).

A 15 degree decrease in impact angle from 90 to 75 degrees also had few significant effects on  $\Delta t$ . For the 2.4m/s impacts, only impacts onto wood and carpet significantly affected  $\Delta t$  ( $P < 0.05$ ). However, at 3m/s, the same reduction in

impact angle (90 to 75 degrees) significantly affected  $\Delta t$  for the carpet-underlay and wood surfaces ( $P < 0.02$ ). At the 3.4m/s impact velocity, again this reduction in impact angle (90 to 75 degrees), did not significantly affect duration of impact for impacts onto carpet-underlay and carpet ( $P < 0.04$ ).

A decrease in impact angle from 75 to 60 degrees had no significant effect on  $\Delta t$  for both the laminate and wood surfaces across all impact velocities ( $P > 0.05$ ). However, for all impact velocities, a 15 degree reduction in impact angle significantly decreased  $\Delta t$  on the carpet-underlay surface ( $P < 0.008$ ). On carpet,  $\Delta t$  only significantly reduced for the 2.4m/s impact for this angle reduction (75 to 60 degrees) ( $P = 0.035$ )

Table 18. The effect of impact angle, impact surface and impact velocity on the duration of impact.

Impact Angle / Degree	Impact Surface	Impact Velocity / m/s	Mean duration of impact / ms Mean (SE)
90	Carpet-underlay	2.4	22(1.6)
		3.0	18.6(0.2)
		3.4	17.8(0.3)
	Carpet	2.4	17.8(0.1)
		3.0	16.9(0.2)
		3.4	16.2(0.2)
	Laminate	2.4	16.8(0.2)
		3.0	17(1)
		3.4	15.6(0.2)
	Wood	2.4	16.7(0.2)
		3.0	16.1(0.4)
		3.4	15.2(0.1)
75	Carpet-underlay	2.4	21.8(0.3)
		3.0	19.9(0.4)
		3.4	18.7(0.4)
	Carpet	2.4	19(0.5)
		3.0	17.2(0.2)
		3.4	16.7(0.4)
	Laminate	2.4	16.8(0.2)
		3.0	16.5(0.3)
		3.4	16(0.1)
	Wood	2.4	17.4(0.2)
		3.0	16.9(0.2)
		3.4	15.9(0.2)
60	Carpet-underlay	2.4	20.5(0.5)
		3.0	19(0.3)
		3.4	17.7(0.2)
	Carpet	2.4	18.6(0.1)
		3.0	18.2(0.7)
		3.4	16.4(0.2)
	Laminate	2.4	16.8(0.5)
		3.0	16.3(0.4)
		3.4	14.1(1.8)
	Wood	2.4	17(0.5)
		3.0	16.7(0.3)
		3.4	15.9(0.4)

#### **4.4 Discussion**

Head injuries in young children as the result of a fall are a common occurrence in the UK <sup>24</sup>, however differentiating between a fall that can or cannot result in a skull fracture and / or ICI remains difficult for clinicians. In Chapter 3 a potential fall height threshold was established of 0.6m, based on the fact that no cases of skull fracture and /or ICI were reported below this height. A novel approach was used to design and manufacture a biofidelic anthropomorphic testing device from infant CT datasets. This led to the development of an infant headform, which was validated against cadaver data. Consequently it allowed for the unique assessment of the effect that angle of impact and friction have on head impact response variables. In conjunction with the effect of other variables, that have been assessed by previous researchers, impact surface and impact velocity (related to fall height). Angle of impact, friction, impact velocity and impact surface significantly affected one or more of the kinematic variables, associated with the severity of head injury.

##### **4.4.1 Impact Angle**

A fall from a carer's arms and a fall from a raised surface were the two most common mechanisms for producing skull fracture and / or ICI (Chapter 3). In such incidents, it is unlikely that a child would fall and impact its head at a 90 degree angle. All previous research, using ATDs, have only investigated 90 degree impacts and as a result, have not considered the potential effects of a decrease in impact angle. They are therefore, unlikely to fully replicate the incidents that lead to minor head or skull fracture and / or ICI in young children. This study has shown that impact angle has a significant effect on kinematic variables associated with head injury severity. The greatest significant effect was on rotational accelerations, where up to a 50% increase in mean  $\alpha_p$  was seen, due to a decrease in impact angle. Interestingly, a decrease of 30 degrees, significantly increased  $\alpha_p$  and  $\Delta\omega$  across all the combinations of impact surfaces and impact velocities tested. A possible explanation for this was that a decrease in impact angle increased the decelerations tangential to the impact surface and as a result, the force exerted on

the headform tangential to the surface would be higher, thus causing a greater moment about the centre of mass of the headform.

The significant effect of impact angle on kinematic variables, associated with head injury severity, adds further complexity to understanding the possible causes of severe head injury in young children as the result of a low height fall. Whilst the rotational kinematic variables increased, the translational variables ( $HIC_R$ ) decreased. A general biomechanical interpretation of this implies that a decrease in impact angle has the potential to increase the risk of diffuse patterns of traumatic brain injury (e.g. bridging vein rupture) as opposed to a focal injury. However, it remains difficult to quantify the increase in injury risk, due to a decreasing angle of impact, because of a lack of clinically assessed thresholds in terms of the kinematic variables. As this is the first study to measure this effect, further biomechanical and clinical work should consider impact angle, so that further understanding can be gained on the effect of this variable.

#### **4.4.2 Impact Velocity**

In accordance with previous research, the impact velocity (associated with fall height), significantly affected the rotational and translational kinematic variables. An increase in impact velocity from 2.4m/s to 3.4m/s (corresponding to an increase of 30cm) significantly increased the  $\alpha_p$ ,  $\Delta\omega$ , peak  $G_R$  and  $HIC_R$ . This effect was evident across the range of impact surfaces and angle of impacts tested. Due to a higher impact velocity, the resultant translation decelerations, both perpendicular and tangential to the surface, would be higher. Since, the forces transferred to the headform would be greater, therefore increasing peak G and HIC. Larger forces, perpendicular and parallel to the impact surface, would result in greater moments being applied about the centre of mass of the headform, consequently increasing  $\alpha_p$  and  $\Delta\omega$ . The significant effect of impact velocity (corresponding to fall height) further highlights the need for an accurate fall height to be recorded in the clinical and forensic context of evaluating head injury

severity from a fall, particularly when considering the significant differences observed with only a 15cm increase in the fall height.

#### **4.4.3 Impact Surface**

Surface stiffness had a more complex effect on the translational and rotational kinematic variables. Comparing wood with carpet-underlay indicated that an increase in surface stiffness increases  $\alpha_p$ , and peak G across all combinations of impact velocity and impact angle. However, comparing carpet-underlay to carpet only showed significant differences across all combinations of impact velocities at an impact angle of 90 degrees, but not for 75 and 60 degree impacts in terms of  $\alpha_p$ . Translational accelerations reduced, with a decrease in impact angle, thereby implying that a certain amount of force is required on impact, prior to the underlay absorbing part of the impact and thus, significantly reducing peak  $\alpha$ . This was illustrated further, by HIC not being significantly different between carpet, with and without underlay, at the lowest impact velocity tested. It did, however, become significant with an increase in impact velocity. The same was true when comparing carpet-underlay to wood at 90 and 75 degree, where there was only a significant difference in HIC at 3m/s and 3.4m/s. Thus it is apparent that the affect of surface varies depending on the impact scenario, increasing height resulted in greater differences between the surfaces and decreasing angle resulting fewer differences. The changing effect of surfaces with impact scenario has been documented by previous authors, Coats and Margulies<sup>3</sup> hypothesised that carpet fully compressed between 0.6 and 0.9m. This was highlighted by insignificant differences in the kinematic variables between carpet and concrete in their research at 0.9m. Whilst this research did not conduct measurement up to 0.9m, it implies that the protective effect of carpet or underlay is not consistent across all fall heights. Previous research has highlighted the importance of considering the full surface composition<sup>6</sup> and not just the top surface layer. This research, with a validated infant headform, supports that finding, considering the effect that carpet & underlay, compared to carpet had on the kinematic variables at the higher impact velocities.

#### 4.4.4 Skin Friction

Coats and Margulies<sup>3</sup> hypothesised that rotational accelerations, during impact, were potentially caused by friction “gripping” the head and thus, causing it to rotate. Two surrogate friction surfaces (Latex and polyamide) were used to assess the effect of friction. The latex skin surrogate increased peak rotational acceleration across 13.9% (n=5) of the 36 different combinations of impact velocity, surface and angle. Four of five of these cases were at the lowest impact velocity of 2.4m/s. The coefficient of static friction for latex ranged from being 81% greater compared to the polyamide on wood, whereas compared with laminate it was 231% greater. However, this increase in the coefficient of friction did not result in proportionate increases in peak rotational accelerations. Thus, whilst this study implies that coefficient of static friction has a limited effect on magnitude of rotational accelerations, at the lowest impact velocity tested, an increase in impact velocity resulted in the effect of friction becoming less significant. Also, a decrease in the angle of impact did not amplify the effect of friction, that is, cause greater headform rotation, as was hypothesised. Whilst on impact friction would prevent sliding between the head and the impact surface, once rolling or rotation has started, the affect of friction reduces. This implies, therefore, that across the range of coefficient of friction values and angles of impact, friction is not the main cause of rotation, but it needs consideration, particularly at lower impact velocities. However, further research is needed to investigate slighter angles of impact, to see if this effect remains constant. Also, more extreme values for the coefficient friction could be investigated, both greater and lesser than the values reported for human skin, to investigate if there is a limit when friction has a significant effect on rotation.



#### 4.4.5 Biomechanics of injury

Understanding the causes of head injury, as the result of trauma, is paramount to improving safety. The causes of different types of traumatic brain injury are commonly attributed to either translational or rotational accelerations (Section 2.3.1). However, this research, along with others, has reported that both significant rotational and translational accelerations can result from a fall, particularly during a 90 degree impact. This highlights that neither form of acceleration occurs in isolation. Consequently, caution should be adopted before a fall is attributed as simply an incident that only results in translational accelerations. A surprising result was the high rotational accelerations that the headform demonstrated during the perpendicular impacts, Figure 20. The neck and body were absent from this study and as such, the range of motion was not constrained to a particular axis. It was expected from the perpendicular impacts that the head would impact and deform and then accelerate back in the direction of impact, as the direction of the resultant force, due to the mass of the head would be perpendicular to the impact point. Integrating the high speed video and accelerometer data, it became apparent that the natural curvature of head combined with non uniform deformation during impact, appeared to migrate the mass of the head such that the resultant force, due to headform mass was offset from the impact point. Thereby causing a moment about the point of contact and producing large rotational accelerations. Coupling this with the rotational acceleration data for the 75° and 60°, where an increase in surface stiffness produced higher values (i.e carpet-underlay vs wood). Therefore initial head deformation could be one of the causes of rotation accelerations during impact. Head curvature has been previously attributed to the potential for a head injury, where Coats *et al* <sup>25</sup> state an irregular curvature in the parietal-occipital area caused their headform to rotate to the left, thus increasing fracture risk on the left. Given curvature and deformation would remain relevant even with the inclusion of the neck and body, it highlights a previously un-investigated variable with respect to head injury severity.

#### 4.4.6 Thresholds

##### 4.4.6.1 Thresholds - Overview

The kinematic variables measured in this study are commonly associated with different types of traumatic brain injury. Determining the injury risk, using these kinematic variables, involves comparing the values to a known threshold. Adult thresholds have been determined by subjecting adult cadavers to injurious and non-injurious impact tests and measuring the impact response<sup>26-29</sup>. Currently there is no published literature where infant or young child cadavers have been subject to injurious impact tests and the impact response, in terms of the kinematic variables, measured. As a result, the thresholds to date for young children have been inferred from adult thresholds<sup>26,30</sup>, by either scaling from human adults or adult primates<sup>13,14,31-33</sup>, reconstructing motor vehicle accidents involving infants using an ATD<sup>34</sup>, or reconstructing infant cadaver impact tests, using an ATD<sup>35</sup> (The impact response in the original tests were not measured). None of the thresholds, however, have been validated against the head injuries that are commonly seen in the paediatric clinical setting. A clinical review of head injuries (see Chapter 3), where the reported mechanism of injury was a fall, established a potential minimum fall height threshold of 0.6m, below which, there were no cases of a skull fracture and / or ICI. Thus, all kinematic variables measured in this chapter should be sub-injurious, thereby giving a marker with which the current kinematic thresholds for head injury from the literature can be assessed. The headform developed and used for experimentation in this study was aimed at infants less than 3 months of age. However, the clinical data in Chapter 3, covered ages up to 48 months; and biomechanical thresholds in the literature cover a wider scope of ages, varying from less than 12 months to 3 years. Consequently, kinematic variables were extracted for heights approximating 0.6m, from previous biomechanical studies using ATDs for ages up to 48 months.

#### 4.4.6.2 Thresholds - Application

Previous research, aimed at young children, using ATDs to determine the risk of head injury, from a low height fall, often do not consider all the kinematic variables prior to assessing the injury risk. A common misinterpretation of the kinematic threshold, when assessing the potential for bridging vein rupture, has been for authors to only measure rotational accelerations and not consider the duration of impact or change in rotational velocity. Whilst adult bridging vein thresholds, in the literature, do not appear relevant to paediatrics, application of just the rotational accelerations would imply a risk of bridging vein rupture in this study. Löwenhielm <sup>27</sup>, documents that both rotational acceleration and velocity thresholds need to be crossed for there to be a risk of bridging vein rupture. Thus, when considered in combination (rotational acceleration and velocity) this data does not imply an injury risk. Again this is true for the threshold proposed by Depreitere *et al* <sup>26</sup>, where it is only relevant to impact durations of less than 10ms. However, no impact duration in this study was below less than 10ms. Whilst duration of impact has been taken into consideration for the translational kinematic variables, using ATDs, by the time durations being defined in HIC<sub>15</sub> and HIC<sub>36</sub>, future research should consider the effect of duration of impact, with respect to rotational kinematic variables.

#### 4.4.6.3 Thresholds – SDH/Bridging vein rupture

Bridging vein rupture thresholds for adults have been reported between rotational acceleration values of 4,500 rad/s<sup>2</sup> and 10,000rad/s<sup>2</sup> with a corresponding change in rotational velocity varying between 30rad/s and 50rad/s<sup>26, 27, 36</sup>. Whilst is generally accepted that these thresholds relate to adults and that there is no accepted method for scaling them, authors often imply an injury risk by applying them. Whilst early literature suggested 23,700rad/s<sup>2</sup> for a SDH using scaling techniques<sup>37</sup>, recently authors suggest not to apply scaling, since no correct scaling technique has been accepted<sup>3</sup>.

The lower thresholds, presented in Figure 20 - Figure 25 are based on impact tests with adult cadavers and provide an “idea of scale” with regard to rotational accelerations and velocities. Thus, under no circumstances should these figures be interpreted as implying injury risk. An overview of the relevant thresholds is outlined in section 2.3.2. However as the relevance of these thresholds to the paediatric clinical setting, have yet to be determined, this research provides a unique opportunity to conduct an assessment. The 4,500 rad/s<sup>2</sup> threshold proposed by Löwenhielm <sup>27</sup>, when taken in isolation, does not appear relevant to the age range investigated, since it implies an injury risk from falls from heights of 0.3m or lower, which does not appear to correlate with the clinical (epidemiological) data. A comparison of this threshold with work previously undertaken by other research groups, using young child ATDs, adds weight to this observation. Figure 6J, Appendix 6 illustrates the values for the rotational accelerations, seen from falls close to 0.6m in the literature, where it can be observed there would be the possibility of bridging vein rupture, using the 4,500 rad/s<sup>2</sup> threshold from heights of 0.6m or lower. This, again contradicts what was observed in the clinical data. The result from the impact testing, in this research, was using an infant ATD (<3months), however, the clinical data (Chapter 3) covered ages ranging from 0 to 48 months. Therefore, using previous research, documented in literature, namely Thompson and Bertocci <sup>21</sup> and Ibrahim and Margulies <sup>38</sup>, allows investigation of a greater age range, where the ATDs were aged 12 month and 18 month respectively. Again, through investigation of Figure 6J, Appendix 6, the 4,500 rad/s<sup>2</sup> proposed by Löwenhielm <sup>27</sup> does not appear relevant across this age range. The original research by Löwenhielm <sup>27</sup> suggested bridging vein rupture was possible, if rotational velocities were greater than 50 rad/s, in combination with rotational accelerations greater than 4,500 rad/s<sup>2</sup>, however, this was later altered by Löwenhielm <sup>36</sup> to 30 rad/s. Investigating only the 90 degree impacts, it can be seen, from Figure 23, that no rotational velocities crossed the lower threshold of 30 rad/s, but for the 75 and 60 degree impacts, they did, thus, questioning the relevance of this threshold children in this age range. The 50 rad/s threshold was not crossed for the ranges of impact angle tested,

therefore, demonstrating greater application of this particular threshold. However, considering previous research, Figure 6I Appendix 6, the values reported by Coats and Margulies<sup>3</sup> cross these thresholds, implying that caution should be adopted and further research conducted prior to its application. Again, investigating the literature where researchers have conducted experiments using a wider age range of ATDs, Figure 6I Appendix 6, rotational velocities appear to reduce with increasing age<sup>21,38</sup>, implying a decreasing risk of injury. This would appear to correlate with a significantly greater number of cases of skull fracture and / or ICI seen in children less than 12months (Chapter 3). However, results from Chapter 3 were not specific to SDH and for the cases with SDH, bridging vein rupture could not be confirmed. One possible explanation is that with increasing age there is the potential for protective reflexes mitigating the potential injurious effects of a fall. Therefore, it is difficult to determine the validity of this correlation at present, though it does provide an area for further research. The 10,000 rad/s<sup>2</sup> threshold for bridging vein rupture proposed by Depreitere *et al*<sup>26</sup>, was only crossed by the stiffest surfaces, at 0.6m, for 90 degree impacts. However, it was crossed by all the surfaces at 0.6m, for 75 and 60 degree impacts and surpassed some surfaces at lower heights at the 75 and 60 degree angles (Figure 20). Taking into account the previous research, where maximum values for heights approximating 0.6m again were reported around 10,000 rad/s<sup>2</sup>, Figure 6J, Appendix 7, it indicates a better correlation for this threshold, compared to the 4,500 rad/s<sup>2</sup> proposed by Löwenhielm<sup>27</sup>. However, as previously stated the threshold is only relevant for cases where the impact duration is less than 10ms. As a result, this threshold does not appear to have application to infants  $\leq 3$  months for heights measured, as all impacts were longer than 10ms, particularly when also taking into consideration previous research<sup>3</sup>. Duration of impact reduced with increasing height, thus the threshold may be relevant at greater heights for infants in this age range, this will be explored further using finite element analysis. Research conducted with ATDs representing older children have documented impact durations of less than 10ms. Thompson and Bertocci<sup>21</sup> conducted drop tests, using a 12 month CRABI dummy and reported impact durations of less than

10ms, along with maximum rotational accelerations of 9,322 rad/s<sup>2</sup>, indicating a potential application of the Depreitere *et al*<sup>26</sup> threshold for older infants. The CRABI 12 month dummy impact response has not been validated against cadaver data, thus, its application would require further investigation. Ibrahim and Margulies<sup>38</sup> conducted tests with an 18 month ATD and again this dummy was not validated against age specific cadaver data. The headform was however stiffer compared to this ATD aimed at infants <3months. Their results also showed impact durations of less than 10ms for a 0.6m fall, in conjunction, the rotational accelerations were greater than 10,000 rad/s<sup>2</sup>, suggesting the potential application of the Depreitere *et al*<sup>26</sup> threshold to the toddler age range. However, in the same study, the 10,000 rad/s<sup>2</sup> and 10ms thresholds were both crossed for a 0.3m fall, which was not substantiated by the clinical data.

#### 4.4.6.4 Thresholds – Skull fracture

Head injury thresholds for translational accelerations, are generally quoted in terms of peak G and HIC. Thresholds for peak G have varied from 50g to 250g, as reported by Cory *et al*<sup>39</sup>. The 50g threshold has been generally quoted as a lower limit for head injury in infants and was documented by Melvin<sup>2</sup>. Whilst the level or risk type for head injury was not documented with this threshold, the level risk does not appear to be substantiated by clinical data, as a fall height of 0.6m resulted in g values of up to 100g. Previous research further adds to this, Figure 6G Appendix 6, with ATDs aimed at older children producing greater values for peak G during impact from 0.6m falls<sup>21,38,40</sup>. A 50% risk of skull fracture has been proposed by Klinich *et al*<sup>34</sup> at 85g and by Van Ee *et al*<sup>35</sup> at 82g in infants (≤12 months). Whilst both thresholds approximate the “upper end” of translational accelerations expected from a 60cm impact, logistic regression of clinical data, in Chapter 3, indicated that 0.6m approximated closer to 5% risk. Therefore, the 82g and 85g were not substantiated by the clinical data. In the same two research papers 50% fracture thresholds in terms of HIC were suggested, Klinich *et al*<sup>34</sup> proposed a HIC value of 220 and Van Ee *et al*<sup>35</sup> proposed a HIC value of 290.

These values are at the upper end of what could be expected from a 0.6m fall related impact, but again, these thresholds represent a 50% risk, whereas 0.6m was closer to a 5% risk, from the clinical data. Again these thresholds were not substantiated. The current National Highway Transport Safety Administration (NHTSA) standard <sup>33</sup> implemented a scaling method of adult thresholds that led to skull fracture thresholds for children  $\leq 12$  month and for 3 year olds. A 5% skull fracture threshold was suggested at a HIC value of 144 for children  $\leq 12$  month and at a value of 216 for a 3 year old. Whilst these thresholds are not exact matches, compared to the clinical data, Figure 6H Appendix 6, they do appear to be the closest match.

### 4.4.7 Limitations

As with all studies, this research has limitations. This study developed only a biofidelic head form, thus, the neck and body were absent. Consequently the effects of the body and neck on the kinematic variables would not have been measured. This uniquely provides an opportunity to assess which variables are influenced solely by the head and further research will measure the effect of the neck and body. Whilst the study only investigated measured heights up to 0.6m, thus not in the injurious range from Chapter 3, given the number of variables measured, it was unrealistic to perform drop tests from greater heights, given the likelihood that the headform would fail. Greater heights will be investigated by finite element analysis.

### 4.4.8 Implications

A validated biofidelic infant headform was developed that uniquely measured the effect that impact angle and skin friction has on kinematic variables, whilst also measuring the effects of previously assessed variables, including impact velocity (corresponding to height) and surface. Impact angle, surface and height, all significantly affected one or more of the kinematic variables. Also, the effect of these three variables was not constant, but varied when one or both of the other

variables changed. For example, a carpet surface did not significantly influence HIC compared to carpet-underlay at the lower impact velocity of 2.4m/s, but did, when the impact velocity increased to 3.4m/s. This therefore reiterates the importance of completing a detailed investigation of the entire scenario leading to a head injury from a fall, prior to assessing the likelihood that a potential head injury, such as skull fracture or intracranial injury. Integrating clinical and biomechanical data, this study uniquely assessed current biomechanical thresholds, so that their relevance to the paediatric clinical setting could be assessed. Few of the thresholds in the literature were substantiated by the clinical data, with the exception of NHTSA standard<sup>33</sup>, therefore, their application should be interpreted with caution.



#### 4.5 Conclusion

A geometrically accurate headform was designed from human infant CT images and manufactured using an additive layer technology. The result was a headform that was validated against human infant cadaver data. After subjecting the headform to impacts tests, it was found that impact velocity (corresponding to fall height), impact angle and surface significantly affected one or more of the kinematic variables.

- A decrease in impact angle increased peak rotational accelerations and peak change in rotational velocities, yet reduced HIC.
- An increase in impact velocity significantly increased peak rotational accelerations, peak change in rotational velocities, peak g and HIC and reduced impact duration.
- Increased surface stiffness, increased peak rotational accelerations, peak change in rotational velocities, peak g and HIC and reduced impact duration. However, this effect varied with impact velocity and angle.

Current biomechanical thresholds were not substantiated by the clinical data, thus implying that the differing dynamic response of infant head potentially needs to be incorporated into thresholds. Investigating the high speed video revealed the potential level of deformation an infant head undergoes during an impact. As a result, the differing response might make an infant head more or less prone to certain forms of traumatic brain injury. As a consequence of these results, finite element analysis will be used to assess how the kinematic variables correlate with material failure properties, to determine if a kinematic thresholds can be established that correlate with the clinical data.

#### **4.6 References**

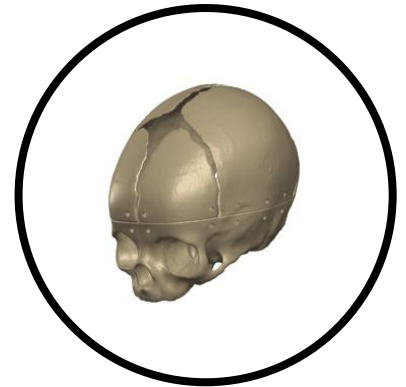
1. Irwin A, Mertz HJ. Biomechanical Basis For The Crabi (Child Restraint Air Bag Interaction) And Hybrid Iii Child Dummies. SAE Publication P-316 Child Occupant Protection 2nd Symposium Proceedings, November 12, 1997, Orlando, Florida, Usa (SAE Technical Paper 973317); 1997.
2. Melvin J. Injury assessment reference values for the CRABI 6-month infant dummy in a rear-facing infant restraint with airbag deployment. *SAE Paper No 950872*. 1995.
3. Coats B, Margulies S. Potential for head injuries in infants from low-height falls. *Journal of Neurosurgery: Pediatrics*. 2008;2(5):321-330.
4. Duhaime AC, Gennarelli TA, Thibault LE, Bruce DA, Margulies SS, Wisner R. The shaken baby syndrome. *Journal of neurosurgery*. 1987;66(3):409-415.
5. Prange M, Coats B, Duhaime A, Margulies S. Anthropomorphic simulations of falls, shakes, and inflicted impacts in infants. *Journal of Neurosurgery: Pediatrics*. 2003;99(1).
6. Cory C, Jones M. Development of a simulation system for performing in situ surface tests to assess the potential severity of head impacts from alleged childhood short falls. *Forensic Science International*. 2006;163(1-2):102-114.
7. Van Ee C, Raymond D, Thibault K, Hardy W, Plunkett J. Child ATD Reconstruction of a Fatal Pediatric Fall. 2009: ASME.
8. Prange M, Luck J, Dibb A, Van Ee C, Nightingale R, Myers B. Mechanical properties and anthropometry of the human infant head. *Stapp car crash journal*. 2004;48:279.
9. Weber W. Experimental studies of skull fractures in infants]. *Zeitschrift für Rechtsmedizin Journal of legal medicine*. 1984;92(2):87.
10. Weber W. [Biomechanical fragility of the infant skull]. *Zeitschrift für Rechtsmedizin Journal of legal medicine*. 1985;94(2):93.
11. Coats B, Margulies S. Material properties of human infant skull and suture at high rates. *Journal of neurotrauma*. 2006;23(8):1222-1232.
12. McPherson GK, Kriewall TJ. The elastic modulus of fetal cranial bone: a first step towards an understanding of the biomechanics of fetal head molding. *Journal of Biomechanics*. 1980;13(1):9-16.
13. Gennarelli T, Thibault L, Ommaya A. Pathophysiologic responses to rotational and translational accelerations of the head. *SAE Technical Paper*. 1972;720970.
14. Gennarelli TA, Thibault LE. Biomechanics of acute subdural hematoma. *The Journal of Trauma and Acute Care Surgery*. 1982;22(8):680-686.
15. Simpleware. ScanIP. Version 4.2. ed2010.
16. DSS. Solidworks. 2011.
17. Galford JE, McElhaney JH. A viscoelastic study of scalp, brain, and dura. *Journal of Biomechanics*. 1970;3(2):211-221.

18. Cheng J, Howard IC, Rennison M. Study of an infant brain subjected to periodic motion via a custom experimental apparatus design and finite element modelling. *Journal of biomechanics*. 2010;43(15):2887-2896.
19. BSI. Structural use of timber. BS 5268-7.1 Recommendations for the calculations basis for span tables. 1989.
20. SAE. SAE J211-1 Instrumentation for Impact Test, Part 1, Electronic Instrumentation. 1995.
21. Thompson AK, Bertocci GE. Paediatric bed fall computer simulation model development and validation. *Computer methods in biomechanics and biomedical engineering*. 2011(ahead-of-print):1-10.
22. Mathworks. Matlab. Version R2011a. ed2011.
23. IBM. SPSS. Version 20. ed2011.
24. Parslow RC, Morris KP, Tasker RC, Forsyth RJ, Hawley CA. Epidemiology of traumatic brain injury in children receiving intensive care in the UK. *Archives of Disease in Childhood*. 2005;90(11):1182-1187.
25. Coats B, Ji S, Margulies S. Parametric study of head impact in the infant. *Stapp Car Crash J*. 2007;51:1-15.
26. Depreitere B, Van Lierde C, Sloten JV, Van Audekercke R, Van Der Perre G, Plets C, et al. Mechanics of acute subdural hematomas resulting from bridging vein rupture. *Journal of neurosurgery*. 2006;104(6):950-956.
27. Löwenhielm P. Strain tolerance of the vv. cerebri sup.(bridging veins) calculated from head-on collision tests with cadavers. *Zeitschrift für Rechtsmedizin*. 1974;75(2):131-144.
28. Mertz HJ, Prasad P, Irwin AL. Injury risk curves for children and adults in frontal and rear collisions. 1997: Society Automotive Engineers Inc. p. 13-30.
29. Prasad P, Mertz HJ. The position of the United States delegation to the ISO working group on the use of HIC in the automotive environment. *SAE transactions*. 1985;94:106-116.
30. Löwenhielm P. Dynamic properties of the parasagittal bridging veins. *International Journal of Legal Medicine*. 1974;74(1):55-62.
31. Holburn AH. Mechanics of head injuries. *Lancet* 2. 1943:438-441.
32. Thibault KL, Margulies SS. Age-dependent material properties of the porcine cerebrum: effect on pediatric inertial head injury criteria. *Journal of Biomechanics*. 1998;31(12):1119-1126.
33. Eppinger R, Sun E, Bandak F, Haffner M, Khaewpong N, Maltese M, et al. Development of improved injury criteria for the assessment of advanced automotive restraint systems–II. *National Highway Traffic Safety Administration*. 1999.
34. Klinich K, Hulbert G, Schneider L. Estimating infant head injury criteria and impact response using crash reconstruction and finite element modeling. *Stapp car crash journal*. 2002;46:165.
35. Van Ee C, Moroski-Browne B, Raymond D, Thibault K, Hardy W, Plunkett J. Evaluation and refinement of the CRABI-6 anthropomorphic test device injury criteria for skull fracture. 2009: ASME.

36. Löwenhielm P. Dynamic strain tolerance of blood vessels at different post mortem conditions. *Journal of bioengineering*. 1978;2(6):509.
37. Cory C, Jones M. Can shaking alone cause fatal brain injury? A biomechanical assessment of the Duhaimé shaken baby syndrome model. *Medicine, science and the law*. 2003;43(4):317-333.
38. Ibrahim N, Margulies S. Biomechanics of the toddler head during low-height falls: an anthropomorphic dummy analysis. *Journal of Neurosurgery: Pediatrics*. 2010;6(1):57-68.
39. Cory C, Jones M, James D, Leadbeatter S, Nokes L. The potential and limitations of utilising head impact injury models to assess the likelihood of significant head injury in infants after a fall. *Forensic Science International*. 2001;123(2-3):89-106.
40. Bertocci GE, Pierce MC, Deemer E, Aguel F, Janosky JE, Vogeley E. Using test dummy experiments to investigate pediatric injury risk in simulated short-distance falls. *Archives of Pediatrics and Adolescent Medicine*. 2003;157(5):480.

---

Chapter 5 – Finite Element  
Analysis of Infant  
Head Impacts



## 5.1 Introduction

Finite element analysis provides a useful tool for understanding the correlation between material response parameters, for example peak stress or strain, of various bone and soft tissue structures of the head and the head impact response in terms qualitative and quantitative kinematic variables. It also allows for greater depth of understanding on the potential causes of traumatic head injury through investigating the dynamic response of the head on impact and how it potentially causes injury to the head. Whilst interpretation and clinical application of finite element analysis remains difficult, it provides a powerful tool for biomechanical engineers to use in conjunction with cadaver tests and experiments using anthropomorphic testing devices, to add depth to the understanding of traumatic head injury. This chapter uses finite element analysis to determine if there is a correlation between infant material failure properties and the kinematic variables. The impact response was evaluated against the clinical thresholds and characteristics from Chapter 3 to investigate if there were any differences.

### *Background*

The initial use of FE analysis to investigate head trauma in infants and young children was confined to investigating head deformations during labour<sup>1, 2</sup>. McPherson and Kriewall<sup>1</sup> developed a finite element model of the parietal bones utilising bone stiffness properties from their previous experiments<sup>3</sup> and used it to provide an understanding of the biomechanics of head deformations during the birth process. The authors also quantified how differences in skull bone stiffness between pre term and terms infants affected head deformation. Lapeer and Prager<sup>2</sup> extended the work of McPherson and Kriewall<sup>1</sup> where they also used FE analysis to understand head moulding during the birth process. However, their FE model was developed through scanning a fetal head model and included the skull and sutures, but no intracranial soft tissue structures. The FE model deformation showed good agreement against clinical deformation measurements from 319 birth deliveries, yet statistical comparisons between the two were not documented<sup>4</sup>.

Thibault and Margulies <sup>5</sup> were one of the first FE analysts to measure deformations, as the result of an impact. Their investigations incorporated experimental tests on human cranial bone and porcine bone suture samples. This material data, gained from experimentation, was then used to measure the effect the infant cranium and sutures have on protecting the brain. The authors developed an idealised FE model of a 1 month infant consisting of the skull, sutures and brain. The material properties of the cranium were varied from those seen in infants (measured by the study) to that of an adult. The authors assumed that the suture properties of infant porcine sutures would be the same as an infant, however Coats and Margulies <sup>6</sup> later proved this to be incorrect as an infant porcine suture was 22-80 times stiffer. The geometry of the FEA mesh was simplified to half an ellipsoid and the base was constrained to prevent displacement and rotation. Two impact loadings from Duhaime *et al* <sup>7</sup> were applied to the model, half sinusoidal with a pulse duration of 10ms and peak loads of 1000N and 5000N. The authors reported that deformations of the model were affected by stiffness of the cranium, increasing peak deformation, from 2mm to 4mm at 1000N and from 4mm to 10mm at 5000N. It was documented by the authors that using infant properties for the cranium led to bilateral and diffuse patterns of strains on the brain, whereas the adult properties led to strains being focal to impact. This led the authors to hypothesise that impact on an infant head may produce diffuse brain injury, while the same load on an adult head would produce a focal injury. However, the authors did not state what it classed as “diffuse”, including details such as the quantity of the elements exceeding a given threshold and their position, relative to the point of impact. Given the simplifications in the geometry and the use of porcine data for the sutures, it makes it difficult to agree with this hypothesis. Whilst the number of limitations of this FE model make it difficult to see if the results are comparable to what would be seen in a human infant, it does highlight that the infant head would deform more during impact and thus, may lead to injuries differing to that of an adult.

Post publication of the material properties for the skull and suture by Margulies and Thibault <sup>8</sup>, Roth *et al* <sup>9</sup> developed a finite element model of a 6 month head in order to assess the differing dynamic response of the head between impact and shaking. In terms of pressure and shear on the brain, shaking was shown to be significantly lower, compared to the 3m/s impact. However, strain on the bridging veins was shown to be comparable between the two scenarios. The authors modelled the bridging veins with springs, yet the stiffness assigned to the springs was not documented, therefore it is unclear if only relative motion between the brain and skull was used to determine potential strain on the bridging veins. Also the material properties used for the skull and suture were later shown to be too stiff by Coats and Margulies <sup>6</sup>; therefore, it is unclear if strain on the bridging veins, due to a fall, were over estimated.

Utilising the same 6 month FE head model, the same research group investigated the effect of scaling an adult FE model, compared to a model built directly from CT images <sup>10</sup>. The accuracy of the scaling method was investigated in terms of head geometry, shape and thickness. In terms of shape and geometry, the scaling method was shown to be inadequate for children less than 6 years old and in terms of bone thickness it was suggested the scaling method cannot be used before the age of 10 years. For the brain shape, again the authors found that scaling did not accurately represent the brain for a 6 month and 3 year old child. The scaled 6 month finite element model was compared to the model with the realistic geometry across three impact conditions; frontal, lateral and occipital impacts at 1m/s. Variations in pressure and stress on the brain and skull between the scaled and 6 month model were documented across the three impact conditions, again, highlighting the need for accurate geometry. The differences in response were attributed to variations in curvature between the skull and brain between the models, thereby leading to differences in deformation and thus, pressure and stress. Also the bone thickness for the scaled model was greater, consequently leading to lower deformations and stress. Finally, using both models to reconstruct an accidental case of a 4.5 month old child who fell, it was shown that



the geometrically accurate 6 month model produced more accurate results, in terms of predicting fracture. This research uniquely highlights that a child's head cannot be considered to be a scaled adult as the quantity and location of high stress will vary, a method that had been previously used in the biomechanical field . However, the limitations of this model are as per Roth *et al*<sup>9</sup>, where the material properties for the skull were later shown to be too stiff<sup>6</sup> and the model was not validated.

The same research group conducted a similar geometric analysis to compare a 3 year old scaled FE head model to a geometrically accurate model, developed directly from CT images. Similar results were seen as with Roth *et al*<sup>10</sup>, in terms of the effects of head geometry, shape, bone thickness and peak shear stress. However, peak pressure on the brain between the two models was similar. This article reiterates the need for geometrically accurate FE models. The same author developed a different finite element 3-year-old head model to reconstruct 25 accidental falls such that neurological injury could be investigated<sup>11</sup>. The 25 cases consisted of patients with no neurological lesions to those with severe lesions. A statistical analysis was performed to determine which output variable was best associated with neurological lesion. Von Mises stress was the best predictor and an injury value of 48KPa was proposed. Yet the impact response of the FE model was not validated, thus the biofidelity of the model is unknown. Also, little is known regarding brain properties for this age range, so it is unclear if the value used were correct, although the authors did take this into consideration through using two different properties.

In the past five years there has been a growth in the number of research institutes exploring the use of finite element analysis in relation to infant head trauma. This is potentially explained by infant human material properties for the skull and suture becoming available in the literature, thus allowing for more accurate representation of the material response<sup>6</sup>. It is also partly explained by greater availability of software that allows for the radiological images to be converted into

3D computer models that can then be exported into computer aided design (CAD) formats such as stereolithography (STL) and also into a mesh that can be run in mesh solvers such as Abaqus (Version 6.10, DSS <sup>12</sup>) or LS DYNA (Livermore Software Corporation). This, in conjunction with increased computational power becoming less expensive, has allowed for infant head FE models to be developed and validated against infant cadaver impact response data.

Post Coats and Margulies <sup>6</sup> experimental work quantifying the material properties of human infant bone and sutures, Coats *et al* <sup>13</sup> developed a finite model of a 5 week old infant head from CT and MRI scans that included this material data. Their aim was to use the FE model to predict fracture from a low height fall, whilst also conducting a parametric test to measure the effect that material properties and anatomical variations have on the impact response. Their parametric test revealed that an increased brain compressibility, brain stiffness (when increased by approximately 3 orders of magnitude) and an increase in suture width from 3mm to 10mm increased one or more of the measured outcomes (peak principle stress, peak force, contact area and duration of impact) by greater than 15%. However, the inclusion of a scalp, inclusion of sutures (measured relative to 3mm suture width), reduction in suture thickness and a 50% reduction in brain stiffness did not affect the measured outcomes by greater than 2%. Their FE model's ability to predict fracture was assessed against the Weber <sup>14,15</sup> cadaver case series. Their model showed good agreement with the cadaver tests, where maximum principle stresses in the parietal bone equated to a 99.8% risk of fracture based upon ultimate tensile stress values from an 82cm fall onto a rigid surface impacting the parieto-occipital area. Their model was also qualitatively assessed in terms of the fracture path, where a high probability of fracture was seen to pass from the lambdoid suture to the centre of the parietal bone. Whilst this FE analysis was a significant step forward in terms of understanding infant head injury biomechanics from a low height fall, the model's impact response was not validated against Prange *et al* <sup>16</sup>. The author attributed this to anatomical differences between the model and cadaver heads used by Prange *et al* <sup>16</sup>, in

particular the suture width. Also based on their analysis, a 50% risk of fracture was equated to a 29-35g impact, which contrasts the cadaver tests conducted by Prange *et al*<sup>16, 13, 17</sup>, as no skull fractures were seen from 15cm or 30cm impacts which had mean acceleration values of 55g and 39g respectively.

After this work a number of researchers have used finite element models of head aimed at young children. A finite element model of a 6 month head was developed and used by Roth *et al*<sup>9</sup> and Roth *et al*<sup>10</sup>. The same research institute also developed a 3-year head FE model<sup>18, 11</sup>. Whilst these finite elements provide an understanding of traumatic head injury, they are limited because their validity could not be assessed with human cadaver data. In the published literature cadaver experiment on paediatric cadaver heads only exist for young infants (<3months)<sup>16</sup>. Thus, subsequent to the FE model created by Coats *et al*<sup>13</sup> both Roth *et al*<sup>19</sup> and Li *et al*<sup>20</sup> have developed validated finite element models of an infant head <3 months. Roth *et al*<sup>19</sup> constructed a model through reconstruction of 230 slices of a CT scan of a 17 day infant head. Mean material properties from the literature were used to represent the membranes, CSF, scalp, suture and the skull. The brain was modelled as viscoelastic and a parametric analysis was conducted on the compressibility and stiffness values, due to a wide range of reported values in the literature. The variation in viscoelastic parameters only led to minor variations in the measured output, including skull deformation, Von Mises stress and peak acceleration; however, greater than 15% increases occurred when the initial shear modulus and bulk modulus increased. These results differed from those by Coats *et al*<sup>13</sup>, potentially as a consequence of using different material models for the brain.

Whilst a number of FE models exist in the literature, they have been confined to a single patient or age. Li *et al*<sup>21</sup> aimed to address this by investigating the effect of head geometry on the impact response of the head. After obtaining 11 head CT images of infants  $\leq 3$  months, the authors completed a mesh morphing procedure of a baseline 6 month head model from Klinich *et al*<sup>22</sup> to develop 0 month,

1.5month and 3 month head models. The morphing procedure altered the head geometry and thickness of the skull and sutures to resemble the age of the model. After this the authors completed a parametric test to measure the effect that geometry (represented only by age), stiffness of the skull, suture, dura, and the scalp and also the brain viscoelastic properties, including the short term and long term shear modulus decay coefficient, have on the impact response. The parametric test was only conducted for a 30cm impact onto the vertex. The authors found that the skull elastic modulus had a significant effect on all the response measurements, something that had not been measured by previous parametric tests<sup>13,19</sup>. In agreement with previous authors the stiffness of the scalp did not affect the stress in the skull or the accelerations on impact<sup>13</sup>. However, the scalp did affect the stress and strain of the suture. In their tests, the stiffness of the skull was seen to be the dominant factor in the parametric test. However, when the stiffness was controlled, the age significantly affected the stress in the skull, whilst the scalp properties affected the peak accelerations. The authors also completed an optimisation of the material properties shown to be significant in the parametric test against the cadaver tests conducted by Prange *et al*<sup>16</sup>. The authors adopted a unique strategy to measure the effect of geometry; however, only the age was used as an indicator of the geometry and no shape index in terms of length, or width of the head or sutures, was documented. The authors used a 6 month head FE model as the baseline model, which was inconsistent given the paper was investigating the 0-3 month range. Also, the authors created models of different ages, but did not consider that material properties change with age, particularly the bone stiffness<sup>6</sup>. Whilst there were a number of limitations of this study, it does again highlight that geometric differences can influence the impact response<sup>20</sup>, echoing what was documented by Coats and Margulies<sup>23</sup>.

### 5.1.1 Aims and objectives

A number of finite element models of the young child head, exist in the literature. Parametric tests have shown that a number of material properties have an effect on the impact response, particularly skull stiffness and brain stiffness and

compressibility. However, given the limited data with which models can be validated, particularly for brain motion and deformation of the skull and brain, it is often difficult to know the material model and properties that accurately represent the human infant impact response. Also, the parametric tests have often been limited to a single scenario, for example a 30cm fall onto the occiput<sup>13</sup>. However, the influence of certain material parameters could vary with a change in the impact scenario, as has been seen with impact surface<sup>23</sup>.

Consequently the aims and objectives of this Chapter were split into three sections to address these issues.

- Develop a finite element model of an infant head that can be validated against the cadaver kinematic response data in the literature. Given that there is only a single study in the literature where cadaver experiments have been conducted and the kinematic response have been recorded<sup>16</sup>, the FE model was designed to resemble the anthropometry of those cadavers. The cadaver ages were 1, 3 and 11 days old, thus the FE model was aimed at the 0-3 month age group.
- Conduct a parametric test that investigates the effect that varying material models and properties have on the impact response of the head. The validated FE model was used as the baseline. Whilst previous parametric studies have been conducted, the aim was to confine the parameters to known values from literature, such that upper and lower ranges could be identified. Previous parametric tests have been confined to a single scenario, thus, the effect of varying material properties was assessed against different impact scenarios. The impact scenarios were varied with respect to the site of impact.
- To perform qualitative and quantitative comparison of the finite element analysis to data from the clinical scenarios reported in Chapter 3. Also, Chapter 4 illustrated a disconnection between biomechanical thresholds and clinical thresholds; therefore, the material response was correlated against the kinematic variables. Chapter 4 highlighted the extent of deformation that an

## Chapter 5 – Finite Element Analysis of Infant Head Impacts

---

infant head undergoes on impact from a fall, which was explored further using finite element analysis.

## **5.2 Materials and Methods**

To fulfil the aims and objectives of this chapter, each section is now split into 3 areas: FE model development and validation; parametric analysis of material properties in conjunction with the impact scenario; and an assessment of finite element model results against the clinical findings and cases.

### **5.2.1 Finite element model development and validation**

#### **5.2.1.1 Overview finite element modelling and image based meshing**

Finite element analysis is a computational technique for modelling a mechanical experiment. It involves developing a two or three dimensional computational model and breaking it down into smaller sections or volumes, commonly known as elements. The model is built up of the smaller elements to represent the total geometry which is subjected to an experiment, such as external load. The reaction of the element is computed, depending on the material properties assigned and any constraints attached. The summation or cumulative response of the individual elements then represents the overall response of the entire model. Finite element models provide a powerful technique for understanding how a model responds under an applied load and how different interactions, constraints and material properties affect the response. However, the accuracy continually needs to be assessed and is dependant on a number of factors, including geometry, material properties and the number of elements or mesh density of the model.

Developing a geometrically accurate model of a complex shape, such as the skull and brain can be difficult and time consuming using standard computational aided design techniques. Image based meshing provides a time efficient tool for the conversion of radiographical image datasets into three dimensional accurate models. Three dimensional images are formed of voxels, with differing greyscale values. Biological tissues can be differentiated, based on differences in the greyscale value, thus allowing the bone and soft tissues to be segmented. Commercially, available packages exist that allow image based model generation, including ScanIP (Version 4.2, Simpleware <sup>24</sup>) and Mimics (Materialise). ScanIP

(Version 4.2, Simpleware<sup>24</sup>) in combination with ScanFE (Version 4.2, Simpleware Ltd<sup>25</sup>) was used during this study for the development of the mesh from radiological datasets. As has been previously stated, FE models consist of a number of elements; however, there are a number of different types of elements ranging from solid, to shell, to membranes. In general terms, an element is made up of nodes, which represents the outer geometry of an element. A 1<sup>st</sup> order hexahedral (hex) element is made up of 8 nodes, which forms a ‘brick’ structure and a 1<sup>st</sup> order tetrahedral (tet) element, consisting of 4 nodes, forming a ‘pyramid’ type structure (*Figure 32*). Second order elements have midsided nodes, thus, turning a hex element into a 20 node element and tet elements into a 10 node element (*Figure 32*). ScanFE (Version 4.2, Simpleware Ltd<sup>25</sup>) allows for models to be constructed with either hex elements, tet elements, or a combination of both<sup>26</sup>.

For the development of hex elements, the software converts the voxels directly into hex elements. Whilst it is desirable to use hex elements, due to the improved computational efficiency, it is often difficult to accurately represent the geometry using only hex elements. In ScanFE (Version 4.2, Simpleware Ltd<sup>25</sup>), using only hex elements resulted in a step surface feature, which was undesirable. For a more realistic surface, ScanFE (Version 4.2, Simpleware Ltd<sup>25</sup>), has an algorithm to use a combination of hex and tet element, where the voxels on the surface are split into tetrahedral elements using a marching cubes approach, resulting in a more realistic surface finish<sup>27, 28</sup>. A further software option is a customizable and flexible FE free algorithm, which extracts the surface using the previous algorithm, remeshes it and the inside is filled with tetrahedral elements using a Delaunay/Advanced front approach<sup>27, 28</sup>.



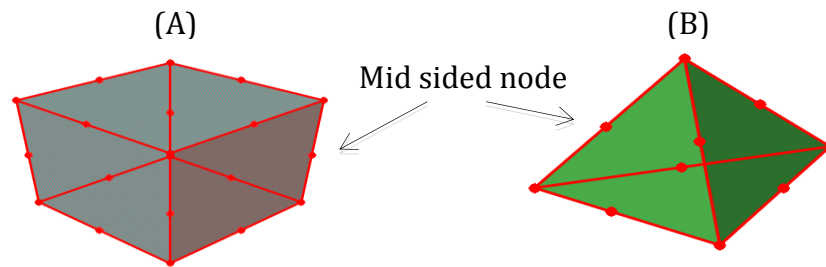


Figure 32. Element types. Hexahedral element with mid sides nodes (A), Tetrahedral element with mid sided nodes (B).

### 5.2.1.2 FE Model Design and Development

#### 5.2.1.2.1 Overview

The initial development of the infant head FE model involved selecting a CT scan that could be used to develop a geometrical accurate FE model. The Prange *et al*<sup>16</sup> infant cadaver data series provides the only data with which impact response can be validated; thus, the FE model was designed to replicate the anthropometry of the cadaver heads. The radiological datasets acquired from Chapter 4 were used for the development of an FE model. The procedure for acquiring the CT images is outlined in section 4.2.1.1.

#### 5.2.1.2.2 CT selection and segmentation

Fifteen datasets were available for the anthropomorphic analysis, prior to the development of the FE model. Again, following the same procedure as outlined in section 4.2.1.1, the CT images were imported into ScanIP (Version 4.2, Simpleware<sup>24</sup>), aligned with the Frankfurt Plane and head length, width and height measurements were taken. A detailed overview of this procedure is outlined in section 4.2.1.1. The procedure of taking measurements from CT images, to select an appropriate scan for the development of FE models, has been used by previous authors<sup>19</sup>. The measurements from each scan are presented in Table 19.

Initial development of the model involved segmenting the different bone and soft tissue structures. A greyscale threshold was applied to the CT dataset, a threshold

between greyscale values of 105-255 was implemented to differentiate the bone. The mandible and the spinal vertebrae were then removed from the model, in accordance with the cadaver heads used by Prange *et al* <sup>16</sup>. A combination of manual and automated filters were used to develop masks for the sutures, brain and meningeal layers. These included fast marching image, cavity fill, boolean and morphological filter. The masks developed for the skull and the intra/extra cranial soft tissues can be seen in *Figure 33*.

*Table 19. Head measurements of the Computed Tomography datasets collected from University Hospital of Wales Cardiff compared to the Prange et al 16 data series.*

Patient age / days	Head length / mm	Head width / mm	Head Hheight / mm	RMS (1 day old)	RMS (3 day old)	RMS (11 day old)
Measurements of infant head in Prange <i>et al</i> <sup>16</sup>						
1 day old	103.0	108.0	112.0			
3 day old	85.0	88.0	104.0			
11 day old	75.0	88.0	92.0			
Measurements from infant head CT images in this dataset						
	124.3	103.8	88.0	18.0	13.1	7.5
56	138.9	106.2	92.0	26.0	20.8	15.6
30	124.5	96.0	90.2	16.5	10.6	8.6
35	136.8	103.6	91.0	24.1	19.0	14.3
84	136.6	98.4	97.8	24.7	18.5	14.9
90	139.8	128.1	100.0	35.8	30.4	21.8
84	132.1	103.0	100.4	24.6	17.8	12.6
3	123.4	100.3	83.2	15.5	11.7	8.6
19	121.6	98.4	90.3	15.9	10.0	6.5
35	135.3	110.1	97.2	26.9	21.0	14.2
60	129.7	110.9	103.0	26.9	20.2	12.7
30	122.9	101.4	94.6	18.7	12.2	6.6
21	128.6	104.6	93.1	21.3	15.5	9.6
104	152.3	118.2	102.1	37.7	32.0	25.4

It can be seen from Table 19 that the CT images that had the lowest RMS error was of a 19 day old male infant.

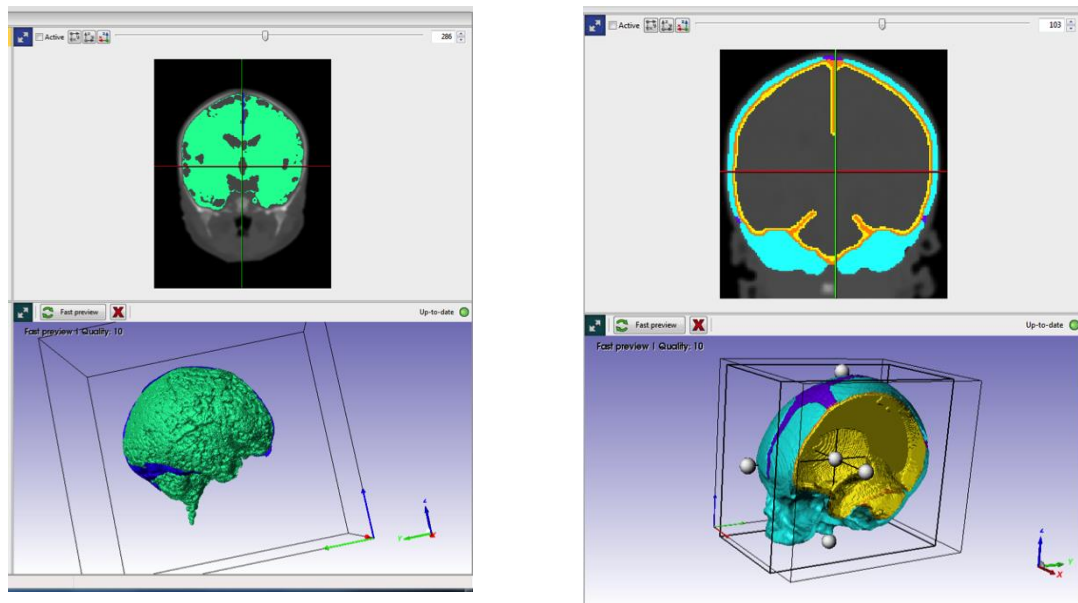
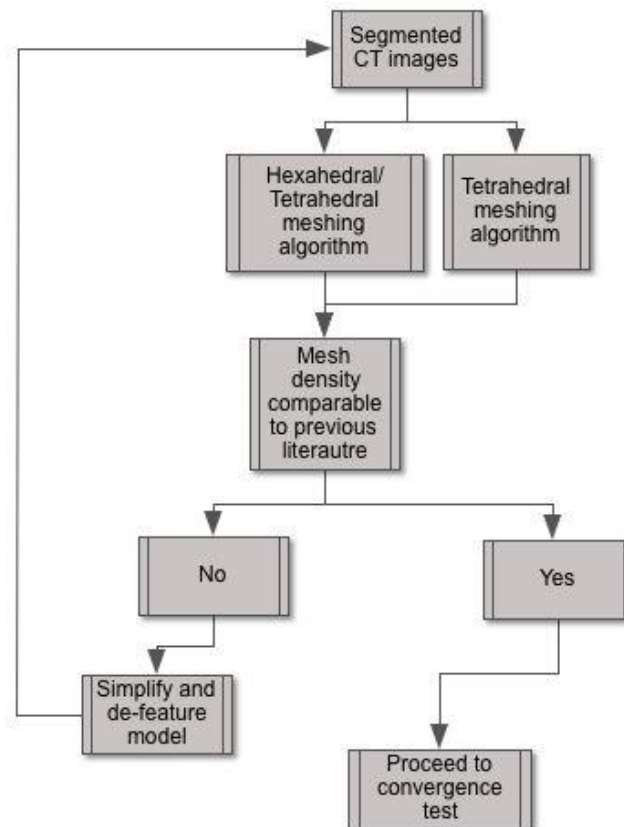


Figure 33. Masks generated of the skull, suture, meningeal layers, and brain for the meshing procedure.

#### 5.2.1.2.3 Meshing Procedure

Following the initial segmentation of the model, the meshing process was completed. As has been previously stated, ScanFE (Version 4.2, Simpleware Ltd<sup>25</sup>) offers two different approaches (once a hexahedral approach was excluded), using either a combination of hexahedral or tetrahedral elements, or just tetrahedral elements. Increased mesh density improves computational accuracy, however, at the expense of computational time. One of the aims of this research was to investigate the head impact response across a range of scenarios, thus, the computational time needed to be reasonable to achieve this. Therefore, to provide an initial estimate of the required mesh density, previous infant FE models were quantified, in terms of their mesh density, computational time and resources. Element densities have ranged from 26,500 to 78,511 (combining both solid and shell elements) <sup>2, 9-11, 13, 18, 19, 21, 22, 29</sup>. Relatively few have documented the computation time and resources used, though the FE model developed by Coats *et al* <sup>13</sup> consisted of 32,881 elements and had a computation run time of 80 hours, using Intel Xeon processors. The validated FE model created by Roth *et al* <sup>19</sup> had

33,700 elements and had a run time of 15 hours. Whilst computational run time will vary depending not only on the number of elements in the model, the type of elements used, computer resources, simulation length and type of software used, it was the original aim to have a density similar to those noted above. The flow diagram, for development of the mesh can be seen in *Figure 34*.



*Figure 34. Flow diagram for the meshing procedure for the finite element model.*

Meshing with the hexahedral/tetrahedral algorithm resulted in a mesh density that was too dense. Post de-featuring (removal of meningeal layers) and re-sampling of the masks of the anatomical features, the maximum mesh density achieved was 230,000. A further decrease in mesh density could be achieved using the hexahedral/tetrahedral or marching cube algorithm through removal of the falx cerebri and the tentorium cerebellum, yet this was undesirable. It could also be achieved through further re-sampling, but again, this resulted in the loss of anatomical features and an unrealistic skull and suture surface, whilst not having

significant gains in element mesh density. Consequently, meshing using only tetrahedral elements resulted in a mesh density comparable with the previous literature; hence, the models used for the convergence test were only meshed using this method. It is well documented that 1<sup>st</sup> order tetrahedral elements suffer from a process known as ‘locking’ that result in a stiffened mesh, unless one has a high mesh density, particularly for contact problems. However, Abaqus (Version 6.10, DSS <sup>12</sup>) has a 2<sup>nd</sup> order modified tetrahedral element that is suited to contact problems with large deformations and exhibits minimal volume locking; thus, this element was used for the development of the model<sup>26</sup>.

A number of finite element packages exist for pre processing, running and postprocessing; however, Abaqus (Version 6.10, DSS <sup>12</sup>) was used due to its availability at Cardiff University. Simulations were initially completed using an Intel i5 four core processor with 8GB of RAM, however as a result of subsequent availability, simulations were also run on the Cardiff University supercomputer (n.b. only aspects of parametric test and assessment of clinical features was conducted on the supercomputer due to subsequent availability).

#### 5.2.1.2.4 Convergence test and final mesh

A mesh convergence test was conducted to determine the optimum mesh for the impact conditions. A 30cm impact onto the vertex was used to evaluate the optimum mesh. The development of each subsequent model reduced the mesh density from the densest mesh (Table 20). The output variable assessed was the peak force. The output variable was normalised relative to the value outputted from the densest mesh. It can be seen from Figure 35 that a reduction in the mesh density below  $60 \times 10^3$  resulted in an increase in error relative to the densest mesh. Also, investigating the computational run time there were significant savings in the computational time, as can be seen through reference to Table 20. Consequently the model with  $60 \times 10^3$  elements was chosen for the remainder of the analysis. The final mesh was consisted of 59,714 2<sup>nd</sup> order modified tetrahedral elements.

Table 20. Computational time for each mesh density assessed for a vertex impact and 40ms time duration.

Mesh Density / $1e^3$	Computational time for 40ms duration / hours
109	244
60	21
50	28
41	15

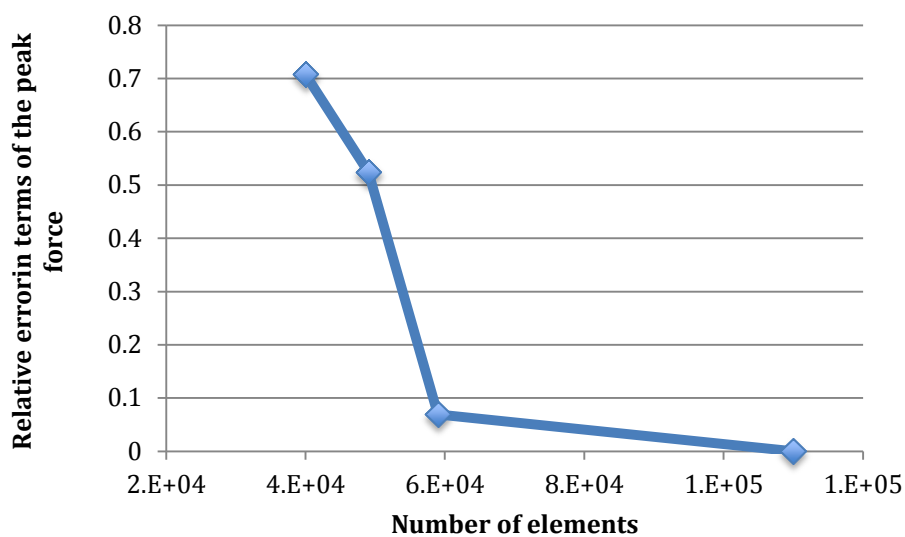


Figure 35. The error in the peak force compared to densest mesh.

### 5.2.1.3 Materials- Model Validation

An overview of the previous literature on the material properties of the cranium and the intra and extra cranium soft tissue structure can be found in section 2.3.3. Previous authors have shown that the skull stiffness has the greatest effect on the dynamic impact response of the head<sup>21</sup>; consequently this property was varied based on properties from the literature, in order to find values that best correlated with the response corridors reported by Prange *et al*<sup>16</sup>.

#### 5.2.1.3.1 Skull

Initial work on fetal cranial bone by McPherson and Kriewall<sup>3</sup> showed that infant bone is orthotropic. High rate testing on infant bone later conducted by Coats and

Margulies <sup>6</sup> also revealed that infant bone is inhomogeneous, with the parietal and occipital bone having different stiffness properties. Despite infant bone exhibiting both orthotropic and inhomogeneous material properties, few authors when modelling infant cranial bone have taken this into consideration <sup>13</sup>. In the literature, two studies that have created validated FE models of an infant head, however both studies modelled the bone as isotropic and homogenous. Roth *et al* <sup>19</sup> created a validated FE model using the mean bone stiffness reported by Coats and Margulies <sup>6</sup> for the 0-2.5 month age range and Li *et al* <sup>20</sup> who used a bone stiffness based on optimised values. Given that bone stiffness has been shown to have a significant influence on the impact response <sup>20,22</sup>, the stiffness was varied in order to find the properties that had the most biofidelic response with respect to the kinematic variables detailed by Prange *et al* <sup>16</sup>. In accordance with Roth *et al* <sup>19</sup> and Li *et al* <sup>21</sup>, the skull was initially modelled as isotropic and four different skull stiffness models were assessed. The initial model (Model B1) assessed was based on the mean skull stiffness properties reported by Coats and Margulies <sup>6</sup> for infants less than 3 months, where the fibre orientation is perpendicular to the long axis (*Table 21*) . Two further models were developed to account for the inhomogeneous nature of infant bone and also the range of values reported by Coats and Margulies <sup>6</sup>. Model B2 was based on the lowest reported stiffness values for the parietal and occipital bones and Model B3 was based on the highest reported stiffness values. The reported material properties for the occipital and parietal bones for infants <3 months can be seen in *Table 21*. Whilst Coats and Margulies <sup>6</sup> did not conduct experiments on frontal bones, McPherson and Kriewall <sup>3</sup> investigated a total of 14 specimens, two with the fibres perpendicular and 12 where the fibres were parallel. The mean and standard deviation of the frontal bones was used to calculate the 5<sup>th</sup> and 95<sup>th</sup> percentile stiffness values, and were used in models B2 and B3. The final baseline model (Model B4) utilised the optimised stiffness values reported by Li *et al* <sup>21</sup>. The skull was modelled as linear elastic, Equation (30), for each of the baseline simulations. The resulting material properties can be seen in *Table 22*.

$$\sigma_{Skull} = E_{Skull}\epsilon_{Skull} \tag{30}$$

Where  $\sigma$  is stress, E is elastic modulus and  $\epsilon$  is strain.

5.2.1.3.2 Sutures

Only a single study in the literature has conducted mechanical tests on human infant sutures. They found that the sutures were linear elastic and were not affected by donor age <sup>6</sup>. Consequently, for baseline models (Models B1, B2 & B3) the mean value reported by Coats and Margulies <sup>6</sup>, for children less than 12 months was used. For the Model B4 the optimised values reported by Li *et al* <sup>21</sup> was used. The sutures were modelled as linear elastic using Equation (31).

$$\sigma_{Suture} = E_{Suture}\epsilon_{Suture} \tag{31}$$

Where symbols have been previously defined.

Table 21. Material properties of the parietal and occipital bones for infants <3 months as reported by Coats and Margulies <sup>6</sup>.

	Elastic modulus / MPa	Ultimate Stress / MPa	Ultimate strain	Strain rate / s <sup>-1</sup>
<b>Age</b>	<b>Occiput</b>			
21 day	550.70	5.80	0.01	12.39
21 day	516.20	4.60	0.01	13.17
1 month	449.20	18.50	0.05	38.76
1.5 month	28.60	8.70	0.01	22.24
1.5 month	57.70	13.50	0.00	19.83
1 month 23 day	421.40	15.10	0.03	17.01
2 month 9 days	186.40	3.08	0.03	25.66
2 month 9 days	186.10	5.70	0.03	17.94
<b>Statistics</b>				
Mean	299.54	9.37	0.02	20.88
Standard deviation	208.68	5.63	0.02	8.46
5 <sup>th</sup>	-109.48	-1.67	-0.01	4.30
10 <sup>h</sup>	32.43	2.16	0.00	10.05
25 <sup>th</sup>	285.56	8.99	0.02	20.31
75 <sup>th</sup>	313.52	9.75	0.02	21.44
90 <sup>th</sup>	566.65	16.58	0.04	31.70



95 <sup>th</sup>	708.55	20.42	0.05	37.45
<b>Age</b>	<b>Parietal</b>			
19 day	336.80	37.80	0.15	103.42
21 day	182.70	8.40	0.05	31.82
1 month	815.50	53.70	0.08	47.06
1.5 month	372.40	19.70	0.07	26.09
1.5 month	518.20	29.60	0.05	24.22
1.5 month	581.30	25.60	0.06	37.95
2 month	297.40	14.20	0.05	73.64
2 month	522.40	27.10	0.08	59.45
<b>Statistics</b>				
Mean	453.34	27.01	0.07	50.46
Standard deviation	197.92	14.15	0.03	27.31
5th	65.41	-0.72	0.01	-3.07
10h	200.00	8.90	0.03	15.50
25th	440.08	26.06	0.07	48.63
75th	466.60	27.96	0.08	52.29
90th	706.67	45.12	0.12	85.41
95th	841.26	54.74	0.14	103.98

### 5.2.1.3.3 Scalp

Previous finite element models of infant heads have found the scalp to have a varying effect on the kinematic response of the head. Coats <sup>30</sup>, compared a FE model with a scalp to one without and observed that the exclusion of the scalp did not affect maximum principle stress, peak force or duration of impact by greater than 15%. In the parametric test using an FE models aimed at infants  $\leq 3$  months, Li *et al* <sup>21</sup> found increasing scalp stiffness from 8.5MPa to 21.3MPa to 34MPa only significantly affected maximum principle stress ( $P=0.004$ ) and strain ( $P=0.002$ ) of the suture. However in the same study, once the skull stiffness was controlled in the parametric analysis, scalp stiffness significantly effect peak head accelerations ( $P=0.002$ )<sup>21</sup>. A parametric test using a 6 month head FE model also concluded that scalp stiffness significantly affected peak accelerations ( $P=0.000$ ) and peak von mises stress ( $P0.025$ ) once the skull stiffness is controlled<sup>29</sup>. Despite the varying significant affect, it was included in all models in this study, due to the previous studies, which found it to have no significant effect only evaluating its importance

over a single scenario. In accordance with previous research, the scalp was modelled as linear elastic, Equation (32), utilising the material properties reported for an adult monkey by Galford and McElhaney <sup>31</sup>, for models B1,B2 and B3<sup>9,10,13,18,19</sup>. For model B4, the optimised values from Li *et al* <sup>21</sup> were used.

$$\sigma_{Scalp} = E_{Scalp}\varepsilon_{Scalp} \quad (32)$$

Where symbols have been previously defined.

#### 5.2.1.3.4 CSF

The CSF is essentially a fluid and to model it as a fluid involves coupling a computation fluid dynamics (CFD) mesh (or ‘Eularian’ mesh) with an FE mesh (or ‘Langarian’ mesh), which is commonly referred to as fluid solid interaction. However, such a problem is computationally expensive, consequently numerous FE models have modelled it essentially as an incompressible soft solid.

Whilst studies have compared different models for representing the CSF, most are based on a comparison to either an analytical model or a simplified physical model. However, Coats *et al* <sup>32</sup> created a finite element model of a piglet brain in order to assess different models of the pia –arachnoid complex, essentially the CSF section and the effect the differing models have on brain strain and brain skull displacement in an in situ animal experiment. Their research found that a spring element and solid element correlated best with the experimental work, in terms of brain displacement and strain, but spring elements were better at predicting intracranial haemorrhaging in the piglets. Thus, in accordance with Coats *et al* <sup>32</sup> and previous research using FE head models <sup>9,11,13,19,21</sup>, the CSF in all models (B1, B2, B3 and B4) in this study was modelled with solid elements with CSF properties.

#### 5.2.1.3.5 Dura

The FE contained the dura folds, the falx cerebri and tentorium cerebellum (*Figure 33*). Only two studies in the literature measured the material properties of human dura. Galford and McElhaney <sup>31</sup> measured the elastic modulus of adult human dura under a free vibration test and reported an elastic modulus of 31.5MPa. Most finite

element models of an infant head in the literature that have included the dura, have used this stiffness value <sup>9-11, 18, 19, 29</sup>. The optimisation procedure used by Li *et al* <sup>21</sup> outputted a stiffness value of 21.28MPa. Bylski *et al* <sup>33</sup> measured the stiffness of fetal dura matter in bi axial tension from 7 fetuses. Whilst the research on fetal dura is more age appropriate to this study, the elastic modulus was not reported. Comparing stiffnesses between the two studies indicates that stiffness of the fetal dura matter is approximately half of that of an adult; thus, the optimised value reported by Li *et al* <sup>21</sup> would likely fall within this range. Due to the uncertainty in scaling between the two studies, the adult values reported by Galford and McElhaney <sup>31</sup> were used in the models B1, B2 and B3 and the optimised value from Li *et al* <sup>21</sup> were used for model B4. The dura was modelled as linear elastic, Equation (35).

$$\sigma_{dura} = E_{dura}\epsilon_{dura} \tag{33}$$

#### 5.2.1.3.6 Brain

In section 2.3.3.5, it was documented that no studies have conducted mechanical/material tests on a sample of human infant brain tissue. Tests conducted on either infant or adults porcine samples or adults humans sample have found considerable variation in the response. Despite this, the majority of previous FE models of an infant head have used a viscoelastic law to model the brain<sup>9, 10, 19, 21, 22</sup>, based on the material tests conducted by Thibault and Margulies <sup>5</sup>, with only Coats *et al* <sup>13</sup> using a hyperelastic model. Even though it has been shown that the brain is inhomogeneous and anisotropic in certain sections<sup>34</sup>, it is difficult to apply it to an infant head model, due to a lack of age specific properties. Thus, in accordance with the majority of infant head FE models, including both validated FE models<sup>9, 10, 19, 21, 22</sup>, the brain was modelled as an isotropic, homogenous, linear viscoelastic material, based on the work by Thibault and Margulies <sup>5</sup> for all models in the validation process. The properties used can be seen in Table 22.

The bulk modulus of the brain affects computational time and stability<sup>13</sup>. Coats *et al* <sup>13</sup> concluded that a bulk modulus of 2.79MPa was sufficient when simulating the skull response for an infant head impact onto a hard surface, although no studies

have measured the bulk modulus of an infant brain. The bulk modulus of an adult brain has been shown to be 2.1GPa, due to anatomical variations between an adult and infant brain, namely axon myelination, there is potential for variation, as has been discussed by previous authors<sup>13</sup>. Roth *et al*<sup>19</sup> published a parametric test on the bulk modulus and found that a decrease in the bulk modulus from the adult value did not affect the peak linear acceleration, deflection or the peak von mises stress in the skull, with increasing only affecting the peak skull stress. Due to its potential for decreasing computational time, whilst maintaining accuracy in the output, the bulk modulus of order of magnitude to that of Coats *et al*<sup>13</sup> was used. The accuracy of this assumption was initially checked prior to proceeding with the validation process; however, this is covered in the parametric section of this work.

### 5.2.1.3.7 Bridging veins

Section 2.3.3.7 outlined that few studies have completed testing on bridging veins, with only a single study completing testing on veins dissected from age appropriate infants. Consequently, as used by Morrison<sup>35</sup>, the force displacement of the sample (name H/2/2 from their research) was used. Non-linear connectors were used to model the veins. Ten pairs of veins were inserted onto the FE model, connecting to the falx cerebri at the intersection with the suture. Lee and Haut<sup>36</sup> described that parasagittal bridging veins drain frontally into the parasagittal sinus, thus; all veins were inserted in forward facing direction. Morrison<sup>35</sup> documented bridging vein mean lengths of 7mm, thus, connector lengths used to model the veins approximated this. The connectors inserted into the FE model can be seen in Figure 36 and are labelled 1 to 10, with 1 most posterior and 10 most anterior.

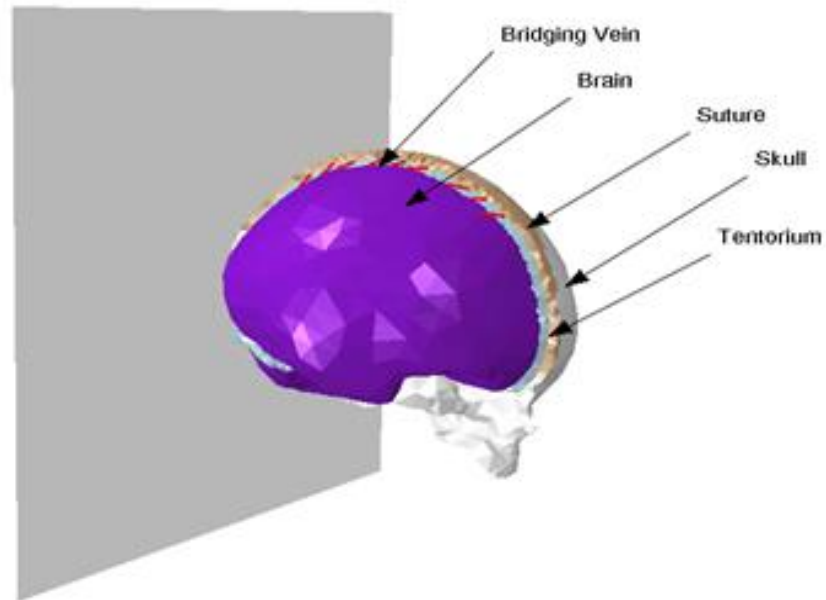


*Figure 36. Connectors used to model bridging veins inserted into model. Connector 1 is most posterior and 10 is most anterior.*

#### 5.2.1.3.8 Materials overview for model validation

An overview of the material properties used for the validation procedure can be seen in Table 22.

Table 22. Material properties used in the different baseline finite element models for the development a validated model.

	Baseline model B1 /MPa	Baseline model B2 /MPa	Baseline model B3 /MPa	Baseline model B4 /MPa
Scalp	16.7	16.7	16.7	8.56
Skull	E1= 299.5 (Occiput)	E1= 28.6 (Occiput)	E1= 550.7 (Occiput)	170.79
	E1= 453.3 (Parietal)	E1= 182.7 (Parietal)	E1= 815.5 (Parietal)	
	E1= 888.3 (Frontal)	E1= 209.3 (Frontal)	E1= 1567.3 (Frontal)	
Suture	8	8	8	8
CSF	0.012	0.012	0.012	0.012
Dura	31.5	31.5	31.5	21.28
Brain	G0 = 5.99 x10 <sup>-3</sup> G <sup>∞</sup> =2.32x10 <sup>-3</sup> β = 0.09248s <sup>-1</sup> K=2.110	G0 = 5.99 x10 <sup>-3</sup> G <sup>∞</sup> =2.32x10 <sup>-3</sup> β = 0.09248s <sup>-2</sup> K=2.111	G0 = 5.99 x10 <sup>-3</sup> G <sup>∞</sup> =2.32x10 <sup>-3</sup> β = 0.09248s <sup>-3</sup> K=2.112	G0 = 5.99 x10 <sup>-3</sup> G <sup>∞</sup> =2.32x10 <sup>-3</sup> β = 0.09248s <sup>-1</sup> K=2.113

### 5.2.1.4 Analysis Procedure

#### 5.2.1.4.1 Time Integration

For non linear dynamic analysis, direct integration must be used by finite element solvers. Two different techniques can be used for this, implicit and explicit time integration. An implicit analysis calculates the inverse stiffness matrix at time  $t+\Delta t$ , and has to be solved at each time step, thus this method is computationally expensive. An implicit model is suited to quasi-static problems and problems with a long time duration. An explicit time integration model works on the central difference method, where the kinematic quantities, such as displacement and velocities for a next time step ( $t+\Delta t$ ), are calculated, based on the current time step <sup>26</sup>. As a result, the stiffness matrix does not need to be created and inverted at each time step; thus, this method is computationally less expensive. Whilst the time steps that can be used by an explicit analysis are limited based on the size of smallest element and the time taken for a stress wave to pass through it, this form

of analysis is suited to contact problems with a short time duration. Due to this, and because previous finite element head models investigating impact have used it<sup>9-11, 13, 18, 19, 21, 22, 29</sup>, an explicit solver was used for all simulations completed by this study.

### 5.2.1.4.2 Interactions and Model environment

Post development of the FE models, the environment in the finite element solver was set up. A tie constraint was used for all interactions with the exception of the interaction between the brain and CSF elements. Different modelling techniques for the brain-skull interaction, which is also referred to as the pia / arachnoid complex, have been used by previous authors<sup>13, 37, 38</sup>. Essentially this interface should be modelled using a fluid structure interaction; however, this area of computational modelling is still developing and requires substantial resources. However, different techniques have been proposed to model this interaction, ranging from using solid CSF elements with a low shear modulus, to using a frictionless sliding contact. Whilst previous parametric tests, using adult FE head models have concluded that head impact response is affected by this interaction, Kleiven and Hardy<sup>37</sup> concluded that localised brain motion is insensitive to the condition used for this interface for low severity impacts. Consequently, initially a sliding contact was used with friction value of 0.2, as proposed by Miller *et al*<sup>38</sup>, an interaction that has been used by previous authors<sup>13, 32, 37, 38</sup>; however, a tie constraint was evaluated in the parametric analysis.

In the cadaver experiments conducted by Prange *et al*<sup>16</sup>, the foramen magnum was sealed for the drop test experiments. Therefore, the foramen magnum was modelled as closed, with a restraint used to prevent nodes from moving through it, for all the FE models used in the validation process. It has been suggested that this foramen should be modelled as a force free opening<sup>13, 39</sup>, however this will be assessed in the parametric section.

#### 5.2.1.4.3 Simulation Procedure

The validation procedure was identical to that outlined by Prange *et al* <sup>16</sup>. The FE model was impacted onto a rigid surface at four different anatomical locations (frontal, parietal, vertex and occiput). Each impact was conducted at two different impact velocities, 1.716m/s and 2.426m/s, which corresponded to fall heights of 0.15m and 0.3m respectively. For each impact, the FE model was placed in contact with the rigid surface and was assigned a predefined impact velocity. Each simulation was run for a 40ms time period.

Prange *et al* <sup>16</sup> also completed compression tests in the anterior-posterior (AP) and left-right (LR) direction at rates of 0.05mm/s, 1.0mm/s, 10mm/s and 50mm/s. Thus, each headform was subject to the same compression test. Each test involved placing the headform between two plates, one plate was fixed in space (constrained in 6 degrees of freedom) and the other was given a translation velocity depending on the compression rate. The plates were placed such that compression was either in the AP or LR direction.

#### 5.2.1.4.4 Output variables and statistical analysis

The contact force between the headform and the rigid surface was exported from Abaqus (Version 6.10, DSS <sup>12</sup>) into Matlab (Version R2011a, Mathworks<sup>40</sup>). The transitional acceleration was calculated in units of g using Equation (25). Following this the peak translational acceleration (peak G), HIC (Equation (2)) and duration of impact were calculated. Force and displacement were exported for each of the compression tests. The stiffness was calculated using Hooke’s Law, Equation (34).

$$F = kx \tag{34}$$

where F is force, k is stiffness and x is displacement.

A one sample student t-test was used to compare peak G, HIC, duration of impact and stiffness between each of the FE models used in the validation process (Models B1, B2, B3 and B4) and the values documented in the cadaver tests by Prange *et al* <sup>16</sup>. Statistical significance was set at p=0.05 and each test was two sided. SPSS (Version 20, IBM<sup>41</sup>) was used for all the statistical comparisons.



## 5.2.2 Parametric study

### 5.2.3 Overview

Prior to proceeding with assessing clinical features using the FE model, a parametric test was used to assess the material properties and interactions used. The aims of this section were to conduct a parametric test to identify an upper and lower limit, in terms of kinematic variables and material output parameters (stress, strain etc), for different anatomical sites of impact. Whilst previous parametric tests have been conducted, using FE models of infant heads, often they have used extreme material properties that are outside a reported range and have often been restricted to a single impact scenario. Therefore, the material properties investigated in this parametric test were confined to reported values in the literature for infants, or to assess optimised values and were subject to 4 different impact scenarios. The impact scenarios were as per the previous section, namely 4 different anatomical sites of impact (vertex, occiput, frontal and parietal, at a 0.3m fall height. All impacts were onto a rigid plate in order to assess the worst-case. The material parameters assessed have been outlined as per the anatomical regions, detailed below. Unless stated the material properties will be as per the baseline model (B4).

#### 5.2.3.1 Skull

The material properties of an infant skull are essentially inhomogeneous and orthotropic<sup>3, 6</sup>. However the material properties of the bone for both validated infant head models in the literature<sup>19, 21</sup> and the optimised model in this study, have modelled it as homogeneous and isotropic. The anatomical site of impact significantly affected head injury severity (Chapter 3), therefore the inhomogeneous and orthotropic nature of infant bone may play an important role in this clinical feature. Consequently three parametric models were developed that included the inhomogeneous nature of infant bone (Parametric model S1-S3) and one where the bone was modelled orthotropic (Parametric model S3). The range of reported material properties for the parietal and occipital bone in infants <3 months by

Coats and Margulies <sup>6</sup> is documented in *Table 21*. The material properties that were changed from the validated baseline model are outlined below.

#### Parametric Model S1

An inhomogeneous model and isotropic model were used, using the lower reported values by Coats and Margulies <sup>6</sup> for infants <3 months age (*Table 21*). The skull properties were the same as the baseline B2 model and the corresponding values can be seen in *Table 21*.

#### Parametric Model S2

The skull was modelled as inhomogeneous and orthotropic for both of these models. Research conducted by McPherson and Kriewall <sup>3</sup> showed that infant skull properties were orthotropic, with different properties when the fibres were parallel or perpendicular to the long axis. The material tests conducted by Coats and Margulies <sup>6</sup> on infant bone were with the fibres perpendicular to the long axis and no testing was completed with the fibre parallel to the long axis. However, only Coats and Margulies <sup>6</sup> completed testing on bone samples from infants between 0-3months. Consequently, to obtain properties where the fibres are parallel to the long axis for each bone for this age range, the values for perpendicular fibres were scaled based on the work by McPherson and Kriewall <sup>3</sup>, a procedure that has been used by previous authors<sup>13</sup>. Based on the work by McPherson and Kriewall <sup>3</sup>, the ratio for parallel to perpendicular for the parietal bones was 4.2:1 and for the frontal bones was 1.8:1. No testing was conducted on occipital bones; therefore, a ratio was assumed to be equivalent of the parietal bones. The skull bones were modelled with solid elements in the FE model in Abaqus (Version 6.10, DSS <sup>12</sup>). An orthotropic solid element material model Abaqus (Version 6.10, DSS <sup>12</sup>) can be defined based on the elastic stiffness matrix<sup>26</sup>, outlined in Equations (35) through to (45).

$$\begin{Bmatrix} \sigma_{11} \\ \sigma_{22} \\ \sigma_{33} \\ \sigma_{12} \\ \sigma_{13} \\ \sigma_{23} \end{Bmatrix} = \begin{bmatrix} D_{1111} & D_{1122} & D_{1133} & 0 & 0 & 0 \\ 0 & D_{2222} & D_{2233} & 0 & 0 & 0 \\ 0 & 0 & D_{3333} & 0 & 0 & 0 \\ 0 & 0 & 0 & D_{1212} & 0 & 0 \\ 0 & 0 & 0 & 0 & D_{1313} & 0 \\ 0 & 0 & 0 & 0 & 0 & D_{2323} \end{bmatrix} \begin{Bmatrix} \epsilon_{11} \\ \epsilon_{22} \\ \epsilon_{33} \\ \gamma_{12} \\ \gamma_{13} \\ \gamma_{23} \end{Bmatrix} \quad (35)$$

$$D_{1111} = E_1(1 - \nu_{23}\nu_{23})\Gamma \quad (36)$$

$$D_{2222} = E_2(1 - \nu_{13}\nu_{31})\Gamma \quad (37)$$

$$D_{2233} = E_2(\nu_{32} - \nu_{12}\nu_{31})\Gamma \quad (38)$$

$$D_{1122} = E_1(\nu_{21} - \nu_{31}\nu_{23})\Gamma \quad (39)$$

$$D_{1133} = E_1(\nu_{31} - \nu_{21}\nu_{32})\Gamma \quad (40)$$

$$D_{2233} = E_2(\nu_{32} - \nu_{12}\nu_{31})\Gamma \quad (41)$$

$$D_{1212} = G_{12} \quad (42)$$

$$D_{1313} = G_{13} \quad (43)$$

$$D_{2323} = G_{23} \quad (44)$$

$$\Gamma = \frac{1}{(1 - \nu_{12}\nu_{21} - \nu_{23}\nu_{32} - \nu_{13}\nu_{31} - 2\nu_{21}\nu_{32}\nu_{13})} \quad (45)$$

The material constants required for this model are  $E_1$ ,  $E_2$ ,  $E_3$ ,  $G_{12}$ ,  $G_{23}$ ,  $\nu_{12}$ ,  $\nu_{23}$  and  $\nu_{13}$ . Where  $E$  is the elastic modulus,  $G$  is the shear modulus,  $\nu$  is poisson's ratio, 1 refers to the direction where the fibres are parallel, 2 refers to direction where the fibres are perpendicular and 3 is the direction perpendicular to both the 1 and 2 direction. However only  $E_2$  is known for each cranial bone and  $E_1$  was calculated based on scaling as previously stated. An assumption was made that  $E_3$  was the equivalent of  $E_2$ . Poisson's ratio ( $\nu_{23}$ ) was assumed to be the equivalent of an adult, as with previous models<sup>31</sup>. An assumption was made that  $E_3$  was the equivalent of

$E_2$ ; thus, due to symmetry  $\nu_{32}$ ,  $\nu_{31}$ , and  $\nu_{21}$  were equal to  $\nu_{23}$ . The shear modulus was calculated using Equation (46)

$$G_{23} = \frac{E_2}{2(1 + \nu_{23})} \tag{46}$$

The non symmetric poisson’s ratio were calculated using Equation (47)

$$\frac{\nu_{12}}{E_1} = \frac{\nu_{21}}{E_2} \tag{47}$$

For non symmetric planes, Huber’s in plane orthotropic equation was used to calculate the shear modulus, Equation (48)

$$G_{12} = \frac{\sqrt{E_1 E_2}}{2(1 + \sqrt{\nu_{12} \nu_{21}})} \tag{48}$$

The resulting material properties can be seen in Table 23.

Table 23. Material constants used to define an orthotropic material

Material constant	Occiput	Parietal	Frontal
E1 / MPa	120.10	767.3	376.70
E2 / MPa	28.60	182.70	209.30
E3 / MPa	28.60	182.70	209.30
$\nu_{12}$	0.19	0.19	0.19
$\nu_{13}$	0.045	0.045	0.11
$\nu_{23}$	0.22	0.22	0.22
G12 / MPa	26.83	171.37	122.67
G13 / MPa	26.83	171.37	122.67
G23 / MPa	11.72	74.88	85.78

### Parametric Model S3

An inhomogeneous model and isotropic model was used, using the highest reported values by Coats and Margulies <sup>6</sup> for infants <3 months age (Table 21). The skull properties were the same as the validation model B3 and the corresponding values can be seen in Table 21.

### 5.2.3.2 Scalp

#### Parametric Model S4

The majority of the FE models that have included the scalp have used consistent values ( $E=16.7\text{MPa}$ ,  $\nu=0.42$ ,  $\rho=1200\text{ kg/m}^3$ ); however, the optimised elastic modulus value documented by Li *et al*<sup>21</sup> was lower ( $E=8.56\text{MPa}$ ), whilst tests conducted on the scalp tissue have reported values between  $0.13\text{MPa}$  and  $29.5\text{MPa}$ <sup>42, 43</sup>, with the tissue stiffening with compression. Parametric tests conducted by previous authors have found variation in importance of inclusion of the scalp<sup>13</sup>. However due to the optimised value differing from a commonly used value by previous FE infant head models<sup>9, 10, 13, 19, 22, 29</sup>, the elastic modulus was increased to this commonly used value. This was so that the effect of this lower optimised value could be quantified.

### 5.2.3.3 Dura

#### Parametric Model S5

It was been previously discussed that few authors have completed testing to determine the mechanical properties of the meningeal layers<sup>31, 33</sup>. Consequently, similar to the scalp, previous infant head FE models have used consistent properties when modelling this layer of soft tissue<sup>9, 10, 19, 22</sup>, based on adult properties<sup>31</sup>. Thus, in this parametric model the stiffness of the meningeal layers was increased from the optimised value of  $21.28\text{MPa}$ , to the commonly used adult value of  $31.5\text{MPa}$ .

### 5.2.3.4 Brain

#### Parametric Model S6

It was discussed in section 5.2.1.3.6, that the bulk modulus can affect computational stability. A value of an order of magnitude suggested by previous authors<sup>13</sup> ( $2.1\text{MPa}$ ) for an infant brain was compared to an adult value ( $2110\text{MPa}$ ).

This was so that the effect could be quantified, prior to using a lower value to save computational resources.

### Parametric Model S7

Previous parametric tests using finite element analysis have shown that the brain material properties ( $G(0)^{21, 29}$ ,  $G(\infty)^{19, 29}$ ,  $\beta^{21, 29}$ ) have a limited effect ( $<15\%^{19, 29}$  or  $P>0.05^{21, 29}$ ) on certain dynamic response variables (peak  $G^{19, 21, 29}$ ,  $HIC^{29}$ , maximum principle stress of the bone<sup>21</sup>, maximum principle strain of the bone<sup>21, 29</sup>, maximum von mises stress of the bone<sup>19, 29</sup>, deflection<sup>19</sup>) of an infant head on impact<sup>19, 21, 29</sup>. Only Roth *et al*<sup>19</sup> found that increasing  $G(0)$  from  $5.99e^{-3}$  to  $5.99e^{-1}$  effected peak  $G$  and skull von mises stress by greater than 15%. However parametric tests leading to these conclusions have used a viscoelastic law. Tests conducted at strains of 50% on porcine and adult sample, have suggest modelling the brain using a 1<sup>st</sup> order Ogden hyperelastic model<sup>34</sup>. Consequently FE models have modelled the brain using this method<sup>13, 32</sup>, where it has been concluded that the brain shear stiffness affects the dynamic response of the head<sup>13</sup>. Due to these differences in the effect of brain material properties, in this parametric test the brain was modelled using a non-linear Ogden hyperelastic law; however, as no human infant properties were reported by Prange and Margulies<sup>34</sup>, the relationship between infant and adult porcine values were used to scale the human adult shear stiffness values to that of an infant ( $\mu_{\text{infant}} = 2.17\mu_{\text{adult}}$ ). This method has been used by previous authors<sup>13</sup>, with resulting values for  $\mu$  and  $\alpha$  of 559Pa and 0.00845 respectively. The density and bulk modulus remained constant with the viscoelastic model.

$$\mu(t) = \frac{\alpha T_{12}(\lambda + \lambda^{-1})}{2(\lambda^\alpha + \lambda^{-\alpha})} \quad (49)$$

where  $\mu(t)$  is the time dependent shear modulus,  $T_{12}$  is the shear stress at time  $t$ ,  $\alpha$  is material constant and  $\lambda$  is the principle stretch ratio at time  $t$ .

### 5.2.3.5 Interactions

#### Parametric Model S8

A constraint was used in the optimised model to prevent nodes from passing through the foramen magnum, as it was closed in the cadaver experiments conducted by Prange *et al*<sup>16</sup>. Previous research has suggested, however, that the foramen magnum be modelled as a force free opening<sup>13, 39</sup>. Consequently, the restraints preventing the nodes from passing through the foramen magnum were removed, in order to assess the effect of this constraint.

#### Parametric Model S9

It has been previously discussed that a number of different methods have been proposed for modelling the brain skull or pia / arachnoid interface<sup>44</sup>. In the optimised model, a slip condition was used with a friction value of 0.2<sup>38</sup>. Whilst this potentially under-restrains this interaction, previous authors have indicated that brain skull motion is insensitive to this contact definition for low severity impacts<sup>37</sup>. No data exists, however, which can validate the brain skull motion in an infant head, meaning a tied constraint was used between the brain and CSF in this parametric model, a restraint that has been shown to be adequate when modelled pressure on the brain<sup>37</sup>. The CSF was modelled with a low shear modulus for all impacts, thus following a similar procedure for this interaction as used by previous authors<sup>45</sup>.

### 5.2.3.6 Bridging vein

In the optimised FE model, connectors used to model the bridging veins were manual inserted and assigned stiffness properties based on the research by Morrison<sup>35</sup>. Due to this properties including length, direction and stiffness were allocated to the connectors. Thus to quantify these assumptions, parametric models were developed.

Parametric S10

In this parametric model the length of the veins was increased to greater levels reported by Morrison <sup>35</sup> as opposed to the mean values. The lengths were increased to an average length of 10mm.

Parametric Model S11

It has previously been discussed that a proposed theory for why a SDH might be more likely from an occipital impact as opposed to frontal impact is due to the bridging veins draining in a forward direction <sup>36</sup>. However draining direction of the bridging veins can vary depending on its location along the superior sagittal sinus <sup>46</sup>. Consequently the direction of the connectors was changed to a posterior direction, as can be seen in *Figure 37*.

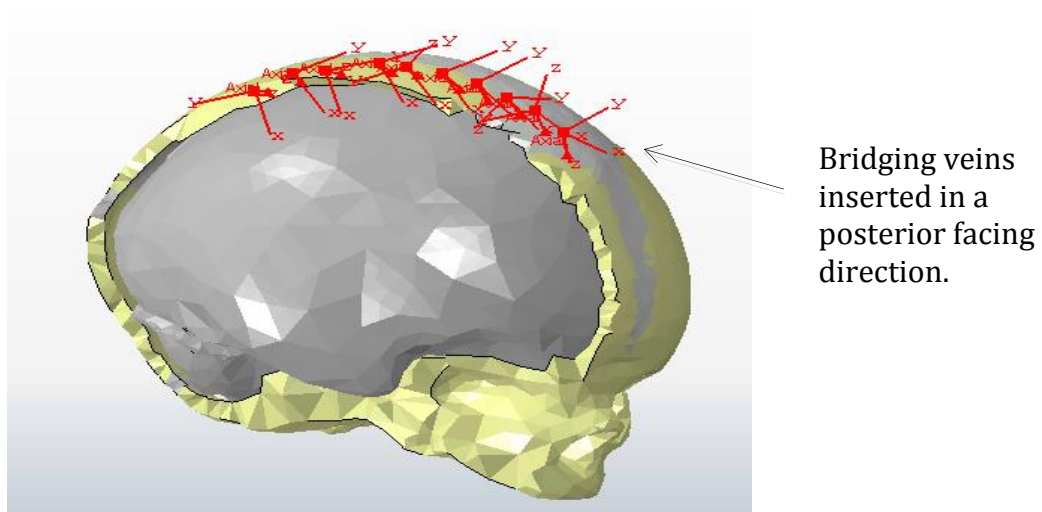


*Figure 37. Connectors inserted into in a posterior facing direction.*

Parametric Model S12

The non linear stiffness assigned to the connectors in the optimised FE model was based on a force displacement graph of an infant bridging vein (H/2/2) reported by Morrison <sup>35</sup>. However, the authors were only able to acquire a small sample of infant bridging veins, thus it is unclear how representative the stiffness is of this



particular age group. Whilst the same authors investigated relative displacement between the brain and skull, instead using a connectors with an assigned stiffness, and concluding that using elastic veins only reduced the peak stretch ratio by 5%<sup>35</sup>. Despite this, the connectors in this parametric model were assigned a stiffness based on vein  $H/1/4$  from Morrison<sup>35</sup>, which effectively increased the stiffness whilst also effectively encompassing a range in which reported adult properties would lie<sup>35,36</sup>.

### **5.2.3.7 Impact scenarios, output variables and statistical comparisons**

#### 5.2.3.7.1 Impact Scenarios

It has been discussed that previous parametric tests, using FE infant head models have been conducted based on a single impact scenario<sup>13,19,21,29</sup>. However, due to the significance of the anatomical site of impact, one of the aims of this section of the research was to measure the effect of material parameters and interactions across a range of scenarios. Consequently each parametric model was subject to four impact scenarios, a 0.3m fall onto the vertex, occiput, frontal and parietal areas. This height was chosen, such that the output variables could be compared between the cadavers experiments by Prange *et al*<sup>16</sup> and also the clinical data from Chapter 3.

#### 5.2.3.7.2 Output variables

Both kinematic variables and material failure properties were assessed in each parametric model. The measured kinematic variables were peak linear acceleration (peak G), head injury criterion (HIC), duration of impact ( $\Delta t$ ), peak rotational acceleration ( $\alpha_p$ ) and peak change in rotational velocity ( $\Delta\omega$ ). The measured material properties were the maximum principle stress ( $\sigma_{MxPrin}$ ) of the skull and peak stretch ratio of all of the bridging veins ( $\lambda_{peak}$ ). The stretch ratio was defined as the deformed length relative to the original length. The final measurement was the deformation of the head. The deformation of the head was measured in three directions, anterior-posterior (AP), left-right (LR) and superior-

inferior (SI). The head strain ( $\varepsilon_{Head}$ ) was defined as the change in length relative to the original length, Equation (50). The maximum head strain ( $\varepsilon_{MxHead}$ ) was taken as the maximum of the head strains in the three directions (AP, LR and SI).

$$\varepsilon_{Head} = \frac{\varepsilon_L - \varepsilon_0}{\varepsilon_0} \times 100 \quad (50)$$

Where  $\varepsilon_L$  is the change in length and  $\varepsilon_0$  is the original in length.

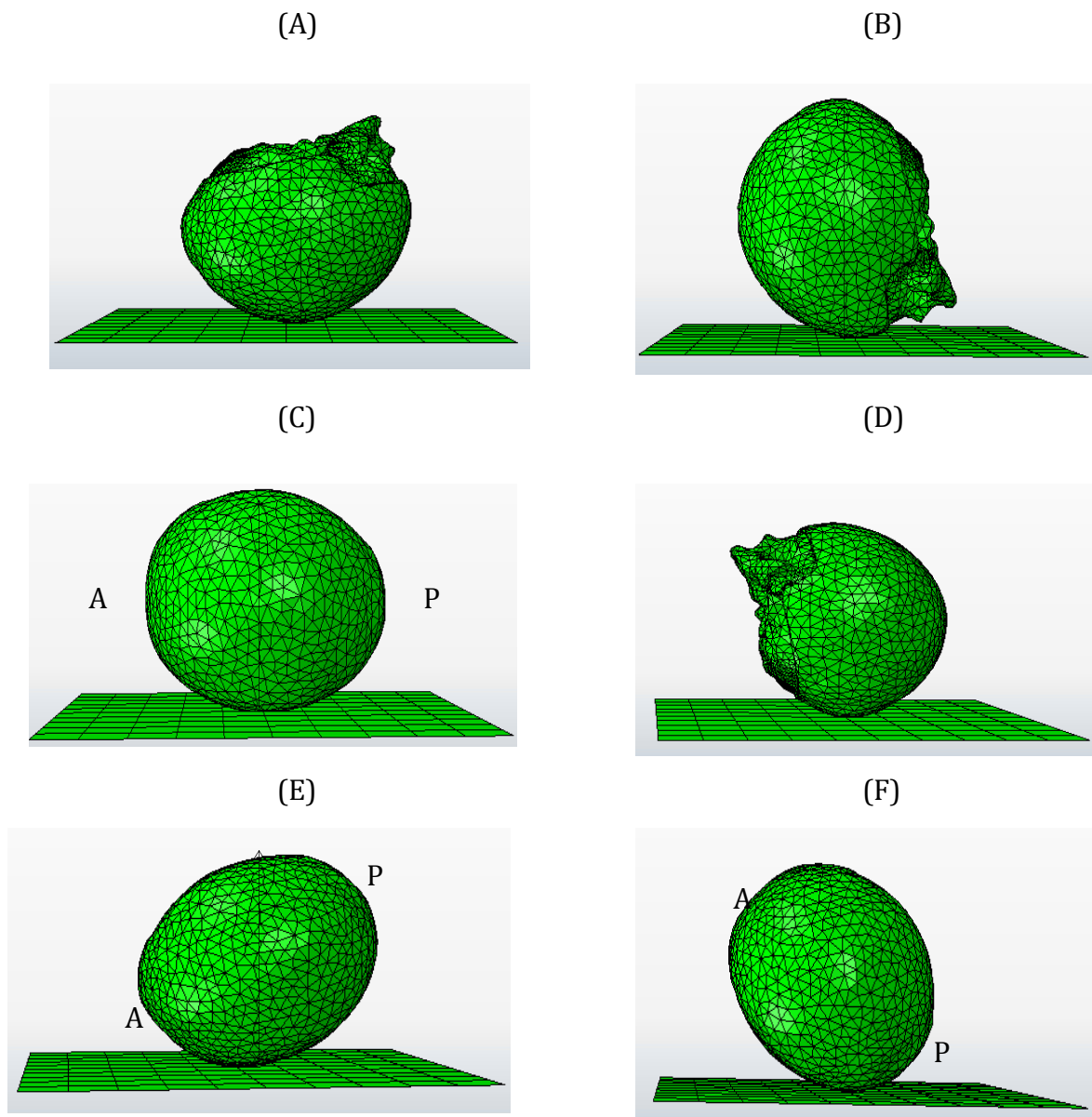


Figure 38. Impact locations used in finite element analysis. A vertex impact with an arrow illustrating superior-inferior (SI) measurements (A), a frontal impact with an arrow illustrating anterior-posterior (AP) measurement (B), a parietal impact with an arrow illustrating the left-right (LR) measurement (C), an occipital impact (D), a fronto-parietal impact with an arrow illustrating a distal-floor (DF) measurement (E), a parieto-occipital measurement (F), A-Anterior of head, P – Posterior of head.

#### 5.2.3.7.3 Statistical Comparisons

All peak variables measured in this section are absolute values and do not include a measure of variation. Consequently statistical significance cannot be evaluated for these parameters. However, a greater than 15% change in a variable was discussed between the respective parametric model and the optimised model, as has been used by previous authors<sup>13, 19</sup>. Each of the parametric models were evaluated against the cadaver experiments conducted by Prange *et al*<sup>16</sup> using same procedure as outlined in section 5.2.1.4.4.

### **5.2.4 Assessment of key clinical features (Height and anatomical site of impact)**

All tests in this section were conducted with the optimised FE model.

#### **5.2.4.1 Impact Scenarios**

Chapter 3 addressed two key clinical differentiating features, namely the height and surface. However, due to limited resources, only heights up to 0.6m were investigated, from Chapter 3, this was essentially sub injurious. Therefore, an aim of this section of the work was to investigate heights within an injurious range using a validated FE model of an infant head. Consequently, four heights were investigated, 0.15m, 0.3m, 0.6m and 1.2m. The lower heights of 0.15m and 0.3m was chosen as ‘sub injurious’ heights and 0.6m was used as borderline threshold based on the findings from Chapter 3. The height of 1.2m was investigated as it correlated with a 9-23% risk of skull fracture and / or ICI, from Chapter 3 and it has commonly been used as a threshold, from the epidemiology literature<sup>47</sup>. The anatomical site of impact was identified as a key differentiating feature from Chapter 3. To investigate this further, the head FE model was impacted onto 6 different anatomical sites; vertex, occiput, frontal, left parietal, fronto-parietal and parieto-occipital. Whilst only the vertex, occiput, frontal and parietal were assessed in Chapter 3, the further two anatomical locations were included to cover a broader area of the head.

The FE head model of the infant head was impacted on the 6 different anatomical locations across the four different heights, thus resulting in 24 different impacts. Each impact was onto a rigid surface, thus equating to a “worst case scenario” in terms of surface. Whilst impact surface has been shown to be significant, due to a disconnect between biomechanical and clinical thresholds. Only the worst case scenario was investigated, such that dynamic response of the head in isolation could be investigated.

An additional impact onto the parieto-occipital area at a fall height of 0.82m was completed so that the high stress zones in the skull could be compared to the fractures patterns documented. Potential fracture zones were defined as stress values in excess of the lowest ultimate stress values reported by Coats and Margulies <sup>6</sup>, Table 21.

#### Output variables

The measured output variables were the same as those in the parametric section of this research (section 5.2.3.7.2). Namely peak G, HIC, duration of impact ( $\Delta t$ ), peak rotational acceleration ( $\alpha_p$ ), peak change in rotational velocity ( $\Delta\omega$ ), maximum principle stress ( $\sigma_{MxPrin}$ ) of the skull, peak stretch ratio of all of the bridging veins ( $\lambda_{peak}$ ) and the maximum head strain ( $\epsilon_{MxHead}$ ). Additionally, a deformational measurement was also taken for the fronto-parietal and parieto-occipital impact. The measurement was taken normal to the impacted surface and was labelled distal to floor (DF), Figure 38.

#### **5.2.4.2 Statistical Comparisons**

The statistical analysis for this section followed the same procedure as outlined in section 5.2.3.7.3. Again, each of the output variables was absolute and thus statistical significance could not be assessed. However, again a >15% difference was used to assess the effect of height and site of impact<sup>13, 19</sup>.

An additional analysis was conducted on the stretch ratio of the connectors used to model the bridging veins. The  $\lambda_{\text{peak}}$  was defined as the peak stretch ratio across all connectors in the FE model. However, in addition, the variation in peak stretch ratio of the individual connectors was assessed between height and site of impact. Parametric and the non parametric equivalence of the two factorial ANOVA were used to determine, if significant differences existed in the peak stretch ratio between height and site of impact. The non parametric equivalent was based on the global ranking of the data. SPSS (Version 20, IBM) was used for all the statistical analysis, where statistical significance was set at  $p = 0.05$ .

### 5.2.5 Nomenclature

*Table 24. Nomenclature of material properties and variables assessed during finite element analysis.*

<b>Symbol</b>	<b>Definition</b>
$\sigma$	Stress
$\epsilon$	Strain
E	Elastic Modulus
G	Shear Modulus
$\lambda_{\text{peak}}$	Peak stretch ratio of bridging veins
$\sigma_{\text{MxPrin}}$	Maximum principle stress
Peak G	Peak linear acceleration
HIC	Head Injury Criterion, Equation (2).
$\Delta t$	Duration of impact
$\alpha_p$	Peak rotational acceleration
$\Delta\omega$	Peak change in rotational velocity

### 5.3 Results

#### 5.3.1 Validation

Each of the four models developed for the validation process were subject to eight different impact scenarios and assessed against the kinematic response for infant cadaver heads reported by Prange *et al*<sup>16</sup>. Model B1 had an inhomogeneous material model for the skull based on the mean stiffness values reported in the literature for infant <3 months<sup>3,6</sup>. A comparison of the output variables between model B1 and those documented by Prange *et al*<sup>16</sup> can be seen in Table 25. Across the 24 output variables assessed, model B1 was significantly different for 11. Vertex impacts were not significantly different for both the 0.15m and 0.3m fall heights (Table 25).

Table 25. Output variables (peak G, HIC, duration of impact) from finite element model (B1). One sample student t-test used to compare FE results to Prange *et al*<sup>16</sup>.

Impact Location	Height / m	Peak G / G	Duration / ms	HIC	P value (Peak G)*	P value (Duration)*	P value (HIC)*
Vertex	0.15	57.1	10.2	88.1	0.383	0.101	0.056
Occiput	0.15	64.9	8.6	106.9	0.022	0.082	0.011
Frontal	0.15	76.1	7.2	128.5	0.032	0.066	0.015
Parietal	0.15	68.6	9.2	109.2	0.006	0.071	0.004
Vertex	0.30	87	9.1	234.8	0.763	0.109	0.115
Occiput	0.30	86.1	8.6	241.9	0.049	0.065	0.006
Frontal	0.30	110.2	6.8	308.1	0.057	0.068	0.04
Parietal	0.30	104.5	8.4	291	0.008	0.054	0.005

• Significance assessed against Prange *et al.* (2004). Assessed using one sample t-test. Grey box indicate significantly different result (P<0.05).

Model B2 also had an inhomogenous material model for the skull, however, the stiffness properties were based on the lowest values reported in the literature for infants <3months<sup>3,6</sup>. A comparison of the output variables, between model B2 and those documented by Prange *et al*<sup>16</sup>, can be seen in Table 26. Across the 24 output variables assessed, model B2 was significantly different for 7, of which, 5 had a significant difference in the variable HIC (Table 26).

Table 26. Output variables (peak G, HIC, duration of impact) from finite element model (B2). One sample student t-test used to compare FE results to Prange et al <sup>16</sup>.

Impact Location	Height / m	Peak G / G	Duration / ms	HIC	P value (Peak G)*	P value (Duration)*	P value (HIC)*
Vertex	0.15	49.0	11.8	71.2	0.896	0.132	0.121
Occiput	0.15	45.6	12.2	66.3	0.203	0.159	0.049
Frontal	0.15	63.1	9.2	94.7	0.064	0.091	0.034
Parietal	0.15	55.2	11.2	80.5	0.019	0.113	0.01
Vertex	0.30	69.9	11.2	170.4	0.555	0.168	0.376
Occiput	0.30	61.3	11.8	142.3	0.882	0.141	0.042
Frontal	0.30	87.7	8.7	222	0.139	0.094	0.099
Parietal	0.30	78.9	10.3	195.1	0.031	0.09	0.018

• Significance assessed against Prange et al. (2004). Assessed using one sample t-test. Grey box indicates significantly different result (P<0.05).

The stiffness properties of the skull of model B3 were based on the highest values reported in the literature for infants <3months <sup>3,6</sup>. A comparison of the output variables between model B3 and those documented by Prange et al <sup>16</sup> can be seen in Table 27. Across the 24 output variables assessed, model B3 was significantly different for 14 (Table 27).

Table 27. Output variables (peak G, HIC, duration of impact) from finite element model (B3). One sample student t-test used to compare FE results to Prange et al <sup>16</sup>.

Impact Location	Height / m	Peak G / G	Duration / ms	HIC	P value (Peak G)*	P value (Duration)*	P value (HIC)*
Vertex	0.15	62.3	0.0094	99.6	0.227	0.09	0.038
Occiput	0.15	73.7	0.0076	125.3	0.013	0.071	0.007
Frontal	0.15	82.1	0.0066	142	0.025	0.061	0.012
Parietal	0.15	72.9	0.0082	120.6	0.005	0.058	0.003
Vertex	0.30	87	0.0091	234.8	0.763	0.109	0.115
Occiput	0.30	100.5	0.0076	287.9	0.021	0.053	0.004
Frontal	0.30	121.1	0.0062	340.6	0.041	0.062	0.031
Parietal	0.30	112.6	0.0075	326.7	0.006	0.043	0.004

• Significance assessed against Prange et al. (2004). Assessed using one sample t-test. Grey box indicate significantly different result (P<0.05).

The final model to be assessed was based on the optimised parameters documented by Li et al <sup>21</sup>. A comparison of the output variables between model B3



and those documented by Prange *et al*<sup>16</sup> can be seen in Table 28. Only three of the twenty four output variables are significantly different to cadaver impacts reported by Prange *et al*<sup>16</sup>, with no impact condition significant different for more than one variable. As a result of the similarities in the output variables, this model was classed as having a similar dynamic response to a human infant head and was used as the baseline model in the parametric assessment.

Table 28. Output variables (peak G, HIC, duration of impact) from finite element model (B4). One sample student t-test used to compare FE results to Prange *et al*<sup>16</sup>.

Impact Location	Height / m	Peak G / G	Duration / ms	HIC	P value (Peak G)*	P value (Duration)*	P value (HIC)*
Vertex	0.15	44	0.013	60.4	0.705	0.164	0.232
Occiput	0.15	49.5	0.0108	77.2	0.106	0.12	0.029
Frontal	0.15	56.6	0.0102	80.3	0.1	0.108	0.55
Parietal	0.15	40.2	0.012	48.4	0.309	0.14	0.063
Vertex	0.30	60.4	0.0126	133.8	0.328	0.234	0.834
Occiput	0.30	65.5	0.0109	170.4	0.475	0.11	0.019
Frontal	0.30	75.6	0.0098	176.5	0.267	0.116	0.192
Parietal	0.30	69.2	0.011	157.6	0.076	0.113	0.039

• Significance assessed against Prange *et al.* (2004). Assessed using one sample t-test. Grey box indicate significantly different result (P<0.05).

A one sample student t-test concluded that the stiffness of the FE model B4 was not significantly different from the cadavers heads used by Prange *et al*<sup>16</sup> (P>0.14) for the 1mm/s, 10mm/s and 50mm/s for both the AP and LR directions. However, the FE model B4 was significantly stiffer for the AP and LR at a compression rate of 0.05mm/s (P<0.007). A comparison of the stiffness values for a 50mm/s compression test between model B4 and those documented by Prange *et al*<sup>16</sup> can be seen in *Figure 39*.

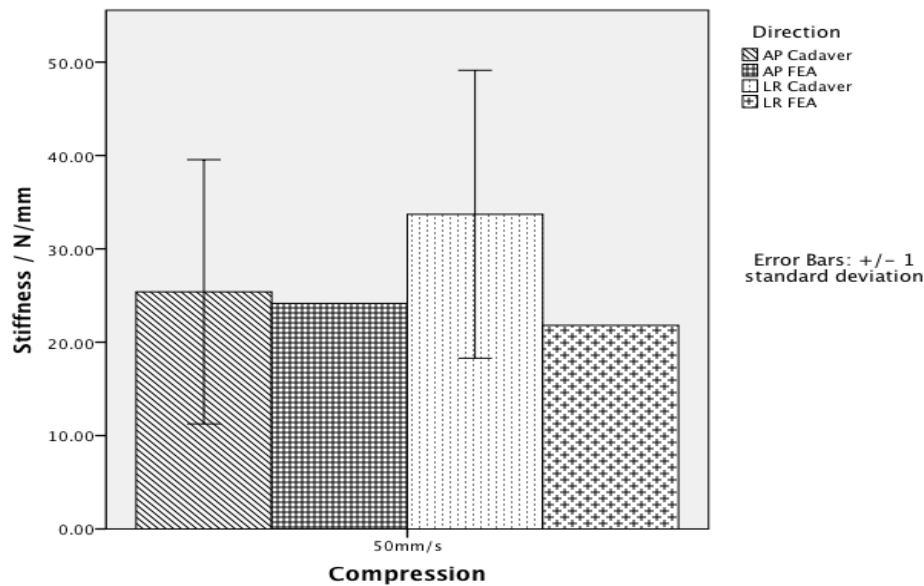


Figure 39. Comparison of compression at rate of 50mm/s in anterior-posterior (AP) and left-right (LR) direction between model B4 and the cadaver head used by Prange *et al*<sup>16</sup>.

### 5.3.2 Parametric Analysis

Each of the parametric models was assessed against the optimised model from the validation process (Model B4). A greater than a 15% difference in the output variable for each parametric model is discussed below.

#### 5.3.2.1 Skull Stiffness

##### Parametric Model (S1)

A greater than 15% difference in peak G was seen for the frontal and vertex impacts, increasing from 76g to 88g for the frontal impact and from 60g to 70g for the vertex impact. Both cases were not significantly different from those reported by Prange *et al*<sup>16</sup> ( $P > 0.13$ ). In terms of HIC, impacts onto all four areas resulted in variations of greater than 15%. In this parametric model, the bone stiffness of the parietal bone was 7% greater, relative to the optimised model, the frontal bone was 23% greater and the occipital bone was 83.3% lower. Consequently HIC increased for the frontal impact by 26% to 222, for the parietal impact by 23% to 195, for vertex by 27% to 170 and for the occipital impact it decreased by 16% to 142. However, this resulted in the HIC values being significantly different from

Prange *et al* <sup>16</sup> for the parietal ( $P < 0.02$ ) and occipital ( $P < 0.05$ ) impacts. This parametric model did not significantly increase rotational accelerations by greater than 15% and only rotational velocities increased by greater than 15% for the frontal impact. The maximum deformation for the frontal, parietal and vertex decreased for this parametric model, yet it was not by greater than 15%. However, deformation for the occipital impact increased by 15%. Similarly the maximum principle stress increased for the frontal, parietal and vertex impacts, but not by greater than 15% and it reduced for an occipital impact by greater than 15%.

#### Parametric S2

In this parametric model an inhomogeneous, orthotropic material was used to define the skull. The material properties were again based on the lower properties reported by Coats and Margulies <sup>6</sup>, as outlined in section 5.2.1.3.1. Compared to the optimised model, peak G increased by greater than 15% only for the vertex impact and HIC increased by 15% for the vertex, occipital and parietal impacts. Duration of impact did not vary by greater than 15%.

Comparisons were also made relative to the Parametric Model S1, so that an orthotropic material representation of the skull could be compared to an isotropic one. Peak G did not vary by greater than 15% for any impact location, when comparing parametric models S2 to S1. Comparing parametric model S2 to S1, thus using an orthotropic model to define the bone instead of a isotropic model, resulted in HIC only varying by greater than 15% for the frontal impact. Duration of impact did not vary by greater than 15%. The greatest change as a result of using an orthotropic material for skull was on the maximum principle stress. It increased by greater than 15% for the vertex, occipital and parietal impacts. However, the increased stress would imply a greater risk of fracture, which disagrees with findings from Prange *et al* <sup>16</sup>, where no fractures were seen.

### Parametric S3

An increase in bone stiffness to the upper properties reported by Coats and Margulies <sup>6</sup> resulted in all variables, varying by greater than 15% from the optimised model. In this parametric model, the bone stiffness of parietal bone was 377% greater relative to the optimised model, the frontal bone was 818% greater and the occipital bone was 222% greater. However, it resulted in all variables being significantly different from Prange *et al* <sup>16</sup> ( $P > 0.05$ ). For a vertex impact peak G increased by 45% to 87g and HIC increased by 75% to 235.

#### **5.3.2.2 Scalp Stiffness**

##### Parametric model S4

In this model the scalp stiffness was increased by 95% from 8.56MPa to 16.7MPa, in order to compare the optimised output to the value commonly used in the literature. This 95% increase in stiffness did not increase peak G by greater than 15% across all four impact locations and only increased HIC by greater than 15% for a vertex impact. The duration of impact, peak deformation and maximum principle stress in the bone did not increase by greater than 15% across all four impacts.

#### **5.3.2.3 Membrane Stiffness**

##### Parametric model S5

The falx cerebri and tentorium cerebellum stiffness was increased in this parametric model by 48% from 21.3MPa and 31.5MPa, due to similar reasons as parametric model S4, such that the optimised output could be compared to a commonly used value. Peak G, HIC, duration of impact, peak deformation and maximum principle stress were not affected by greater than 15% across the four impact scenarios.

#### 5.3.2.4 Bulk Modulus

Parametric model S6

The bulk modulus was decreased from 2110MPa to 2.1MPa in this parametric model, however this did not affect peak G, HIC or duration of impact by greater than 15%. Only for an occipital impact was the maximum principle stress in the bone affected by greater than 15%, where it increased by 25% to 18.8MPa.

#### 5.3.2.5 Brain Stiffness

Parametric model S7

A hyperelastic material model for the brain was compared to a viscoelastic model. Across all four impact locations peak G, HIC, duration of impact, peak deformation and maximum principle stress were not affected by greater than 15%.

#### 5.3.2.6 Interactions

Parametric model S8

The foramen magnum was closed in the optimised in the order for the model to be comparable to the infant cadaver heads used by Prange *et al* <sup>16</sup>. However, in order to test this constraint, a parametric model was developed, where the foramen magnum was open such that nodes were free to pass through. However, this change in the constraint did not affect the output variables peak G, HIC, duration impact, peak deformation or skull maximum principle stress by greater 15%.

Parametric model S9

In this parametric model, a tie constraint was used for the interaction between the brain and CSF. Similarly to parametric model S8, no affects of greater than 15% were seen on the output variables.

#### 5.3.2.7 Bridging Veins

Parametric Model S10

In this parametric model the length of the connectors were increased. However, this did not affect ( $\lambda_{\text{peak}}$ ) by greater than 15% across all impact scenarios investigated.

#### Parametric Model S11

The direction of connectors used to model the bridging veins was altered from an anterior facing direction to a posterior direction. However, this change in direction also did not affect  $\lambda_{\text{peak}}$  by greater than 15%.

#### Parametric Model S12

The stiffness of the connectors in this model was increased to highest reported by values by <sup>35</sup>. However again this did not affect  $\lambda_{\text{peak}}$  by greater than 15%.

### **5.3.3 Assessment of key clinical features using validated FE model**

The assessment of the key clinical features (height and location of impact) was assessed for each of the output variables.

#### **5.3.3.1 Peak G**

An increase in height increased peak G across all impact locations as can be seen in *Figure 40*. All increases in height resulted in peak G increasing by greater than 15% for all impact locations. For the increase in height from 0.15m to 0.3m, the smallest increase in peak G was onto the parieto-occipital area, where it increased by 25% from 44g to 55g and the greatest increase was onto the parietal region where it increased by 72.6% from 40g to 69g. For the further increase in height from 0.3m to 0.6m, the least amount peak G increased by was 21% and was for an impact onto the vertex area increasing from 60g to 75g. The greatest increase was again onto the fronto-parietal area, increasing from 71g to 102g (44%). The final increase in height from 0.6m to 1.2m, further increased the magnitude of peak G. Again increasing least for an impact onto parietal area (13%, 84g to 95g) and most onto the fronto-parietal (28%, 102g to 131g).

The peak linear acceleration did not have a linear association with fall height as can be seen in *Figure 40*, although peak g does appear to have a logarithmic relationship with fall height.

The variation in peak G between sites of impact varied with height. An increase in height increased the difference in peak G between the sites of impact (*Figure 40*). For the 0.15m fall height, the maximum difference in peak G was between the frontal and parietal impacts, where the frontal impact increased peak G by 42.5% to 57g. The mean value for peak G across all sites of impact for a 0.15m fall height was  $47 \pm 2g$ . At an increased fall height of 0.3m, an impact onto the parieto-occipital area had the lowest peak G value of 55g. At this height an impact onto the frontal area increased peak G by 38.2% to 76g. The mean value for peak G across all sites of impact for a 0.3m fall height was  $66 \pm 3g$ . A further increase in fall height to 0.6m again resulted in a parieto-occipital impact having the lowest peak G value of 70g. However, a fronto-parietal impact had the highest value of 102g, an increase of 45.7%. The mean value for peak G across all sites of impact for a 0.6m fall height was  $85 \pm 5g$ . At the final fall height of 1.2m, again the lowest peak G value of 80g was for an impact onto the parieto-occipital area and the highest was 131g (an increase of 63.8%) for a fronto-parietal impact. The mean value for peak G across all sites of impact for a 1.2m fall height was  $101 \pm 8g$ .

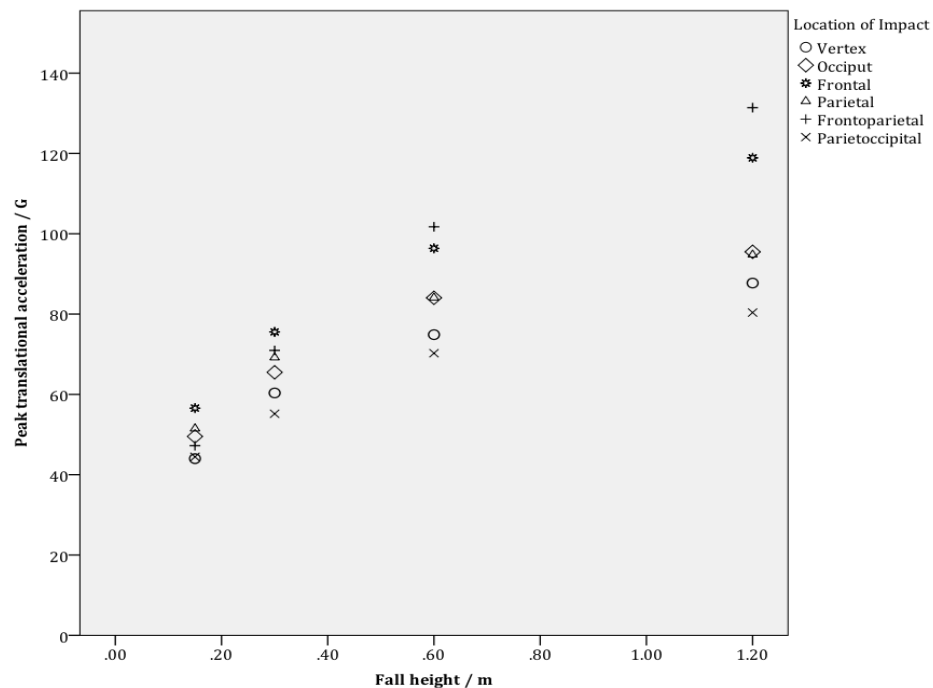


Figure 40. Variation of peak G with changing height and location of impact.

### 5.3.3.2 HIC

A similar pattern was seen for HIC as for peak G. Again all increases in height increased HIC across all impact locations, as can be seen in Figure 41. All increases in height resulted in HIC increasing by greater than 15% for all impact locations. For the increase in height from 0.15m to 0.3m, the smallest increase in HIC was onto the parieto-occipital area, where it increased by 79% from 57 to 102 and the greatest increase was onto the parietal region, where it increased by 226% from 48 to 158. For the further increase in height from 0.3m to 0.6m, the least amount HIC increased by was 68%, for an impact onto the parietal area increasing from 158 to 166. The greatest increase was again onto the fronto-parietal area, increasing from 150 to 329 (119%). The final increase in height from 0.6m to 1.2m, further increased HIC. Again, increasing least for an impact onto parietal area (37%, 266 to 365) and most onto the fronto-parietal (80%, 329 to 592).

However, HIC also did not have a linear association with fall height, as can be seen in Figure 41. HIC appears to have a logarithmic relationship with fall height and it varied with site of impact.



The variation in HIC between sites of impact varied with height. An increase in height increased the difference in HIC between the sites of impact (*Figure 41*). For the 0.15m fall height, the maximum difference in HIC was between the frontal and parietal impacts, where the frontal impact increased HIC by 65.3% to 80. The mean value for HIC across all sites of impact for a 0.15m fall height was  $64 \pm 5$ . At an increased fall height of 0.3m, an impact onto the parieto-occipital area had the lowest HIC value of 102. At this height an impact onto the frontal area increased HIC by 72.5% to 159 compared to a parieto-occipital impact. The mean value for HIC across all sites of impact for a 0.3m fall height was  $148 \pm 11$ . A further increase in fall height to 0.6m again resulted in a parieto-occipital impact having the lowest HIC value of 181. However a frontal impact had the highest value of 339, an increase of 87.3%. The mean value for HIC across all sites of impact for a 0.6m fall height was  $284 \pm 25$ . At the final fall height investigated, of 1.2m, again the lowest HIC value of 263 was for an impact onto the parieto-occipital area and the highest was 592 (Increase of 125.1%) for a fronto-parietal impact. The mean value for HIC across all sites of impact for a 1.2m fall height was  $424 \pm 53$ .

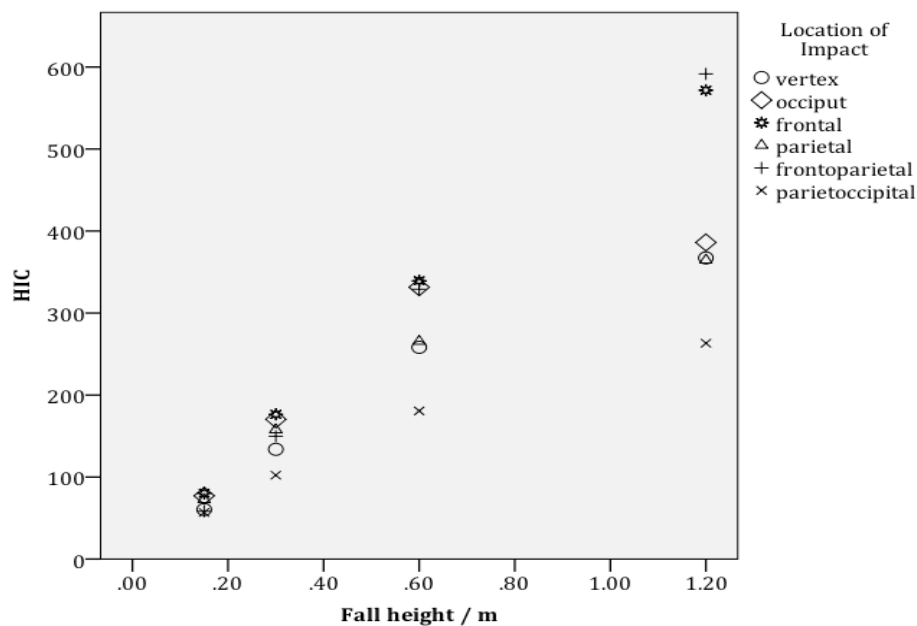


Figure 41. Variation of HIC with changing height and site of impact.

### 5.3.3.3 Duration of impact

An increase in height reduced duration of impact, as can be seen in Figure 42. A vertex impact had the longest duration of impact across the heights investigated. At a 0.15m impact, the duration of impact for a vertex impact was 13ms and it decreased to 11.6ms when the fall height increased to 1.2m. Further comparisons can be seen in Figure 42. Duration of impact was affected by site of impact, as can be seen in Figure 42. At a 0.15m fall height a frontal impact reduced the duration of impact by 21.5% to 10.2ms. The lowest duration of impact was 8.6ms for a frontal impact at a fall height of 1.2m.

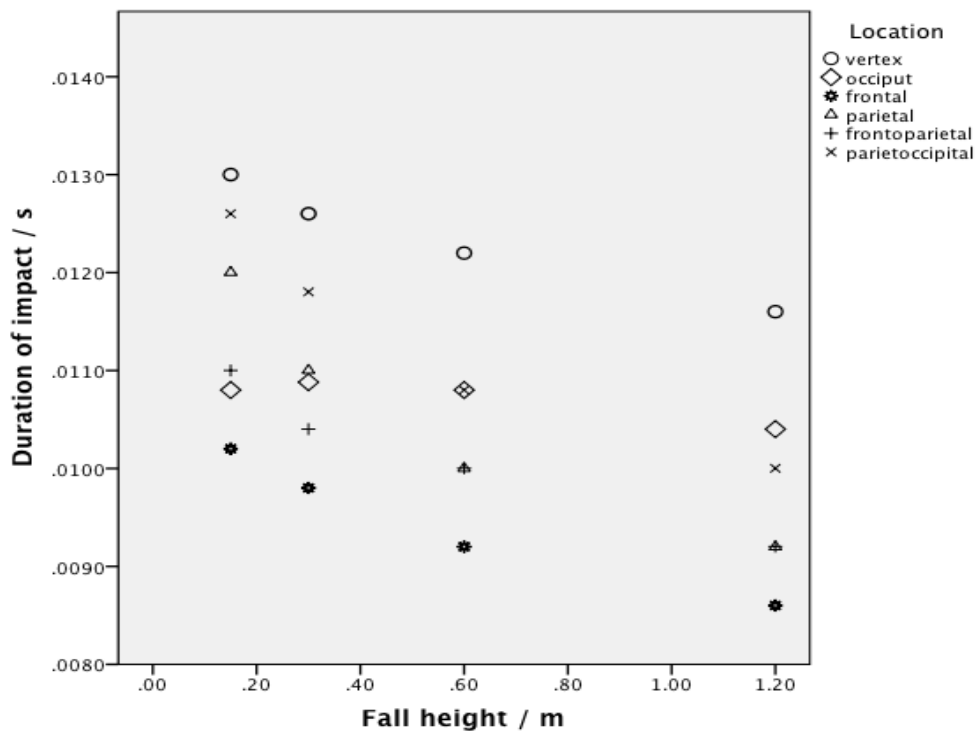


Figure 42. Variation in duration of impact between fall height and site of impact.

### 5.3.3.4 Rotational acceleration

Each site of impact demonstrated rotation about 3 axis: the sagittal, coronal and axial planes. An example of the rotational accelerations in 3 planes for an occipital impact can be seen in Figure 43. The largest rotational acceleration for an occipital

impact was in the sagittal plane, as can be seen in Figure 43. Only maximum rotations, in terms of both rotational accelerations and velocities, from all three planes, will be discussed for the remaining sites of impact. The frontal and vertex impacts had the largest rotation about the sagittal plane, for the parietal and parieto-occipital impacts it was about the axial plane and fronto-parietal impact was about the coronal plane.

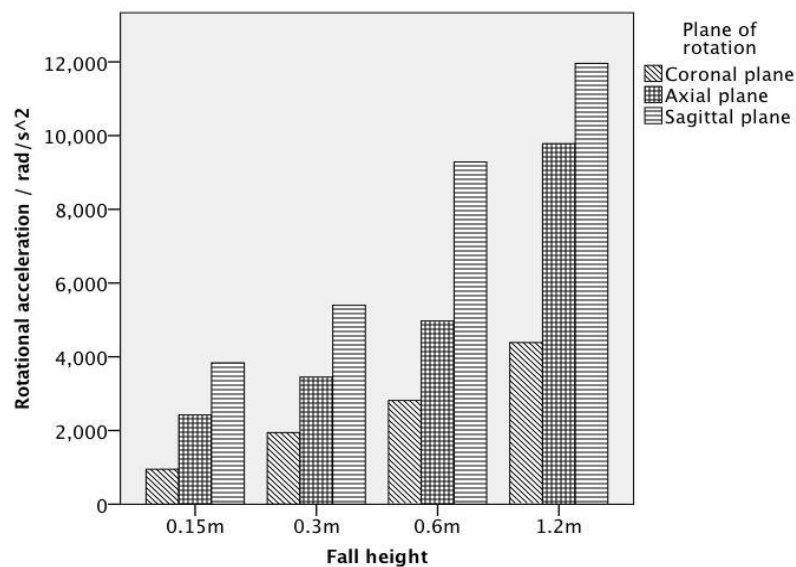


Figure 43. Peak rotational acceleration in the sagittal, coronal and axial planes for an occipital impact,

Peak rotational accelerations varied with both height and site of impact. An increase in height increased rotational accelerations for all sites of impact. The greatest peak rotational acceleration was 13,951 rad/s<sup>2</sup> for a frontal impact at a fall height of 1.2m, a reduction in fall height to 0.6m, 0.3 and 0.15m decreased rotational accelerations to 8,399 rad/s<sup>2</sup>, 5,788 rad/s<sup>2</sup> and 4,015 rad/s<sup>2</sup> respectively. The effect of fall height for other impact locations can be seen in Figure 44.

The site of impact influenced the peak rotational accelerations. Relative to a frontal impact at a fall height of 1.2m, both vertex and occipital impacts reduced peak rotational accelerations in the sagittal plane; a vertex impact reduced it to

11,952 rad/s<sup>2</sup> (decrease of 14.3%) and an occipital to 11,957 rad/s<sup>2</sup> (decrease of 14.3%). A parietal impact also reduced peak rotational accelerations to 9,389 rad/s<sup>2</sup>, however, the peak rotational acceleration was in the axial plane. The effect of site of impact on peak rotational accelerations varied with height, as can be seen in Figure 44. At a fall height of 0.6m an occipital impact increased peak rotational accelerations by 10.5% to 9284 rad/s<sup>2</sup> compared to a frontal impact. Further comparisons can be made by reference to Figure 44. A comparison of rotational accelerations and velocities with SDH and bridging vein rupture thresholds can be made with reference to Figure 44.

Chapter 5 – Finite Element Analysis of Infant Head Impacts

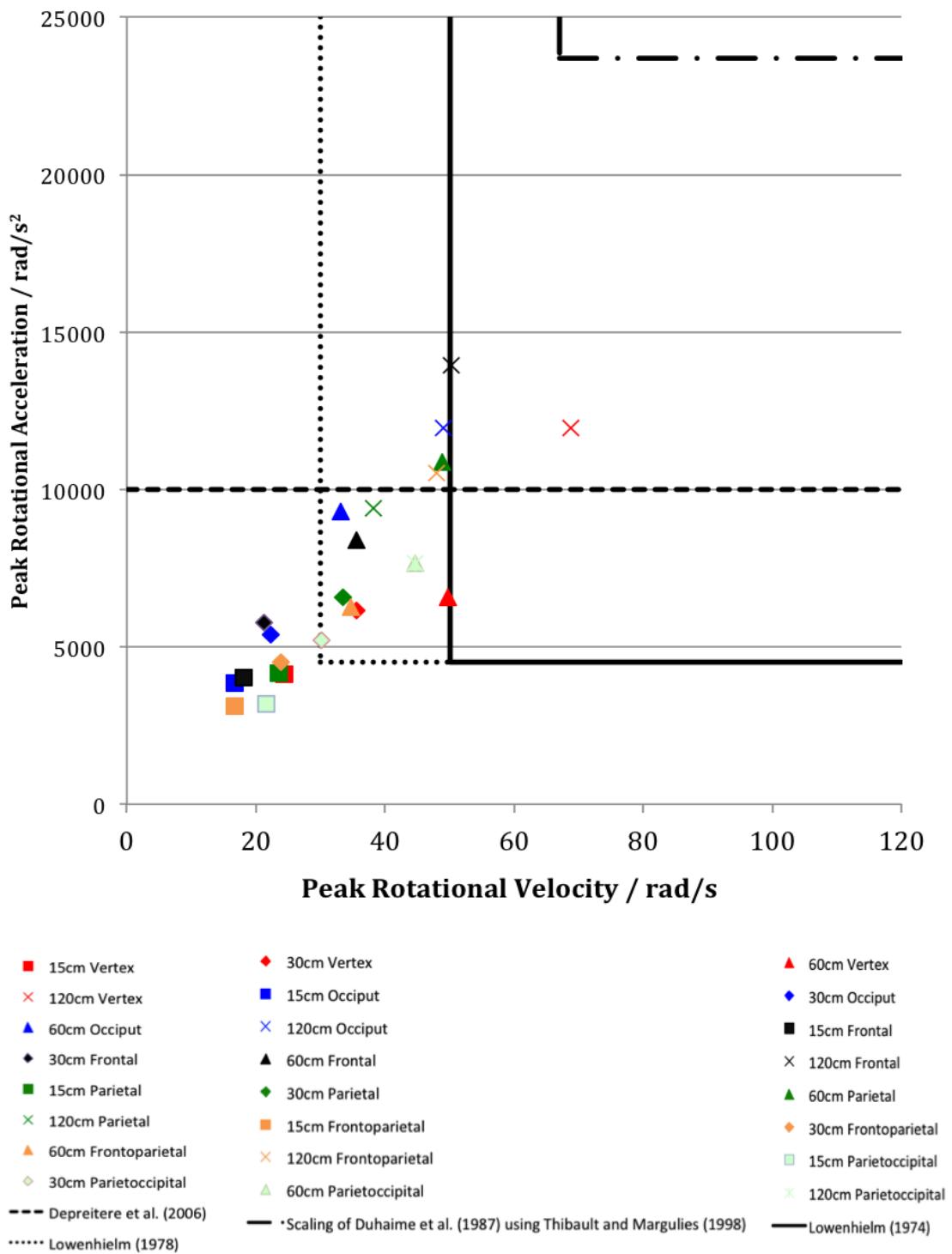


Figure 44. Peak rotational accelerations versus peak change in rotational velocities for all fall heights and sites of impact investigated.

### 5.3.3.5 Peak change in rotational velocity ( $\Delta\omega$ )

Similar to peak rotational accelerations, peak change in rotational velocity varied with both height and site of impact. An increase in height increased  $\Delta\omega$  for all sites of impact. The greatest  $\Delta\omega$  was 68.8 rad/s for a vertex impact at a fall height of 1.2m, a reduction in fall height to 0.6m, 0.3 and 0.15m decreased  $\Delta\omega$  to 49.7 rad/s, 35.5rad/s and 24.4 rad/s, respectively. The effect of fall height for other impact locations can be seen in Figure 44.

The site of impact influenced the peak rotational accelerations. Relative to a vertex impact at a fall height of 1.2m, both frontal and occipital impacts reduced peak  $\Delta\omega$  in the sagittal plane; a frontal impact reduced it to 50.2 rad/s (decrease of 27.1%) and an occipital impact to 49 rad/s (decrease of 28.7%). A parietal impact also reduced peak  $\Delta\omega$  to 38.2 rad/s, however, the peak  $\Delta\omega$  was in the axial plane. The affect of site of impact on peak  $\Delta\omega$  varied with height, as can be seen in Figure 44. At a 0.3m fall height, a frontal impact decreased peak  $\Delta\omega$  by 40.2% to 22.2 rad/s, compared to a vertex impact. Further comparisons can be made by reference to Figure 44.

### 5.3.3.6 Head deformation

In Chapter 3, using an anthropomorphic testing device the potential level of deformation that an infant head undergoes on impact was illustrated, Figure 45. The FE model was used to investigate head deformations further. Deformations were measured in the superior-inferior direction (SI), anterior-posterior (AP) and left lateral-right lateral (LR) directions. A distal to floor (DF) measurement was also taken for the fronto-parietal and parieto-occipital impacts. Each high-speed video of the impacts from Chapter 4 were analysed to acquire an estimation of the deformations in SI direction. An example of the measurements taken can be seen in Figure 45.

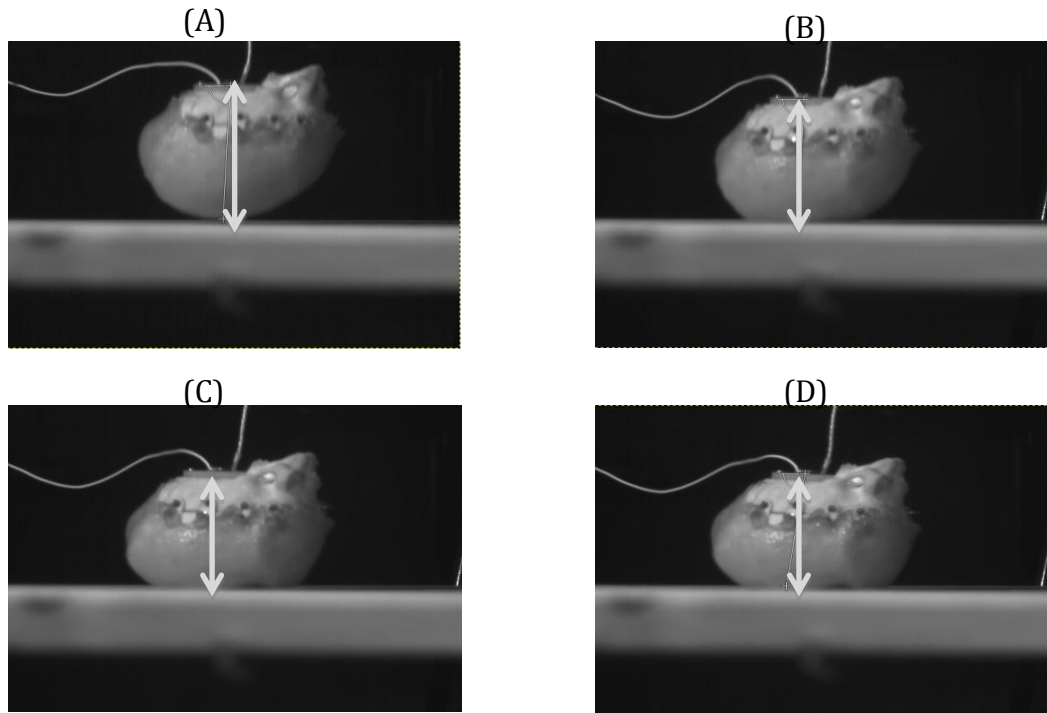


*Figure 45. Estimation of headform deformation using the high-speed video from 0.6m fall onto wood. Prior to impact to impact no head deformation (A), 10.5mm deformation at 4ms post impact (B), 15.5mm deformation at 7ms post impact (C), 14.4mm deformation 10ms post impact (D).*

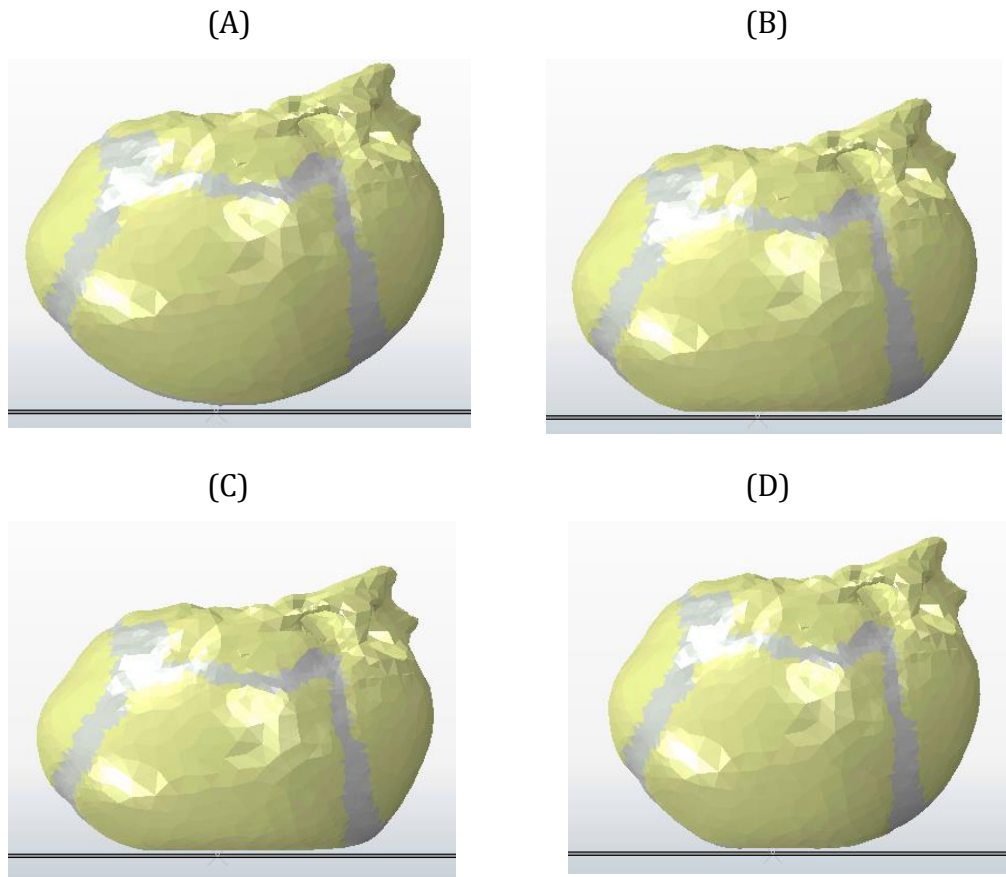


Figure 46. Vertex impact for a 0.6m fall height with the FE model. Prior to impact to impact no head deformation (A), 11.6mm deformation at 4ms post impact (B), 12.9mm deformation at 7ms post impact (C), 8.5mm deformation 10ms post impact (D).

The deformations for the vertex impacts for the FE model were compared to that of the ATD. A comparison of deformations between the two can be seen in *Figure 46*.

Post comparing the deformations from the ATD to the FE, the strain measurement in each direction was quantified. An example output of strain in the SI, AP and LR direction for a 0.6m impact onto the occipital impact can be seen in *Figure 48*. The strain in each direction for all occipital impacts can be seen in *Figure 49*. However for the comparison between impacts only the maximum strain was used, thus, in the occipital example (*Figure 48* and *Figure 49*) this would be the AP direction.



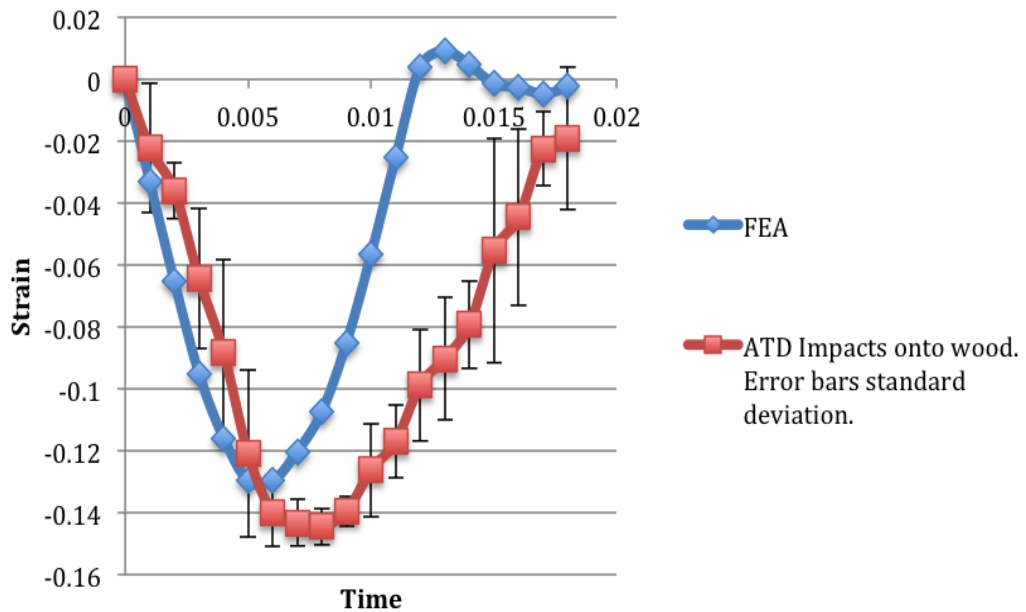


Figure 47. Comparison of deformation between the finite element model (FE) and the anthropomorphic testing device (ATD).

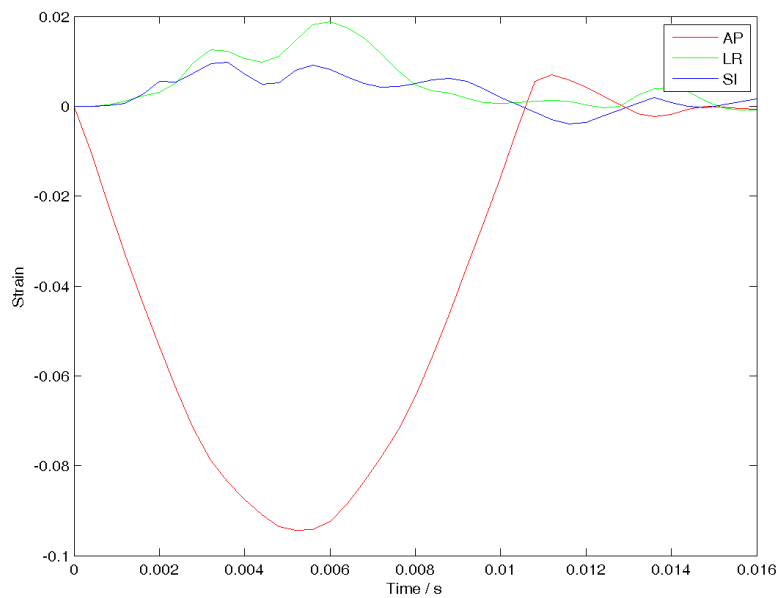


Figure 48. Example of impact response from an 0.6m occipital impact. Anterior-posterior (AP), left-right (LR), superior-inferior (SI).

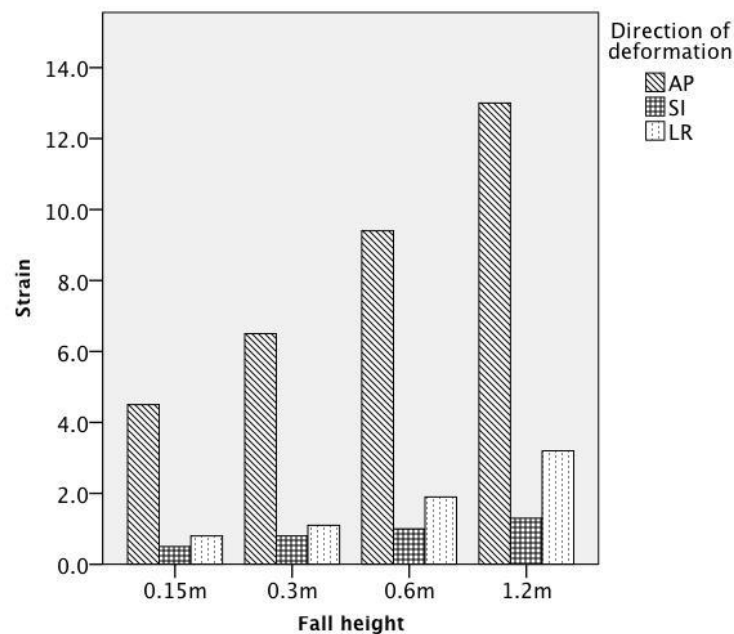


Figure 49. Strain in anterior-posterior (AP), superior-inferior (SI) and left-right (LR) directions for all occipital impacts.

Peak head strain increased with height, as can be seen in Figure 50. The greatest strain of 18.8 %, was for a vertex impact at a fall height of 1.2m. This corresponded to a deformation of 18.3mm in the SI direction. A decrease in the height to 0.6m, 0.3m and 0.15m decreased the peak head strain to 13%, 9.5% and 6.9%, respectively, for a vertex impact. The effect of height across the other sites of impact can be seen in Figure 50. The greatest variation in strain, between the sites of impact was between vertex and frontal impacts. At a 1.2m fall height peak strain for a frontal impact reduced to 10.1% compared to a vertex impact (A decrease of 46.5%). The variation in peak head strain between the sites of impact varied with height. For a 0.15m fall height, the peak strain for a frontal impact was 4.2% (a decrease of 40.2%). Further comparison can made through investigation of Figure 50.

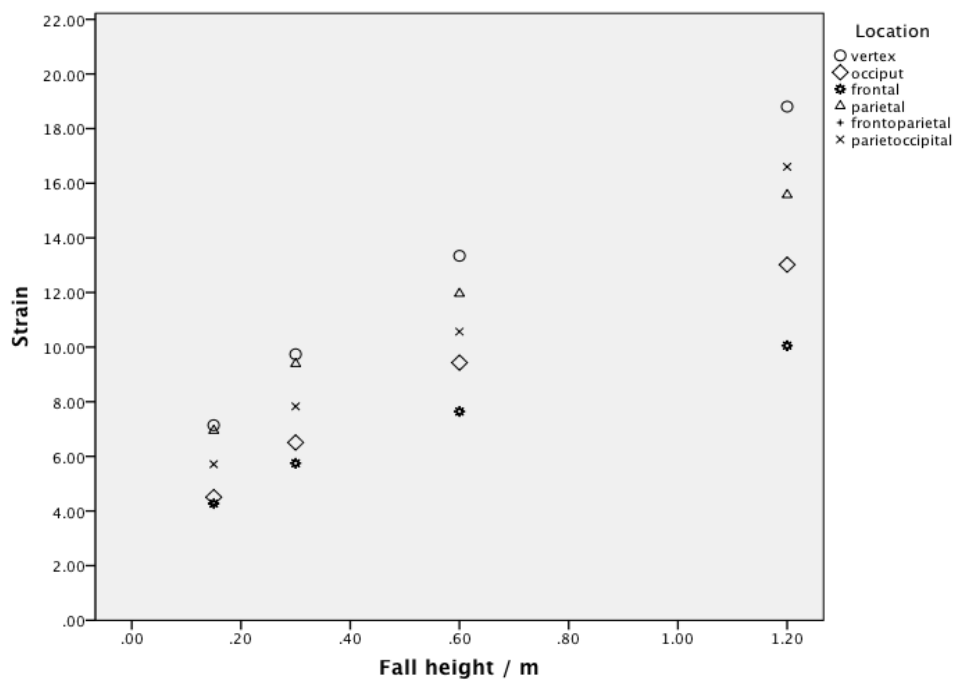


Figure 50. Peak head strain for all sites of impact across all fall heights investigated.

### 5.3.3.7 Maximum principle stress of the bone

The location of the maximum principle stress varied depending on the site of impact: for a parietal impact the location was the parietal bone, an occipital impact was in the occipital bone, a frontal impact was in the frontal bone, a vertex impact was to the parietal bones, a fronto-parietal impact was the frontal bone and the parieto-occipital was the occipital bone.

The maximum principle stresses for an occipital impact, at fall heights of 0.15m, 0.3m, 0.6m and 1.2m was 11.0MPa, 15.0MPa, 16.3MPa and 16.5MPa, respectively. Thus, increases in height from 0.3m to 0.6m and 1.2m did not increase maximum principle stress by greater than 15%. The stress values for an occipital impact at 0.15m, 0.3m, 0.6m and 1.2m equated to a fracture risk of 61.4%, 84.1%, 89.1% and 89.7% respectively, utilising a normal distribution of the ultimate stress values for the occipital bone reported by Coats and Margulies <sup>6</sup> for infants <3 months old.

The maximum principle stresses for a parietal impact at fall heights of 0.15m, 0.3m, 0.6m, and 1.2m was 9.3MPa, 11.1MPa, 15.1MPa and 23.6MPa, respectively. Thus, all increases in height increased maximum principle stress by greater than

15% for the parietal impacts. The stress values for a parietal impact at 0.15m, 0.3m, 0.6m and 1.2m equated to a fracture risk of 10.5%, 13.0%, 20% and 40.5%, respectively. These values are based on the ultimate stress values for the parietal bone reported by Coats and Margulies<sup>6</sup> for infants <3 months old.

The maximum principle stresses for a vertex impact at fall heights of 0.15m, 0.3m, 0.6m, and 1.2m was 5.8MPa, 9.0MPa, 12.4MPa and 13.6MPa, respectively. Thus, all increases in height with exception of 0.6m to 1.2m increased maximum principle stress by greater than 15% for the vertex impacts. The stress values for a parietal impact at 0.15m, 0.3m, 0.6m and 1.2m equated to a parietal fracture risk of 6.7%, 10.1%, 15.1% and 17.2%, respectively.

The maximum principle stresses for a parieto-occipital impact at fall heights of 0.15m, 0.3m, 0.6m, and 1.2m was 6.2MPa, 9.2MPa, 14MPa and 17.4MPa, respectively. These stresses were in the occipital bone and the fracture risk equated for the heights measured equated to 28.7%, 48.8%, 79.4% and 92.3%, respectively. At this impact location there were also high stresses in the parietal bone, for fall heights 0.15m, 0.3m, 0.6m and 1.2m the corresponding parietal stresses were 4MPa, 5.7MPa, 7.6MPa and 9.4MPa, respectively. The corresponding parietal bone fracture risks were 5.2%, 6.6%, 8.5% and 10.7%, respectively.

Frontal impacts at fall heights of 0.15m, 0.3m, 0.6m and 1.2m had maximum principle stresses of 4.8MPa, 6.6MPa, 8.7MPa and 12.3MPa, respectively. Due to no failure properties being reported for the infant frontal bone, fracture risk cannot be reported.

The maximum principle stress values were correlated with peak G (Figure 51) and HIC values across all sites of impact (Figure 51). It can be seen from Figure 51, that there are two distinct correlations, one for the frontal and fronto-parietal impacts and another for the remaining impact locations, for both peak G and HIC. A linear regression was conducted based on these two correlations, with the constants of

the linear regression shown in Table 29. A linear regression was also completed for the individual sites of impact, for both peak G and HIC, and the constants of the linear regression are shown in Table 29.

It has been previously been stated that the mean peak G value for a 0.6m fall height was 85g, with a range of 70g to 131g. Utilising the linear regression this equated to a maximum principle stress value of 8.6MPa (7.1MPa -13.3MPa) for the frontal and fronto-parietal impacts and a value of 15.9MPa (13.1MPa – 24.5MPa) for the remaining sites of impact. The corresponding parietal fracture risks for these stress values were 9.7% and 21.7% respectively and the corresponding occipital fracture risks were 44.6% and 87.7% respectively. The value of maximum principle stress at 85g, using the regression analysis for the individual sites of impact, can be seen in Table 29.

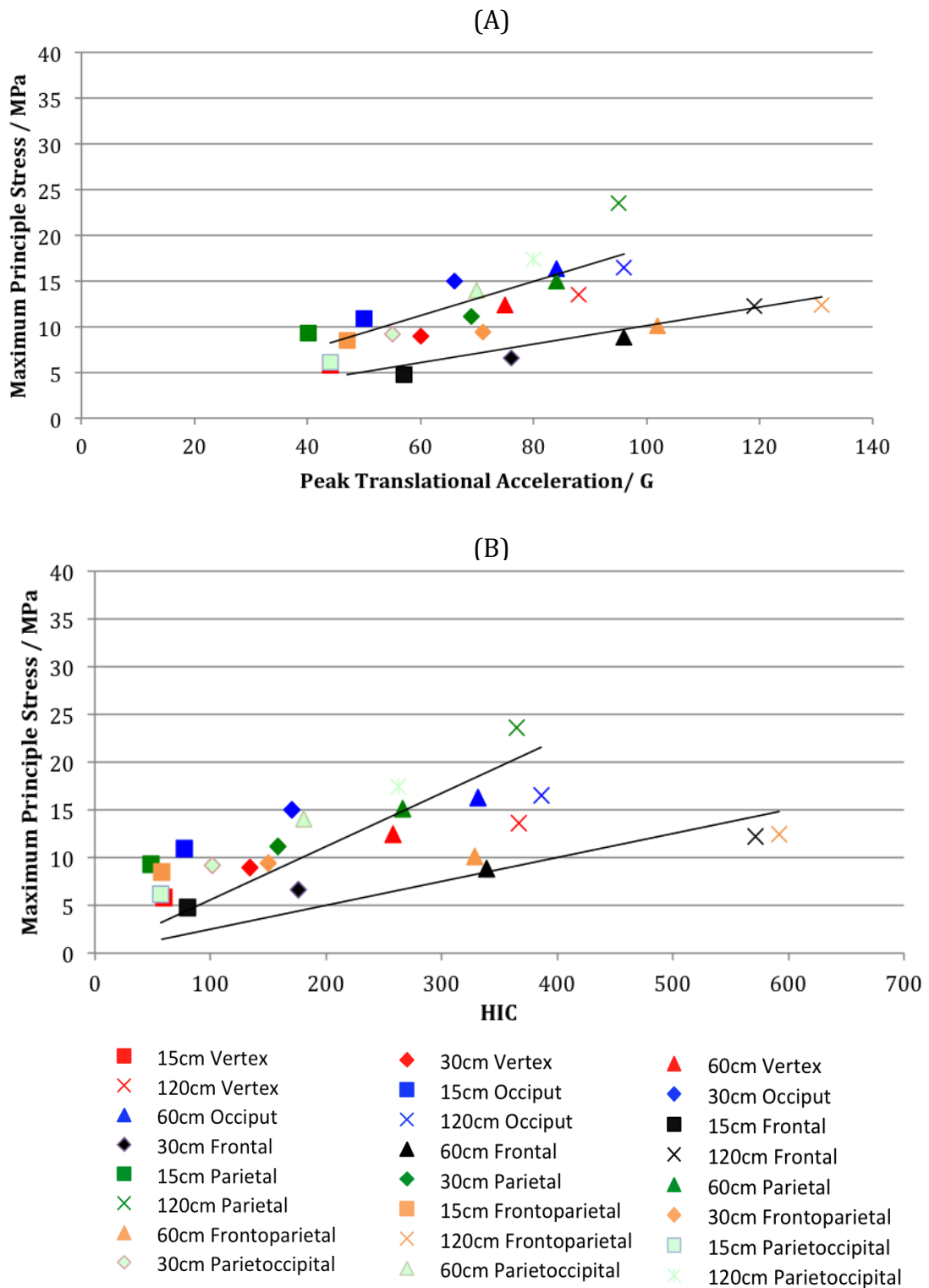


Figure 51. Correlation between maximum principle stress values and peak G (A), correlation between maximum principle stress and HIC (B).

Table 29. Output variables of linear regression of peak G and HIC with maximum principle stress.

Data used for regression analysis	Gradient	R squared	t statistic	P value	
<b>Peak G</b>					Maximum principle stress at a peak G of 85g
Vertex, occipital, parietal and parieto-occipital combined	0.19 (CI 0.17-0.2)	0.97	22.63	<0.01	15.9
Vertex	0.15 (CI 0.14-0.17)	1	27.97	<0.01	13.1
Occipital	0.19 (CI 0.15-0.23)	0.99	15.42	<0.01	16.5
Frontal	0.1 (CI 0.08-0.11)	0.99	22.43	<0.01	8.1
Parietal	0.21 (CI 0.13-0.27)	0.97	9.53	<0.01	17.2
Fronto-parietal	0.11 (CI 0.06-0.15)	0.96	8	<0.01	9.1
Parieto-occipital	0.19 (CI 0.14-0.24)	0.98	12.58	<0.01	16.5
Frontal and fronto-parietal combined	0.1 (CI 0.08-0.12)	0.97	14.55	<0.01	8.6
<b>HIC</b>					Maximum principle stress at a HIC value of 284
Vertex, occipital, parietal and parieto-occipital combined	0.06 (CI 0.05-0.07)	0.91	12.65	<0.01	15.8
Vertex	0.04 (CI 0.02-0.06)	0.94	6.84	0.01	12.4
Occipital	0.05 (CI 0.02-0.09)	0.89	4.85	0.02	14.7
Frontal	0.02 (CI 0.01-0.03)	0.94	7.1	0.01	6.8
Parietal	0.06 (CI 0.04-0.08)	0.97	10.34	<0.01	18.2

Fronto-parietal	0.03 (CI 0-0.05)	0.78	3.28	0.05	7.4
Parieto-occipital	0.07 (CI 0.05-0.09)	0.98	12.98	<0.01	20.6
Frontal and fronto-parietal combined	0.02 (CI 0.02-0.03)	0.85	6.25	<0.01	7

Similarly for HIC, at a 0.6m fall height the mean HIC value was 284 with a range of 218 to 467. Again, using the linear regression this equated to a maximum principle stress of 7.0MPa (5.4MPa -11.6MPa ) for the frontal and fronto-parietal impacts and a value of 15.8MPa (12.2MPa – 26.0MPa) for the remaining sites of impact. The corresponding parietal fracture risks for these stress values were 7.9% and 21.7%, respectively and the corresponding occipital fracture risks were 34.0 % and 87.4%, respectively. The value of maximum principle stress at a HIC value of 284, using the regression analysis for the individual sites of impact can be seen in Table 29

#### Potential fracture patterns

The stresses in the skull bones that exceeded the ultimate stress ( $\sigma_{UTS}$ ) values reported by Coats and Margulies <sup>6</sup>, were evaluated in order to assess potential skull fracture patterns. All scenarios of fall heights of 1.2m were investigated. In conjunction, a single 0.82m fall onto the parieto-occipital area was assessed so that comparisons could be made with infant skull fracture patterns reported by Weber <sup>14, 15</sup>.

The 0.82m parieto-occipital impact indicated high stress zones travelling from the left lambdoid suture, across the parietal bone, towards to squamous suture and also across the occipital bone (Figure 52).



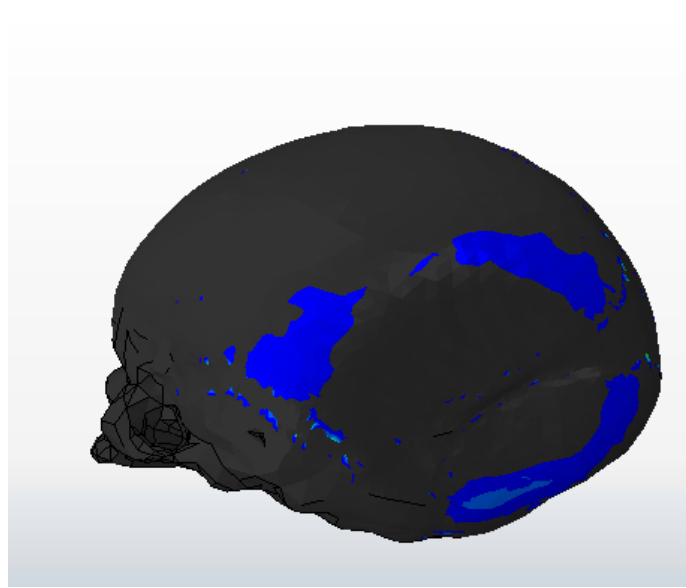


*Figure 52. Stress zones (blue) in excess ultimate stress for 0.82cm parieto-occipital impact. View from left parieto-occipital area, looking from posterior left to anterior right.*

The stress zones in excess of the  $\sigma_{UTS}$  values for a vertex impact are shown in *Figure 53*, where a symmetrical bi-parietal pattern can be seen. The stress zones appear to travel from the posterior aspect of the sagittal suture toward the middle of the coronal suture. The high stress zones for a parietal impact are shown in *Figure 54*. It can be seen that the high stress zones appear to travel from the left lambdoid suture, across the centre of parietal bone towards the coronal suture.

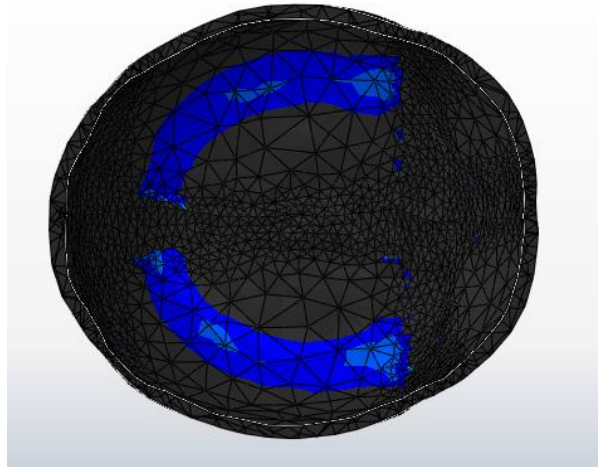


*Figure 53. A 1.2m fall onto vertex illustrating stress zones in excess of bone ultimate stress values. Intracranial view of skull in an inferior superior direction*

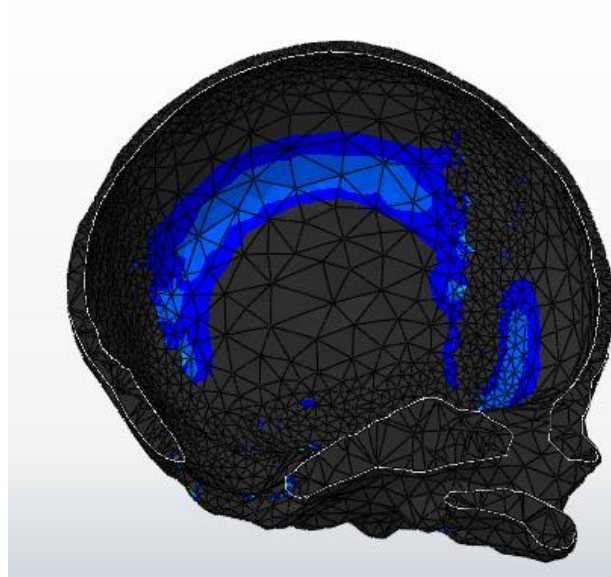


*Figure 54. A 1.2m fall onto parietal area illustrating stress zones in excess of bone ultimate stress values. Intracranial view from right to left.*

### 5.3.3.8 Bridging Veins

On impact, each connector used to model the bridging veins had a different response, an example of the stretch ratio versus time of impact for all veins on the left side for a 60cm occipital impact can be seen in Figure 55.

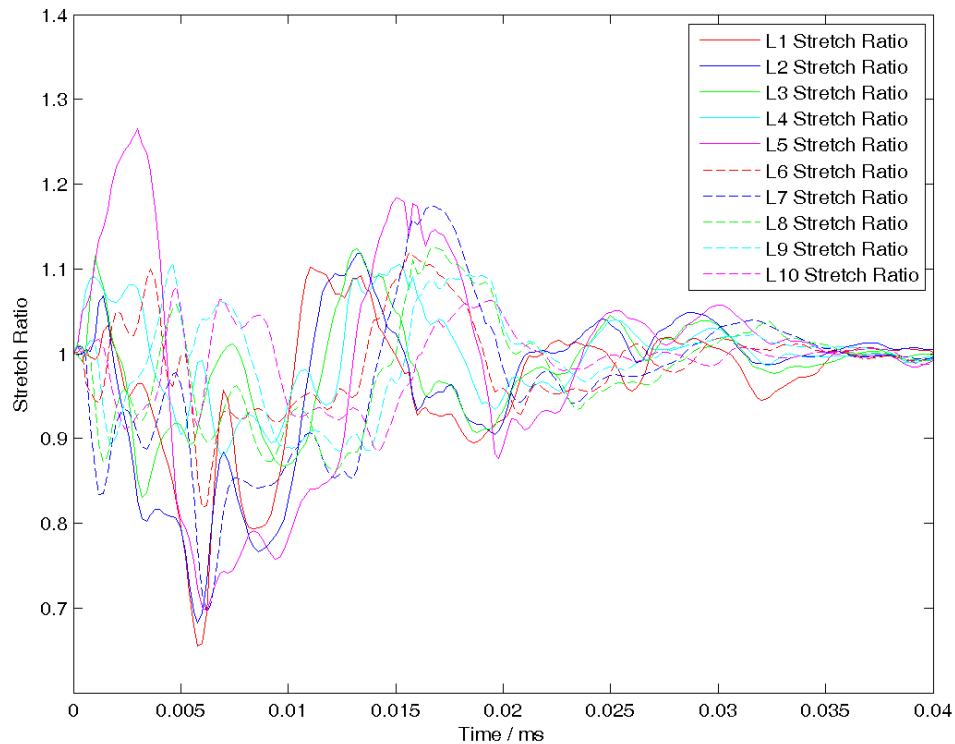


Figure 55. Stretch ratio versus time for the left sides connectors for a 0.6m vertex impact.

A two factorial ANOVA indicated that both height and site of impact significantly influenced peak stretch ratio of the connectors ( $P < 0.001$ ). The effect of height varied with site of impact. Most increases in height significantly increased the peak stretch ratio ( $P < 0.05$ ). However, certain increases in height for certain impacts did not, for example an increase in height from 0.6m to 1.2m for a vertex impact did not significantly increase the peak stretch ratio ( $P = 0.265$ ). A vertex impact significantly increased the peak stretch ratio of the bridging veins relative to all other sites of impact for the 0.3m, 0.6m, and 1.2m fall heights ( $P < 0.05$ ). An occipital impact did not significantly increase the peak stretch ratio of the bridging veins relative to a frontal impact across all heights investigated ( $P > 0.23$ ). Parietal impacts reduced peak stretch ratio of the bridging veins relative to an occipital

impact, but only significantly for the 0.15m and 1.2m fall heights ( $P \leq 0.15$ ). A parietal impact also reduced the peak stretch ratio of the bridging veins, relative to an occipital impact, but only significantly for the 1.2m fall heights ( $P = 0.007$ ).

The peak stretch ratio across all connectors for each height and site of impact were also assessed and can be seen in Figure 56. The vertex impact had greatest  $\lambda_{\text{peak}}$  across all sites of impacts and the highest value was 1.31 at 1.2m fall height. All reductions in height reduced peak stretch ratio for a vertex impact, but not by greater than 3%. For the remaining sites of impact, a reduction in height reduced  $\lambda_{\text{peak}}$ , but again, not by greater than 15%. Excluding the vertex impacts, only small difference (<6%) existed in  $\lambda_{\text{peak}}$  between sites of impact.

The location of  $\lambda_{\text{peak}}$  varied with site of impact and height. Each connector was labelled 1 to 10, with 1 being the most posterior to 10 being the most anterior. The location of  $\lambda_{\text{peak}}$  for a vertex impact was connector number 5, thus, the middle aspect of the FE model. This was also the location of  $\lambda_{\text{peak}}$  for 0.15m, 0.3m and 0.6m occipital impacts. However, for a 1.2m impact onto the occipital region, the location varied to connector number 3. The  $\lambda_{\text{peak}}$  for the frontal impacts, at fall heights of 0.15m, 0.3m and 0.6m was located in posterior aspect in connector number 1. However, the location of  $\lambda_{\text{peak}}$  moved in an anterior direction to connector number 7, for the 1.2m impact. The location of  $\lambda_{\text{peak}}$  for parietal impact, was in the anterior aspect of the FE model in either connector 9 or 10 across the four fall heights investigated. The location of  $\lambda_{\text{peak}}$  for the fronto-parietal impact had a similar pattern to the frontal impacts, where its location was in posterior aspect for the 0.15m, 0.3m and 0.6m fall heights (connector 1) and was located in the anterior aspect for the 1.2m fall (connector 10). Finally, for the parieto-occipital impact, the location of  $\lambda_{\text{peak}}$  varied with height, however, generally it was located in the anterior aspect of model (connectors 7-9) for the 0.15m, 0.6m and 1.2m impacts.

The effect of site impact varied with height, when comparisons were made relative to a vertex impact. All other sites of impact reduced peak stretch ratio by greater than 15% for a 0.15m fall height, but not for the 1.2m fall height relative to a vertex impact. Excluding the vertex impacts, the peak stretch ratio increased with increasing height for all other sites of impact, but again not by greater than 15%. Again excluding the vertex impacts, differences existed in peak stretch ratio between sites of impact but not by greater than 15%.

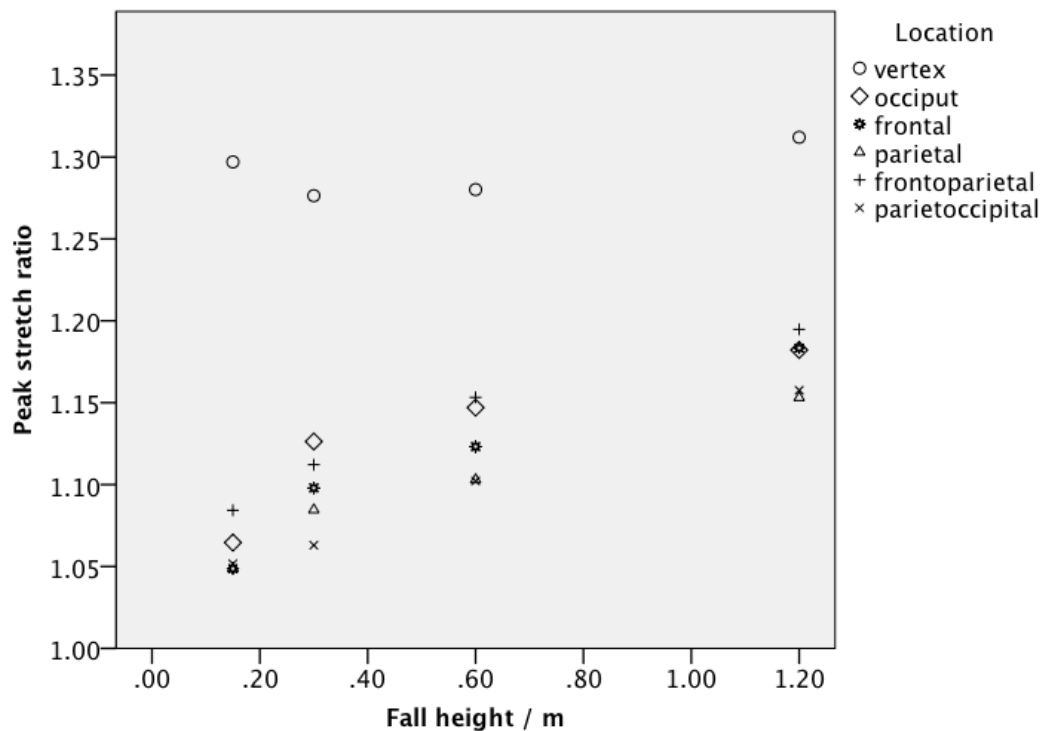


Figure 56. Peak stretch ratio for each fall height and site of impact.

The relationship between kinematic variable and peak stretch ratio was correlated with peak rotational acceleration and peak change in rotational velocity. It can be seen from *Figure 57* that once vertex impacts were excluded, a correlation exists between peak change in rotational acceleration and the peak stretch ratio of the bridging veins. A linear regression was completed between both peak rotational acceleration, peak change in rotational velocity and peak stretch ratio, the outputs can be seen in Table 30. Using linear regression, 10,000 rad/s<sup>2</sup> correlated with a peak stretch ratio of 1.15 and change in rotational velocity of 50 rad/s correlated with peak stretch ratio of 1.17.

*Table 30. Linear regression outputs*

<b>Data used for regression analysis</b>	<b>Gradient</b>	<b>R squared</b>	<b>t statistic</b>	<b>P value</b>
Rotational Acceleration	0.0001	0.79	8.41	<0.01
Rotational Velocity	0.0306	0.91	13.64	<0.01

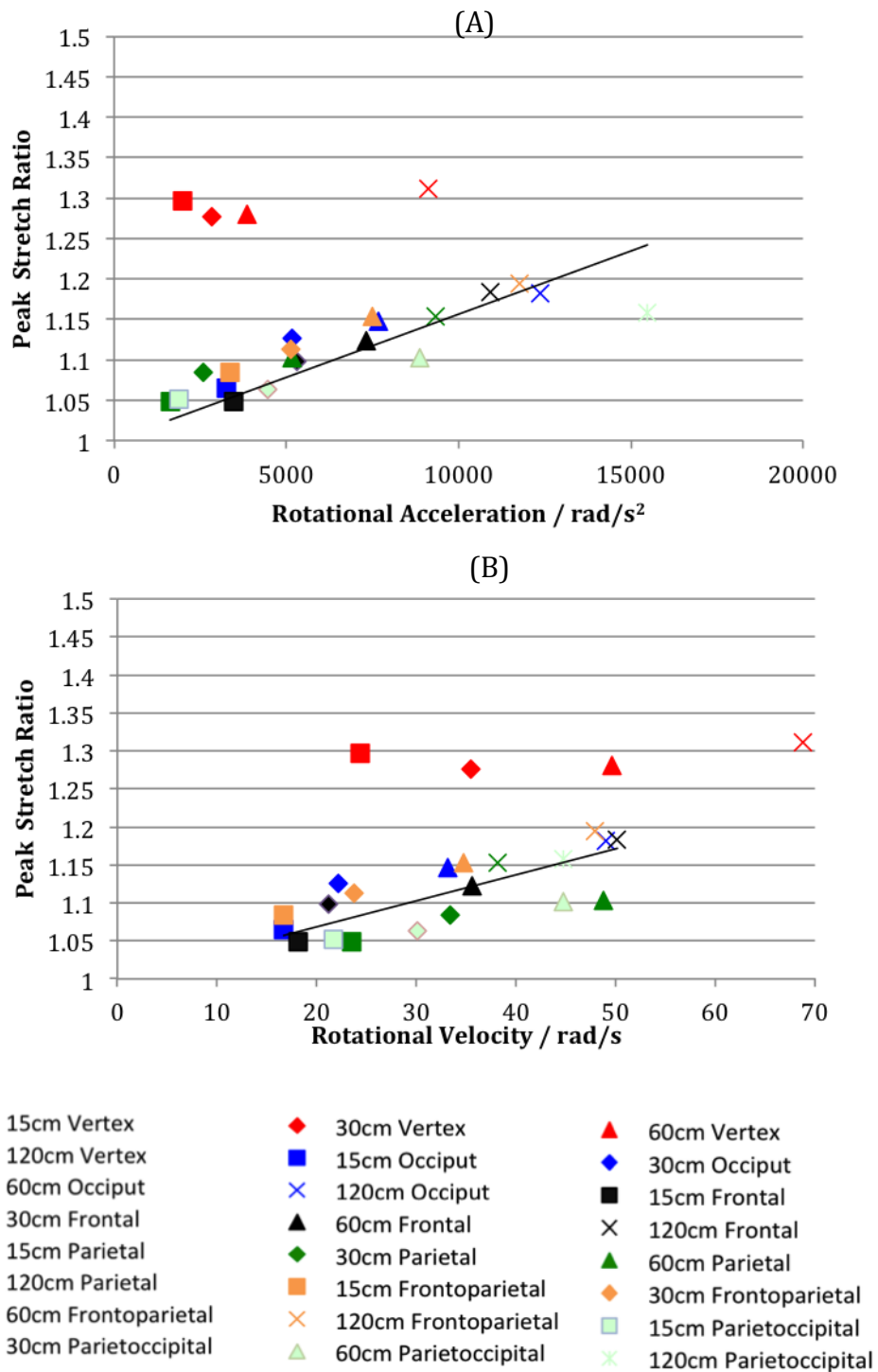


Figure 57. Correlation between peak rotational acceleration and peak stretch ratio (A), correlation between peak rotational change in rotational velocity and peak stretch ratio (B).

## 5.4 Discussion

A finite element model of the infant head was developed and validated against human cadaveric data. A parametric test was conducted, using an FE model, to assess the effect that material properties have on the dynamic response of the head across a range of scenarios. The skull stiffness was shown to have the greatest effect on the output variables, including peak G, HIC and maximum bone principle stress. The validated FE model was subsequently used to investigate key clinical features, namely height and site of impact, where both were both found to influence one or more of the output variables by greater than 15%.

### 5.4.1 Validation

All biomechanical models, whether computational or physical, need to be assessed against human data such that their biofidelity can be quantified. A limited amount of infant cadaver data exists which FE models can be validated against. This combined with the developmental nature of an infant head, makes it difficult to develop a validated infant head FE model that is also representative of a particular age group. Due to this, few previous authors have developed finite element models that have been validated against cadaver impacts<sup>19, 21, 29</sup>. Consequently the design of the FE model was tailored, such that its geometry was similar to the cadaver heads used by Prange *et al*<sup>16</sup>. Four different material properties of the skull were assessed in the validation process, three using an inhomogenous model and one using a homogenous model. The FE model utilising the highest reported values for skull stiffness by Coats and Margulies<sup>6</sup> for infants < 3months, resulted in a stiffened headform. A decrease in the stiffness to the mean reported skull stiffness values, also resulted in a stiffened headform, particularly for the parietal and occipital impacts. A previous FE model using an inhomogenous model based on mean properties reported by Coats and Margulies<sup>6</sup>, also resulted in a stiffened headform relative to the cadaver impacts.

In terms of the assessed inhomogenous skull properties, the model, based on the lowest skull stiffness values reported by Coats and Margulies<sup>6</sup>, had the closest similarities to Prange *et al*<sup>16</sup>, with only 7/24 output variables having significantly



different results. However, the FE model, based on optimised properties and using homogenous skull properties had the most similar dynamic response to the cadavers head, with only 3/24 output variables being significantly different. A further assessment of the optimised model in compression, again showed no significant difference in the FE model stiffness at compression rates of 1mm/s, 10mm/s and 50mm/s. The FE model, based on the optimised properties was stiffer for the 0.05mm/s compression rate, however, this rate was not comparable to a low height fall, so it was deemed acceptable. Thus, it was concluded that the model had a dynamic response similar to the cadaver heads and was therefore, classed as validated. Whilst significant differences exist for the model, based on the optimised properties, the evaluation criteria was strict, relative to that used by previous authors <sup>19,29</sup>, investigating stiffness, peak G, HIC and duration of impact. In the validated model developed by Roth *et al* <sup>19</sup>, the authors investigated the level of correlation in the acceleration versus time graphs, but only one of four had a 100% correlation. Li *et al* <sup>29</sup> developed a validated 6 month FE model and investigated stiffness, peak G and time. Despite the authors acknowledging the headform was stiff, relative to cadaver impacts, it was still classed as validated as the differences were small. Thus the FE models in this study have been subject to more stringent criteria, in terms of their bio fidelity. However, the differences could still be attributed to reasons used by other authors <sup>29</sup>, namely that differences in age exist between the model and the cadavers and also that site of impact could have been slightly different between the two studies.

### 5.4.2 Parametric Analysis

A parametric analysis was used to measure the effect that material properties and interactions have on the dynamic response of the head on impact. Uniquely, the parametric test was conducted across a range of scenarios, such that the effect of differing impact locations could be assessed. Whilst the optimised model was validated against infant cadaver data, limited studies have conducted tests on infant bone and soft tissue and those that have, have found variation in the output. Consequently their values were investigated such that their effect could be quantified.

### 5.4.2.1 Skull Stiffness

Skull stiffness had the greatest effect on the output variables, as has been concluded by previous authors<sup>19, 21, 29</sup>. The elastic modulus in the parametric test was varied between lowest and highest reported values from the literature for an infant head<sup>3, 6</sup>. Using an inhomogenous material model, based on the lowest reported values for the given age, resulted in the Young's modulus of the parietal bone only being 7% greater, relative to the value used in the optimised model. However, this still resulted in a 23% increase in HIC, illustrating how a small variation in stiffness can still have a considerable affect on the dynamic response of the head. Increasing the stiffness further, to the highest reported values, resulted in a Young's modulus of the parietal bone that was 377% greater than that used in the optimised model. This resulted in HIC increasing by 107%, relative to the optimised model. Considerable variations were seen when comparing the output from the FE model, using the lowest reported values for skull stiffness to that using highest reported values. Peak G varied from 69g to 113g for a parietal impact and from 60g to 87g for a vertex impact. However, certain outputs of the FE model, using lowest reported stiffness properties (Parametric model S1) and all of the outputs using the highest reported stiffness properties (Parametric model S3) were significantly different from infant cadaver tests conducted by Prange *et al*<sup>16</sup> ( $P < 0.05$ ). Despite this it does identify a potential range of values that could exist within an infant head response based purely on material properties. However, due to limited validation data, the accuracy of the outputs is unclear. Previous authors have discussed how anatomical variations within a given age range can affect the impact response<sup>13, 21</sup>. This, combined with the range of skull stiffness properties highlights how natural human variation needs to be considered when evaluating the potential impact response.

Uniquely, a comparison was made between an orthotropic and isotropic material model for the skull. Translation variables including peak G and HIC were not affected by greater than 15% when comparing the two. The only output variable that was affected was the maximum principle stress in the bone. The orthotropic

model increased the maximum principle stress, however, this indicated a greater risk of fracture. This disagreed with cadaver findings where no fractures were seen across all tests at 30cm.

#### 5.4.2.2 Scalp Stiffness

The scalp stiffness was increased by 95%, relative to the optimised value in order to compare the optimised value with commonly used values. Scalp stiffness did not have a greater than 15% influence on most of the output variables across the range of scenarios tested, with the exception of HIC for a vertex impact. Previous authors using a FE model of an infant head to investigate the scalp material properties have found variation in their results. Coats *et al*<sup>13</sup> compared two FE models, one with the scalp and one without and found that only the maximum contact area was affected by greater than 15%. Three different scalp stiffness properties were investigated in the parametric test conducted by Li *et al*<sup>21</sup> using a FE head representing infants <3 months, 8.5MPa, 21.23MPa and 34MPa. The authors concluded that scalp stiffness did not significantly affect peak G, maximum principle stress or strain on the bone, but did significantly affect maximum principle stress and strain on the suture ( $P < 0.05$ )<sup>21</sup>. However in the same study, once the skull stiffness was controlled in the parametric analysis, scalp stiffness significantly effect peak head accelerations ( $P = 0.002$ )<sup>21</sup>. The same authors completed a parameter test using a 6 month FE head model, where the elastic modulus varied between 8.35MPa and 33.4MPa. The scalp stiffness was shown to significantly influence peak G and von mises stress on the skull<sup>29</sup>. Whilst research of FE head models aimed at infants <3months indicates that scalp stiffness does not affect the impact response, including the majority of variables in this study. Given research aimed at older infants has shown its importance, consideration is needed prior to selecting appropriate stiffness value.

#### 5.4.2.3 Membrane Stiffness

The effect of membranes on impact response of infant head FE model has been investigated by few authors<sup>21,29</sup>, with some not including the soft tissue structures in their model<sup>13</sup>. In the 3 month FE model developed by Li *et al*<sup>21</sup>, the membranes stiffness was varied in their parametric test, but it did not significantly affect any of the parameters measured by the authors. The same was true for the 6 month head model developed by the authors<sup>29</sup>. Similar results were seen in this study, where an increase in membrane stiffness by 48% did not influence any of variables measured by greater than 15%.

#### 5.4.2.4 Bulk Modulus of the Brain

Coats *et al*<sup>13</sup> concluded that bulk modulus was an important factor on maximum principle stress on the skull and suggest a value in the same order of magnitude of 2.79MPa or greater should be used. Roth *et al*<sup>19</sup> investigated bulk modulus in a parametric test and concluded an order of magnitude decrease in the bulk modulus from 2110MPa to 211MPa did not affect peak G, deflection or von mises stress by greater than 15%. However, an order of magnitude increase to 21,100MPa did decrease the von mises stress of the skull by greater than 15%. In this study, a decrease in the bulk modulus from 2110MPa to 2.1MPa did not affect the translation variables, peak G and HIC. However, for the occipital impact, the maximum principle stress did increase by greater than 15%, which implied a greater risk of fracture compared to what was from cadaver impact tests<sup>16</sup> and the clinical findings from this study. Consequently a bulk modulus of 2.1MPa was used for the remainder of the study.

#### 5.4.2.5 Brain Stiffness

Previous parametric tests conducted using FE infant head models have found variation in the results with regards to the effect of brain stiffness properties<sup>13,19,21,29</sup>. In previous studies, that have modelled the brain using a viscoelastic law<sup>19,21,29</sup>, it has been concluded that the brain stiffness properties, long term shear

modulus and time decay, do not affect impact response variables. Only Roth *et al*<sup>19</sup> concluded that the short term shear modulus ( $G(0)$ ) had an affect on the impact response, where an order of magnitude increase in the  $G(0)$  increased peak  $G$  and decreased skull von mises stress by greater than 15%. However, an increase in  $G(0)$  in the parametric tests conducted by Li *et al*<sup>21</sup> and Li *et al*<sup>29</sup> did not significantly influence the impact response variables measured by the authors. Coats *et al*<sup>13</sup> however, modelled the brain as using a hyperelastic law, also found that an decrease the brain stiffness to an adults value (257Pa) did not affect peak force, peak principle stress and contact area by greater than 15%. However when the brain shear stiffness was increase by a factor of 4, from 559Pa to 2.9KPa, max principle stress peak force and contacts area did increase by greater than 15%<sup>13</sup>. Whilst parametric tests, conducted by previous authors, indicate the brain properties have a limited influence on the impact response variables associated with skull fracture, an increasing amount of research suggests moelling the brain using a hyperelastic law<sup>13, 32, 34</sup>. Consequently, the commonly used viscoelastic law was compared to a hyperelastic law, and a greater than 15% difference in the impact response variables measured by this study was not seen. Therefore, suggesting a viscoelastic law is an adequate representation for a low height fall investigation, using finite element analysis. However, it needs to be noted that whilst variables associated with brain injury were investigated, namely rotational acceleration, rotational velocity and HIC, variables specific to the brain were not measured and thus, could be affected when comparing a viscoelastic to a hyperelastic law.

#### **5.4.2.6 Bridging Veins**

Failure of the parasagittal bridging veins form an integral part of one of the main hypothesised mechanisms of a subdural haemorrhage<sup>48</sup>. However, few studies have used finite element analysis to investigate the potential strains on the bridging veins in the infant head, due to a fall, partly due to no data being available to validate the head. The veins were modelled as non- linear connectors and were manually inserted into the model, as has been used by previous authors<sup>35</sup>.

However, due a number of unknown parameters and a lack of data with which to validate, it is difficult to know the correct method for modelling strains on the veins. Despite these limitations, a parametric test was conducted to investigate what potentially affects strains on the veins. None of the previously discussed material property variations affected the peak stretch ratio on the bridging vein by greater than 15%. Two different methods were used to model the brain skull interface, one using a slip condition and another using a tie constraint. Surprisingly again this did not affect  $\lambda_{\text{peak}}$  by greater than 15%. However, Kleiven and Hardy <sup>37</sup>, using an adult FE head model investigated brain skull motion and concluded that brain skull relative motion was not sensitive to the brain skull contact definition for low severity impacts. In their analysis a 3m/s impact was used for investigation of relative skull brain motion. Whilst few authors investigated head trauma in infants using FE analysis have included bridging veins, unlike adult FE head model that have included the bridging veins <sup>45, 49</sup>. Kleiven <sup>45</sup> has investigated the effect of impact direction on the prediction of a SDH. In the FE model 11 pairs of parasagittal vein were inserted into their model. The length and direction of each vein varied along the length of the superior sagittal sinus. However, in general terms the vein in the frontal aspect of the head was orientated in a posterior direction and those in the posterior aspect of the head were orientated in a frontal direction. The authors concluded that the greatest strain occurred in the shortest veins, which were orientated in the plane of motion<sup>45</sup>. In this study, when the veins were changed from an anterior direction to a posterior direction, the  $\lambda_{\text{peak}}$  reduced for the occipital impact by 5.8% and increased for the frontal impact by 0.02%. Given that an anterior facing vein, for an occipital impact, would be in the plane of motion and posterior facing vein would be in the plane of motion for a frontal impact, there are similarities with Kleiven <sup>45</sup>. Also, when the length of the vein was increased in this study,  $\lambda_{\text{peak}}$  reduced for the occipital, frontal and parietal impacts, but increased for the vertex. However, neither length or direction of vein in this study affected  $\lambda_{\text{peak}}$  by greater than 15%. These differences are potentially attributed to differences in impact scenarios, where the Kleiven <sup>45</sup> investigations were a 5m/s impact onto a padded surface. They may

also be attributed to differences in the head stiffness between an infant and adult, where their model was of an adult head; thus, they did not have sutures and the bone stiffness was two orders of magnitude greater than that used in the study<sup>45</sup>.

### 5.4.3 Assessment of key clinical features

#### 5.4.3.1 Height

Fall height was shown to have an effect on the output variables, including the kinematic (translation and rotational), deformation and material failure properties measured by the FE model. In Chapter 3, only sub injurious heights were investigated, thus the FE model allowed further investigation of potentially injurious heights. However, the translational parameters, peak G and HIC, had a logarithmic, as opposed to linear relationship, with fall height. Previous authors have documented a similar relationship, with a decreasing slope with fall height was observed with respect to peak G<sup>29</sup>. However, the same relationship was not documented for HIC by the same authors<sup>29</sup>. The differences might be attributed to the site of impact as the relationship between height and HIC varied with site of impact in this study. This FE analysis further highlights the need for an accurate fall height to be recorded in a clinical setting and the relation with injury will be discussed in the threshold section of this chapter (Section 5.4.5).

#### 5.4.3.2 Site of impact

Analysis of the clinical data (shown in Chapter 3) showed that site of impact was significantly different between children with a minor head injury and those with a skull fracture and / or ICI. Few previous authors have assessed the affect that site of impact has on the dynamic response of an infant head. This might partly be attributed to the findings reported by Prange *et al*<sup>16</sup> in the cadaver head impact tests. In their experiments, three different cadavers heads were impacted onto five different locations at two different heights. Peak G, HIC and duration of impact were not significantly different between sites of impact in their results. Whilst across the series of heads tested, site of impact was not significant, evaluating each head on an individual basis suggests differently. For example comparing a left

parietal to a vertex impact for the 11 day specimen, peak G increased by 62% from 46.1g to 74.6g and comparing forehead impact to a vertex impact, HIC increased by 104% from 47 to 96. Thus it is clear, even from the cadaver tests, that site of impact can have a considerable effect on translational variables.

In this research, site of impact affected kinematic (translation and rotational) variables, deformation and material failure properties. The stiffest regions of the head were the frontal areas, which resulted in the greatest values for peak G and HIC and lowest levels of deformation and duration of impact. The frontal bones are known to be thicker relative to the parietal and occipital bone<sup>50</sup>, which explains the increased stiffness. However, whilst having increased peak G and HIC, it does not necessarily correlate to an increased injury risk. The increased thickness makes the bone less prone to fracture, as was seen from the lower maximum principle stress values for the frontal bone in this study. The least stiff regions, were impacts focal to the sutures, thus the vertex and parieto-occipital areas. This resulted in a reduced peak G and HIC and greater deformation. The stiffness of sutures is an order of magnitude lower relative to bone, which explains the increased deformation. Impacts focal to sutures also resulted in high stress on both adjacent bones, however, the implication of this will be discussed further in the threshold section (Section 5.4.5).

In the validated model a homogenous elastic modulus was used for the skull, thus the Young's modulus was the same for each of the skull bones. However, frontal bones potentially have a greater Young's modulus<sup>3</sup>, as documented in the parametric analysis. Thus, the differences between site of impact could potentially be greater, as was seen in the parametric analysis. For example, the frontal impact increased peak G by 15.2% from 66g to 76g relative to the occiput for the validated model, however, using an inhomogenous model (parametric model S1), peak G increased by 44.3% from 61g to 88g. Whilst authors have investigated age relevant material properties of occipital and parietal bone<sup>6</sup>, few studies have investigated the frontal bones<sup>3</sup>. Thus, further research is required on the



properties of the frontal bone, in order to further ascertain potential differences between site of impact. However, the findings further illustrate the importance of considering site of impact when assessing the likelihood of a given head injury.

In terms of rotational kinematic variables, site of impact also affected the plane of maximum rotational acceleration and change in rotational velocity. Rotations in the sagittal plane were greatest for frontal, vertex and occipital impacts, but a parietal impact had the greatest rotations in the axial plane. Previous authors have discussed how rotations, in different planes, potentially leads to different forms of head injury risk<sup>23, 51</sup>. Coats and Margulies<sup>23</sup> found that the axial rotations were higher from occipital impacts and suggested that future animal studies should focus on this plane of motion as it causes the highest rotation from occipital impact. Sagittal rotations are thought to cause rupture of the parasagittal bridging veins in humans<sup>45, 48</sup> and adult primate studies have shown a greater severity of diffuse axonal injury from coronal rotations<sup>51</sup>. Given that rotation in different planes varied with site of impact, the potential for different types of traumatic brain injury could vary with site of impact. However, injury specific to the brain was not investigated using the FE model, as it was not seen in the clinical setting, thus, it is difficult to quantify this hypothesis. Also, the greatest sagittal rotational was again for the stiffer frontal impact. However, the increased value for rotational acceleration and velocity again should not necessarily relate to an increase in injury risk, relative to an occipital impact. It has been discussed by previous authors that other factors, such as bridging vein orientation can potentially affect the likelihood of failure<sup>35, 36</sup>, however, again this has been discussed in the thresholds section of the discussion (Section 5.4.5).

Site of impact also affected the potential level of fracture risk and stress distribution in each bone. The results of FE modelling suggested the greatest risk of fracture was for the occipital bone for the parieto-occipital and occipital impacts.

Ultimate stress values for the occipital bone of infants are lower, relative to the parietal bone<sup>6</sup>, which might explain the increased risk. However, as previously stated, a homogenous model for the skull was used in this study, with a Young's modulus of 170.79MPa. Utilising a normal distribution of the reported Young's modulus for the parietal and occipital bones for infants <3months, this value approximated an 8th percentile stiffness for the parietal bone and 27th percentile stiffness of occipital bone. This means the occipital bone has a greater relative stiffness. Investigation of the parametric model S1 in the parametric analysis, where an inhomogenous model based on lower reported values was used, still indicated a greater relative risk compared to the parietal bone.

The implications of site of impact will be discussed further in the threshold section, along with the affect of site of impact on the stretch ratio of the bridging veins.

#### 5.4.4 Deformation

In Chapter 3, the potential level of deformation that an infant head undergoes was illustrated. The validated FE was used to quantify the potential levels of deformation for different anatomical sites of impact and across a range of heights. Few authors have investigated deformation. Thibault and Margulies<sup>5</sup> suggested that an infant head is at a greater risk of diffuse patterns of injury as compared to an adult head, because of the greater malleability of the infant head. However, the authors did not quantify their definition of diffuse and stiffness values used for the sutures were later shown to be invalid by Coats and Margulies<sup>6</sup>. Roth *et al*<sup>19</sup> reported the level of deflection in their parametric analysis, which was conducted for frontal impacts at fall heights of 30cm. Deflection values were reported between 6.7mm and 7.8mm in their parametric analysis<sup>19</sup>, the equivalent impact in this test had deformation in the anterior-posterior direction of 6.9mm. In this study, deformation increased with height and varied with site of impact, as previously stated. The greatest deformation was seen during impacts focal to the sutures, namely the vertex and parieto-occipital impact. However, the potential

implication of head deformation has been discussed in the thresholds section of this discussion (Section 5.4.5).

#### 5.4.5 Threshold

##### 5.4.5.1 Skull fracture

In Chapter 3 a potential fall height threshold of 0.6m was established for skull fracture and / or intracranial injury. An anthropomorphic testing device was designed and built to compare the clinical threshold with current biomechanical skull fracture thresholds. A disconnect was indicated when comparing the two. Skull fracture was investigated, using the finite element head model. At a 0.6m fall height, parietal fracture was estimated to be 20% for a parietal impact and 15.2% for a vertex impact, based on maximum principle stress and ultimate stress values for infant cranial bone <sup>6</sup>. In comparison to the clinical data this over estimated the risk at this height. At a 1.2m fall height, the risk of skull fracture and/or ICI was estimated between 9.3% and 23.4%. The corresponding parietal fracture risk was estimated at 40% for a parietal impact, again over estimating the risk. The parietal fracture risks at 0.15m and 0.3m were 10.5% and 13%, respectively. In the cadaver tests conducted by Prange *et al* <sup>16</sup>, three cadaver heads were impacted onto five different areas (vertex, left parietal, right parietal, frontal and occiput). Isolating the vertex and parietal impacts, there were 9 impacts for each fall height <sup>16</sup>, none of which resulted in fracture. Consequently the FE analysis again overestimated the risk. The occipital fracture risk was greater relative to parietal, with a 0.6m fall indicating an 89.9% risk, thus, also over estimating the injury risk. Whilst the FE analysis overestimated the risk, the skull stress values were comparable or less to those reported by previous authors. Coats <sup>30</sup> reported maximum principle occipital stress values of 20MPa at a 0.3m fall height and 32MPa at 0.6m fall height onto concrete. In the validated head model aimed at infants  $\leq 3$  months, developed by Li *et al* <sup>21</sup>, the skull stress values were not reported. In the same study, however, a parametric study was conducted for 0.3m fall onto the vertex. Peak principle values were reported between 12-16MPa for the parametric models that did not assess skull stiffness and between 3-25MPa in

those that did. The 30cm frontal impact conducted by Roth *et al* <sup>19</sup> using a validated FE model resulted in a peak von mises stress of 12MPa, a value similar to those reported in this study. The 6 month FE model developed by Li *et al* <sup>29</sup> had peak stress values of 25MPa at a 0.3m fall height and 30MPa at 60cm. Whilst these value are higher than reported in this study, the FE model was aimed at an older age, Li *et al* <sup>29</sup>.

It is clear it remains difficult to establish a threshold that agrees with the cadaver impact tests conducted by Prange *et al* <sup>16</sup> (no fracture at fall heights of 0.15m and 0.3m), the cadaver test conducted by Weber <sup>14,15</sup> (high risk of fracture at 0.82m) and finally a threshold that concurs with what was seen clinically (no risk of skull fracture at heights <0.6m). The 50% occipital fracture risk developed by Coats <sup>30</sup> for an impact force of 280N, correctly predicted skull fracture at 0.82m. However, it indicated a 50% risk for fall heights <0.3m, which differed from the findings by Prange *et al* <sup>16</sup>. The 50% fracture risk, at a peak G of 82g and HIC 290, developed by Van Ee *et al* <sup>17</sup>, also over predicted the possibility of skull fracture at 0.3m (5-20%) and indicated an approximate 50% risk at 0.6m (Chapter 3). However, using the validated finite element model in this study, a 0.6m fall height had a mean peak G value of 85g and HIC value of 284. Utilising the linear regression, this corresponded to a parietal fracture risk of 22%. Thus, this study has a closer correlation with clinical data, but still over estimates the risk in the lower height regions. The current NHTSA standard<sup>52</sup>, suggested a 5% skull fracture threshold for children aged <1 year old at an HIC value of 144. Utilising the FE analysis this corresponds to fall height of approximately 0.3m. An HIC value of 144 corresponded to a parietal fracture risk of 9% and occipital fracture risk of 40% in this study. An HIC value 284, thus, approximately a 0.6m impact, equated to a fracture risk of 20% from the NHTSA standard<sup>52</sup>, therefore, showing similarities between the thresholds from this FE analysis and the NHTSA standard. However, the NHSTA standard appeared to better correlate with the sub injurious heights from the clinical study (Chapter 3).

The similarities in the peak G and HIC threshold values between this study and those reported by Van Ee *et al*<sup>17</sup>, shows that a greater correlation is being developed in biomechanical thresholds and also greater alignment with what is seen clinically. Whilst differences still exist in the level of risk, the similarities between the two is a positive step in the right direction. Whilst caution needs to be adopted prior to application, particularly considering an 85g impact corresponds to a lower fall height than 0.6m for the frontal and fronto-parietal impacts. Also, an infant head stiffens with age. In the validated 6 month head developed by Li *et al*<sup>29</sup>, an 85g impact corresponded to a fall height of approximately 0.35m and 0.6m fall had a peak G value of 122g on a hard surface (Concrete). It is well known that thresholds, in terms of translational parameters, vary with age, the NHTSA published HIC fracture thresholds for 1, 3 and 6 year old children<sup>52</sup>. Thus, combining this research with the results reported by Li *et al*<sup>29</sup>, suggests a threshold that varies with smaller age increments, potentially every 3 months. Also, given the effect of bone stiffness from the parametric analysis, in combination with the previous authors, discussing the effect of anatomical variation, patient specific characteristic may have to be taken into consideration.

Skull fracture patterns were initially evaluated against the fractures reported in the cadaver cohort by Weber<sup>14,15</sup>. In the cohort, skull fracture patterns were documented in 20 cases. However, there were only three cases of infants  $\leq 3$  months who had been dropped onto a hard surface (stone). In all three cases, the skull fracture patterns appeared to travel from the lambdoid suture in a direction towards the centre of the parietal bone and then move in an inferior direction towards the squamous suture. The FE analysis for a 0.82m fall onto the parieto-occipital area indicated high stress zones that match this pattern. The FE analysis also indicated high stresses on the occipital bone. However, only one of three cases reported by Weber<sup>14,15</sup> also had occipital fracture. Previous authors, using FE analysis, also documented a potential fracture of moving from the lambdoid suture towards the centre of parietal bone<sup>6</sup>. Investigating all fracture patterns reported by Weber<sup>14,15</sup>, including all ages and surfaces tested, 13 of the 20 had

this pattern. Following the similarities in the stress pattern between the FE model and the Weber<sup>14, 15</sup> cases, stress patterns in differing sites of impact were investigated. A vertex impact illustrated a symmetric stress pattern on the left and right parietal bones. A similar bi-lateral parietal pattern was documented by Roth *et al*<sup>19</sup>, whilst investigating a 1m fall onto the vertex. The clinical cases were also objectively evaluated in terms of fracture patterns, where a fracture moving from a lambdoid suture toward to centre of the parietal bone was documented. Whilst there is good agreement in the fracture patterns between what was seen clinically, cadaver experiments and FE analysis, further research is required to validate potential fracture patterns prior to application and greater material failure properties are required such as infant bone shear strength.

### 5.4.5.2 Bridging vein rupture

Bridging vein rupture thresholds exist in terms of rotational accelerations and velocities<sup>53-56</sup>. However, comparing these thresholds with what was seen clinically to the experimental results using the anthropomorphic testing device, again indicated a disconnect. Investigating peak rotational accelerations and peak change in rotational velocities, seen in FE analysis with SDH thresholds, resulted in similar conclusions. The Löwenhielm<sup>57</sup> threshold of 4,500 rad/s<sup>2</sup>, when used in isolation, did not appear relevant as both the 0.3m and 0.6m impacts resulted in accelerations in excess of this threshold. The original threshold suggested by Löwenhielm<sup>57</sup> suggested that a change in rotational velocity of 50rad/s was required, in conjunction with the 4,500 rad/s<sup>2</sup>. In Chapter 4, it was suggested that this threshold was potentially relevant, as no cases passed it. Greater heights were investigated using the FE model, where this threshold was only crossed for isolated cases (1.2m impact onto the frontal and vertex areas). Thus, again suggesting that this threshold might be relevant. In Chapter 3, the 10,000 rad/s<sup>2</sup> threshold for bridging vein rupture proposed by Depreitere *et al*<sup>53</sup>, was deemed potentially relevant. However, this threshold is only applicable for impact durations of <10ms. All impact durations were >10ms for testing completed using the ATD. Incorporating the FE analysis, the impact duration decreased with height

and was affected by the site of the impact. This resulted in impacts onto the stiffer parts of the head, namely the frontal aspects, at fall heights of 1.2m having impacts durations <10ms. Thus, suggesting potential application of this threshold. However, for both the threshold proposed by both sets of authors<sup>53, 57</sup>, a corresponding level of risk has not been established, therefore, it is difficult to fully assess their potential application. Also it needs to be reiterated that it was unknown if any of the intracranial injuries seen in Chapter 3 were the result of bridging vein rupture. However, a further assessment of these thresholds against bridging vein strain was completed and has been outlined below.

In this study, connectors were used to model the bridging veins in the FE model. Few studies have measured the properties of the bridging veins<sup>35, 36, 57, 58</sup> and fewer FE models of infant heads have included a representation of them<sup>35, 59</sup>. Only a single study has investigated the potential strain on the bridging veins in infant heads as the result of impact using finite element analysis. Morrison<sup>35</sup> investigated the potential strains on the veins between shaking and impact. However, in their model the skull was modelled as a rigid body and for an impact simulation, their model was subject of two and a half sinusoidal linear accelerations of magnitude 160g and 300g and impact duration of 10ms and 8ms, respectively<sup>35</sup>. The greatest linear acceleration in this research was 131g for a 1.2m fall, onto the fronto-parietal region, thus 160g and 300g corresponds to higher fall heights than measured by this study. However, the peak stretch ratio for the 160g and 300g was 1.14 and 1.23 respectively. The bridging vein strains reported in this study are higher, compared to those documented by Morrison<sup>35</sup>, which might be explained by the skull being modelled a deformable structure as opposed to a rigid body.

Due to disconnect between biomechanical thresholds, for bridging vein rupture and the clinical findings, the rotational kinematic variables were correlated with peak stretch ratio. Once vertex impacts had been excluded, a correlation was seen between both rotational acceleration and change in rotational velocity and peak

stretch ratio. Post linear regression analysis, a rotational acceleration of 10,000 rad/s<sup>2</sup> corresponded with peak stretch ratio of 1.15 and peak change in rotational velocity of 50 rad/s, correlated with a peak stretch ratio of 1.17. These values do not exceed average failure values reported in the literature<sup>35, 36, 57, 58</sup>. Thus, the relationship between rotational accelerations and bridging vein strain needs to be explored further for a malleable infant head. It noteworthy that these results only reflect the type of incidents explored by this study ('low height fall') and should not be extrapolated for different types of incidents.

Average failure properties of the bridging veins have been reported between 1.43 and 1.56<sup>35, 36, 57, 58</sup>. The strains on the connectors did not exceed these values for any of the scenarios investigated, although infant bridging vein failure has been reported for stretch ratios as low as 1.15. However, this was based on a small sample of the bridging veins, and it is unclear if it is representative of the target population. The ultimate stretch ratios of the connectors were significantly influenced by height and site of impact ( $P < 0.05$ ). The largest peak stretch ratios were seen for the vertex impacts. Therefore, possibly suggesting the greatest risk of failure for this particular type of incident ('low height fall') would be from an impact focal to the parasagittal veins. The location of peak stretch ratio correlated well with what has been reported by previous authors in an adult FE head model, namely the highest strains were in the central or posterior central locations<sup>37</sup>. The potential level of deformation that an infant head undergoes on impact has been highlighted by this study, where the greatest was seen for a vertex impact. Given the malleability of an infant head, on impact, the blood vessel intra-cranially and focally could be subject to increased strain, relative to a stiffened skull. Thus, an infant head may be at a greater risk of vein rupture from this hypothesised mechanism. The potential susceptibility of an infant head, to different types of trauma, due to it being more malleable, has been highlighted by previous authors<sup>5</sup>, although bridging vein strain was not investigated. This hypothesised mechanism would appear to concur with recent clinical studies that have indicated the potential for a SDH focal to an impact and more specifically focal to fracture<sup>60, 61</sup>.



However, in such cases it is unclear if the SDH is a result of bridging vein rupture. The connectors used to model the bridging veins were placed in a specific location, thus, the potential affects of this mechanisms would need to be explored further with other vasculature included in the model. For example, in Chapter 3, the extra-axial haemorrhages were reported as focal to the fracture, however, bridging vein rupture is not a potential cause of all extra axial haemorrhages. Thus, investigation of this hypothesised mechanism would need to include vasculature such as the middle meningeal artery, when researching it as a potential cause of an epidural haemorrhage.

In this study, as previously stated, the greatest peak stretch ratio of bridging veins was seen for the vertex impacts and only small variations were seen across the other sites of impact. It has been hypothesised that there is greater risk of bridging vein rupture from occipital impacts<sup>35-37</sup>. Due to bridging vein draining in a frontal direction to the superior sagittal sinus, it is hypothesised that from an occipital impact that the brain moves in a directions towards the site of impact and the skull in an opposite direction, thus putting the vein in tension<sup>36</sup>. However, for a frontal impact, again the brain moves toward the site of impact and the skull in opposite direction, however, the vein would be put into compression as opposed to tension. The results from this analysis do not appear to concur with this hypothesis of a greatest risk from an occipital impact. Whilst peak stretch ratios were greater for occipital impacts, compared to frontal impacts, for 0.15m, 0.3m, and 0.6m, that maximum increase was only 2.6% and for a 1.2m impact it was lower relative to a frontal impact. However, in the parametric analysis the direction was changed such that the vein drained in a posterior direction, this reduced peak strain for the occipital impacts but again only by a small percentage (maximum of 5.8%). In a frontal impact, the strains were relatively unchanged for this change in vein direction and thus not agreeing with this hypothesis. A potential reason for these differences is due to anatomical variations between an infant and adult head, as has been previously stated. An infant head is not as stiff as an adult head and thus would have a greater deformation on impact. Therefore, whilst the brain moves

towards the site of impact, due to the inertia force, this is counter acted by a positive pressure induced as the result of the local deformation. Whilst this remains an hypothesis, partly due to bridging vein strain, brain skull motion and deformation not being validated, it provides an area of further research on how the dynamic response of the infant head differs from that of an adult.

Failure of bridging veins, as the result of relative motion between the brain and skull is one proposed mechanism of traumatic brain injury. However, there are other hypothesised mechanisms, including pressure gradients resulting in shear stresses, as discussed in section 2.3.1. However, these mechanism are not specific to an extra axial haemorrhage. Due to injury, specific to brain not seen in the clinical aspect of the research and rarely documented in the literature, it is unclear if this mechanism has an effect from low height fall incident. However, given the level of deformation of infant head on impact, pressure gradient would be expected. Greater research on the material properties of different parts of the brain would aid in exploring these other mechanisms further.

### 5.4.6 Limitations

A single FE model was developed, thus geometric variations were not assessed. Given previous authors have found anatomical variations to have an effect on impact response, their effect needs to be further assessed. However, all variations would need to be quantified against cadaver impacts, such that the models remain validated. Surface was not investigated using the FE model, as the dynamic response of head, for a worst cases scenario, needed to be quantified and it was also previously assessed in Chapter 4. Therefore the effects of surface at greater heights needs to be explored.

### 5.4.7 Implications

The location of high stress zones on the skull, illustrated using the FE analysis, highlight the role that site of impact and the sutures have on the stress distribution around the skull. An impact close to sutures (vertex and parieto-occipital impacts)

appeared to cause high stress on both adjacent bones. This has implications in the clinical setting, with particular reference to complex fractures. Certain types of complex fracture, namely bilateral and fractures of multiple bones, have raised debate with a potential association with abusive head trauma<sup>62-64</sup>. However, research conducted by previous authors is inconclusive with regards to its association<sup>65,66</sup>. Whilst further research is required to further assess the ability of the FE model to predict skull fracture patterns, the results to date indicate the possibility of bilateral or multiple bone fracture from a single point of impact. However, the potential of such fracture would depend on the site of impact. The greatest strain on the bridging veins in this model were seen on those impacts most focal to the veins and at areas of greatest deformation. Thus, further reiterating the importance of the site of impact and the role of sutures on head impact dynamics for an infant head.

## 5.5 Conclusion

A biofidelic infant head finite element model was designed from CT images. The dynamic impact response of the FE model was assessed against human infant cadaver data. Four FE models were assessed in the validation process and the FE model based on the optimised parameters showed the best correlation with cadaver data.

Subsequently the model was used to conduct a parametric test to assess the effect that material properties have on the impact response of the head.

- Skull stiffness had the greatest effect on the dynamic response of the head. Small increases in stiffness of 7% increased HIC by 26%. Given the potential range of skull stiffness values, based on upper and lower value for infants <3months, it identifies a wide range of potential values for an infant head. However, upper values were outside a validation window in terms of cadaver impacts.
- Scalp stiffness, meningeal stiffness (falx cerebri and tentorium cerebellum), bulk modulus and brain stiffness model (viscoelastic vs hyperelastic) of the brain did not affect the majority of output variables by greater than 15%.

Post this assessment, the FE model was used to investigate two key differentiating features of the clinical findings, namely height and anatomical site of impact.

### Height

- Increase in height increased translation kinematic variables. The mean value of peak G and HIC at the clinical defined threshold of 0.6m fall height was 85g and 284g, respectively. This showed greater alignment between current biomechanical skull fracture thresholds in infants.
- The results of FE model indicated closer correlation is being developed between previous bio mechanical thresholds and those seen from a clinical setting.

### Site of impact

- The stiffer parts of the head were in the frontal areas and least stiff were on impact focal to the suture. Whilst this resulted in increased values for translation kinematic parameter (peak G and HIC), it did not indicate a greater injury risk. Relative bone thickness, along with local material properties need to be taken into consideration. Indicating threshold for injury should potentially vary with site of impact.
- The greatest risk of fracture was from an occipital impact, although the results did not correlate with clinical findings. Impacts focal to the suture also indicate high stress in adjacent bones, suggesting potential of fracture of multiple bones from a single point of impact. For example an impact to the vertex illustrated high stress zones on the left and right parietal bones. Whilst further research is required to validate fracture patterns, it highlights the potential for a bi-parietal fracture from a vertex impact.
- The greatest strain on the connectors used to model the bridging veins was at the most focal impact point, the vertex. Impacts, close to suture, had the greatest deformation. This potential indicates the greatest strain on underlying blood vessels could potentially be dependent on the site of impact in conjunction with focal stiffness characteristics.

## 5.6 References

1. McPherson GK, Kriewall TJ. Fetal head molding: An investigation utilizing a finite element model of the fetal parietal bone. *Journal of Biomechanics*. 1980;13(1):17-26.
2. Lapeer R, Prager R. Fetal head moulding: finite element analysis of a fetal skull subjected to uterine pressures during the first stage of labour. *Journal of Biomechanics*. 2001;34(9):1125-1133.
3. McPherson GK, Kriewall TJ. The elastic modulus of fetal cranial bone: a first step towards an understanding of the biomechanics of fetal head molding. *Journal of Biomechanics*. 1980;13(1):9-16.
4. Sorbe B, Dahlgren S. Some important factors in the molding of the fetal head during vaginal delivery-a photographic study. *International Journal of Gynecology & Obstetrics*. 1983;21(3):205-212.
5. Thibault KL, Margulies SS. Age-dependent material properties of the porcine cerebrum: effect on pediatric inertial head injury criteria. *Journal of Biomechanics*. 1998;31(12):1119-1126.
6. Coats B, Margulies S. Material properties of human infant skull and suture at high rates. *Journal of neurotrauma*. 2006;23(8):1222-1232.
7. Duhaime A-C, Gennarelli TA, Thibault LE, Bruce DA, Margulies SS, Wiser R. The shaken baby syndrome: a clinical, pathological, and biomechanical study. *Journal of neurosurgery*. 1987;66(3):409-415.
8. Margulies S, Thibault K. Infant skull and suture properties: measurements and implications for mechanisms of pediatric brain injury. *Journal of Biomechanical Engineering*. 2000;122:364.
9. Roth S, Raul J-S, Ludes B, Willinger R. Finite element analysis of impact and shaking inflicted to a child. *International journal of legal medicine*. 2007;121(3):223-228.
10. Roth S, Raul J, Willinger R. Biofidelic child head FE model to simulate real world trauma. *Computer methods and programs in biomedicine*. 2008;90(3):262-274.
11. Roth S, Vappou J, Raul J, Willinger R. Child head injury criteria investigation through numerical simulation of real world trauma. *Computer methods and programs in biomedicine*. 2009;93(1):32-45.
12. DSS. Abaqus/Cae. Version 6.10-2 ed2010.
13. Coats B, Ji S, Margulies S. Parametric study of head impact in the infant. *Stapp Car Crash J*. 2007;51:1-15.
14. Weber W. Experimental studies of skull fractures in infants]. *Zeitschrift für Rechtsmedizin Journal of legal medicine*. 1984;92(2):87.
15. Weber W. [Biomechanical fragility of the infant skull]. *Zeitschrift für Rechtsmedizin Journal of legal medicine*. 1985;94(2):93.
16. Prange M, Luck J, Dibb A, Van Ee C, Nightingale R, Myers B. Mechanical properties and anthropometry of the human infant head. *Stapp car crash journal*. 2004;48:279.
17. Van Ee C, Moroski-Browne B, Raymond D, Thibault K, Hardy W, Plunkett J. Evaluation and refinement of the CRABI-6 anthropomorphic test device injury criteria for skull fracture. 2009: ASME.

18. Roth S, Raul J, Ruan J, Willinger R. Limitation of scaling methods in child head finite element modelling. *International Journal of Vehicle Safety*. 2007;2(4):404-421.
19. Roth S, Raul JS, Willinger R. Finite element modelling of paediatric head impact: Global validation against experimental data. *Computer methods and programs in biomedicine*. 2010;99(1):25-33.
20. Li Z, Hu J, Reed MP, Rupp JD, Hoff CN, Zhang J, et al. Development, validation, and application of a parametric pediatric head finite element model for impact simulations. *Annals of biomedical engineering*. 2011;39(12):2984-2997.
21. Li Z, Hu J, Reed MP, Rupp JD, Hoff CN, Zhang J, et al. Development, Validation, and Application of a Parametric Pediatric Head Finite Element Model for Impact Simulations. *Annals of Biomedical Engineering*. 2011:1-14.
22. Klinich K, Hulbert G, Schneider L. Estimating infant head injury criteria and impact response using crash reconstruction and finite element modeling. *Stapp car crash journal*. 2002;46:165.
23. Coats B, Margulies S. Potential for head injuries in infants from low-height falls. *Journal of Neurosurgery: Pediatrics*. 2008;2(5):321-330.
24. Simpleware. ScanIP. Version 4.2. ed2010.
25. Simpleware. ScanFE. Version 4.2. ed2010.
26. Abaqus User's Manual. *Dassault Systemes*. 2010.
27. ScanIP with +FE and + NURBS Modulues and +CAD Module Reference Guide Release 8. *Simpleware Ltd*. 2012.
28. Young P, Beresford-West T, Coward S, Notarberardino B, Walker B, Abdul-Aziz A. An efficient approach to converting three-dimensional image data into highly accurate computational models. *Philosophical Transactions of the Royal Society A: Mathematical, Physical and Engineering Sciences*. 2008;366(1878):3155-3173.
29. Li Z, Luo X, Zhang J. Development/global validation of a 6-month-old pediatric head finite element model and application in investigation of drop-induced infant head injury. *Computer methods and programs in biomedicine*. 2013;112(3):309-319.
30. Coats B. *Mechanics of Head Impacts in Infants*: University of Pennsylvania; 2007.
31. Galford JE, McElhaney JH. A viscoelastic study of scalp, brain, and dura. *Journal of Biomechanics*. 1970;3(2):211-221.
32. Coats B, Eucker SA, Sullivan S, Margulies SS. Finite element model predictions of intracranial hemorrhage from non-impact, rapid head rotations in the piglet. *International Journal of Developmental Neuroscience*. 2012.
33. Bylski DI, Kriewall TJ, Akkas N, Melvin JW. Mechanical behavior of fetal dura mater under large deformation biaxial tension. *Journal of Biomechanics*. 1986;19(1):19-26.
34. Prange M, Margulies S. Regional, directional, and age-dependent properties of the brain undergoing large deformation. *Journal of Biomechanical Engineering*. 2002;124:244.

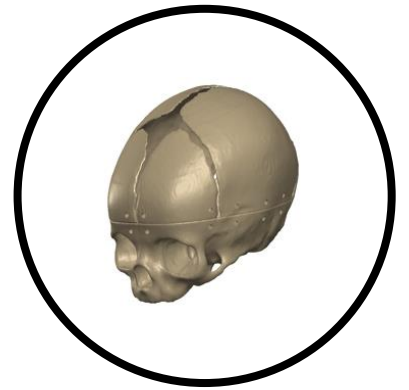
35. Morrison N. The Dynamics of Shaken Baby Syndrome: The University of Birmingham; 2002.
36. Lee MC, Haut RC. Insensitivity of tensile failure properties of human bridging veins to strain rate: Implications in biomechanics of subdural hematoma. *Journal of Biomechanics*. 1989;22(6-7):537-542.
37. Kleiven S, Hardy WN. Correlation of an FE model of the human head with local brain motion-consequences for injury prediction. SAE CONFERENCE PROCEEDINGS P; 2002: SAE; 1999. p. 123-144.
38. Miller RT, Margulies SS, Leoni M, Nonaka M, Chen X, Smith DH, et al. Finite Element Modeling Approaches Of Predicting Injury In An Experimental Model Of Severe Diffuse Axonal Injury 1998. Report No.: 0768002931.
39. Ji S, Margulies S. In vivo pons motion within the skull. *Journal of biomechanics*. 2007;40(1):92-99.
40. Mathworks. Matlab. Version R2011a. ed2011.
41. IBM. SPSS. Version 20. ed2011.
42. Gadd CW, Nahum AM, Schneider DC, Madeira RG. Tolerance and properties of superficial soft tissues in situ. *SAE Technical Paper 700910*. 1970.
43. Raposio E, Nordström RE. Biomechanical properties of scalp flaps and their correlations to reconstructive and aesthetic surgery procedures. *Skin Research and Technology*. 1998;4(2):94-98.
44. Sauren A, Claessens M. Finite element modeling of head impact: The second decade. Proceedings of the International IRCOBI, Conference on Biomechanics of Impact; 1993. p. 241-254.
45. Kleiven S. Influence of impact direction on the human head in prediction of subdural hematoma. *Journal of neurotrauma*. 2003;20(4):365-379.
46. Brockmann C, Kunze SC, Schmiedek P, Groden C, Scharf J. Variations of the superior sagittal sinus and bridging veins in human dissections and computed tomography venography. *Clinical imaging*. 2012;36(2):85-89.
47. Duhaime AC, Alario AJ, Lewander WJ, Schut L, Sutton LN, Seidl TS, et al. Head injury in very young children: mechanisms, injury types, and ophthalmologic findings in 100 hospitalized patients younger than 2 years of age. *Pediatrics*. 1992;90(2):179.
48. Gennarelli TA, Thibault LE. Biomechanics of acute subdural hematoma. *The Journal of Trauma and Acute Care Surgery*. 1982;22(8):680-686.
49. Zhang L, Bae J, Hardy WN, Monson KL, Manley GT, Goldsmith W, et al. Computational study of the contribution of the vasculature on the dynamic response of the brain. *Development*. 2002;2002:22-0014.
50. Margulies S, Coats B. Experimental Injury Biomechanics of the Pediatric Head and Brain. *Pediatric Injury Biomechanics*: Springer; 2013. p. 157-189.
51. Gennarelli TA, Thibault LE, Adams JH, Graham DI, Thompson CJ, Marcincin RP. Diffuse axonal injury and traumatic coma in the primate. *Annals of neurology*. 1982;12(6):564-574.
52. Eppinger R, Sun E, Bandak F, Haffner M, Khaewpong N, Maltese M, et al. Development of improved injury criteria for the assessment of advanced automotive restraint systems-II. *National Highway Traffic Safety Administration*. 1999.



53. Depreitere B, Van Lierde C, Sloten JV, Van Audekercke R, Van Der Perre G, Plets C, et al. Mechanics of acute subdural hematomas resulting from bridging vein rupture. *Journal of neurosurgery*. 2006;104(6):950-956.
54. Löwenhielm P. Strain tolerance of the vv. cerebri sup.(bridging veins) calculated from head-on collision tests with cadavers. *Zeitschrift für Rechtsmedizin*. 1974;75(2):131-144.
55. Löwenhielm P. Mathematical simulation of gliding contusions. *Journal of Biomechanics*. 1975;8(6):351-356.
56. Löwenhielm P. Tolerance level for bridging vein disruption calculated with a mathematical model. *Journal of bioengineering*. 1978;2(6):501.
57. Löwenhielm P. Dynamic properties of the parasagittal bridging veins. *International Journal of Legal Medicine*. 1974;74(1):55-62.
58. Meaney DF. Biomechanics of acute subdural hematoma in the subhuman primate and man. 1991.
59. Raul J-S, Roth S, Ludes B, Willinger R. Influence of the benign enlargement of the subarachnoid space on the bridging veins strain during a shaking event: a finite element study. *International journal of legal medicine*. 2008;122(4):337-340.
60. Feldman KW, Bethel R, Shugerman RP, Grossman DC, Grady MS, Ellenbogen RG. The cause of infant and toddler subdural hemorrhage: a prospective study. *Pediatrics*. 2001;108(3):636.
61. Thomas AG, Hegde SV, Dineen RA, Jaspán T. Patterns of accidental craniocerebral injury occurring in early childhood. *Archives of disease in childhood*. 2013;98(10):787-792.
62. Hiss J, Kahana T. The medicolegal implications of bilateral cranial fractures in infants. *The Journal of Trauma*. 1995;38(1):32.
63. Hobbs CJ. Skull fracture and the diagnosis of abuse. *Archives of Disease in Childhood*. 1984;59(3):246.
64. Meservy CJ, Towbin R, McLaurin RL, Myers PA, Ball W. Radiographic characteristics of skull fractures resulting from child abuse. *American Journal of Roentgenology*. 1987;149(1):173.
65. Kemp AM, Dunstan F, Harrison S, Morris S, Mann M, Rolfe K, et al. Patterns of skeletal fractures in child abuse: systematic review. *BMJ: British Medical Journal*. 2008;337.
66. Leventhal JM, Thomas SA, Rosenfield NS, Markowitz RI. Fractures in young children: distinguishing child abuse from unintentional injuries. *Archives of Pediatrics and Adolescent Medicine*. 1993;147(1):87.

---

Chapter 6 – Final  
Conclusions



## **6.1 Final Conclusions**

The primary aim of this thesis was determine the potential head injuries that can result from incidents commonly referred to as a low height fall in young children. From existing literature, this particular type of incident lacked a clear definition, and there was no clear threshold in terms of fall height for skull fracture or the different forms of intracranial injury. While biomechanical thresholds aimed at young children exist, they have not been assessed against the head injuries seen in a clinical setting. Consequently a clinical study was undertaken to establish differentiating features between minor head injury, and those resulting in skull fracture and/or ICI in young children. In conjunction with this, biomechanical testing devices, a physical anthropomorphic model and a finite element model of an infant head were developed. These devices were used to assess the clinical differentiating features from a biomechanical perspective, in order to evaluate thresholds for skull fracture and ICI in terms of kinematic variables. A number of key findings were identified in relation to head injury severity which are outlined below.

### **6.1.1 Key findings**

#### **6.1.1.1 Clinical**

- The clinical study established a potential fall height threshold between minor head injury and that resulting in a skull fracture and/or ICI of 0.6m.
- The anatomical site of impact was shown to significantly influence head injury severity as a consequence of a fall. A greater proportion of skull fractures and/or ICIs were the result of impacts onto the parietal/temporal or occipital areas.
- A significantly greater proportion of skull fractures and/or ICIs were in children <12months old, and resulted from impacts onto wooden surfaces.

### 6.1.1.2 Biomechanical

- Investigating the fall height threshold from the clinical study using the biomechanical models (physical and computational), suggested that current biomechanical thresholds in the literature were not fully substantiated by the clinical data. However this research does show greater coherence between the two fields of study. The skull fracture threshold of 82g or a HIC value of 290 proposed by previous authors<sup>1</sup> approximates a 0.6m fall, based on combining the physical and FE model results. In conjunction the current NHTSA standard<sup>2</sup> for infants, had similarities in level of skull fracture risk with the FE model, where a HIC value of 284 equated to a 20% skull fracture risk. Whilst there are discrepancies in the level of risk associated with such a fall height, the greater cohesion between the two fields of study adds greater confidence in the potential application of the threshold.
- Adult bridging vein rupture thresholds were not substantiated by the clinical data, particularly when using rotational accelerations in isolation. However when duration of impact was considered in conjunction with rotational acceleration, better similarities were seen. However, the necessary rotational accelerations required to cause bridging vein rupture in an infant or young child is still unknown.
- Site of impact was shown from the clinical study to influence head injury severity. The results from the FE analysis further supported this result. The greatest strain on the connectors used to model the bridging veins were from the most focal impacts. Impacts focal to the sutures also resulted in a stress distribution in excess of ultimate tensile stress values on adjacent bones, thus suggesting the possibility of fracture of multiple bones from a single point of impact.
- The potential level of head deformation that an infant head can undergo from a low height fall was highlighted by this study. Whilst it is widely known that an infant head is more malleable compared to an adult head, the implications of this reduced stiffness is still unknown. This greater ability to deform on impact could potentially place underlying blood vessels (parasagittal bridging veins,

middle meningeal artery etc) under increased strain, particular when site of impact is taken into consideration. This however needs to be explored further.

### 6.1.2 Future Research

In the clinical aspect of this research a number of covariates (height, age, anatomical site of impact and surface impacted) that significantly affected head injury severity in young children were identified. Due to the relative rarity of significant head injury in young children, there was too small a sample size to develop an accurate multivariate regression model. Thus future research should aim at collecting a larger dataset such that the interaction between these covariates can be further assessed. The clinical aspect of this research was based on accidental head trauma, and thus evaluated the significant covariates associated with the fall height threshold. However this research has implications in relation to abusive head trauma. A false history of a fall is often offered by parents of children who have been abused, and thus knowledge of the relevant variables associated with significant head injury resulting from falls in young infants will help to assess the plausibility of any history offered.

An infant head can undergo considerable deformation on impact, as has been documented by this study. Also the greatest strain on the bridging veins, modelled using connectors, was from the most focal impacts, which were also the site of the greatest deformation. As has been previously documented, an infant head is more malleable compared to that of an adult. Thus this greater ability to deform on impact, could be associated with causing greater strain on underlying blood vessels. However this needs to be assessed further, particularly through including a greater a number of parts to represent the different blood vessels, whilst also altering localised stiffness values and considering further sites of impact. The relationship between fracture of multiple bones and site of impact is enormously important to clinicians, and merits further exploration, specifically with regard to varying anatomical sites of impact. Further failure properties of infant bone would allow also allow greater research into potential fracture patterns.

Only infants <3 months were investigated using the biomechanical models, due to limited data with which to validate against. However age variations need to be considered, particularly when evaluating biomechanical thresholds. Consequently as further age appropriate cadaver data becomes available, biomechanical models need to be developed and assessed against the clinical features from this study.

Finally a number of material properties were assessed using the FE model. However anatomical variations such as suture width have the potential to affect the dynamic response on impact<sup>3</sup>. Therefore in order to identify a potential range of values in terms of kinematic variables, anatomical variations need to be considered. This would also be beneficial when evaluating unique anatomical features such as increased CSF thickness.

### **6.1.3 Implications**

The greatest impact of this research should be in the clinical setting. Whilst greater research is required around the proposed fall height threshold, this data could aid clinicians with regards to evaluating the potential head injuries that can result when presented with a history of a low height fall. Once a clear history has been obtained, and the relative distance between the head and impacted surface has been estimated, the thresholds proposed in this study can be used to inform an evaluation of the likelihood of a given head injury. Clinicians when presented with a skull fracture and / or ICI in a young child with a history of a fall height below 0.6m, should be skeptical of its validity. Fall heights between 0.6m and 1.2m should also be interpreted with caution, as whilst this study has shown it to be possible to sustain a significant head injury from this height, the risk appears to be low. An incident that clinicians should be mindful of is a fall from a carer's arms, as it has been shown by this study and other authors<sup>4</sup> as a common accidental incident that can lead to skull fractures and / or ICI.

Whilst fall height is an essential variable to consider when evaluating the severity of an incident, this research has shown that other variables such as the surface impacted, age, impact angle, and, importantly, anatomical site of impact can influence head injury severity. These conclusions from the clinical data were supported by both forms of biomechanical evidence. The anatomical site of impact appeared to be a feature that was collected in a clinical setting, thus this research has shown it should be considered further by clinicians when evaluating the likelihood of a given head injury.

Natural variation in material properties was shown to have an effect on kinematic response. However this would be difficult to assess in a clinical setting, although it potentially needs to be considered from a medico-legal point of view.

Overall this study set out to determine the head injuries that can result from a low height fall in a young child. While there is still no clear definition of this type of incident, this study has provided a threshold for skull fracture and / or ICI along with a better understanding of the level of risk associated with different heights, whilst also outlining the importance of other variables including age, surface impacted and the anatomical site of impact. These findings were supported by both clinical and biomechanical evidence.

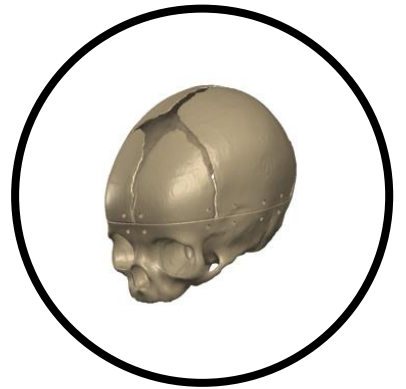
## 6.2 References

1. Van Ee C, Moroski-Browne B, Raymond D, Thibault K, Hardy W, Plunkett J. Evaluation and refinement of the CRABI-6 anthropomorphic test device injury criteria for skull fracture. 2009: ASME.
2. Eppinger R, Sun E, Bandak F, Haffner M, Khaewpong N, Maltese M, et al. Development of improved injury criteria for the assessment of advanced automotive restraint systems–II. *National Highway Traffic Safety Administration*. 1999.
3. Coats B, Ji S, Margulies S. Parametric study of head impact in the infant. *Stapp Car Crash J*. 2007;51:1-15.
4. Thomas AG, Hegde SV, Dineen RA, Jaspan T. Patterns of accidental craniocerebral injury occurring in early childhood. *Archives of disease in childhood*. 2013;98(10):787-792.



---

## Chapter 7 – Appendices



7.1 Appendix 1

**Assessment of Head Injuries in Infants (2 years or younger)**

**Section 1- Patient Details**

Patient Initials: \_\_\_\_\_ Case Number: \_\_\_\_\_  
 DOB: \_\_\_\_\_ Gender: F [ ] M [ ]  
 Age: \_\_\_\_\_ Height (m) & Weight (Kg): \_\_\_\_\_

**Section 2- Incident Description**

**Brief Description of Incident:**  
 .....

**Number of witnesses of Incident:** .....

(If No witnesses present also complete Section 3)

**Weather conditions if the incident occurred outside:**  
 Dry [ ] Wet [ ] Windy [ ] Snow [ ] Ice [ ] Fog [ ]

**Clothing worn by child:**  
 Hat [ ] Helmet [ ] Gloves [ ] Scarf [ ] Padded Jumper [ ] Padded trousers [ ]

**Activity prior to incident:**  
 Walking [ ] Sitting [ ] Lying (Supine) [ ] Lying (Prone) [ ] Other [ ] .....

In the case of falls  
**Fall Height:** .....

**Apparatus/Furniture Fallen from:**  
 Bed [ ] Chair [ ] Table [ ] Cot [ ] Other [ ] .....

**Surface fallen onto (If fallen onto object include details):**  
 Stairs [ ] Floor [ ] Object [ ] (Details: .....) )

**Material fallen onto:** Concrete [ ] Carpet [ ] Mattress [ ]


In the case of high velocity Impacts  
**Was it a car incident:** Yes [ ] No [ ]  
**If yes, description of car and speed:** .....

**If no description of object including suspected shape, speed, weight and material:** .....

**Section 4-Injury Description**

**Brief description of injuries sustained:**  
 .....

**Primary Point of Impact on head (Indicate location):**  
 .....



**Scans required:** CT [ ] MRI [ ] X-Ray [ ]

**Any previous head injuries:** Yes [ ] No [ ]

For non witnessed cases  
**Confidence level in primary impact site:** 20% [ ] 40% [ ] 60% [ ] 80% [ ] 100% [ ]

**Time between injury and presentation:** .....Hours If-6hours, cause of delay .....

<b>Section 5-Child Development</b>		
Developmental Milestone	Age achieved (months)	Reference
Rolling front to back		3 months
Rolling back to front		6 months
Sitting		6 months
Crawling		12 months
Cruising		15 months
Walking		18 months
Ascend stairs		24 months

**For use after consultation:**  
 Consider seeking advice from a colleague if ANY of the following are present.

Indicator	Check
Incompatible/Inconsistent history: Please give details:	
Under 1 year of age	
Injuries unrelated to fracture (new/old bruises, cuts in unusual places)	
Previous fracture	
Metaphyseal Lesion	
Unreasonable delay in presentation to A&E	
Injury unexplained by adult	
More than one fracture from this incident	

Figure 1A – First draft of head injury assessment form.

Chapter 7 – Appendices

**HEAD INJURY ASSESSMENT FORM (CHILDREN UNDER 10 YEARS)**

**Patient Details**

Surname: \_\_\_\_\_ Forename: \_\_\_\_\_  
 Hospital Number: \_\_\_\_\_ DOB: / / \_\_\_\_\_  
 Gender: F [ ] M [ ]  
 Height: \_\_\_\_\_ Weight: \_\_\_\_\_

**HISTORY**

Time of injury: date: / / time: \_\_\_\_\_ Time of examination: date: / / time: \_\_\_\_\_

Was the incident witnessed?  
 Yes, seen by accompanying person  
 Yes, seen by 3<sup>rd</sup> party  
 Someone present but took time  
 No

History given by? (mother, father etc) \_\_\_\_\_

Describe how the incident occurred?  
 \_\_\_\_\_  
 \_\_\_\_\_  
 \_\_\_\_\_

Where did the incident occur? (e.g. living room, playground, kitchen) \_\_\_\_\_

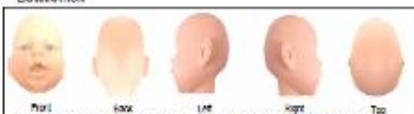
What was the child doing BEFORE the incident?  
 Walking [ ] Sitting [ ] Lying on back [ ] Lying on front [ ]  
 Rolling [ ] Raising [ ] Standing [ ] Running [ ]  
 Other [ ] \_\_\_\_\_

What was the position of the child AFTER the incident?  
 Sitting [ ] Lying on back [ ] Lying on front [ ]  
 Standing [ ] Other [ ] \_\_\_\_\_

Questions with \*\* are essential for study determining how hard the head hit a surface

\*\* Do you know which part of the body the child landed on? Y/N  
 If yes, please state: \_\_\_\_\_

**EXAMINATION**



Front Back Left Right Top

Please illustrate on the above diagram the location of the head injury/injuries with appropriate measurements of lacerations and bruises in cm.  
 No Lacerations [ ] No Bruises [ ]

**Specific Symptoms**

Unconscious when seen? Y/N \_\_\_\_\_


Specific Symptoms	Y/N	GUIDANCE FOR CT REQUEST
Loss of consciousness	Y/N	Leading to Fracture CT REQUEST
Amnesia	Y/N	Leading to Fracture CT REQUEST
Mechanism of injury	Y/N	Leading to Fracture CT REQUEST
Swelling	Y/N	3 or more discrete palpable CT REQUEST
Redness (not below forehead)	Y/N	Leading to Fracture CT REQUEST
Redness on forehead	Y/N	Leading to Fracture CT REQUEST
Unilateral pupil dilation	Y/N	Leading to Fracture CT REQUEST
Unilateral pupil constriction	Y/N	Leading to Fracture CT REQUEST
Age < 1 year, GCS < 7	Y/N	Leading to Fracture CT REQUEST
Age < 1 year, GCS (best eye) < 10	Y/N	Leading to Fracture CT REQUEST
Suppression of eye or pupillary response to injury or noise	Y/N	Leading to Fracture CT REQUEST
Seizures	Y/N	Leading to Fracture CT REQUEST
Any eye of head and/or facial asymmetry, tearing, eye, and/or eyelid full, redness, bruising or swelling, bulging, or other signs	Y/N	Leading to Fracture CT REQUEST
High speed MVC (pedestrian, cyclist, vehicle occupant) or motor bike (excluded from this assessment)	Y/N	Leading to Fracture CT REQUEST

Other neurological symptoms \_\_\_\_\_

Fontanelle / Sutures? Normal [ ] Bulging / sunken [ ] Head Circumference? .....cm

Evidence of injury to the neck? Y/N \_\_\_\_\_

Please illustrate and annotate any other injuries



**NEUROLOGICAL EXAMINATION**

Doctor MUST document responsiveness, pupil and limb movement responses in boxes 1, 2 & 3 on observation chart opposite.

Evidence of abnormal behaviour / speech	Y/N	Retinal haemorrhages	Y/N
Abnormal visual recognition / behaviour	Y/N	Apparent loss hearing / facial weakness	Y/N
Abnormal eye movement	Y/N	Incoordination / abnormal movement patterns	Y/N

**INVESTIGATIONS AND RESULTS**

CT [ ] MRI [ ] X-Ray (Skull) [ ] X-Ray (Neck) [ ] Other [ ] \_\_\_\_\_

Reason for further investigations? \_\_\_\_\_

Results from further investigations? \_\_\_\_\_

**DIAGNOSIS**

[ ] Minor HI, fully orientated, no evidence of skull fracture (on clinical or radiological grounds)  
 [ ] Minor HI, fully orientated, with skull fracture  
 [ ] Disorientated / drowsy  
 [ ] Difficult to assess  
 [ ] Moderate / severe head injury  
 [ ] Other diagnosis / injury  
 Describe: \_\_\_\_\_

Has the child had any previous visits to the ED? Y/N \_\_\_\_\_

Who was the form filled out by?  
 Paediatrics A&E-Nurse [ ] Cons [ ] Reg [ ]  
 Other: \_\_\_\_\_

**Discharge details**

Has a child protection referral been made? Y/N \_\_\_\_\_

Has a Health Visitor / School Nurse referral been made? Y/N \_\_\_\_\_

**Patient Outcome:**  
 Discharged home [ ]  
 Transfer to other hosp [ ] where? \_\_\_\_\_  
 Trans to acute ward / HDU / PICU [ ]  
 Other: \_\_\_\_\_

Reason for admission: \_\_\_\_\_

Other treatment, e.g. sutures, tetanus and antibiotics \_\_\_\_\_

Head injury instructions explained and given? Y/N \_\_\_\_\_

**TETANUS STATE**  
 Covered [ ] Needs Booster [ ] Needs Course [ ]  
 Not Known [ ]

**DRUG THERAPY**  
 [ ] None  
 [ ] Unknown

**ALLERGIES**  
 [ ] None  
 [ ] Unknown

Does the child have any disabilities or pre-existing illnesses?  
 Yes [ ] No [ ] If Yes \_\_\_\_\_

**Head Injury Observation**

At least one full set of observations from boxes 1, 2 and 3 must be recorded

Time	EYES OPEN	BEST VERBAL RESPONSE	BEST MOTOR RESPONSE	Pupils	Limb Movement	Temp	BLOOD PRESSURE mmHg	PULSE RATE	PUPIL SCALE (mm)	RESPIRATORY RATE	REVERSED GRIMACE	MACE/AVICE	GCS VALUE
1													
2													
3													
4													
5													
6													
7													

Figure 1B-Head Injury Assessment Form

## 7.2 Appendix 2

### Height of head centre of gravity (HHCoG)

Body measurements were interpolated from Schneider *et al*<sup>1</sup> and the World Health Organisation<sup>2</sup> in order to calculate the position of the vertex of the head relative to the supporting surface. For example if it was clearly documented that a child was standing on a table then the standing height (Stx) for the correct age (months) and gender was used from the World Health Organisation (WHO) growth tables<sup>2</sup>. Sitting heights (Six) to the vertex of the head for each age and gender were interpolated from the WHO<sup>2</sup>, where mean sitting heights are reported in 3 month age groups. Consequently age and gender appropriate fall height distances were calculated to the head vertex for both sitting and standing positions, but not to the CoG of the head. Snyder *et al*<sup>3</sup> reported the location of the CoG of 14 paediatric cadaver heads. However in their research the CoG position was documented relative to the centroid of the occipital condyles. As the position of this anatomical landmark wasn't documented with respect to the vertex of the head, different co-ordinate systems were aligned such that the distance from the vertex to the CoG of the head could be calculated. Loyd *et al*<sup>4</sup> reported head measurements to different anatomical landmarks for children  $\leq 4$  years and the position from the vertex of the head to nasion (the intersection of the frontal bone and two nasal bones) was documented. Schneider *et al*<sup>1</sup> also reported the position of nasion with respect to centroid of the occipital condyles, consequently the nasion was used as a point to align co-ordinate reference frames between the two studies<sup>1, 4</sup>. As a result a distance in the superior to inferior direction was calculated from the vertex of the head to the CoG. This distance was subtracted from the standing and sitting heights for the relevant age and gender. The calculation of each measurement for each age and gender is outlined below along with an example calculation of the position of the head CoG.

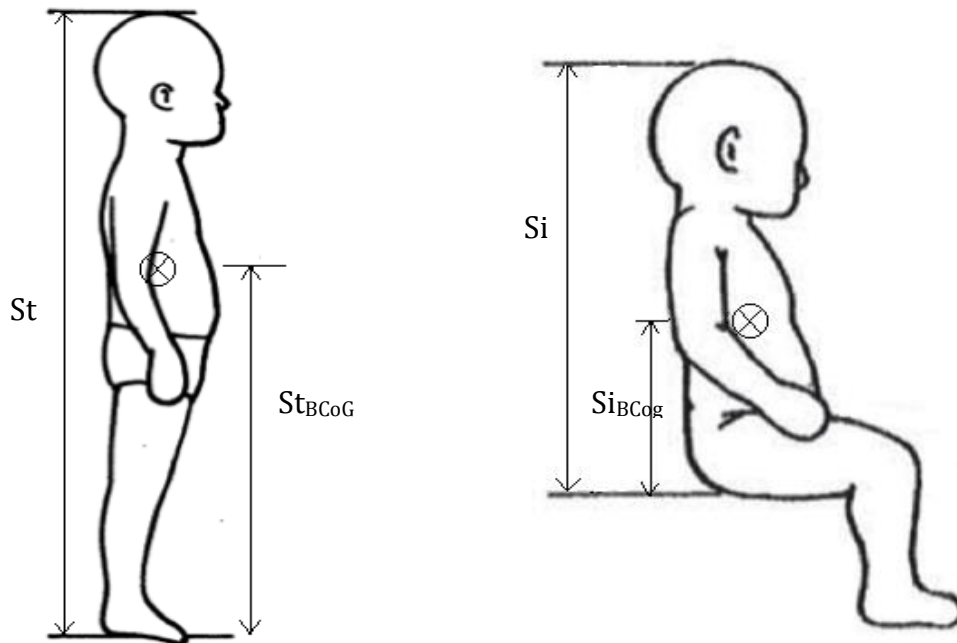


Figure 2A. Standing ( $St_x$ ) and sitting ( $Si_x$ ) heights used. Images edited from Schneider et al <sup>1</sup>.

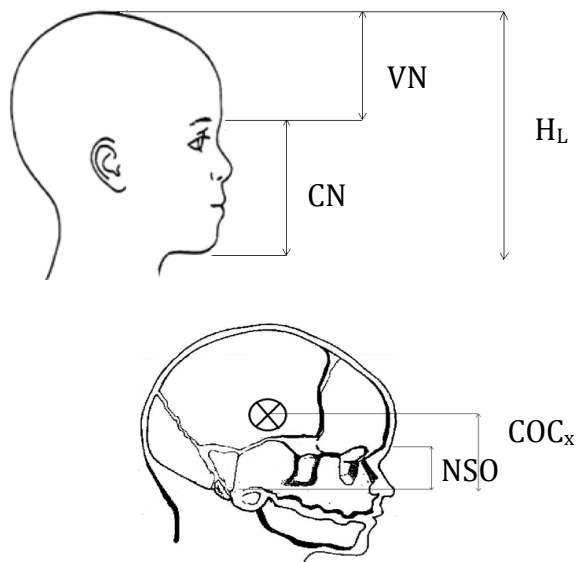


Figure 2B. Alignment of co-ordinate systems to calculate the position of centre of gravity of the head. (A) Head measurements taken from Snyder et al <sup>3</sup> to calculate the distance from the vertex to nasion. (B) Measurements taken from

Schneider *et al* <sup>1</sup> to calculate the distance from the nasion to the centre of gravity of the head.

The different measurements used are shown in Figure 2A and Figure 2B, with definitions shown in Table 31. The distance from the vertex of the head to the nasion wasn't documented by Loyd *et al* <sup>4</sup>, however length of the head ( $H_{Lx}$ ) and distance from the chin to nasion ( $CNS_x$ ) in the superior inferior directions were. However the measurements were documented for 3 month age groups, therefore data needed to be interpolated in order to get measurements per age (months). As such the data from Schneider *et al* <sup>1</sup> was extracted and 1st order logarithmic curves were fitted for both head length (Equation(51)) and chin to nasion distances (Equation (52)). The  $r^2$  (Coefficient of determination) for each equation were 0.95 and 0.9 respectively.

$$H_{Lx} = 1.415 \ln(m) + 12.935 \quad (51)$$

$$CNS_x = 0.532 \ln(m) + 5.8953 \quad (52)$$

$m$  = Age of child in months

The distance from the vertex to the nasion to the nasion was calculated via Equation (1).

$$VNS_x = H_{Lx} - CNS_x \quad (53)$$

Loyd *et al* <sup>4</sup> published an equation for distance between the centroid of the occipital condyles and nasion, Equation (35). However no equation was published for the distance between the centroid of the occipital condyles and the centre of gravity of the head. Consequently, based on the data from the published 14 paediatric cadaver heads, a 3rd order logarithmic fit was created with an  $r^2$  value of 0.84, Equation (36).

$$NSOC_x = 0.00302CL^2 + 0.31CL - 9.44 \quad (54)$$

$$COC_x = -0.0449\ln(m)^3 - 0.1383\ln(m)^2 + 3.0673 \ln(m) + 41.84 \quad (55)$$

$$CL = \text{Head length} + \text{head width} + \text{head circumference} \quad (56)$$

Detailed below is a calculation of the position of the centre of gravity of the head . :The example given is for a child in the standing position prior to falling, For a child in the sitting position, six replaces Stx in the calculation below)

Position of the CoG of the head with respect to the nasion,

$$\begin{aligned} \text{Positon of the CoG of the head wi}h\text{ respect to nasion (CoGNSx)} & \quad (57) \\ & = \text{COCx} - \text{NSOCx} \end{aligned}$$

Position of the CoG with respect to the vertex of the head,

$$\begin{aligned} \text{Positon of the CoG of the head wi}h\text{ respect to vertex (CoGVx)} & \quad (58) \\ & = \text{VNSx} - \text{CoGNSx} \end{aligned}$$

Position of the CoG with respect to weight bearing surface,

$$\text{HCoGx} = \text{Stx} - \text{CoGVx} \quad (59)$$

Table 31 -Nomenclature of the measurements used to calculate the position of the centre of gravity of the head relative to the impact surface.

Symbol	Definition
Stx	Standing Height
Six	Sitting Height
StBCoG	Location of the body centre of gravity for a standing position
SiBCoG	Location of the body centre of gravity for a sitting position
CNSx	Distance from the chin to the nasion
HLx	Head length (Distance from the vertex to the chin)
HCoGx	Position of the centre of gravity of the head with respect to the weight bearing surface.
BCoGx	Position of the body centre of gravity with respect to the weight bearing surface
VNSx	Distance from the vertex of the head to nasion
NSOCx	Distance from the centroid of the occipital condyles to the

	nasion of the head
COCx	Distance from the centroid of the occipital condyles of the head to the centre of gravity of the head
CL	Characteristic Length

As the measurements were only documented in 3 month age ranges per gender, data were interpolated to deduce measurements for each age (months). Equations (60), (61), (62) and (63) were developed for the male StBCoG , female StBCoG , male SiBCoG and female SiBCoG respectively (Refer to Table 31 for definitions).

$$St_{BCoG}(Male) = 0.0181\ln(m)^2 + 0.0006 \ln(m) + 0.323 \quad (60)$$

$$St_{BCoG}(Female) = 0.0211 \ln(m)^2 - 0.0139 \ln(m) + 0.3295 \quad (61)$$

$$Si_{BCoG}(Male) = -0.0018 \ln(m)^2 + 0.0091 \ln(m) + 0.2309 \quad (62)$$

$$Si_{BCoG}(Female) = -0.0056 \ln(m)^2 + 0.0324 \ln(m) + 0.134 \quad (63)$$

Depending on the gender and position of the child prior to falling, the position of the body centre of gravity with respect to the weight bearing surface (BCoGx) was summated with the documented fall height (Hf) to calculate the position of the head centre of gravity body with respect to the impacted surface (HBCoG), Equation (8). Depending on the position prior to falling and gender, BCoGx was calculated using either Equation (60), (61), (62) or (63).

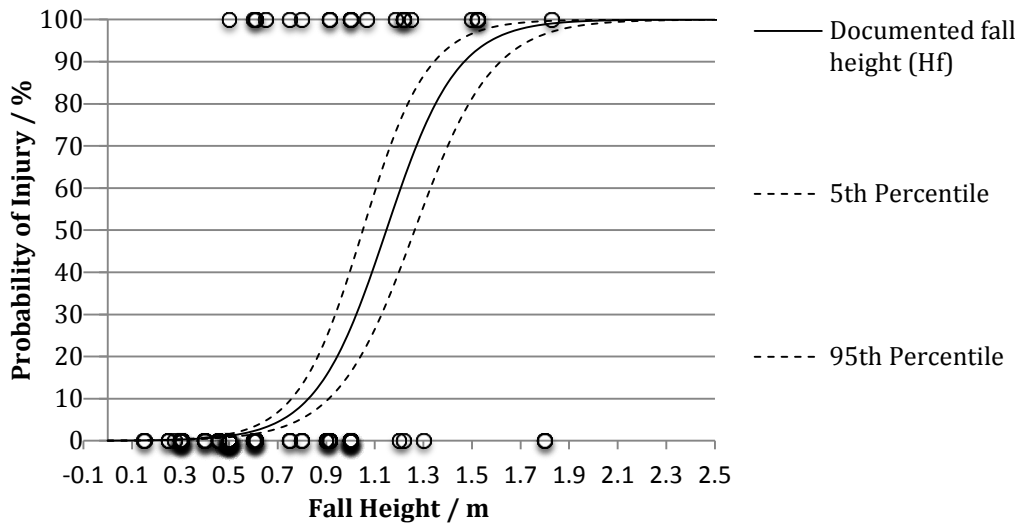
#### Crawling position

If it was clearly stated that the child was crawling prior to the fall then both the position of the body centre of gravity and the head were based on the arm length from the shoulder to the hand. The measurement were taken from Snyder *et al* <sup>3</sup>.



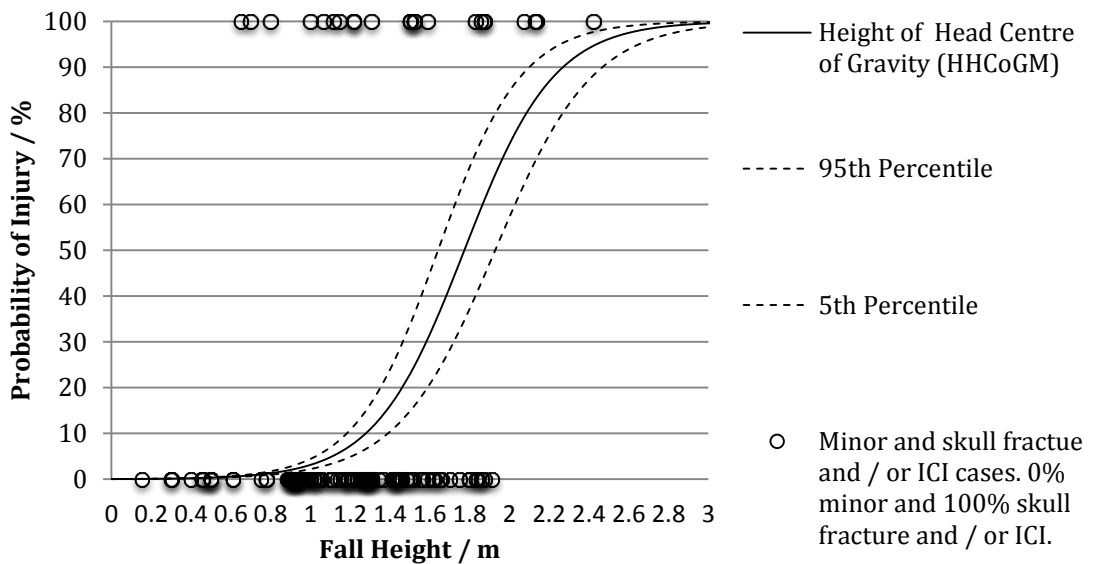
**7.3 Appendix 3**

Figure 3A. Logistic Regression Curve illustrating the probability of sustaining



a skull fracture and or ICI, based on the documented fall height ( $H_f$ ).

Figure 3B. Logistic Regression Curve illustrating the probability of sustaining



a skull fracture and or ICI, based on height of head CoG with maximum imputation ( $H_{HCoGM}$ ).

Chapter 7 – Appendices

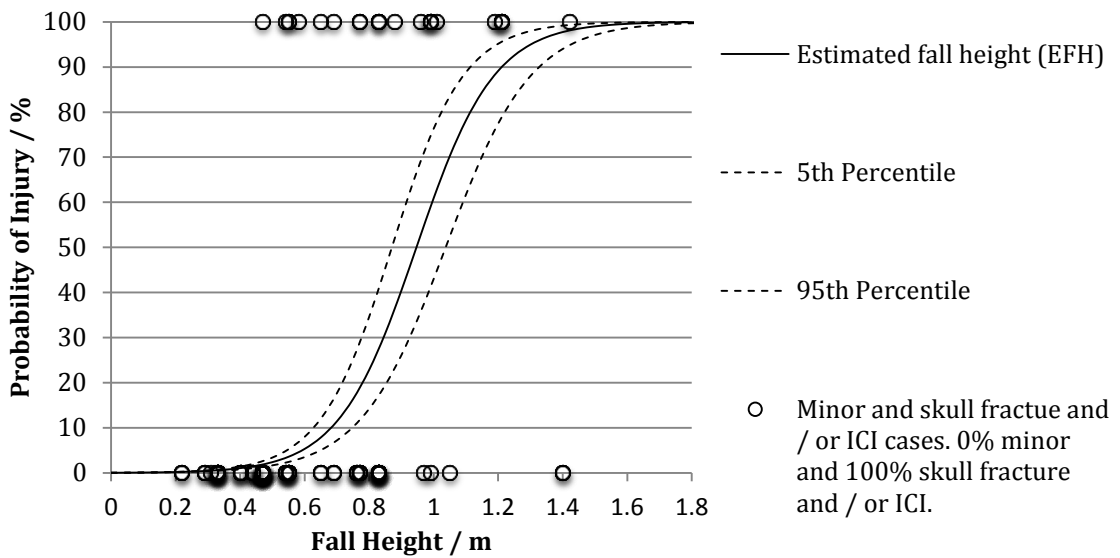


Figure 3C. Logistic Regression Curve illustrating the probability of sustaining a skull fracture and or ICI, based on the estimate fall height (EFH).

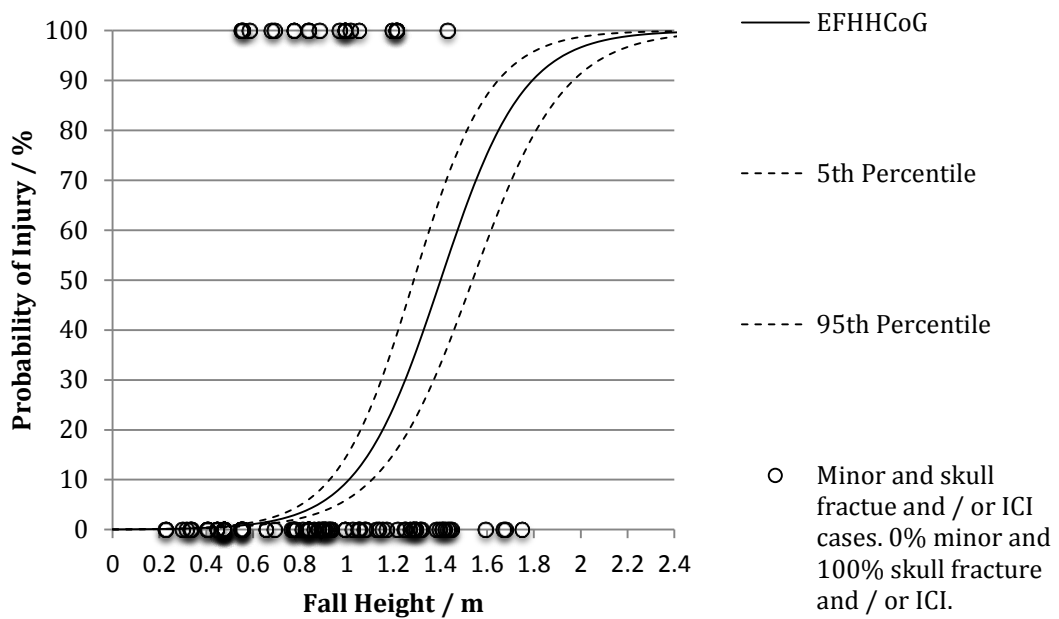


Figure 3D. logistic Regression Curve illustrating the probability of sustaining a skull fracture and or ICI, based on the estimate fall height with head height incorporated (EFH<sub>HCoG</sub>)

7.4 Appendix 4

**Table 4A – Review of clinical literature to determine previous head injuries reported from a low height fall in children**

<u>Article</u>	<u>Study Method</u>	<u>Age</u>	<u>Fall height classification</u>	<u>Head Injuries</u>	<u>Abuse considered</u>	<u>Fall witnessed by observer</u>
Bechtel <i>et al</i> <sup>5</sup> (2004) <a href="#">ENREF 5</a>	Prospective study of children admitted with a head injury undergoing a CT over a 2 year period	<24 months	<u>Measurement</u> - Unclear <u>Classification</u> - Unclear <u>Cut off</u> - <1.22m cut	≤ 1.22m - n=47/67 <u>Skull fracture</u> - n=40/67 <u>SDH</u> - n=18/67 <u>EDH</u> - N=10/67 <u>SAH</u> - n=2/67 (Head injuries not sub categorised by mechanism)	<u>Excluded</u> / <u>Separated out</u> – Yes (Abuse cases separated out based on algorithm)	Yes – (Witnessed by more than one adult)
Claudet <i>et al</i> <sup>6</sup> (2013)	Retrospective review over 4 year period of pre mobile infants admitted with head as the result of a fall.	<9 months	<u>Measurement</u> – Unclear <u>Classification</u> - Unclear <u>Cut off</u> - <0.9m	<u>Skull fracture &lt;0.9m</u> – 4% of 104 cases <u>Traumatic brain injury &lt;0.9m</u> – 2% of 48 cases <u>Traumatic brain injury</u> – mean fall height 0.91±0.3m	<u>Excluded</u> / <u>Separated out</u> - Unclear	Recorded if witnessed, but cases not separated out
Duhaime <i>et al</i> <sup>7</sup> (1992)	Prospective study of 100 patients admitted with a head injury.	≤24 months	<u>Measurement</u> - Height classed as distance through which head travelled. <u>Classification</u> - Specific heights used when available,	<u>Simple fracture</u> as likely to occur from <1.22m as >1.22m. <u>Complex fracture</u> - All non inflicted depressed	<u>Excluded</u> / <u>Separated out</u> – Yes (Developed classification	Combined (Height of fall estimated when cases not witnessed)

			otherwise fall from couches 0.46 - 0.61m, beds 0.61-0.76m, changing tables 0.91m, falls from arms greater than 1.22m. <u>Cut off</u> - <1.22m	fractures from falls >1.22m. Basilar and bilateral fracture associated with falls >1.22m. <u>EDH</u> 3 occurred from falls <1.22m.	criteria based on history and injuries. Suspected abuse cases separated out)	
Feldman <i>et al</i> <sup>8</sup> (2001)	Propsective study over a three year period of patients with a SDH	≤36 months	<u>Measurement</u> - Height measurement unclear. <u>Classification</u> - Unclear <u>Cut off</u> - <1.83m classified as 'indeterminate' cause, and ≤1.22m in mechanism classification.	<u>SDH</u> (≤1.22m) - n=5/12 (n.b this is based on indeterminate classification, no cases in the unintentional group	<u>Excluded</u> / <u>Separated out</u> – Yes (Multiple classification system of accidental and abuse)	
Greenes and Schutzman <sup>9</sup> (1997)	Retrospective review children admitted with a isolated skull fracture over a 3 year period.	<2 years	<u>Measurement</u> - Height used clear. <u>Classification</u> - Authors used documented height when available and used an estimate when it was not. Fall from bed (0.61m), fall from couches (0.46m), fall from table (0.76m), fall from adults arms (1.22m). <u>Cut off</u> - <0.91m and <1.52m used	Simple fracture (n=78/101) Depressed fracture (n=22/101) Multiple fracture (n=9) Fall <1.52m - n=55 Fall<0.91m -n=18	<u>Excluded</u> / <u>Separated out</u> – Yes (Potential abuse cases separate out	Unclear
Gruskin and	Retrospective	<2	<u>Measurement</u> – Unclear	<u>Skull fracture and / or</u>	Excluded/sepa	Unclear

Chapter 7 – Appendices

Schutzman <sup>10</sup> (1999)	study of children evaluated for head trauma over 1 year period.	years	<u>Classification</u> – specific height used when available. Otherwise estimated, falls sitting 0.3m, from chair, another child’s arms, standing position or a childrens bicycle 0.6m, from couch bed or baby swing 0.9m, from adults arms, shopping cart, crib, table or changing table 1.2m, from bunk bed 1.8m <u>Cut off</u> – 0.91 and 1.2m-1.5m	<u>ICI (&lt;0.9m and &lt;12 month)</u> – n=8/72 <u>Skull fracture and / or ICI (&lt;0.9m and ≥12 month)</u> – n=1/66 <u>Skull fracture and / or ICI (1.2-1.5m and &lt;12 month)</u> – n=10/31 <u>Skull fracture and / or ICI (1.2-1.5m and ≥12 month)</u> – n=1/16	rated out – Yes (If referred to social services and injuries felt to be intentional)	
Hettler and Greenes <sup>11</sup> (2003)	Retrospective review of children admitted with a traumatic intracranial injury over a 7 year period.	≤ 3 years	<u>Measurement</u> - Unclear <u>Classification</u> - Height used when available but otherwise estimated based on description. Falls from standing, couch or bed were ≤0.91m and falls from tables counters or adults arms were considered >0.91m. <u>Cut off</u> - Falls classed as ≤0.91m and >0.91m.	<u>SDH (≤0.91m)</u> - n=21/39 <u>EDH (≤0.91m)</u> - n=13/39 <u>SAH (≤0.91m)</u> - n=9/39 <u>Haemorrhagic contusion</u> - n=5/30	<u>Excluded</u> / <u>Separated out</u> – Yes (Algorithm developed)	Unknown if accidental cases witnessed
Ibrahim <i>et al</i> <sup>12</sup> (2011)	Retrospective review of children	≤48 months	<u>Measurement</u> - Surface height used.	<u>Skull fracture (≤0.91m)</u> - n=49/67 (Infant), n=7/31	<u>Excluded</u> / <u>Separated out</u>	Unknown

Chapter 7 – Appendices

	<p>admitted with a fall over a 6 year period.</p>		<p><u>Classification</u> – Heights estimated based on description when not available. <u>Cut off</u> -Heights classed as <math>\leq 0.91m</math>, <math>&gt;0.91m</math> &amp; <math>&lt;10ft</math> and <math>\geq 10ft</math>.</p>	<p>(Toddler) <u>Multiple Skull fracture (<math>\leq 0.91m</math>)</u> - n=5/67 (Infant) <u>Primary ICI w/o skull fracture (<math>\leq 0.91m</math>)</u> - n=8/67 (Infant), n=7/31 (Toddler) <u>Primary ICI with skull fracture (<math>\leq 0.91m</math>)</u> - n=29/67 (Infant), n=6/31 (Toddler) (Primary-Defined as including Epidural Haemorrhage (EDH), SDH, Subarachnoid Haemorrhage (SAH), intraventricular haemorrhage, parenchymal haemorrhage or contusion or axonal injury, Secondary - Defined as cerebral oedema, ischaemic infarct, or loss of gray / white matter)</p>	<p>– Yes (E codes indicative of abuse excluded along also if child protection team had suspicion of abuse then cases also excluded)</p>	
--	---	--	--	--	---	--

Chapter 7 – Appendices

Johnson <i>et al</i> <sup>13</sup> (2005)	Prospective review of children referred to an A&E department with a head injury from a fall over a 8 month period.	<5 years	<u>Measurement</u> - Unclear <u>Classification</u> – Fall height recorded. <u>Cut off</u> – Specific heights used	<u>Skull fracture</u> – n=4/72 (32 underwent skull radiography), 3 simple fractures ( 2 from falls just over a 1m and 1 who fell 0.8-0.9m) and 1 basal fracture from 3m fall.	<u>Excluded</u> / <u>Separated out</u> – Yes Only accidental cases included	Yes – Accidental cases witnessed by carer and corroborated by second observer
Leventhal <i>et al</i> <sup>14</sup> (1993)	Retrospective review over a 4 year period of children presenting with fractures	<3 years	<u>Measurement</u> – Unclear <u>Classification</u> - Height measurements used unclear. Unclear if heights estimated based on description. <u>Cut off</u> - <0.6m,	<u>Simple fracture</u> (<0.6m - n=8 <u>Complex fracture</u> 0.6-1.19m - n=6/23 ( n.b. parietal bone most common fracture area	<u>Excluded</u> / <u>Separated out</u> – Yes ( Cases separated into abuse, accidental and unknown, based on review of multiple clinical opinions	Yes Accident witnessed by neutral observer
Lyons and Oates <sup>15</sup> (1993)	Retrospective review over a 9 year period of children who fell from a bed	≤ 5 years	<u>Measurement</u> - Unclear <u>Classification</u> – Beds 25in, bed rails 41in, crib 32in, crib rail 54in <u>Cut off</u> - Unclear	1 Skull fracture in a child who fell from a crib	Unclear	Unclear
Myhre <i>et al</i> <sup>16</sup>	Retrospective	<36	<u>Measurement</u> – Unclear	<u>Skull fracture</u> <0.8m -	Cases	Yes- Accidental

Chapter 7 – Appendices

(2007)	review of children admitted over a 10 year period with traumatic head injury	months	≤1m defined as low impact. <u>Classification</u> - Unclear <u>Cut off</u> - Define height sub categories as <0.8m, 0.8-1.2m and >1.2m	n=7/39 <u>Skull fracture</u> 0.8-1.2m - n=10/39 <u>SDH &lt;0.8m</u> - n=8/27 <u>SDH 0.8-1.2m</u> - n=1/27 <u>EDH &lt;0.8m</u> - n=1/12 <u>EDH 0.8-1.2m</u> - n=7/12 <u>Parenchymal</u> - None reported from a fall ≤1m ( n.b.. Cases classed as abuse or intermediate were not subcatergorised relative to mechanism. 63% of SDH classed as abuse)	separated into abuse, accidental and intermediate.	cases were witnessed by someone other than caretaker.
Nimityongskul and Anderson <sup>17</sup> (1987)	Retrospective review over a 5 year period of children who were reported to have fall from bed, chair or cribe while in hospital.	≤16 years	<u>Measurement</u> - Unclear <u>Classification</u> – Cribs 38in, beds 23-34in, wagon 12in <u>Cut off</u> - Unclear	1 occipital fracture	Not specified	Unclear
Park <i>et al</i> <sup>18</sup> (2004)	Retrospective review of children admitted as the result of a fall over a 5 year period.	<6 years	<u>Measurement</u> - Unclear <u>Classification</u> – Falls from chair, table, bed and sofa <1m, fall from window, balcony and stairs >1m	<u>Skull fracture w/o intracranial haemorrhage (&lt;1m)</u> – n=19/38 <u>Intracranial</u>	<u>Excluded</u> – Yes (Identification unclear)	Yes - Height of fall based on that stated by witnesses or paramedics



			<u>Cut off</u> - <1m	<u>haemorrhage (&lt;1m)</u> – n=7/38		
Reece and Sege <sup>19</sup> (2000)	Retrospective review of children admitted with a head injury over a five year period	<6.5 years	<u>Measurement</u> - Unclear <u>Classification</u> - Unclear <u>Cut off</u> - <1.22m cut off used but definition of height unclear.	<u>Simple fracture (&lt;1.22m)</u> - n=38/62 <u>Complex fracture (1.22m)</u> - n=5/62 <u>SDH (&lt;1.22m)</u> - n=5/62 <u>SAH (&lt;1.22m)</u> -n=1/62 <u>Brain Contusion (&lt;1.22m)</u> - n=2/62	<u>Excluded</u> / <u>Separated out</u> – Yes (No history provided. Physical findings inconsistent, positive skeletal survey. Confession or witnessed abuse)	Yes -Only witnessed cases included
Shugerman <i>et al</i> <sup>20</sup> (1996)	Retrospective of patients admitted with a SDH or EDH over a 6 year period	≤ 3 years	<u>Measurement</u> - Unclear <u>Classification</u> - Unclear <u>Cut off</u> - <1.83m cut off.	<u>EDH</u> - 34 reported cases of which 31 accidental. 16 from fall ≤1.83m. SDH - 25 unintentional but mechanisms not reported	<u>Excluded</u> / <u>Separated out</u> – Yes (Cases classed as abuse based on hospital or CPS findings)	Unclear
Schutzman <i>et al</i> <sup>21</sup> (1993)	Retrospective review of children with a EDH over a	≤ 19 years	<u>Measurement</u> - Unclear <u>Classification</u> - Unclear <u>Cut off</u> - <1.52m cut off.	<u>EDH (&lt;1.52m)</u> - n=24/53 ( n.b. only 13 < 2years old. 19 temporal and 10	<u>Excluded</u> / <u>Separated out</u> – No, not	Unclear

Chapter 7 – Appendices

	10 year period			temperoparietal	discussed	
Tarantino <i>et al</i> <sup>22</sup> (1999)	Retrospective review of emergency department log over a 2 year period of children who presented from a fall.	<10 months	<u>Measurement</u> - Unclear <u>Classification</u> – falls from bed, couch or other surface or being dropped by carer classed as ≤1.22m <u>Cut off</u> - ≤1.22m	11.4% of cases isolated skull fracture or long bone fracture	Separated out – work up on suspicious cases, multidisciplinary investigation	Unclear
Thomas <i>et al</i> <sup>23</sup> (2013)	Retrospective review of imaging and clinical data in children admitted with head injury over a 5 year period	≤24 months	<u>Measurement</u> – Unclear <u>Classification</u> - Reported fall heights used. Height estimate based on the surface fallen from when not available. Unclear if surface height or the height of the head. <u>Cut Off</u> – Specific heights used	<u>Fracture and / or ICI</u> (n=54) -Mean height 1.32m (No cases <0.5m) <u>Isolate skull fracture</u> (n=23) - Mean height 1.4m <u>Intracranial haemorrhage</u> (n=21) - Mean height 1.5m <u>Thin SDH beneath fracture</u> (n=17) - mean 1.57m <u>EDH</u> (n=1) - 1m <u>Parenchymal Injury</u> (n=2) - mean 3m	<u>Excluded</u> / <u>Separated out</u> – Yes (Either no remaining suspicion of abuse, if suspicion remaining cases excluded)	Either independent witness or mechanism regarded clinically appropriate
Thompson <i>et al</i> <sup>24</sup> (2011)	Prospective study to determine severity of injuries	≤48 months	<u>Measurement</u> – Height of furniture and body CoG investigated. At home	<u>Moderate/Serious injuries</u> (fracture and isolated SDH) - Mean	<u>Excluded</u> / <u>Separated out</u> – Yes (cases	Recorded whether witnessed but

Chapter 7 – Appendices

	in children as a consequence of a short furniture fall over a 1 year period (n.b. not specific to head injuries)		investigations also completed. <u>Classification</u> - Specific heights used and at home investigations were completed. <u>Cut off</u> – No cut off used.	furniture height 0.76m, mean centre of body mass height 0.91m. <u>SDH</u> - Two cases with fall heights of 0.86m and 1m	reviewed by physician to determine likelihood of abuse)	not excluded. Used to inform abuse criteria.
Vinchon <i>et al</i> <sup>25</sup> (2010)	Prospective study of children hospitalised with a head injury to compared those with an inflicted head injury and those with accidental trauma.	<24 months	<u>Measurement</u> - Unknown <u>Classification</u> – Trivial fall classed as fall from arms or hospital beds <u>Cut off</u> – Not used	<u>Skull fracture</u> – (n=2/5) <u>SAH</u> – (n=3/5)	<u>Excluded or separated out</u> – Yes (Multidisciplinary team using Duhaime algorithm)	Yes independent witness public area.

## 7.5 Appendix 5

### Aim

To determine how accurate people estimate the height of household objects so that comparison can be made with a study undertaken by previous authors.

### Method

Students and staff at the canteen in the Newydd Meirionnydd building at the University of Hospital of Wales Cardiff were asked to estimate the height of three household objects. These household objects were a chair, a desk and table. All people investigated were  $\geq 18$  years old. Each person was presented with 3 objects and then asked to estimate the vertical height of each object and write the answers on a piece of paper. The percentage error was evaluated between estimated height and true height of each object (Equation 1).

$$\text{Percentage Error} = \frac{\text{Estimated height} - \text{True Height}}{\text{True Height}} \times 100 \quad (64)$$

### Results

In total 99 people estimated the height of three different household objects, therefore totalling 297 height estimations. Seventy one per cent of the cases were overestimated ( $n=208/299$ ) and 29% were under estimated ( $n=86/299$ ).

On average the height of the furniture was overestimated by 11%.

Fifty four per cent of people overestimated height for the chair and 45.3% of people underestimate the height. On average people overestimated the height of a chair by 4.3%. Seventy six per cent of people overestimate the height and 23.2% people underestimated the height of the table. On average the table was overestimated by 12.4%. Finally 80.6% of people overestimate the height of the desk and 19.4% underestimated the height. On average the desk was overestimate by 15.9%.

### Conclusion

It is clear that the population sample overestimated the height of the household objects by an average of 11%. This agrees with a similar finding from previous authors<sup>24</sup>.

7.6 Appendix 6

Table 6A -Variation in the coefficient of static friction between material surrogates and human skin.

Material	$\mu$ Wood	Significant difference between human (volar) on wood and surrogate material / P value	Significant difference between human (saturated) on wood and surrogate material / P value	$\mu$ Laminate	Significant difference between human (volar) on laminate and surrogate material / P value	Significant difference between human (saturated) on laminate and surrogate material / P value	$\mu$ Carpet	Significant difference between human (volar) on carpet and surrogate material / P value	Significant difference between human (saturated) on carpet and surrogate material / P value
Latex	1.52	<0.001	<0.001	1.19	<0.001	0.58	1.79	<0.001	<0.001
Chamois	1.31	<0.001	0.001	0.83	0.483	0	1.96	<0.001	<0.001
Leatherette	0.57	0.006	0.07	0.66	0.254	0	1.12	<0.001	0.002
Polyamide	1.01	0.012	0.101	1.33	<0.001	0.35	2.21	<0.001	<0.001
Polypropylene	0.44	<0.001	0.009	0.34	<0.001	<0.001	0.95	0.001	0.067
50% Polyamide 50% wool	0.99	0.02	0.016	0.35	<0.001	<0.001	0.78	0.252	0.78
Saturated Polyamide & wool	1.12	0.001	0.018	0.68	0.351	<0.001	1.27	<0.001	<0.001

Table 6B- Coefficient of static friction between different surfaces and human skin.

	Hydration	
Surface	Volar	Saturated
wood	0.8 (0.07)	0.8 (0.12)
laminated	0.77 (0.09)	1.24 (0.09)
carpet	0.71 (0.06)	0.77 (0.09)

Table 6C-A comparison between latex and polyamide & wool mix to determine the effect of friction on headform rotation during impact, with varying impact velocity, impact surface and angle of impact.

Impact Velocity (m/s)	Impact Surface	Latex / rad/s Mean±SE	Polyamide & wool mix / rad/s Mean±SE	P value
90 Deg (Perpendicular to surface)				
2.4 m/s	Carpet and Underlay	4.7(0.8)	6(0.4)	0.183
	Carpet	13.6(1.9)	18(1.2)	0.094
	Laminate	11.9(0.9)	13.4(2.3)	0.58
	Wood	17.4(0.6)	12.5(1.7)	0.028
3.0 m/s	Carpet and Underlay	13.2(0.9)	16(0.9)	0.081
	Carpet	14.7(1.2)	16.6(2.3)	0.504
	Laminate	18.6(1)	19.3(1)	0.624
	Wood	19.7(0.4)	12.9(2.4)	0.063
3.4 m/s	Carpet and Underlay	10.3(2.7)	15.3(0.4)	0.086
	Carpet	18.7(2.1)	17.5(3.3)	0.778
	Laminate	24(3.1)	20.5(2.8)	0.443
	Wood	20.8(2)	21.6(4.4)	0.875
75 Deg to Vertical				
2.4 m/s	Carpet and Underlay	20.7(0.5)	24.2(0.4)	0.002
	Carpet	24.5(0.6)	23.1(0.2)	0.087
	Laminate	25.5(0.9)	25.3(0.4)	0.865
	Wood	26.8(0.3)	26.3(0.6)	0.464
3.0 m/s	Carpet and Underlay	26.6(0.8)	29.9(0.9)	0.032
	Carpet	30.8(0.7)	30.3(0.4)	0.578
	Laminate	30.4(0.6)	33.6(0.9)	0.042
	Wood	30.8(1.6)	32.2(0.7)	0.456
3.4 m/s	Carpet and Underlay	32.4(0.4)	34(1.3)	0.351
	Carpet	29(4.8)	38.7(1)	0.094
	Laminate	39.7(3)	39.1(1.7)	0.868
	Wood	39(1)	40.8(1)	0.267
60 Deg to Vertical				
2.4 m/s	Carpet and Underlay	26.5(1.6)	29.9(0.5)	0.083



## Chapter 7 – Appendices

	Carpet	27.5(0.2)	32.5(0.4)	0
	Laminate	38.3(6.4)	30.8(1.2)	0.313
	Wood	35.8(0.5)	31.4(1.5)	0.027
3.0 m/s	Carpet and Underlay	37.9(1.3)	37.2(0.8)	0.665
	Carpet	36.6(0.8)	40.9(1.8)	0.109
	Laminate	40.1(0.5)	37.2(1.5)	0.117
	Wood	42.1(0.9)	39.5(0.9)	0.074
3.4 m/s	Carpet and Underlay	42.9(2)	48.1(2.5)	0.155
	Carpet	41.3(4.1)	48.4(2.4)	0.168
	Laminate	50.5(2.3)	46.5(1.4)	0.188
	Wood	46.4(1.8)	46.5(0.7)	0.97

Chapter 7 – Appendices

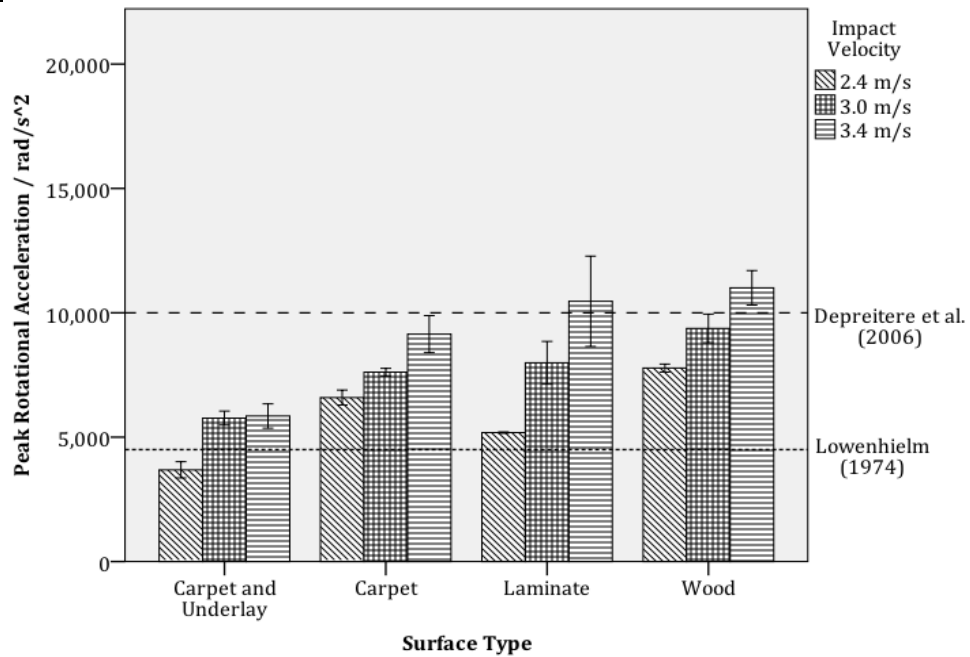


Figure 6A. The effect that changing impact velocity and impact surface have on peak rotational acceleration at a 90 degree impact angle for the latex skin surface.

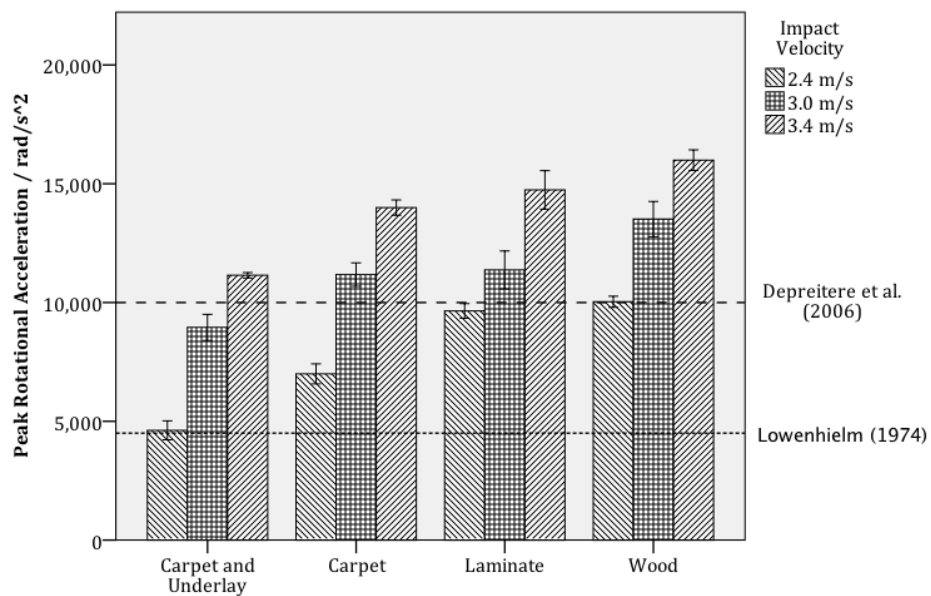


Figure 6B. The effect that changing impact velocity and impact surface have on peak rotational acceleration at a 75 degree impact angle for the latex skin surface.

6C.  
effect

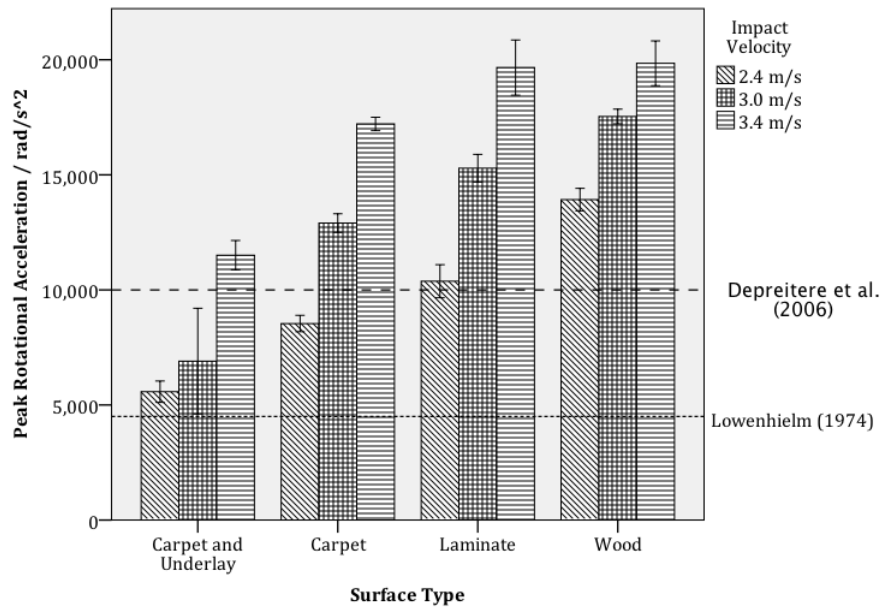


Figure  
The  
that

changing impact velocity and impact surface have on peak rotational acceleration at a 60 degree impact angle for the latex skin surface

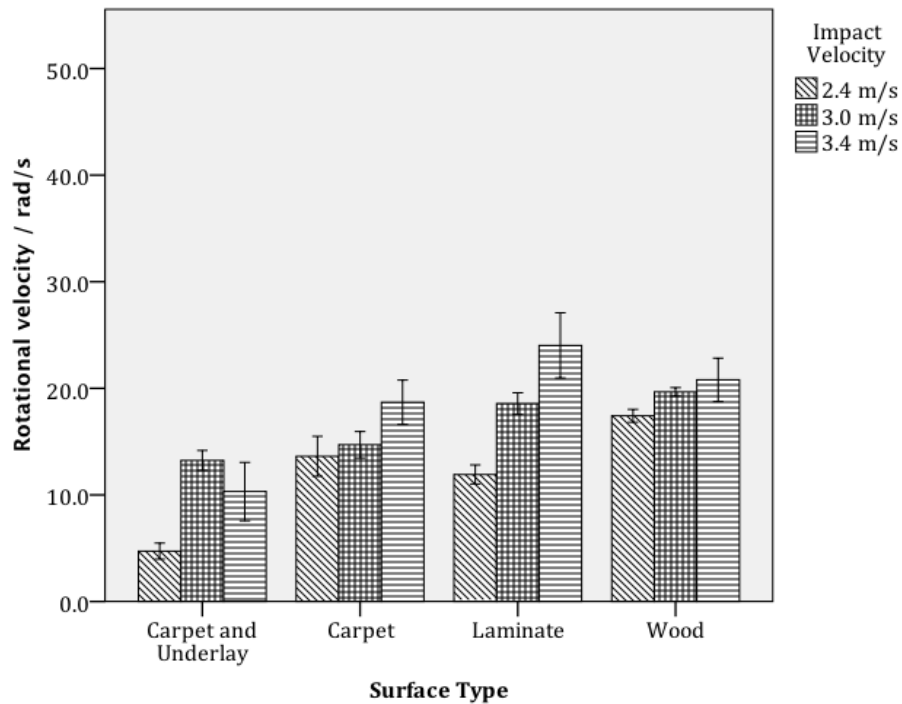


Figure 6D. The effect that changing impact velocity and impact surface have on rotational velocity at a 90 degree impact angle for the latex skin surface.

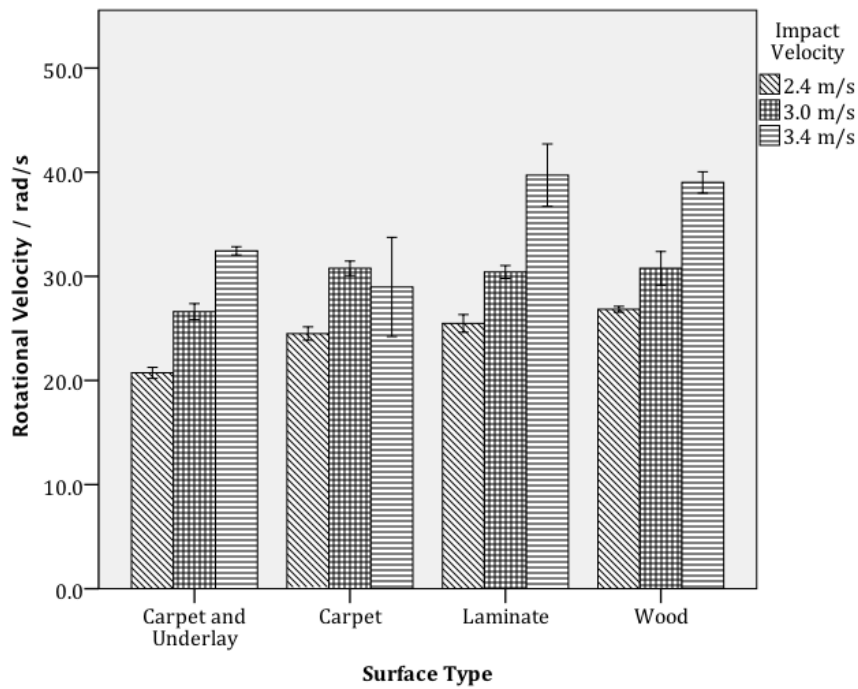


Figure 6E. The effect that changing impact velocity and impact surface have on rotational velocity at a 75 degree impact angle for the latex skin surface.

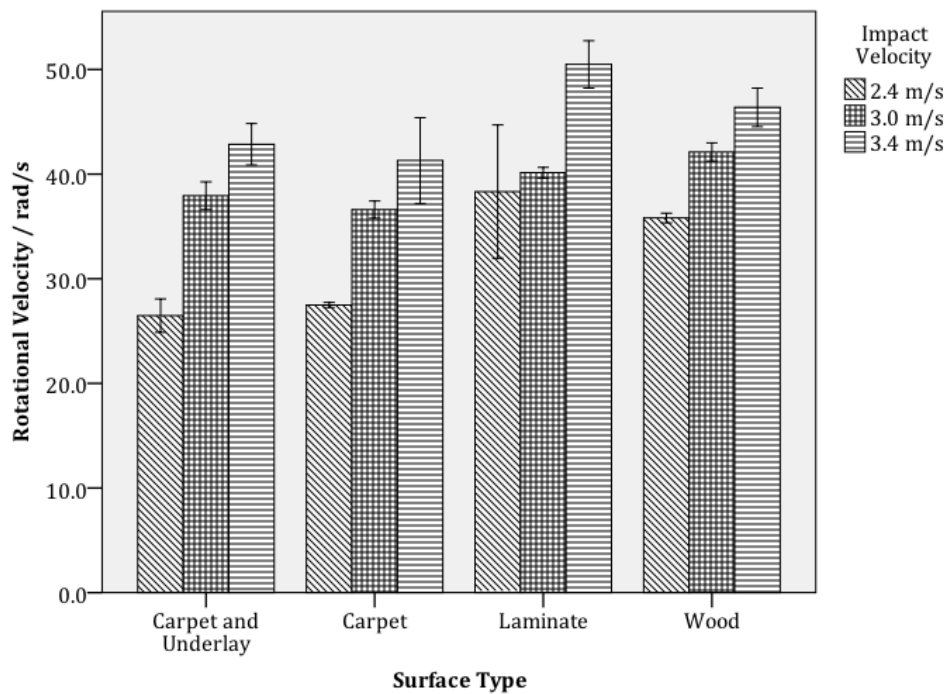


Figure 6F. The effect that changing impact velocity and impact surface have on rotational velocity at a 60 degree impact angle for the latex skin surface.

Chapter 7 – Appendices

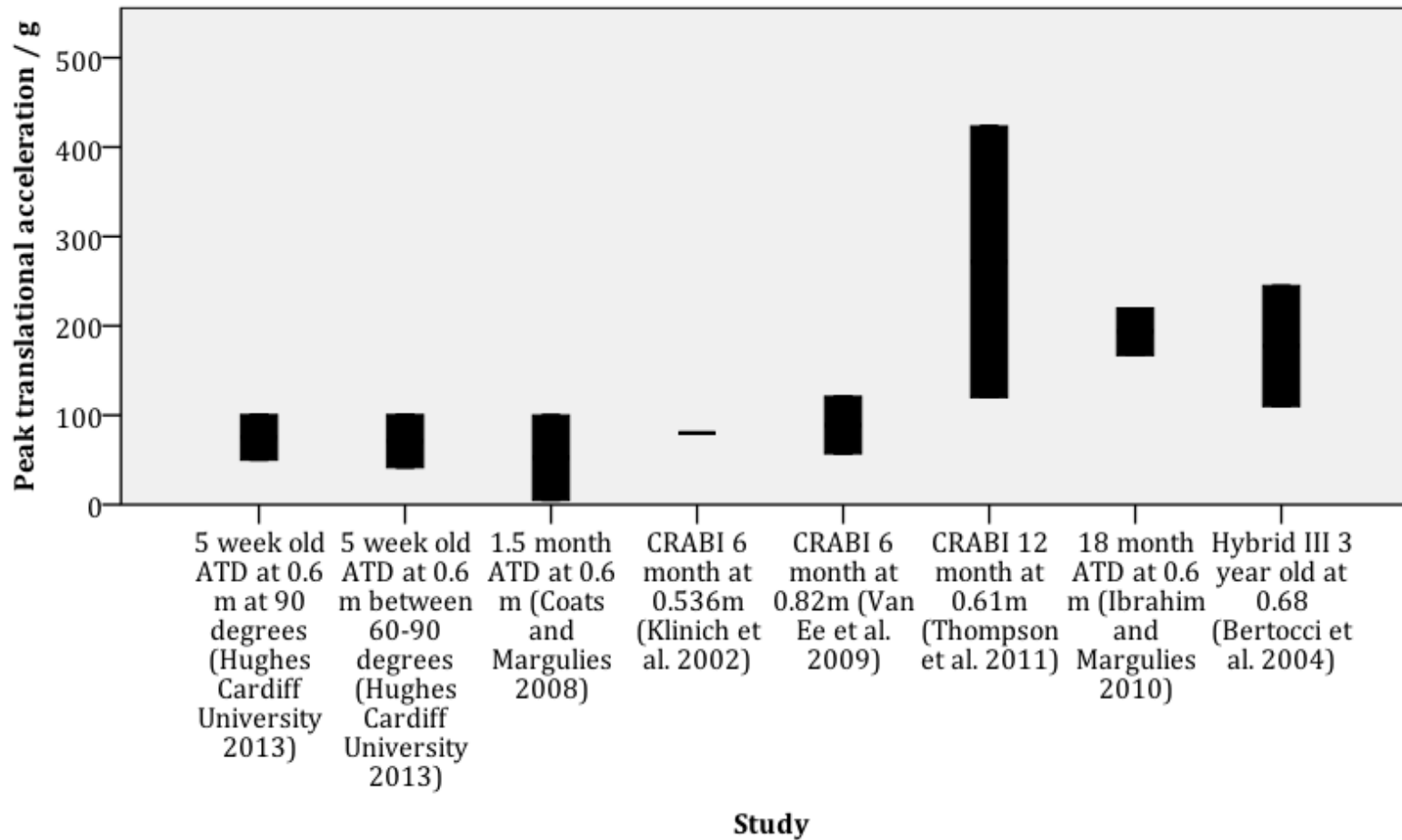


Figure 6G. Peak translational accelerations measured using ATDs of different ages at a height of or close to 0.6m by different authors.

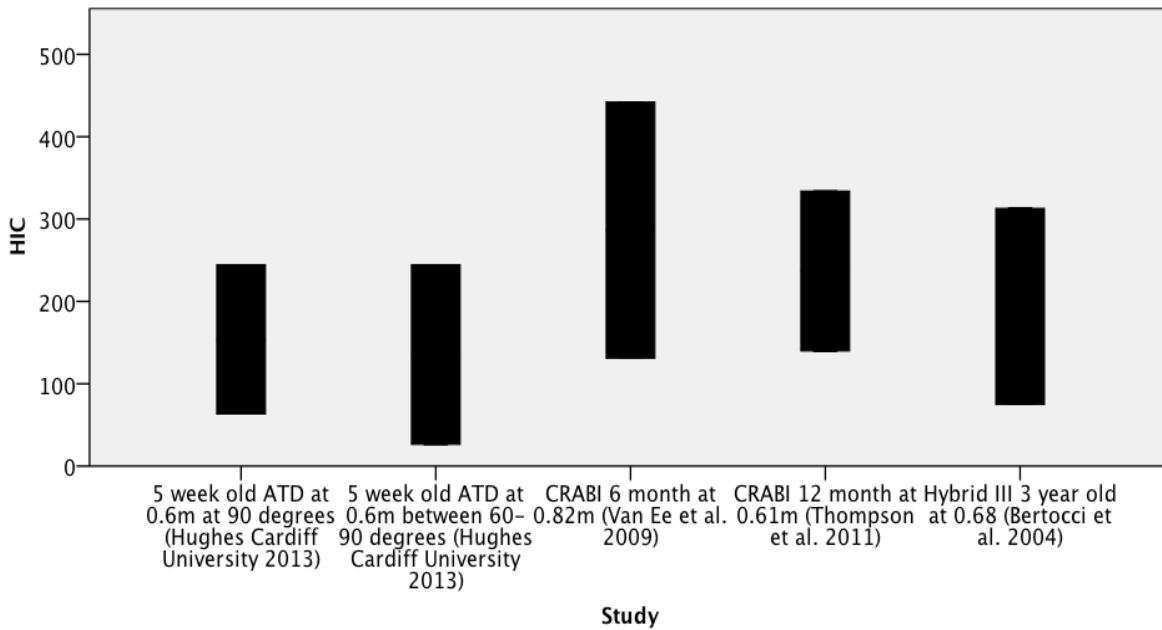


Figure 6H. HIC measured using ATDs of different ages at a height of or close to 0.6m by different authors.

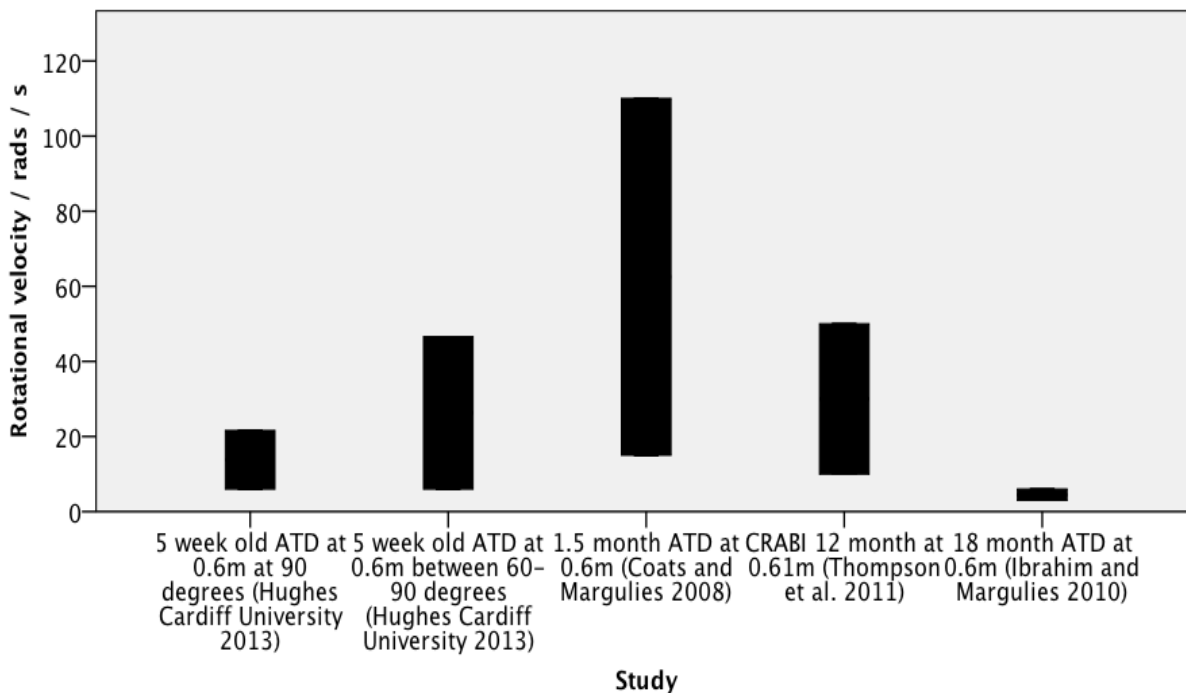


Figure 6I. Rotational velocity measured using ATDs of different ages at a height of or close to 0.6m by different authors.

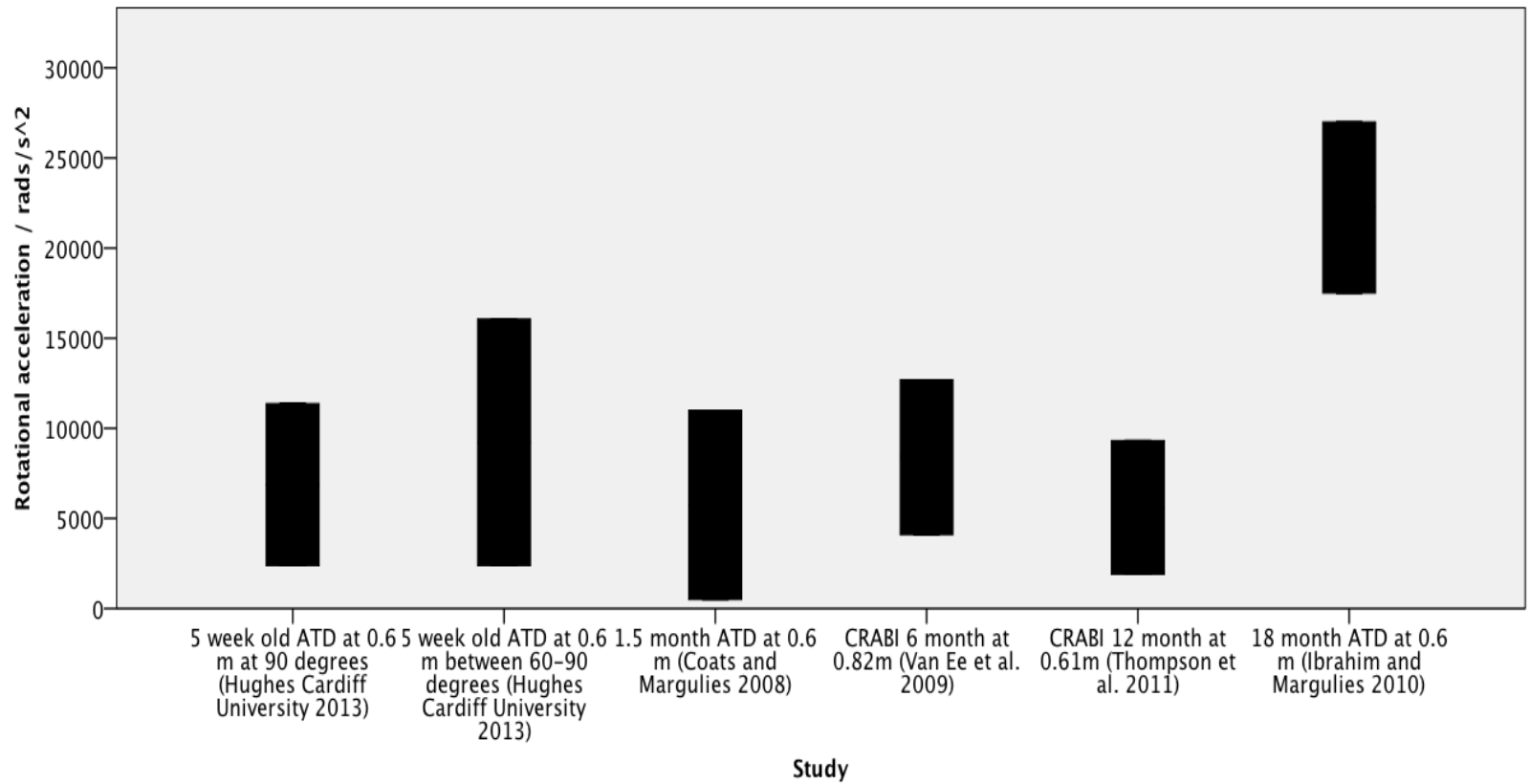


Figure 6J. Peak rotational accelerations measured using ATDs of different ages at a height of or close to 0.6m by different authors.

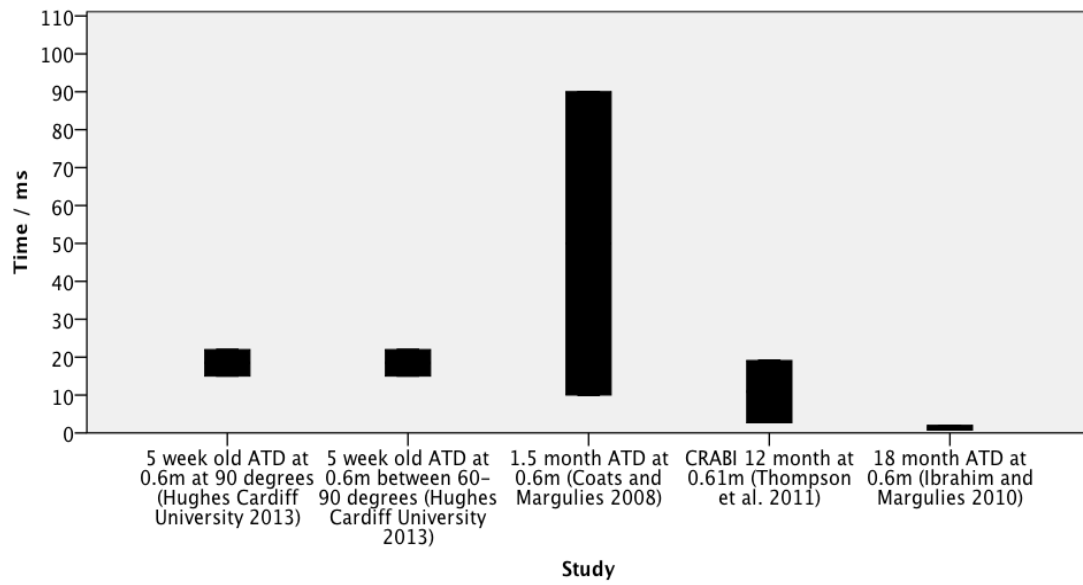


Figure 6K. Duration of impact measured using ATDs of different ages at a height of or close to 0.6m by different authors.



## 7.7 References

1. Schneider L, Lehman R, Pflug M, Owings C. Size and shape of the head and neck from birth to four years. Final report 1986.
2. WHO. The WHO Child Growth Standards. <http://www.who.int/childgrowth/standards/en/>. Published 2011. Accessed 18/8/2011, 2011.
3. Snyder RG, Spencer ML, Owings CL, Schneider LW. Physical Characteristics of Children. *US Consumer Product Safety Commission, Bethesda, MD*. 1975.
4. Loyd AM, Nightingale R, Bass CR, Mertz HJ, Frush D, Daniel C, et al. Pediatric head contours and inertial properties for ATD design. *Stapp car crash journal*. 2010;54:167.
5. Bechtel K, Stoessel K, Leventhal JM, Ogle E, Teague B, Lavietes S, et al. Characteristics That Distinguish Accidental From Abusive Injury in Hospitalized Young Children With Head Trauma. *Pediatrics*. 2004;114(1):165-168.
6. Claudet I, Gurrera E, Honorat R, Rekhroukh H, Casasoprana A, Grouteau E. [Home falls in infants before walking acquisition]. *Archives de pediatrie: organe officiel de la Societe francaise de pediatrie*. 2013;20(5):484-491.
7. Duhaime AC, Alario AJ, Lewander WJ, Schut L, Sutton LN, Seidl TS, et al. Head injury in very young children: mechanisms, injury types, and ophthalmologic findings in 100 hospitalized patients younger than 2 years of age. *Pediatrics*. 1992;90(2):179.
8. Feldman KW, Bethel R, Shugerman RP, Grossman DC, Grady MS, Ellenbogen RG. The cause of infant and toddler subdural hemorrhage: a prospective study. *Pediatrics*. 2001;108(3):636.
9. Greenes DS, Schutzman SA. Infants with isolated skull fracture: what are their clinical characteristics, and do they require hospitalization? *Annals of emergency medicine*. 1997;30(3):253-259.
10. Gruskin KD, Schutzman SA. Head trauma in children younger than 2 years: are there predictors for complications? *Archives of pediatrics & adolescent medicine*. 1999;153(1):15.
11. Hettler J, Greenes DS. Can the initial history predict whether a child with a head injury has been abused? *Pediatrics*. 2003;111(3):602-607.
12. Ibrahim NG, Wood J, Margulies SS, Christian CW. Influence of age and fall type on head injuries in infants and toddlers. *International Journal of Developmental Neuroscience*. 2011.
13. Johnson K, Fischer T, Chapman S, Wilson B. Accidental head injuries in children under 5 years of age. *Clinical radiology*. 2005;60(4):464-468.
14. Leventhal JM, Thomas SA, Rosenfield NS, Markowitz RI. Fractures in young children: distinguishing child abuse from unintentional injuries. *Archives of Pediatrics and Adolescent Medicine*. 1993;147(1):87.
15. Lyons TJ, Oates RK. Falling out of Bed: A Relatively Benign Occurrence. *Pediatrics*. 1993;92(1):125-127.
16. Myhre M, Grøgaard J, Dyb G, Sandvik L, Nordhov M. Traumatic head injury in infants and toddlers. *Acta paediatrica*. 2007;96(8):1159-1163.

17. Nimityongskul P, Anderson LD. The likelihood of injuries when children fall out of bed. *Journal of Pediatric Orthopaedics*. 1987;7(2):184.
18. Park SH, Cho BM, Oh SM. Head injuries from falls in preschool children. *Yonsei Medical Journal*. 2004;45:229-232.
19. Reece RM, Sege R. Childhood Head Injuries: Accidental or Inflicted? *Arch Pediatr Adolesc Med*. 2000;154(1):11-15.
20. Shugerman RP, Paez A, Grossman DC, Feldman KW, Grady MS. Epidural hemorrhage: is it abuse? *Pediatrics*. 1996;97(5):664-668.
21. Schutzman SA, Barnes PD, Mantello M, Scott RM. Epidural hematomas in children. *Annals of emergency medicine*. 1993;22(3):535-541.
22. Tarantino CA, Dowd MD, Murdock TC. Short vertical falls in infants. *Pediatric emergency care*. 1999;15(1):5.
23. Thomas AG, Hegde SV, Dineen RA, Jaspán T. Patterns of accidental craniocerebral injury occurring in early childhood. *Archives of disease in childhood*. 2013;98(10):787-792.
24. Thompson AK, Bertocci G, Rice W, Pierce MC. Pediatric short-distance household falls: Biomechanics and associated injury severity. *Accident Analysis and Prevention*. 2011;43(1):143-150.
25. Vinchon M, de Foort-Dhellemmes S, Desurmont M, Delestret I. Confessed abuse versus witnessed accidents in infants: comparison of clinical, radiological, and ophthalmological data in corroborated cases. *Child's nervous system*. 2010;26(5):637-645.